RADCAT RADAR MEASUREMENT PROGRAM

GENERAL DYNAMICS
FORT WORTH, TEXAS

24 NOVEMBER 1971

RADC-TR-72-7
Final Technical Report
November 1971

RADCAT RADAR MEASUREMENT PROGRAM

Sponsored by
U. S. Army Advanced Ballistic Missile Defense Agency
A 31657-13-Z-659

Contractor: General Dynamics
Contract Number: F30602-72-C-0025
Effective Date of Contract: 12 July 1971
Contract Expiration Date: 12 September 1971
Amount of Contract: $18,000.00

Principal Investigator: Dave Cisco
Phone: 817 732-3404

Project Engineer: David L. Tauroney
Phone: 315 330-4233

Rome Air Development Center
Air Force Systems Command
Griffiss Air Force Base, New York

RADCAT RADAR MEASUREMENT PROGRAM

D. O. Cisco

General Dynamics

Approved for public release;
distribution unlimited.

This research was supported by the U. S. Army Advanced Ballistic Missile Defense Agency and was monitored by David L. Tauroney, RADC (OCTT), GAFB, NY 13440 under Contract F30602-72-C-0025.

PUBLICATION REVIEW

This technical report has been reviewed and is approved.

RADC Project Engineer
DANIEL L. TAURONEY

JAMES L. RYNNING
Colonel, USAF
Chief, Surveillance & Control Division

F O R E W O R D

This report is a documentation of the RADCAT Vehicle 002 radar cross section measurements program which was sponsored by the U.S. Army Advanced Ballistic Missile Defense Agency. The program was conducted during the period 15 August 1971 to 15 November 1971 under Contract number F30602-72-C-0025 for Rome Air Development Center under the auspices of RADC Project Engineer Mr. Daniel L. Tauroney.

This report, designated as General Dynamics Report No. FZE-1143, was prepared by Mr. D. O. Cisco. Major contributions to this program were made by Mr. W. A. Pierson.

This technical report has been reviewed and is approved.

RADC Project Engineer
DANIEL L. TAURONEY

A B S T R A C T

The results of a radar cross section measurement program involving the precision Radar Calibration Target (RADCAT) Vehicle 002 are presented herein. Coherent long-pulse signatures obtained at measurement frequencies of 1.28, 2.85, and 5.65 gigahertz are presented and discussed in relation to similar data obtained in 1967 on the RADCAT Vehicle 001. Short-pulse measurements, coherent at 5.65 gigahertz and noncoherent at 2.4 gigahertz, were also obtained on RADCAT Vehicle 002 and are presented. Comparisons are made between the long-pulse response of Vehicles 001 and 002, between signatures of Vehicles 001, 002, and those from a half-scale model of the calibration target, and between the long-pulse response of Vehicles 001, 002, and the computed response based on a physical optics formulation.

TABLE OF CONTENTS

T A B L E O F C O N T E N T S (cont'd.)

LIST OF FIGURES

L I S T O F F I G U R E S (cont'd).

L I S T O F F I G U R E S (cont'd.)

LIST OF FIGURES (cont'd.)

L I S T O F F I G U R E S (cont'd.)

L I S T O F F I G U R E S (cont'd.)

LIST OF FIGURES (cont'd.)

L I S T O F F I G U R E S (cont'd.)

L I S T O F F I G U R E S (cont'd.)

L I S T O F F I G U R E S (cont'd.)

L I S T O F F I G U R E S (cont'd.)

L I S T O F F I G U R E S (cont'd.)

L I S T O F F I G U R E S (cont'd.)

L I S T O F T A B L E S

SECTION 1

INTRODUCTION AND SUMMARY

1.1 INTRODUCTION

The Convair Aerospace Division of General Dynamics recently completed a radar cross section measurements program involving the acquisition of a limited set of signatures of the Radar Calibration Target (RADCAT) Serial Number 002. This program was expressly designed to define, conduct and examine the minimum set of long-pulse and short-pulse measurements considered feasible for determining the validity of using radar cross section data previously obtained on RADCAT Vehicle 001 to represent the radar cross section characteristics of RADCAT Vehicle 002. Having performed the original measurements on RADCAT Vehicle 001 in 1968, this Division was in an excellent position to reconstruct as accurately as possible the radar range configuration, target mounting configuration, and system parameters which were employed during the 1968 measurements program.

This report documents the measurements performed on vehicle 002, the basis upon which the signatures from vehicle 001 and 002 were compared, and the conclusions and recommendations which resulted from the signature comparison. Due to the limited scope of this program, the short-pulse signatures corresponding to vehicle 002 were not processed to the same extent as were those recorded on vehicle 001. As a consequence, the comparison performed between the scattered response from the two vehicles involved long-pulse signature data exclusively.

In addition to presenting the measured long-pulse and short-pulse response of RADCAT vehicle 002, a considerable volume of ancillary signature data have also been included in this document. These additional data correspond to selected measurements performed on RADCAT vehicle 001, and those which were performed at this facility in 1967 on a 1/2-scale model of the calibration target. The purpose of including these data is to allow engineering personnel more closely associated with the overall RADCAT program to redefine, if they so desire, the basis for determining the usefullness of existing RADCAT vehicle 001 data.

1.2 SUMMARY

The information presented in this report is intended to document the procedures which were employed to obtain high quality long-pulse and short-pulse signature data on RADCAT vehicle Serial Number 002, the basis upon which the response from vehicle 001 and vehicle 002 were compared, and the conclusions which were drawn as they relate to the similarity of scattering characteristics between the two vehicles.

Section 2 of this report contains a complete presentation of all coherent long-pulse data acquired on RADCAT vehicle 002. Included in these data are both the amplitude and phase response at V/V, H/H, 45/45, and V/H polarizations as measured at the frequencies of 1.28, 2.85, and 5.65 gigahertz. The coherent short-pulse response at the measurement frequency of 5.65 gigahertz is presented in the form of a plot of the calibrated peak amplitude response versus

aspect angle, and relative phase (modulo 2π) versus aspect angle. The short-pulse amplitude response obtained at 2.4 gigahertz is also presented in Section 2 in the form of a plot of the calibrated peak amplitude response versus aspect angle.

Section 3 compares the long-pulse response of vehicle 002 to that of vehicle 001. The specific scattering characteristics which are compared are

1) Sensitivity of target response to change in roll angle orientation

2) Sensitivity of target response to change in polarization

3) Sensitivity of target response to change in frequency

4) Pattern symmetry about either end-on aspect orientation

5) Pattern symmetry about either broadside aspect orientation

In order to establish a baseline for comparing one vehicle to the other in terms of these characteristics, the response from each vehicle is separately compared to that computed through the use of a physical optics formulation, as well as the scattered response from a perfectly conducting half-scale RADCAT model.

Conclusions and recommendations regarding the use of signature data available on vehicle 001 to represent the radar cross section characteristics of vehicle 002 are presented in Section 4. Since the basic response pattern (lobe structure) from each vehicle is quite similar, the existing data library for vehicle 001 may be used to represent vehicle 002 subject to the introduction of a bias level to compensate for a difference in absolute radar cross section. It is noted, however, that the value selected

to compensate in the broadside region may not provide acceptable compensation in the end-on region. An alternative to modifying the vehicle 002 data is to simply utilize the signatures acquired during this program for future calibration purposes.

Five appendices have been included in this document to support the technical contents of Section 2 through 4. Appendix A describes the radar systems and operational procedures employed during the radar cross section measurement portion of this program. Appendix B contains pertinent calibration data, recorded background levels, field probes, and system linearity data acquired prior to target measurement. Appendix C contains the long-pulse reponse of vehicle 001 corresponding to measurement frequencies of 1.28, 2.85, and 5.65 gigahertz, the roll angle orientations of zero and sixty degrees, and transmitter/receiver polarizations of V/V, H/H, 45/45, and V/H. Appendix D consists of a complete listing of the calibrated C-band and S-band short-pulse response of vehicle 002 as a function of aspect angle. Appendix E describes the physical optics formulation utilized to compute the radar cross section response of an 8-foot cylinder with 2:1 oblate spheriodal ends, and Appendix F contains the S-, C-, and X-band long-pulse response of a perfectly conducting half-scale RADCAT vehicle model.

SECTION 2

RADCAT VEHICLE 002 MEASURED RESPONSE

2.1 GENERAL

Radar cross section measurements were performed on the RADCAT Vehicle Number 002 using both long- and short-pulse radar systems which are located on this Division's Radar Cross Section Range. Three separate coherent long-pulse radars were utilized to perform measurements at L-, S-, and C-band frequencies of 1.28, 2.85, and 5.65 gigahertz respectively. Coherent high-resolution signatures were obtained through the use of a C-band short-pulse radar system which is characterized by a 3-dB pulse width of approximately 0.8 nanoseconds at 5.65 gigahertz.

Since the measurement program conducted at the Convair Aerospace Division of General Dynamics was to be the sole opportunity to acquire RCS data on this vehicle prior to launch, an additional set of high resolution measurements were performed and are submitted herein. These additional data correspond to signatures acquired using this Division's S-band short-pulse radar system which is characterized by a 3-dB pulse width of 1.4 nanoseconds at an operating frequency of approximately 2.4 gigahertz.

The radar cross section signatures presented in this section are entirely those corresponding to the RADCAT Vehicle Number 002. The reader is referred to Appendix A for a description of the radar systems which were utilized during this program as well as a summary of pertinent operational procedures which were followed during

this measurement program. Analog recordings of calibration, background, and field probe data may be found in Appendix B.

2.2 LONG-PULSE MEASUREMENTS

Coherent long-pulse measurements were performed in accordance with the measurements matrix shown in Table 2.1. Use was made of the triangular shaped designator which is located on one end-cap of the vehicle in order to establish both an aspect-angle and roll-angle reference orientation. As noted in the sketch of Figure 2-1, zero-degrees aspect corresponds to a coincident alignment of the Radar-Line-of-Sight (RLOS) and the longitudinal axis of the vehicle such that the triangular indicator is toward the radar. A zero-degree roll angle orientation corresponds to a positioning of the target such that the triangular indicator appears vertically above the attachment assembly; a sixty-degree roll angle is obtained by rotating the vehicle in a clockwise direction.

Figures 2-2 to 2-49 contain the long-pulse amplitude and phase response of RADCAT Vehicle 002 for all measurement conditions noted in Table 2.1. The amplitude response is shown calibrated in dBsm; phase has been calibrated in degrees, modulo 2π. The title block in the upper right-hand corner of each figure contains information regarding the target roll angle, frequency and polarization at which the measurements were taken.

Table 2.1 RADCAT LONG-PULSE MEASUREMENT MATRIX

FREQUENCY GHz	POLARIZATION	PITCH ANGLE (DEGREES)	ROLL ANGLE (DEGREES)	ASPECT ANGLE (DEGREES)
1.28±.001	VV HH VH π/4 π/4	0	0, 60	0 TO 360 (0.1° INCREMENTS)
2.85±.003	VV HH VH π/4 π/4	0	0, 60	0 TO 360 (0.1° INCREMENTS)
5.65±.006	VV HH VH π/4 π/4	0	0, 60	0 TO 360 (0.1° INCREMENTS)

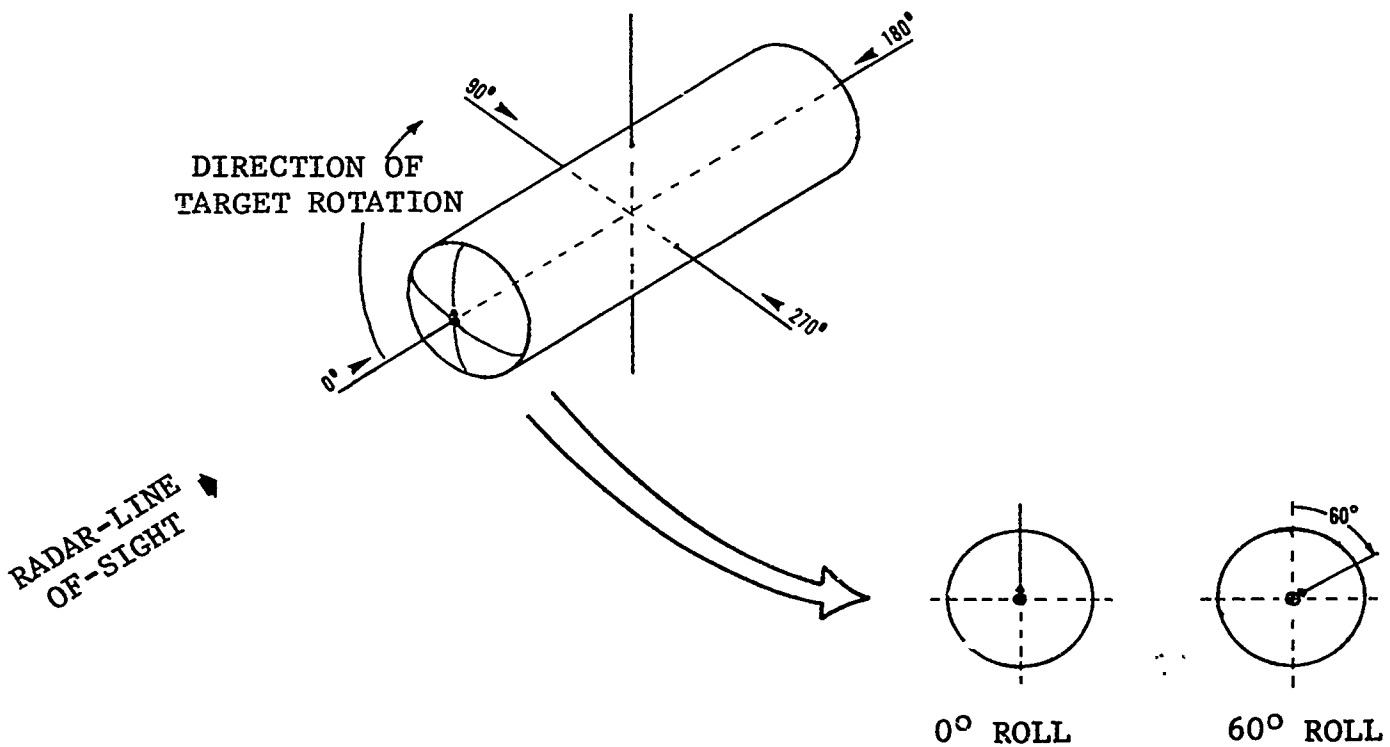

Fig. 2-1 TARGET ORIENTATION CONVENTION FOR LONG-PULSE MEASUREMENTS

THIS PAGE INTENTIONALLY LEFT BLANK

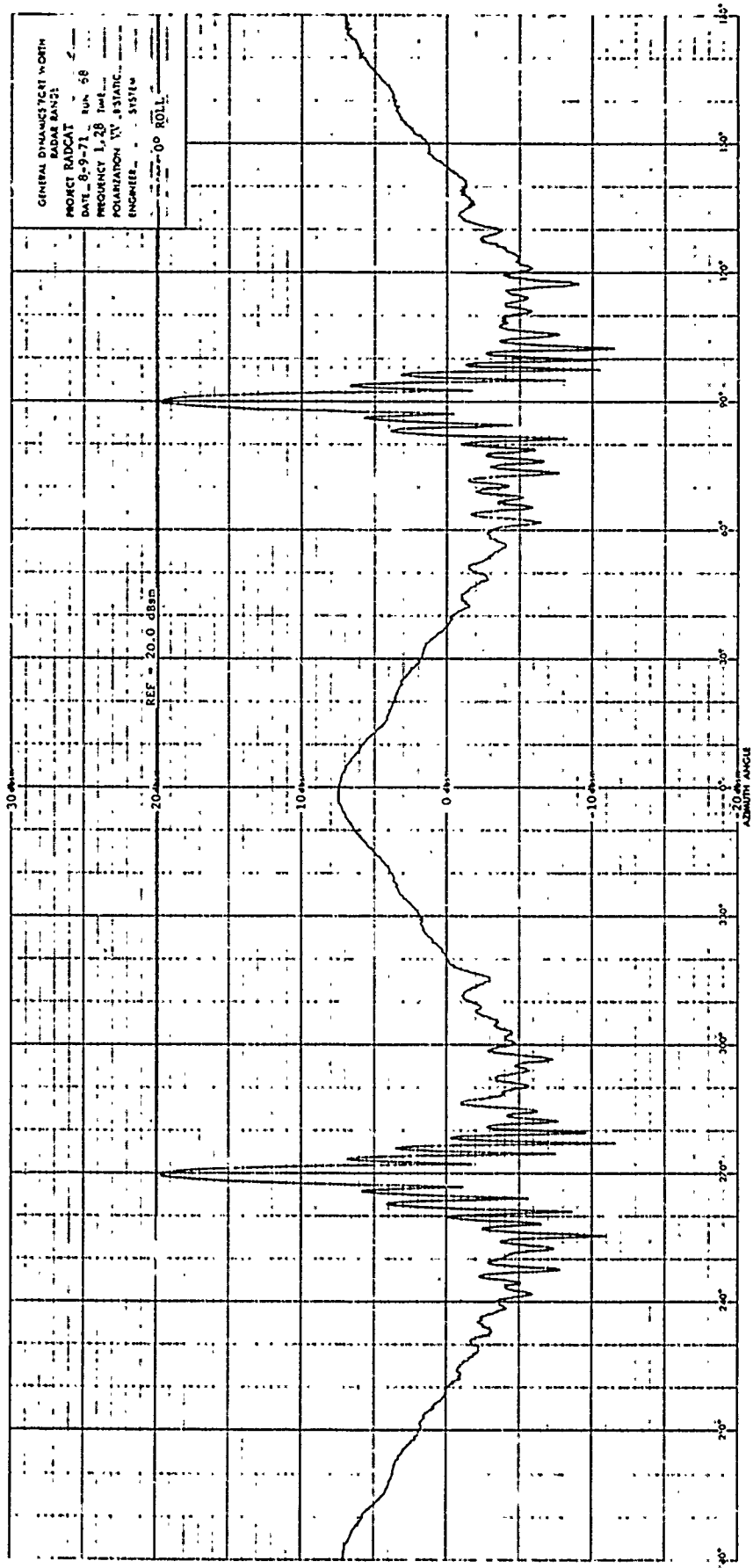

Fig. 2-2 VEHICLE 002 AMPLITUDE RESPONSE; L-BAND, VV POLARIZATION, 0-DEGREE ROLL

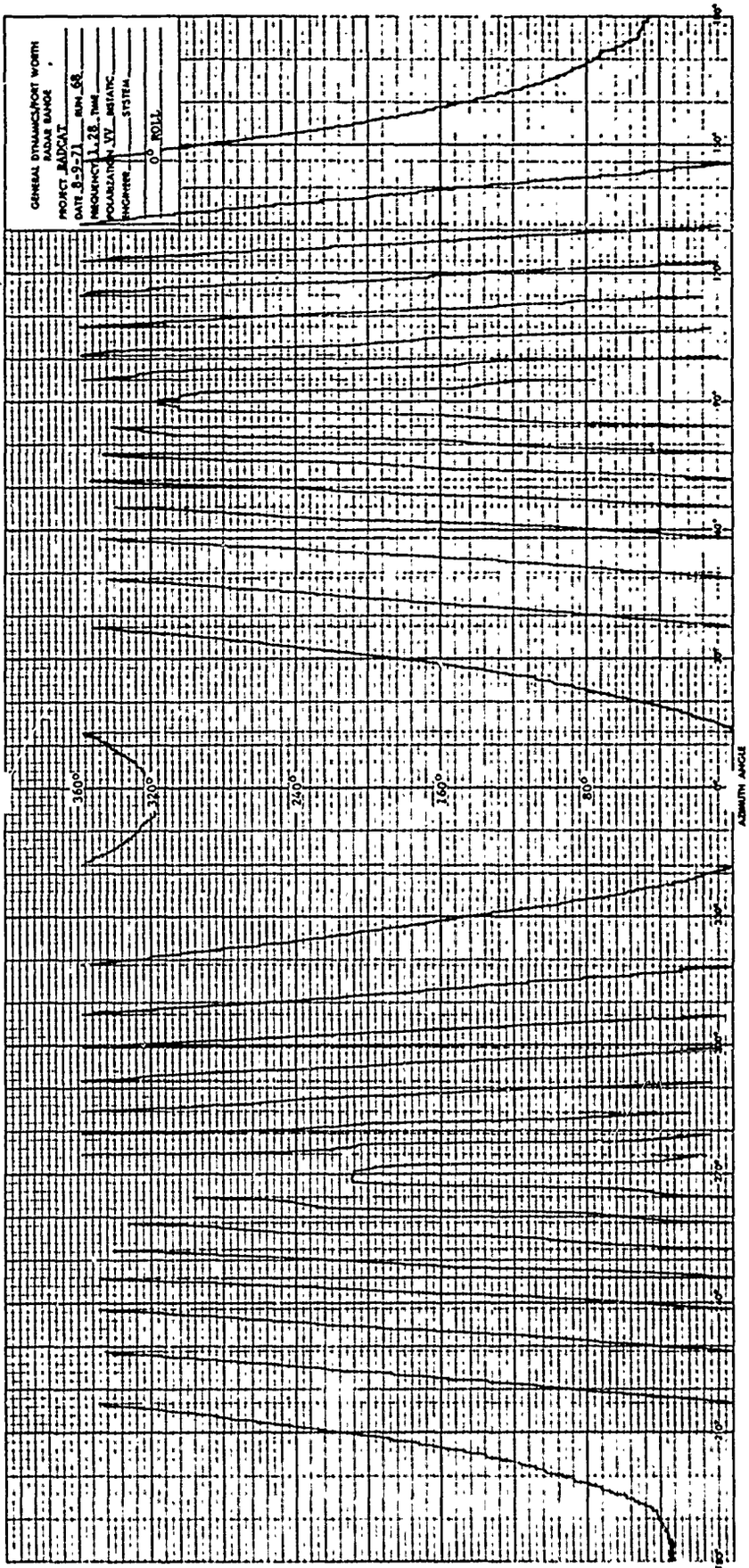

Fig. 2-3 VEHICLE 002 PHASE RESPONSE; L-BAND, VV POLARIZATION, 0-DEGREE ROLL

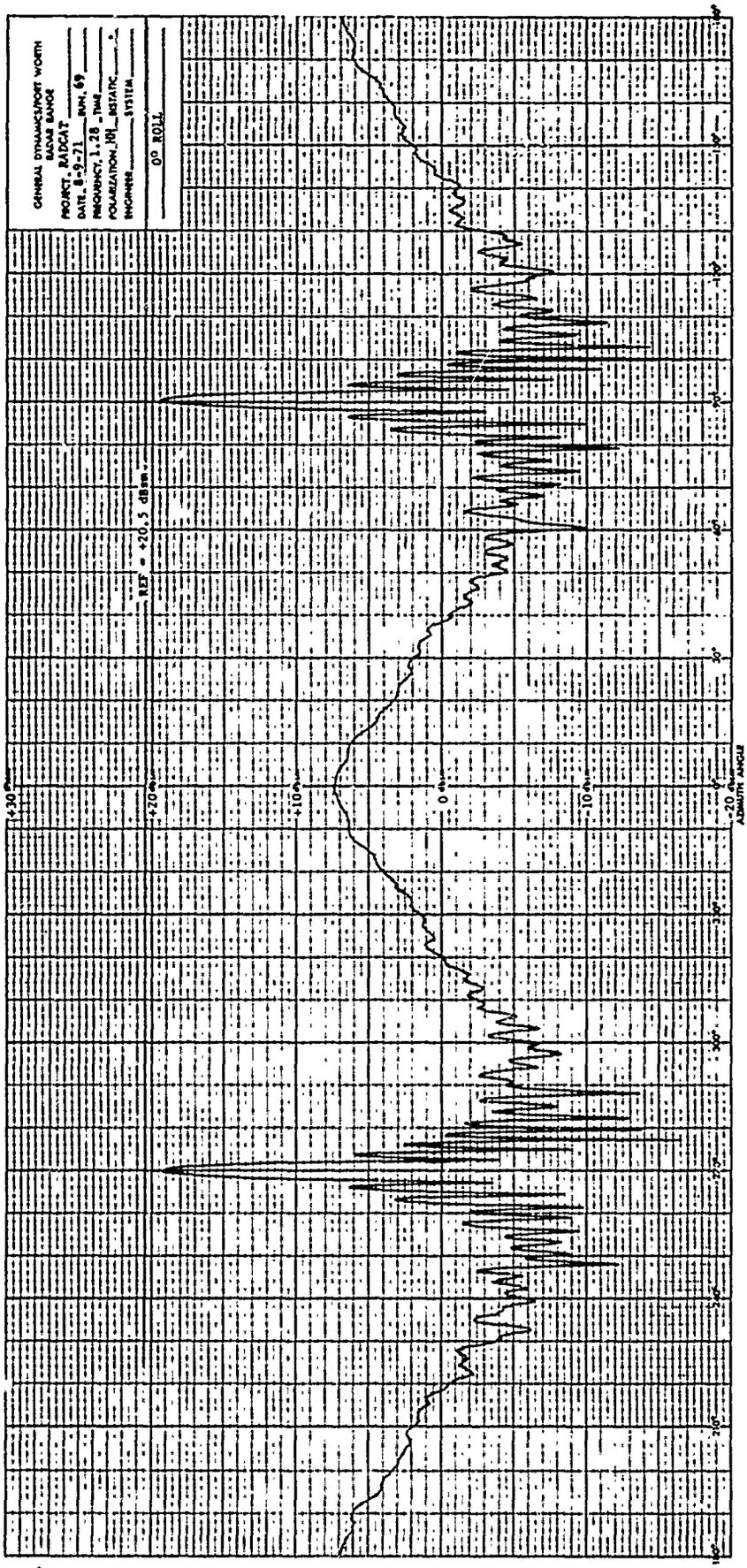

Fig. 2-4 VEHICLE 002 AMPLITUDE RESPONSE; L-BAND, HH POLARIZATION, 0-DEGREE ROLL

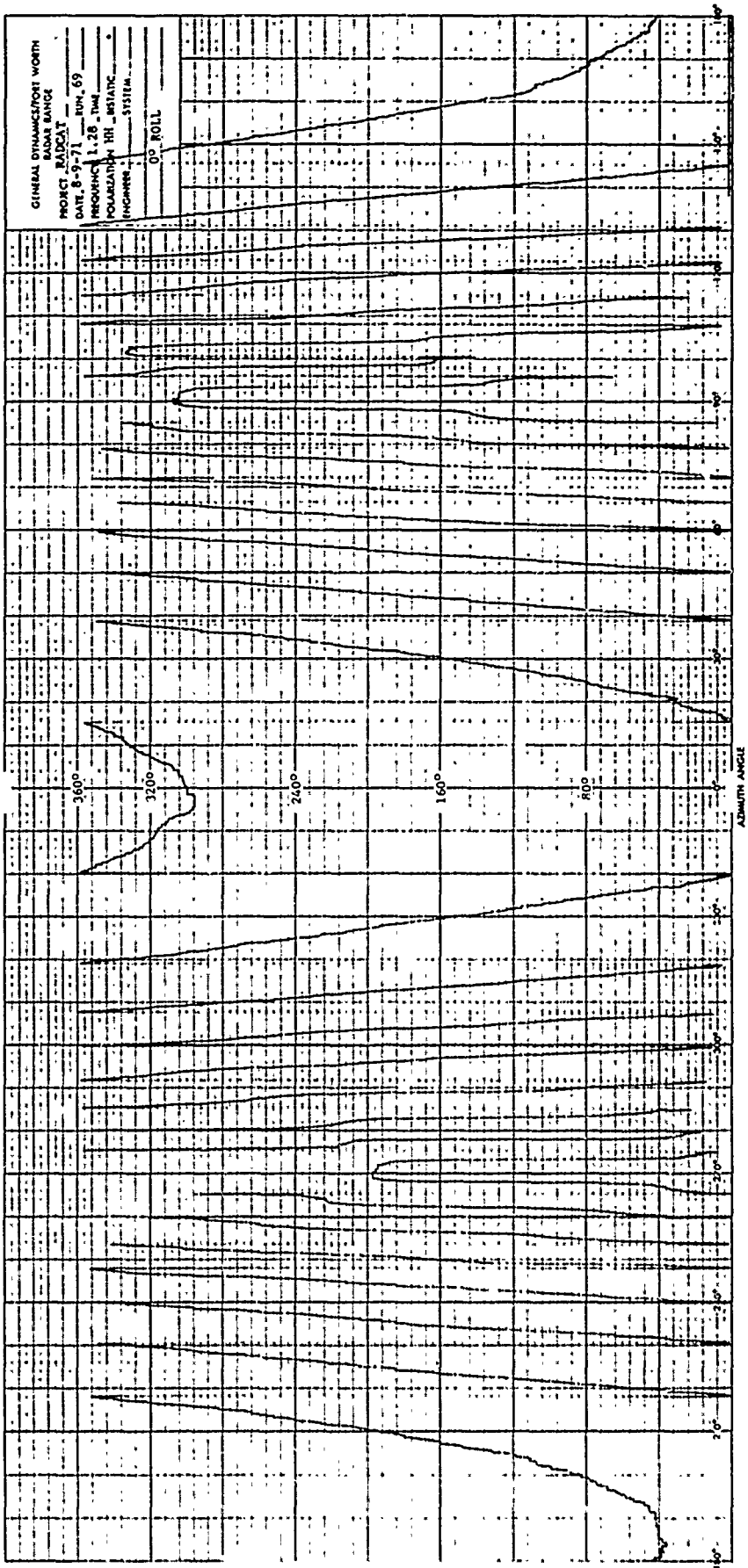

Fig. 2-5 VEHICLE 002 PHASE RESPONSE; L-BAND, HH POLARIZATION, 0-DEGREE ROLL

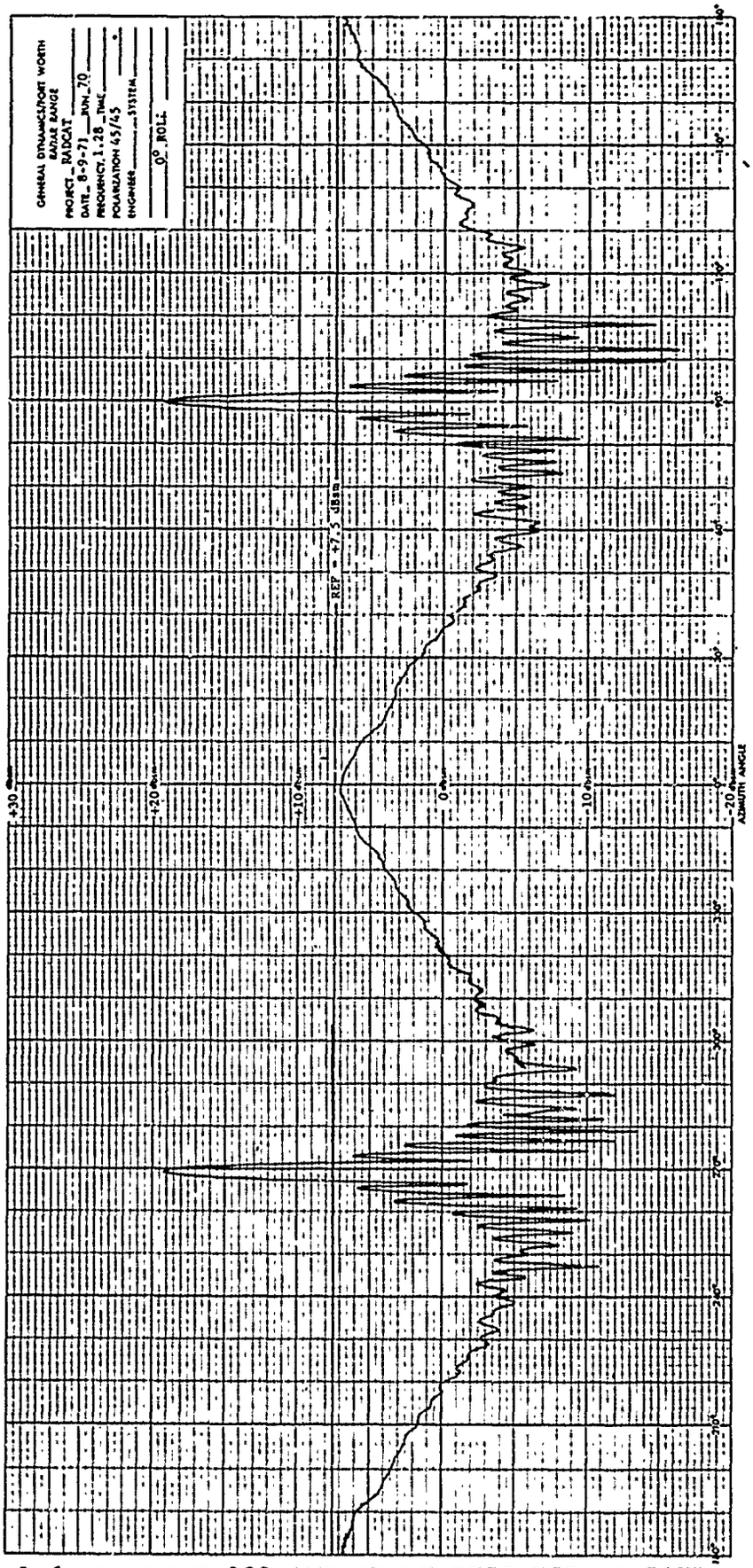

Fig. 2-6 VEHICLE 002 AMPLITUDE RESPONSE; L-BAND, $\pi/4$ $\pi/4$ POLARIZATION, 0-DEGREE ROLL

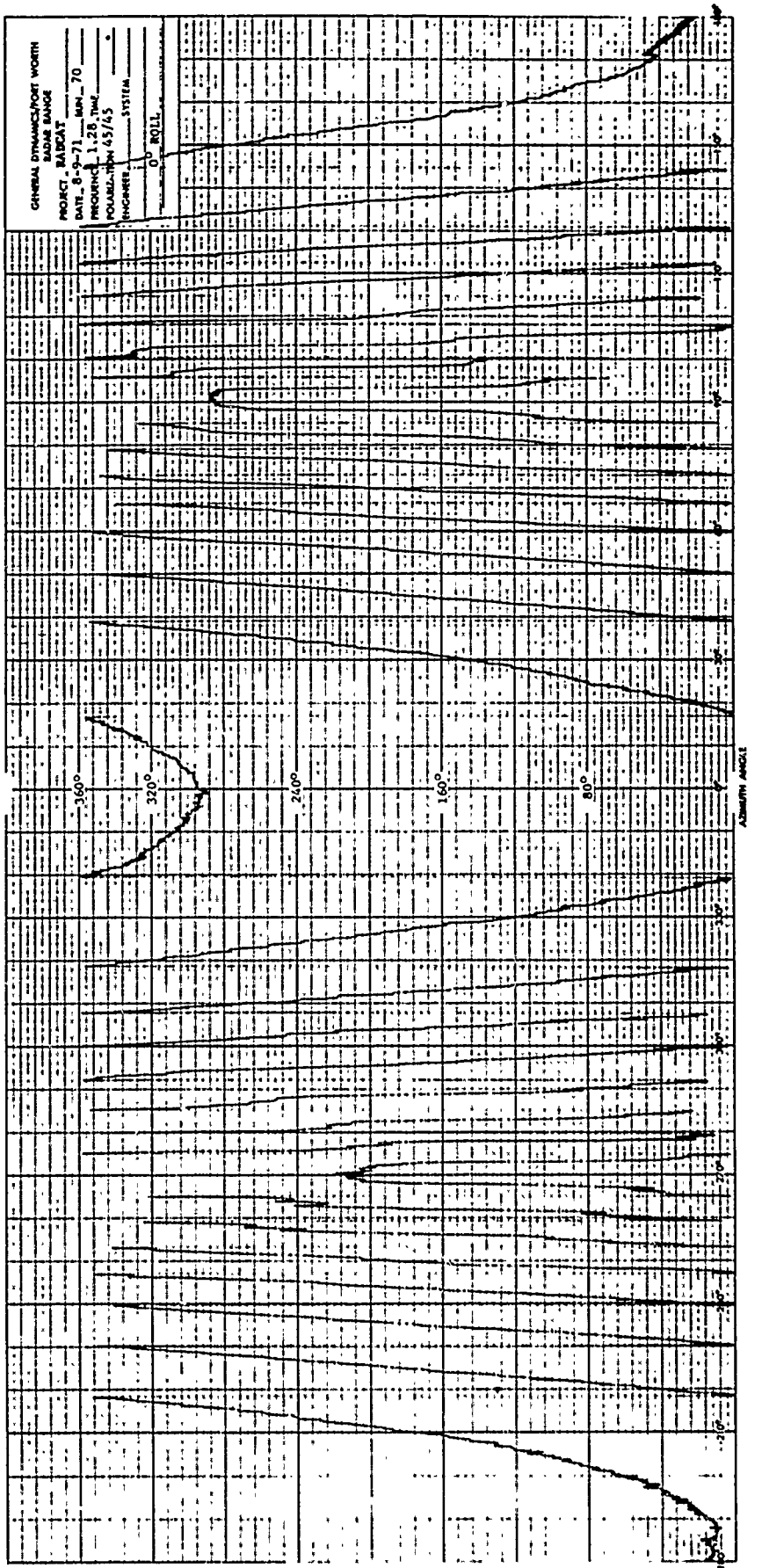

Fig. 2-7 VEHICLE 002 PHASE RESPONSE; L-BAND, $\pi/4$ $\pi/4$ POLARIZATION, 0-DEGREE ROLL

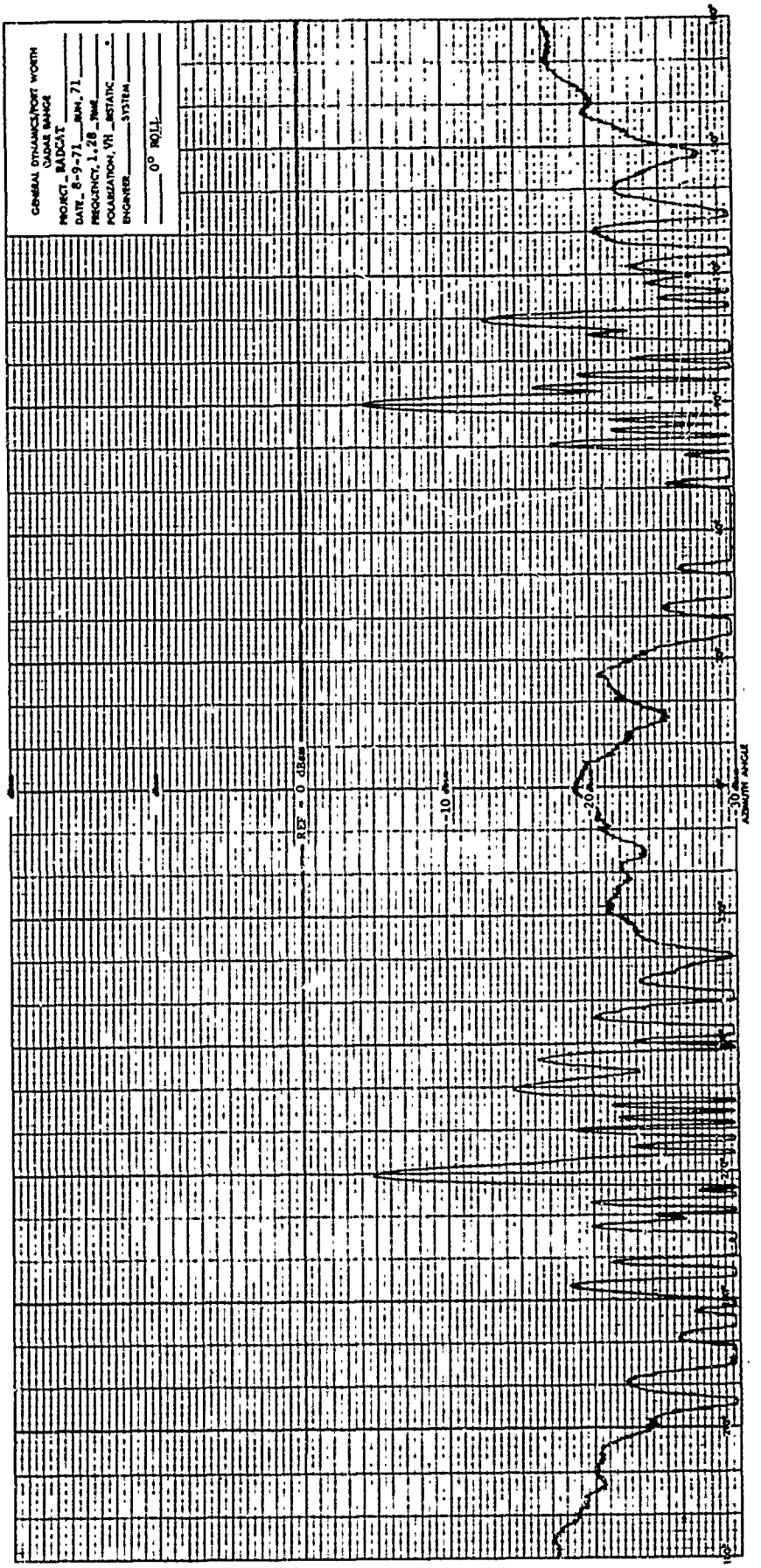

Fig. 2-8 VEHICLE 002 AMPLITUDE RESPONSE; L-BAND, VH POLARIZATION, 0-DEGREE ROLL

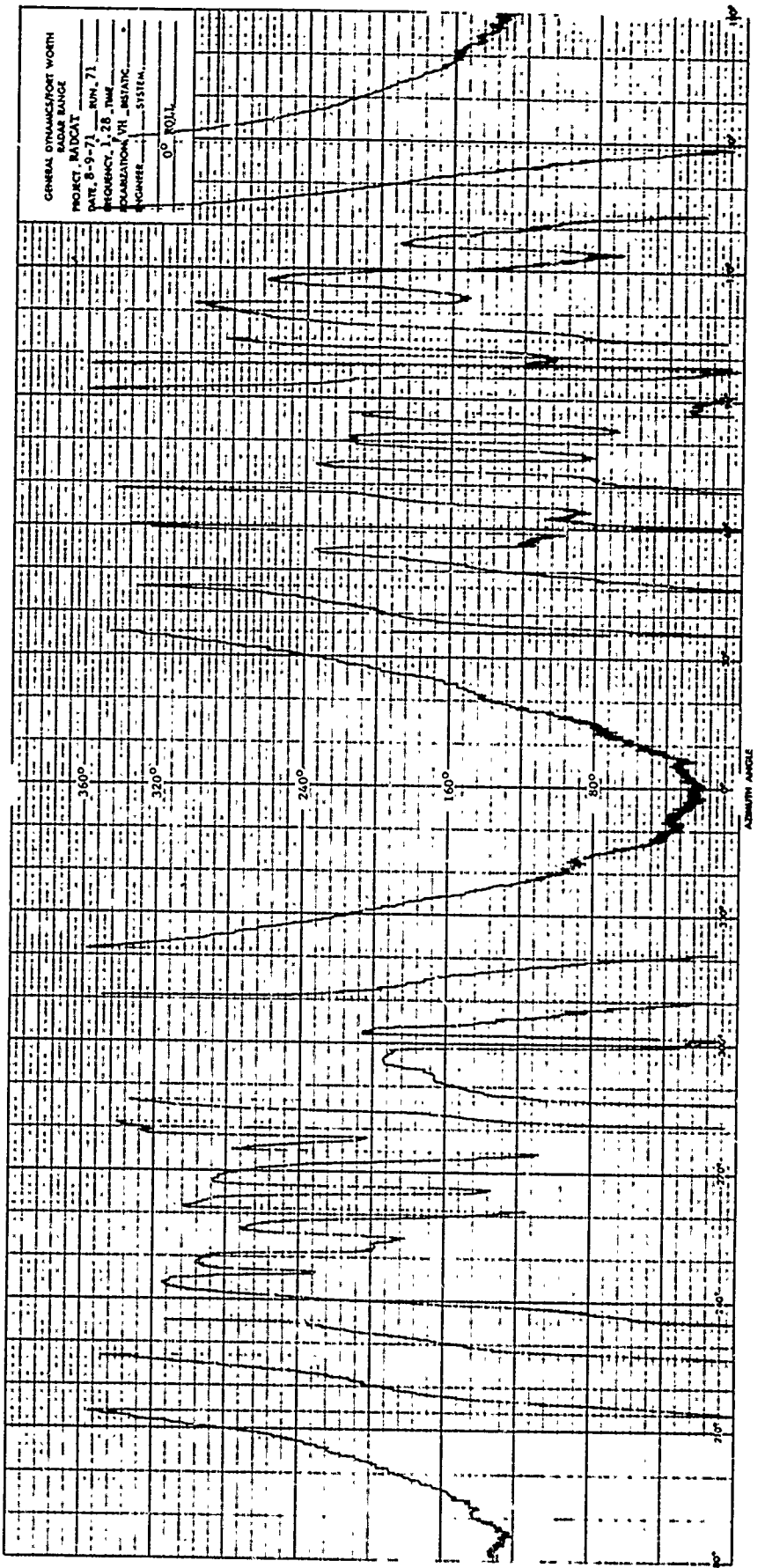

Fig. 2-9 VEHICLE 002 PHASE RESPONSE; L-BAND, VH POLARIZATION, 0-DEGREE ROLL

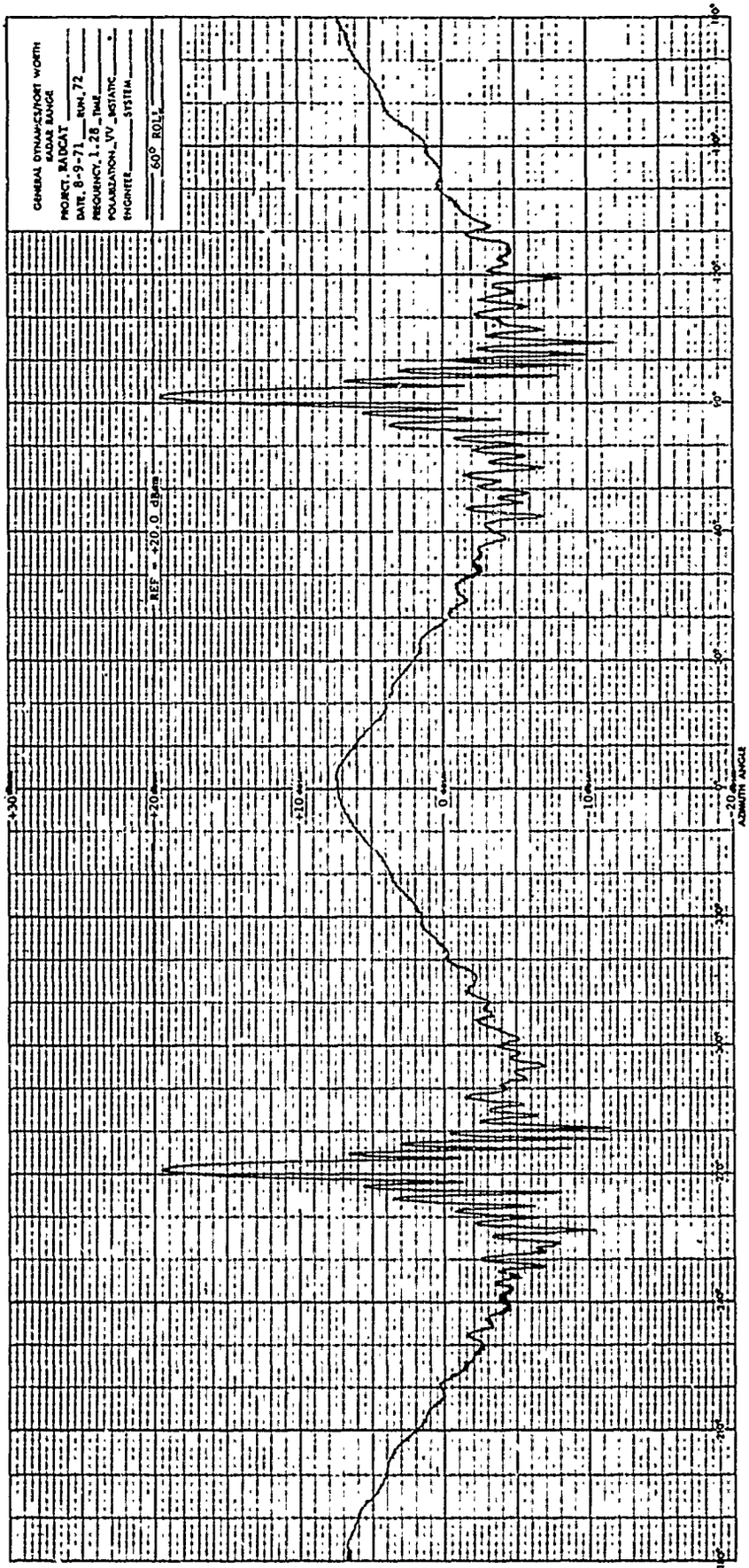

Fig. 2-10 VEHICLE 002 AMPLITUDE RESPONSE; L-BAND, VV POLARIZATION, 60-DEGREE ROLL

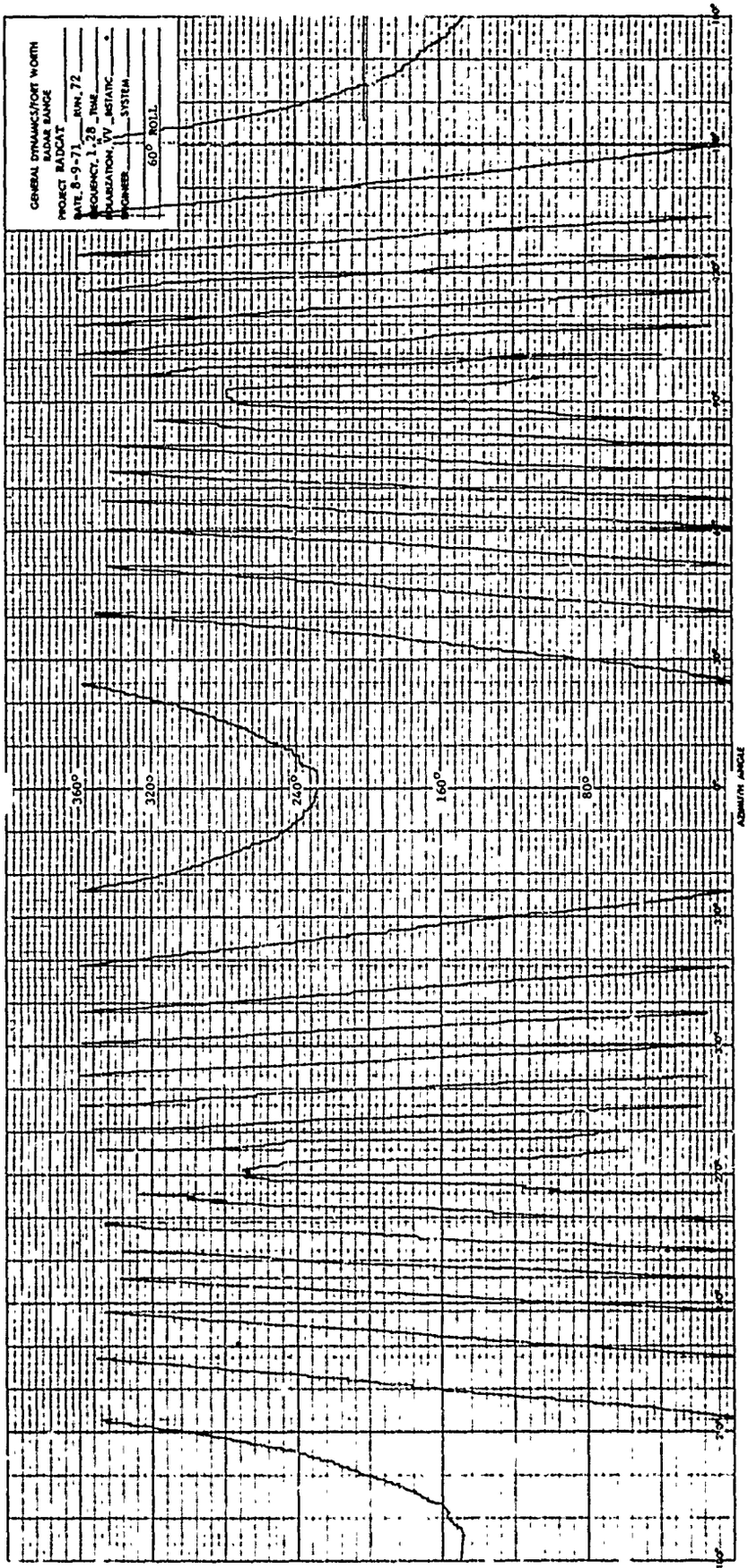

Fig. 2-11 VEHICLE 002 PHASE RESPONSE; L-BAND, VV POLARIZATION, 60-DEGREE ROLL

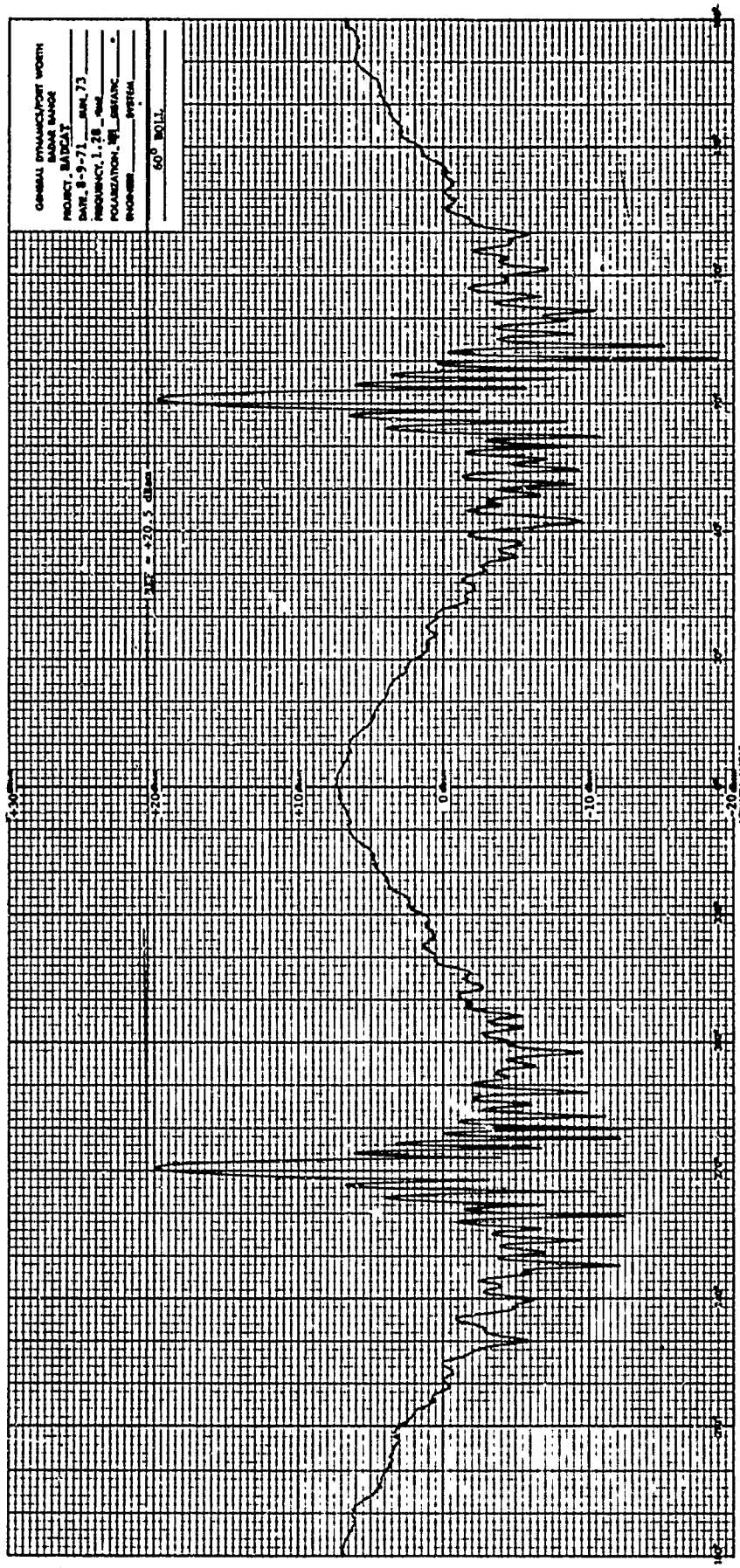

Fig. 2-12 VEHICLE 002 AMPLITUDE RESPONSE; L-BAND, HH POLARIZATION, 60-DEGREE ROLL

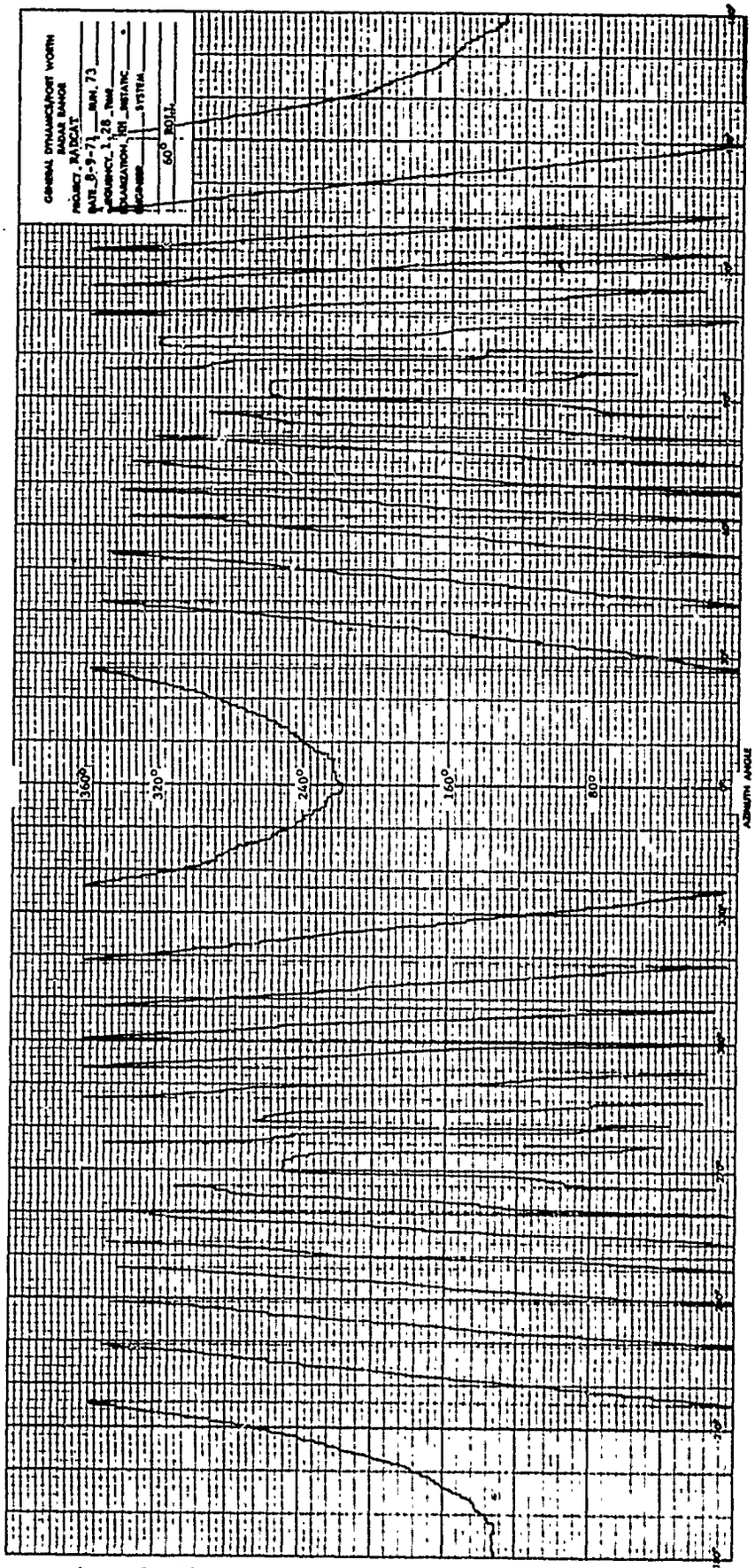

Fig. 2-13 VEHICLE 002 PHASE RESPONSE; L-BAND, HH POLARIZATION, 60-DEGREE ROLL

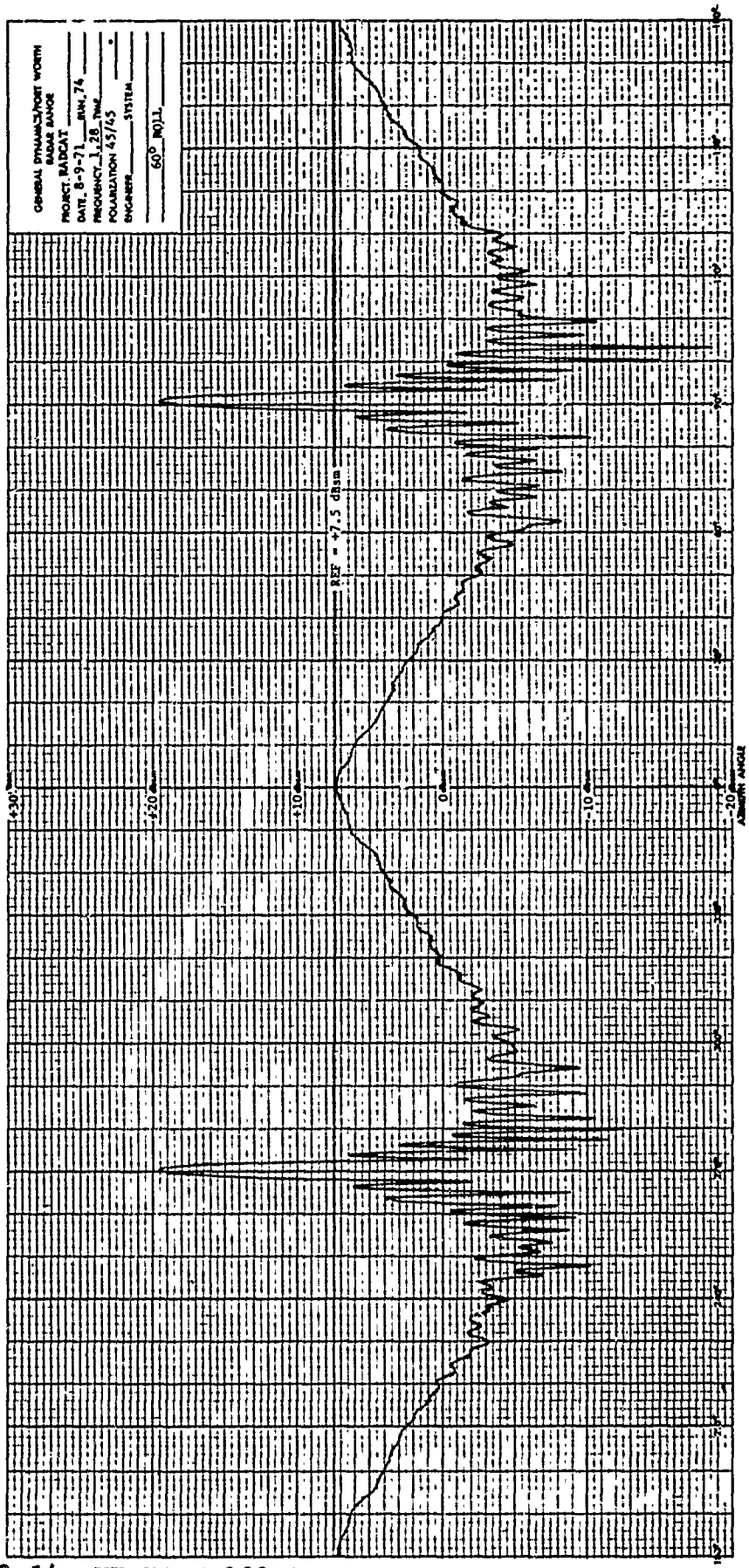

Fig. 2-14 VEHICLE 002 AMPLITUDE RESPONSE; L-BAND, $\pi/4$ $\pi/4$ POLARIZATION, 60-DEGREE ROLL

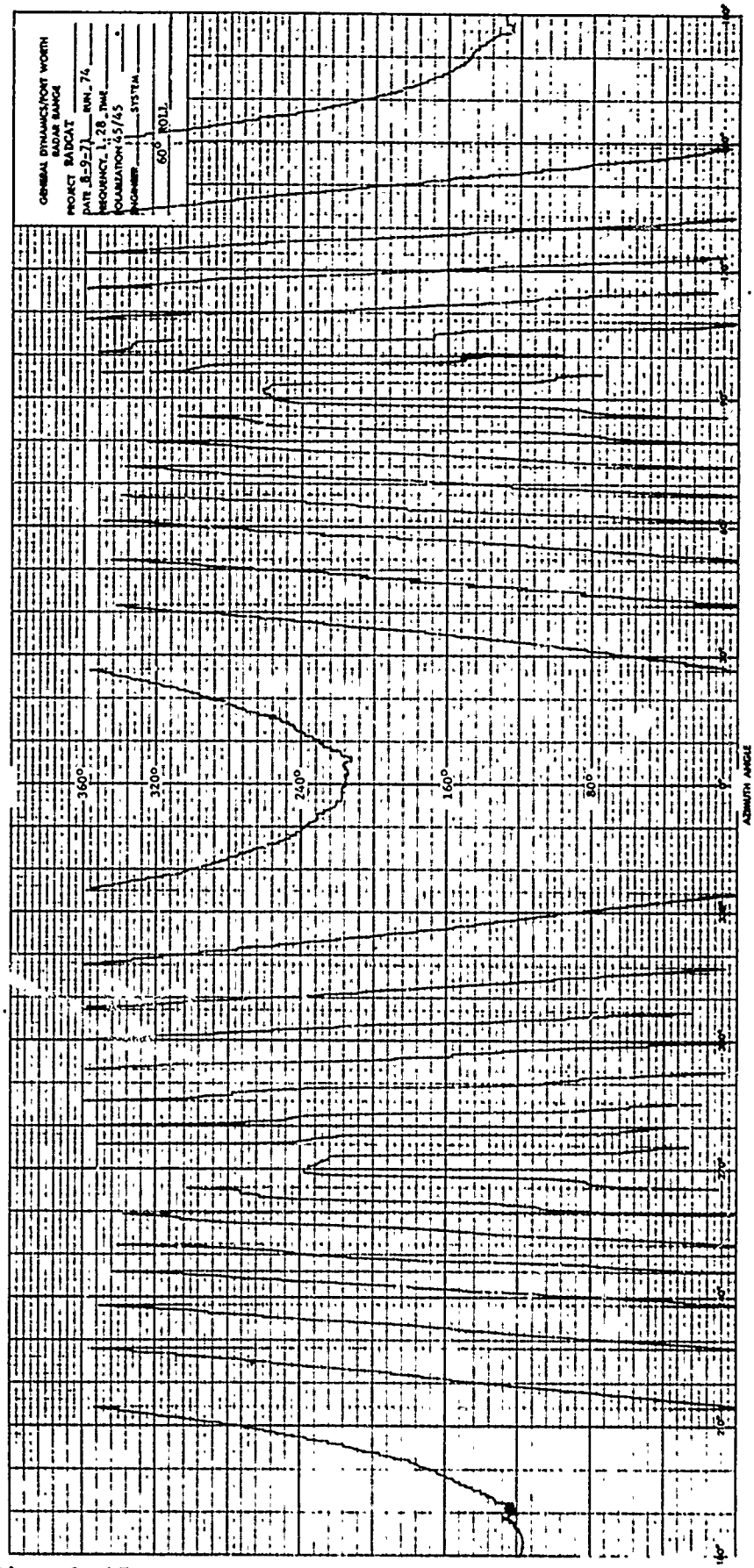

Fig. 2-15 VEHICLE 002 PHASE RESPONSE; L-BAND, $\pi/4$ $\pi/4$ POLARIZATION, 60-DEGREE ROLL

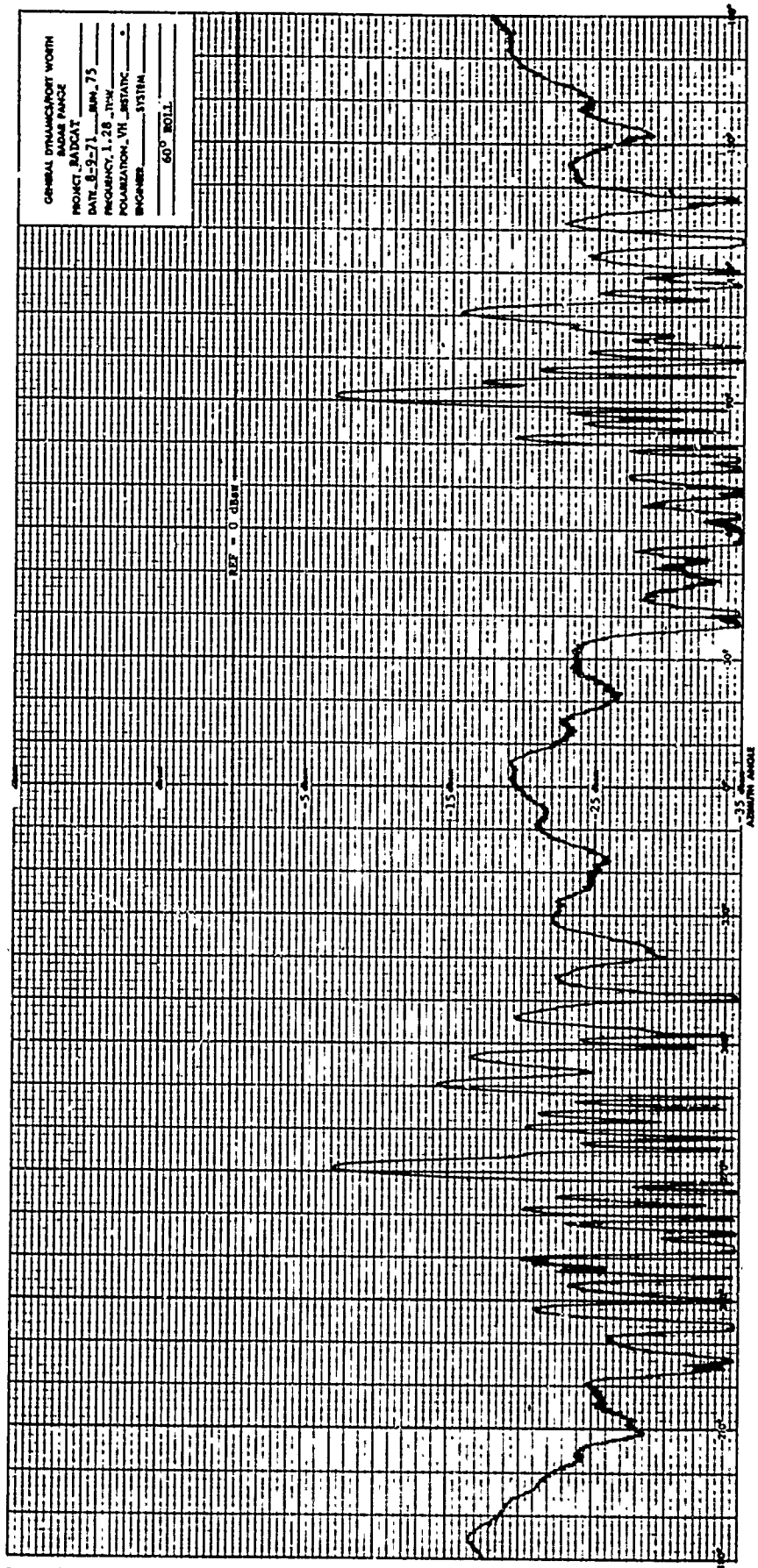

Fig. 2-16 VEHICLE 002 AMPLITUDE RESPONSE; L-BAND, VH POLARIZATION, 60-DEGREE ROLL

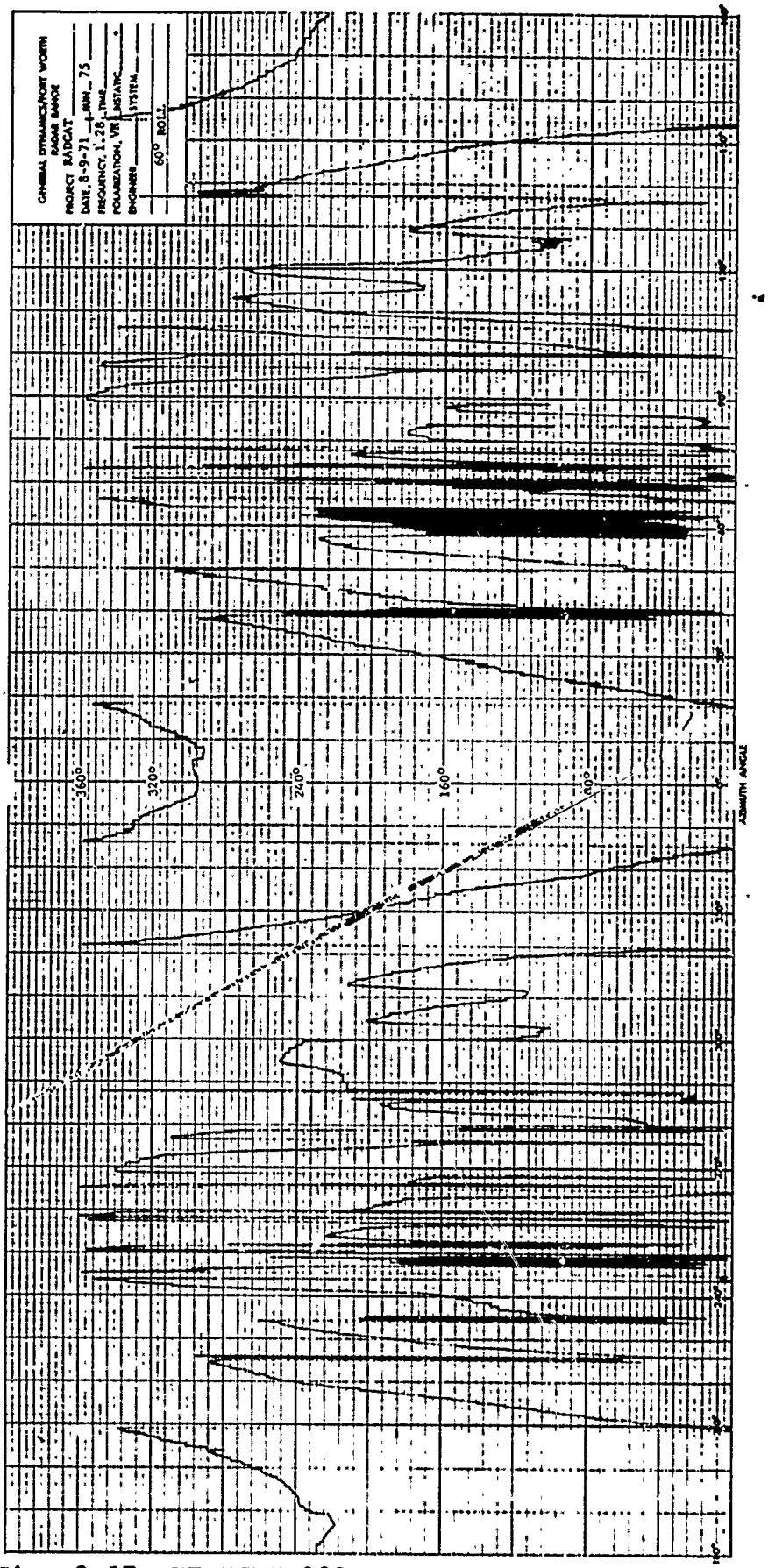

Fig. 2-17 VEHICLE 002 PHASE RESPONSE; L-BAND, VH POLARIZATION, 60-DEGREE ROLL

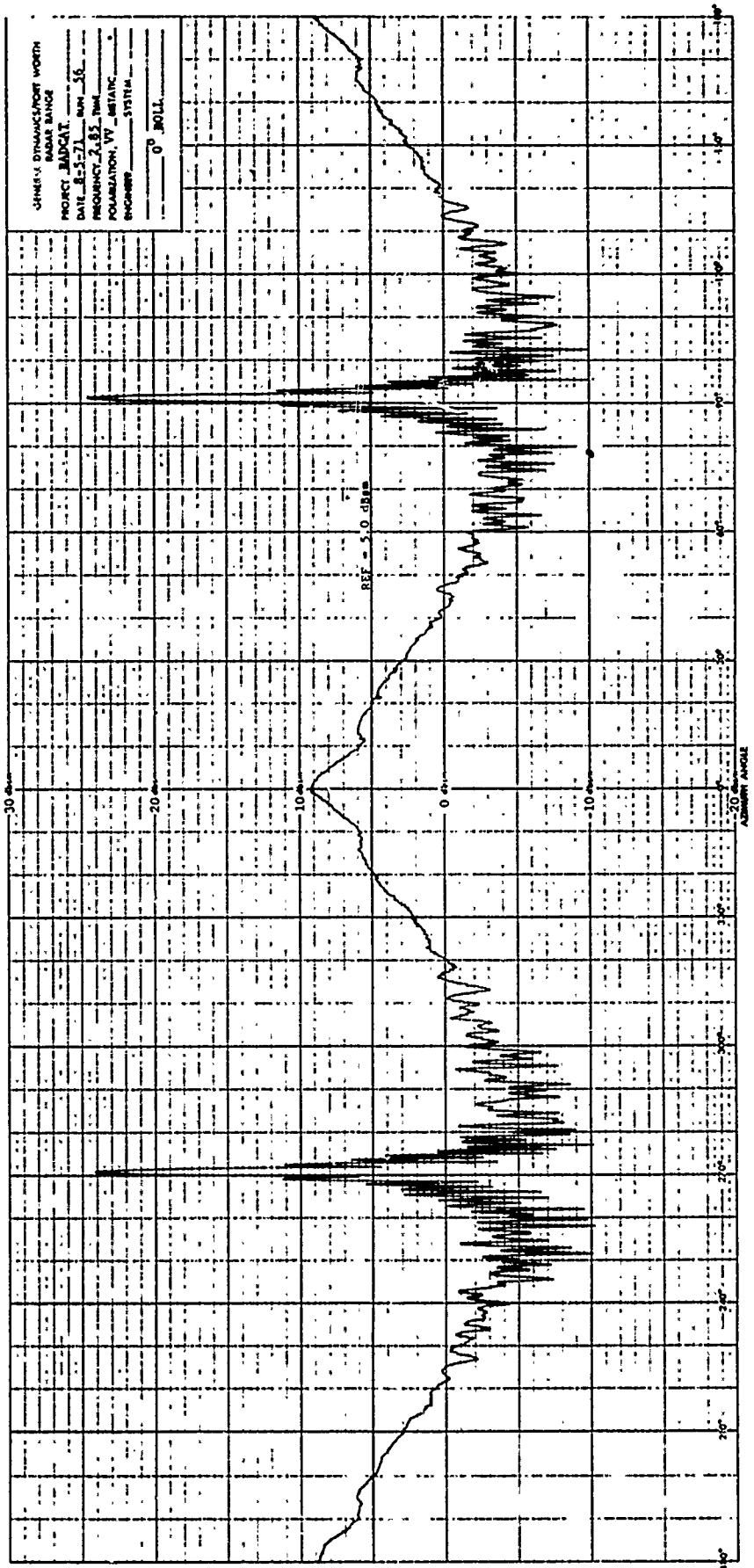

Fig. 2-18 VEHICLE 002 AMPLITUDE RESPONSE; S-BAND, VV POLARIZATION, 0-DEGREE ROLL

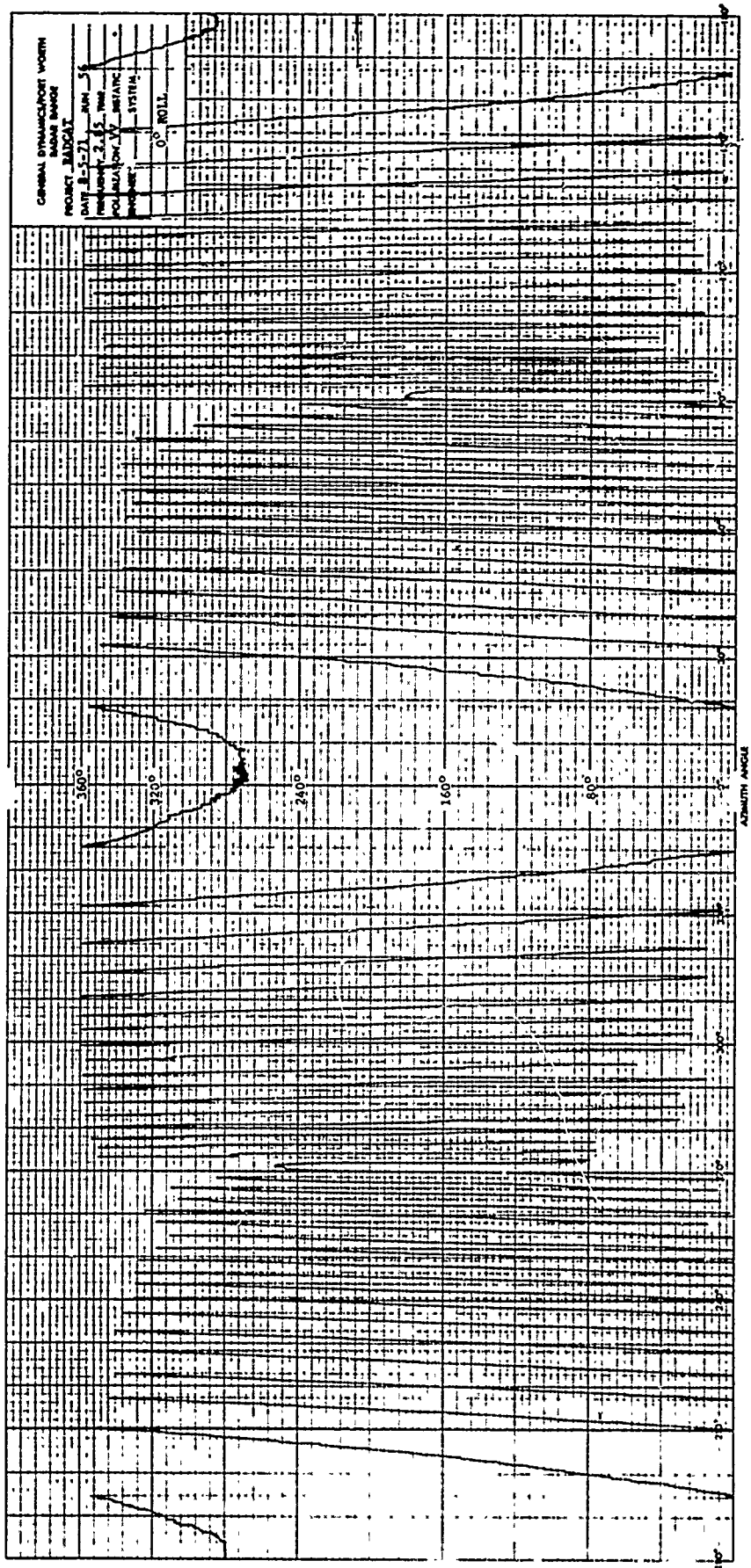

Fig. 2-19 VEHICLE 002 PHASE RESPONSE; S-BAND, VV POLARIZATION, 0-DEGREE ROLL

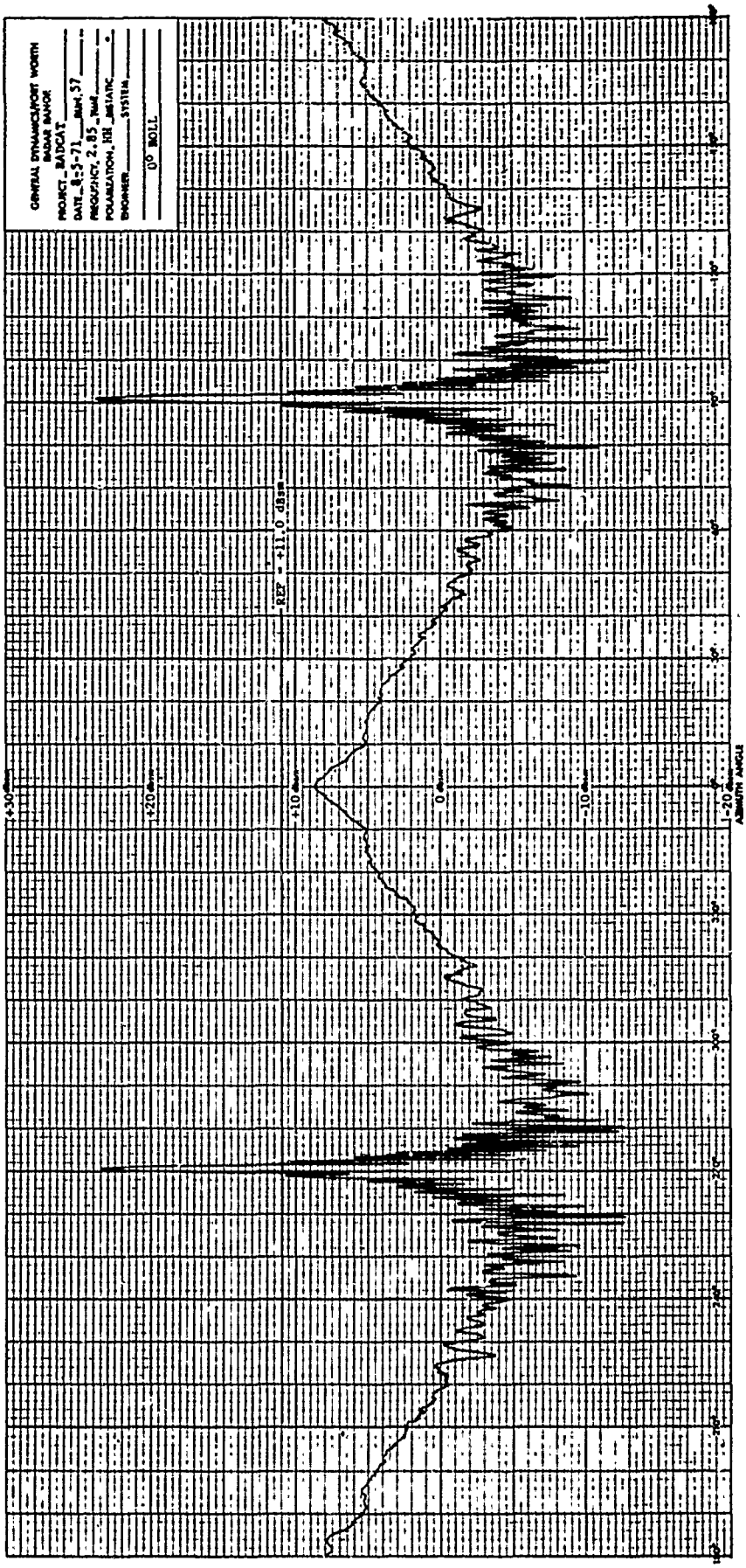

Fig. 2-20 VEHICLE 002 AMPLITUDE RESPONSE; S-BAND, HH POLARIZATION, 0-DEGREE ROLL

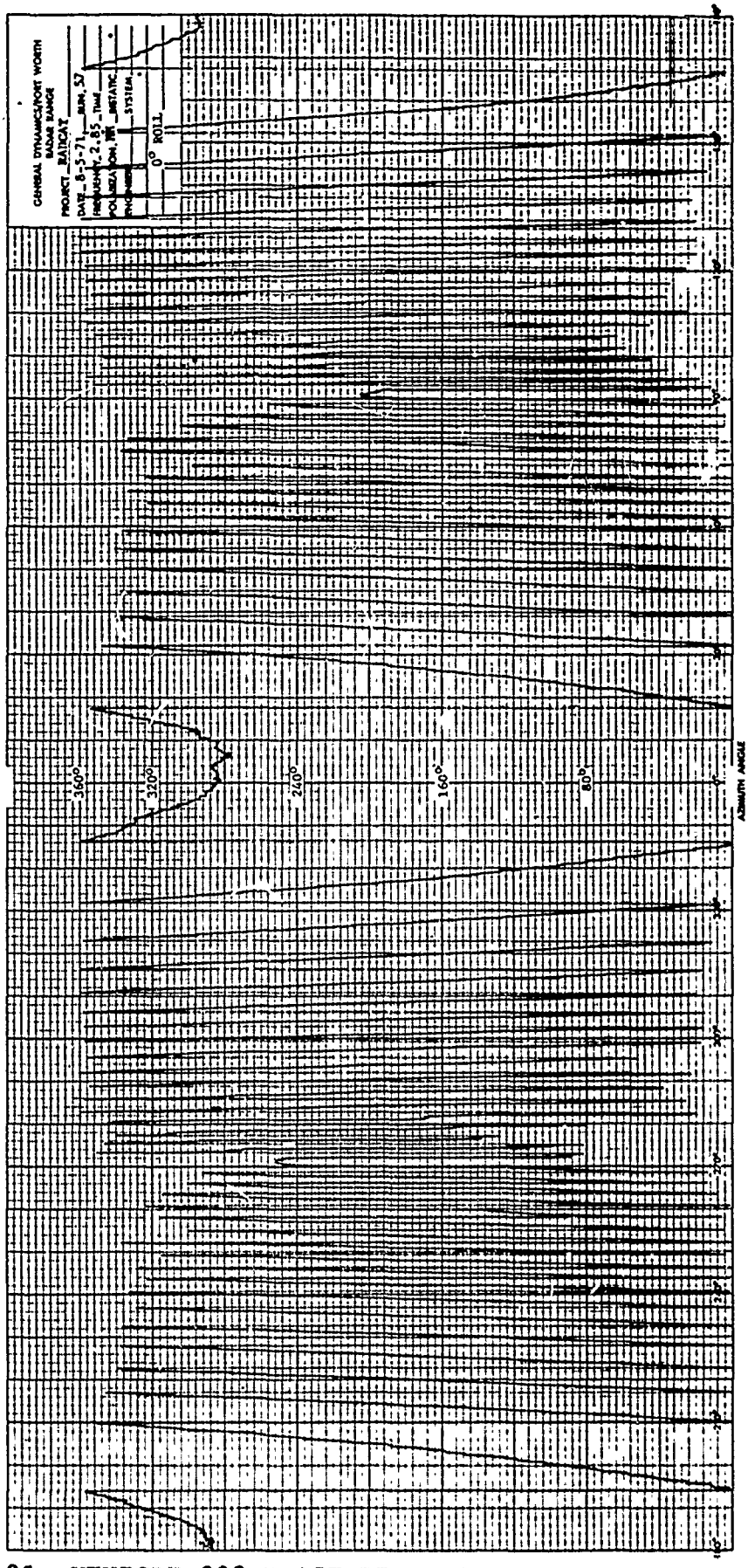

Fig. 2-21 VEHICLE 002 PHASE RESPONSE; S-BAND, HH POLARIZATION, 0-DEGREE ROLL

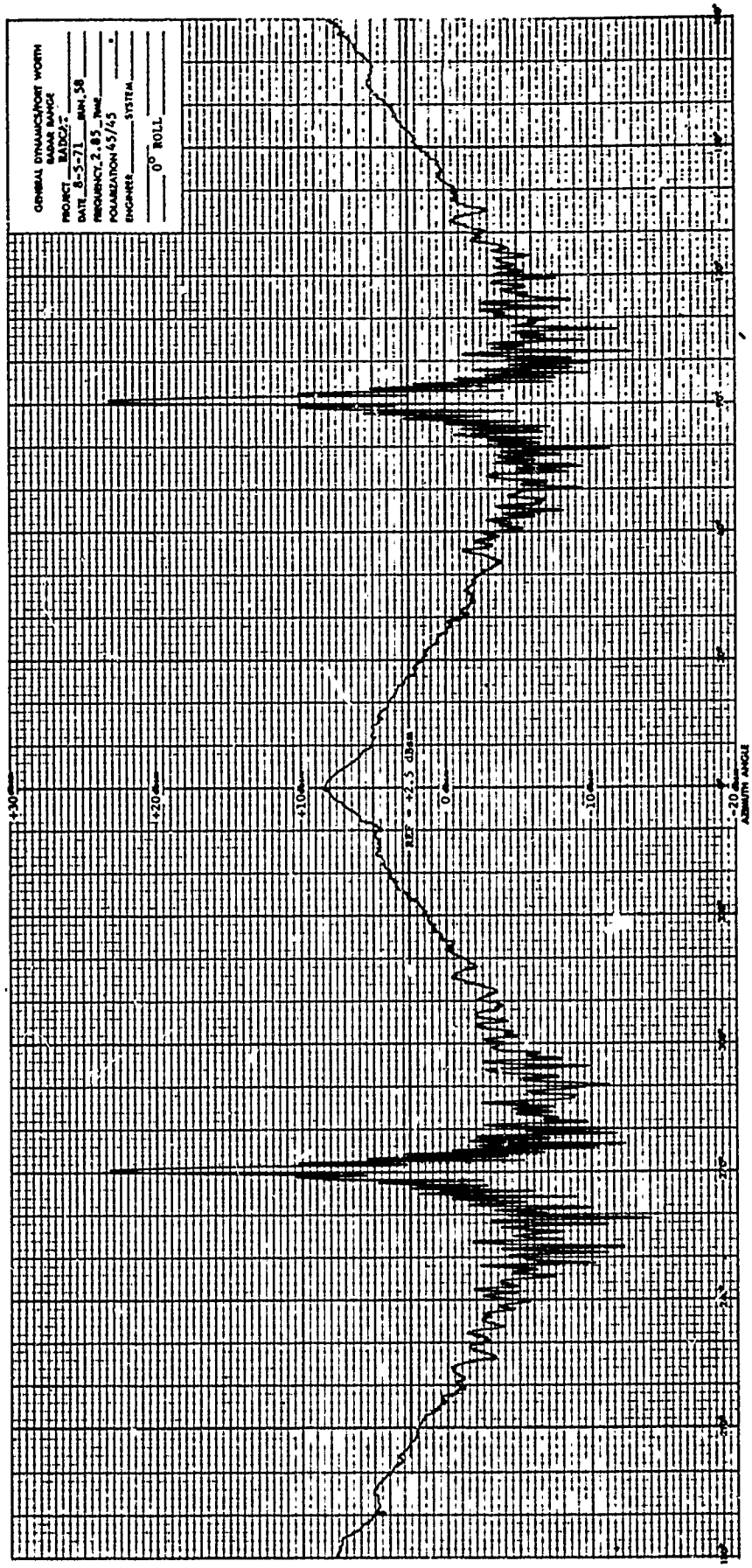

Fig. 2-22 VEHICLE 002 AMPLITUDE RESPONSE; S-BAND, $\pi/4$ $\pi/4$ POLARIZATION, 0-DEGREE ROLL

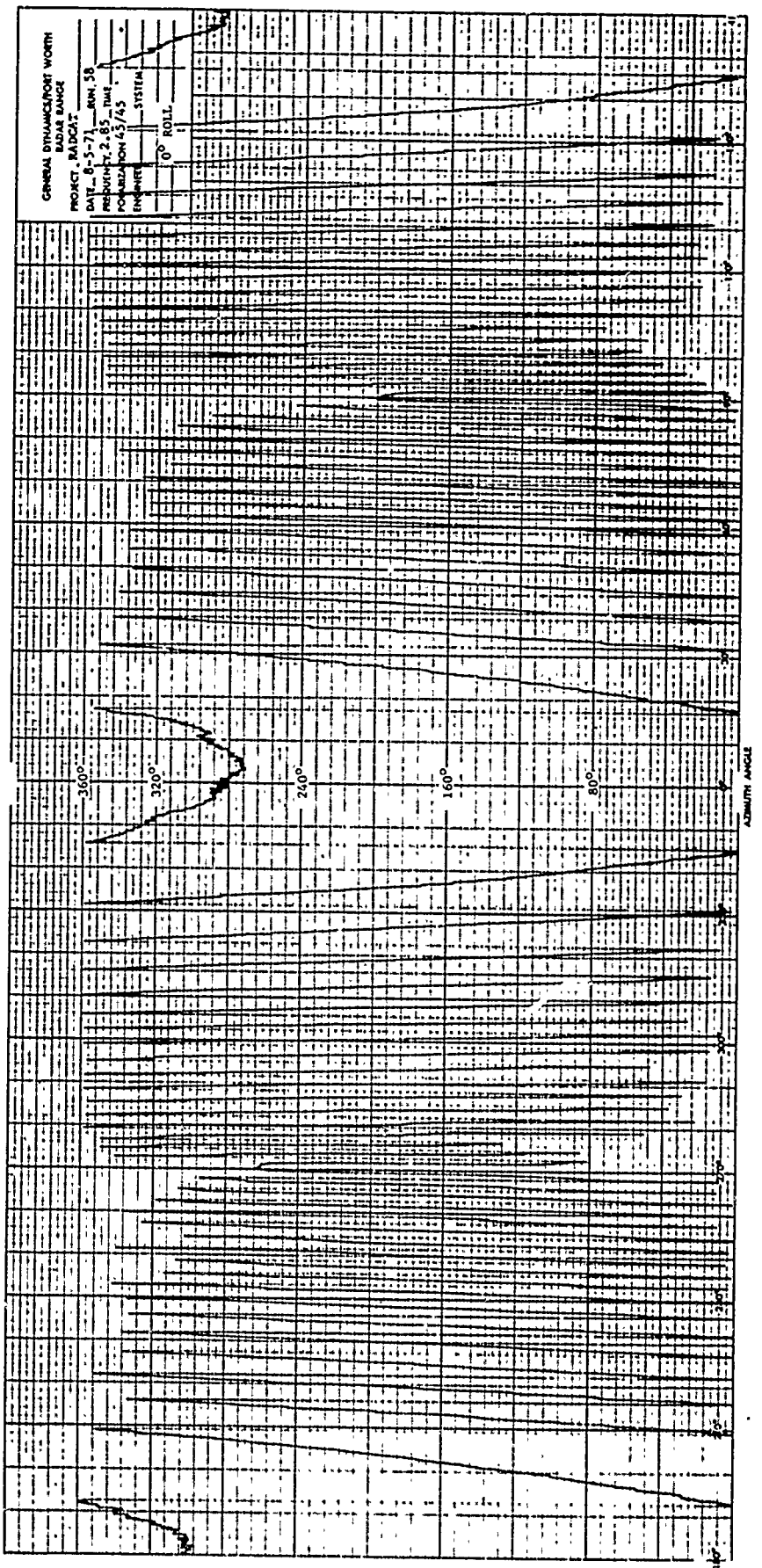

Fig. 2-23 VEHICLE 002 PHASE RESPONSE, S-BAND, $\pi/4$ $\pi/4$ POLARIZATION, 0-DEGREE ROLL

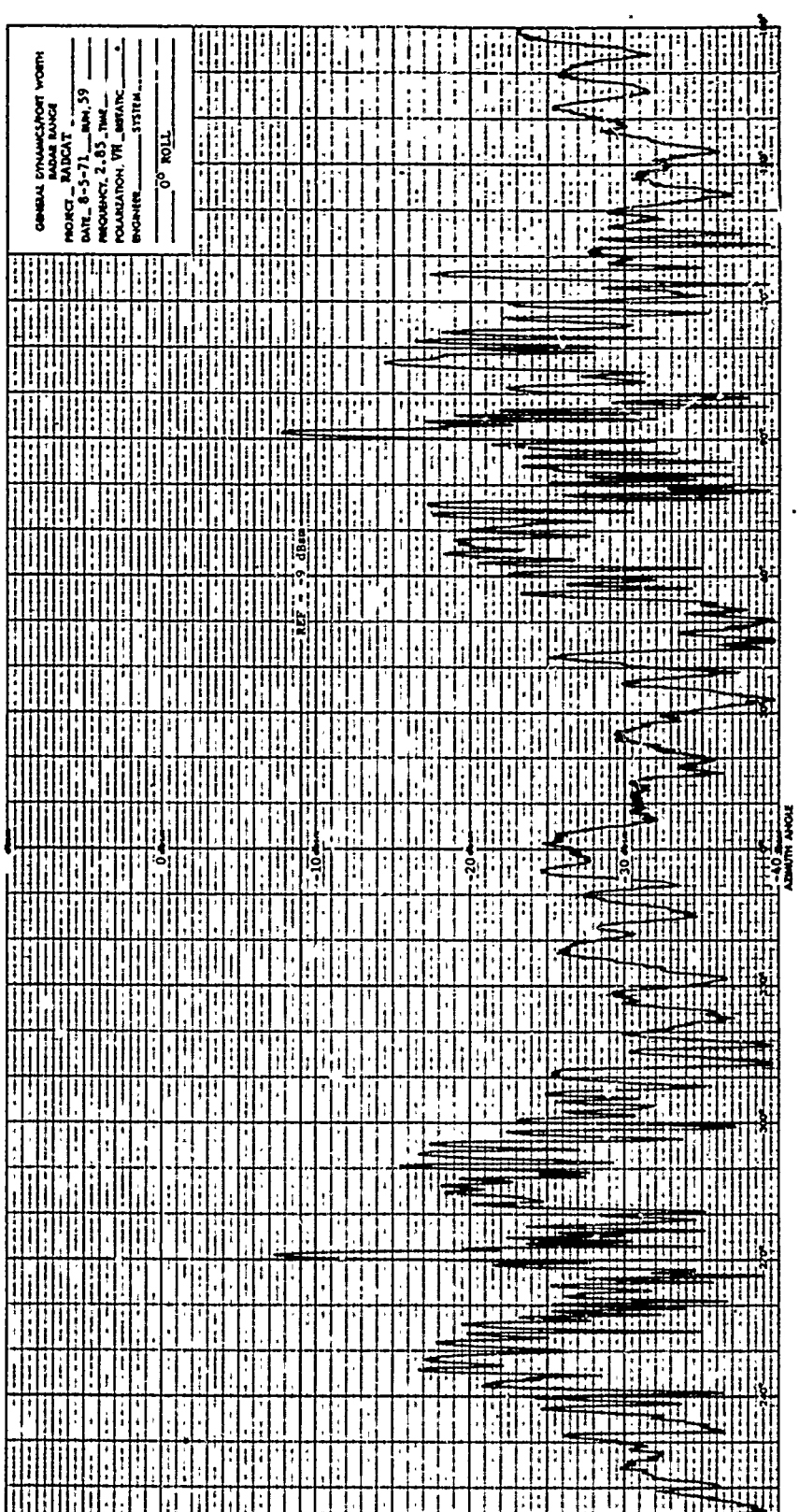

Fig. 2-24 VEHICLE 002 AMPLITUDE RESPONSE; S-BAND, VH POLARIZATION, 0-DEGREE ROLL

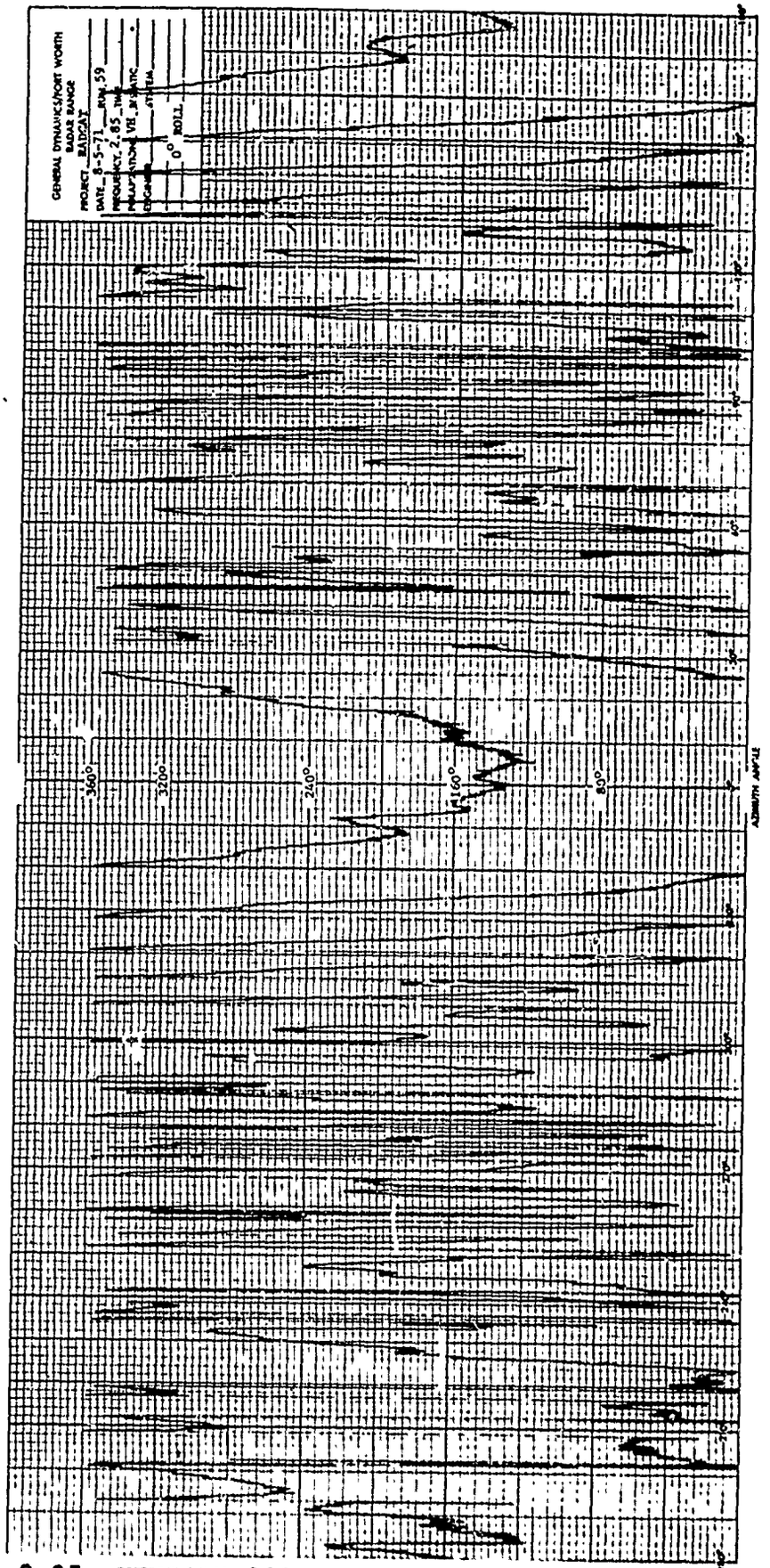

Fig. 2-25 VEHICLE 002 PHASE RESPONSE; S-BAND, VH POLARIZATION, 0-DEGREE ROLL

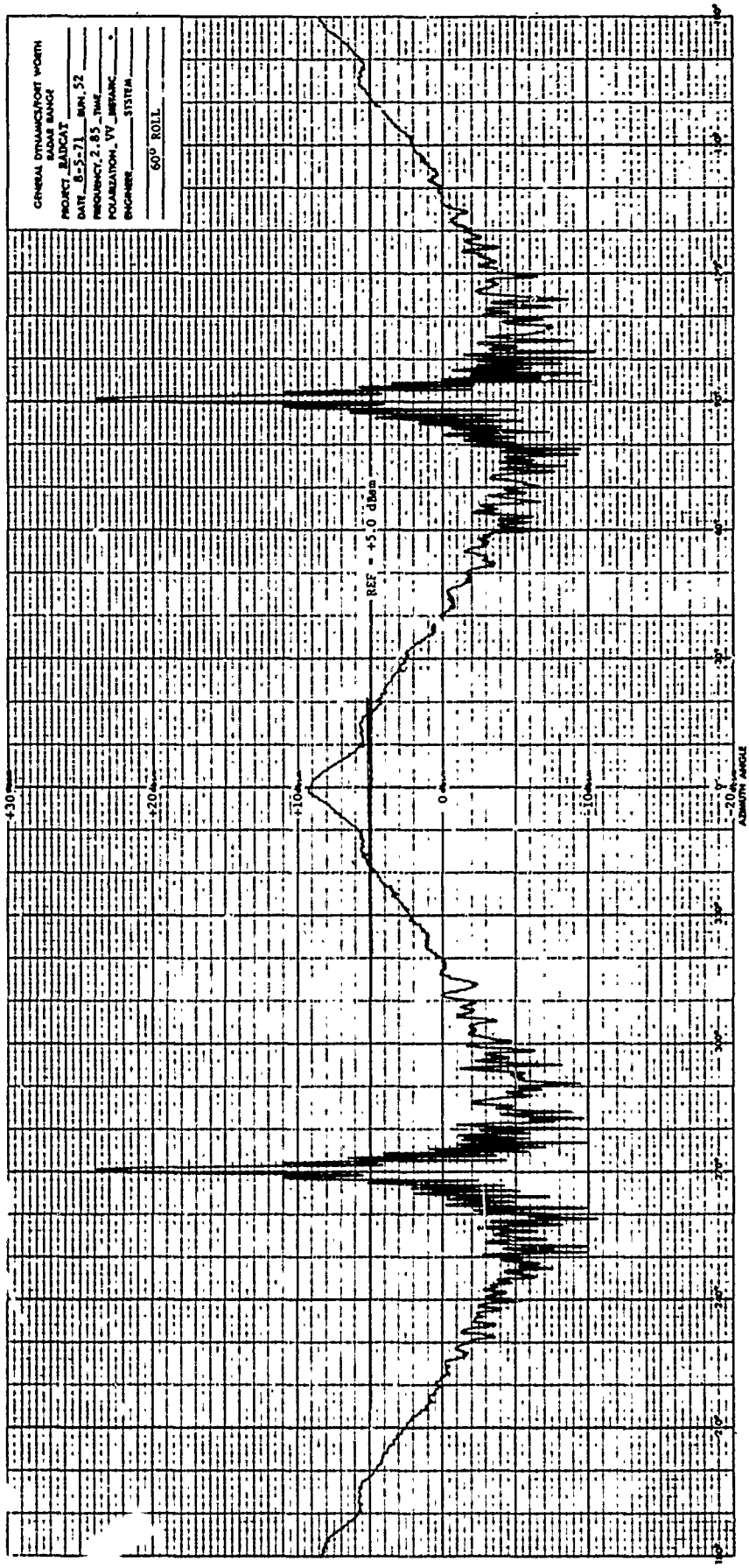

Fig. 2-26 VEHICLE 002 AMPLITUDE RESPONSE; S-BAND, VV POLARIZATION, 60-DEGREE ROLL

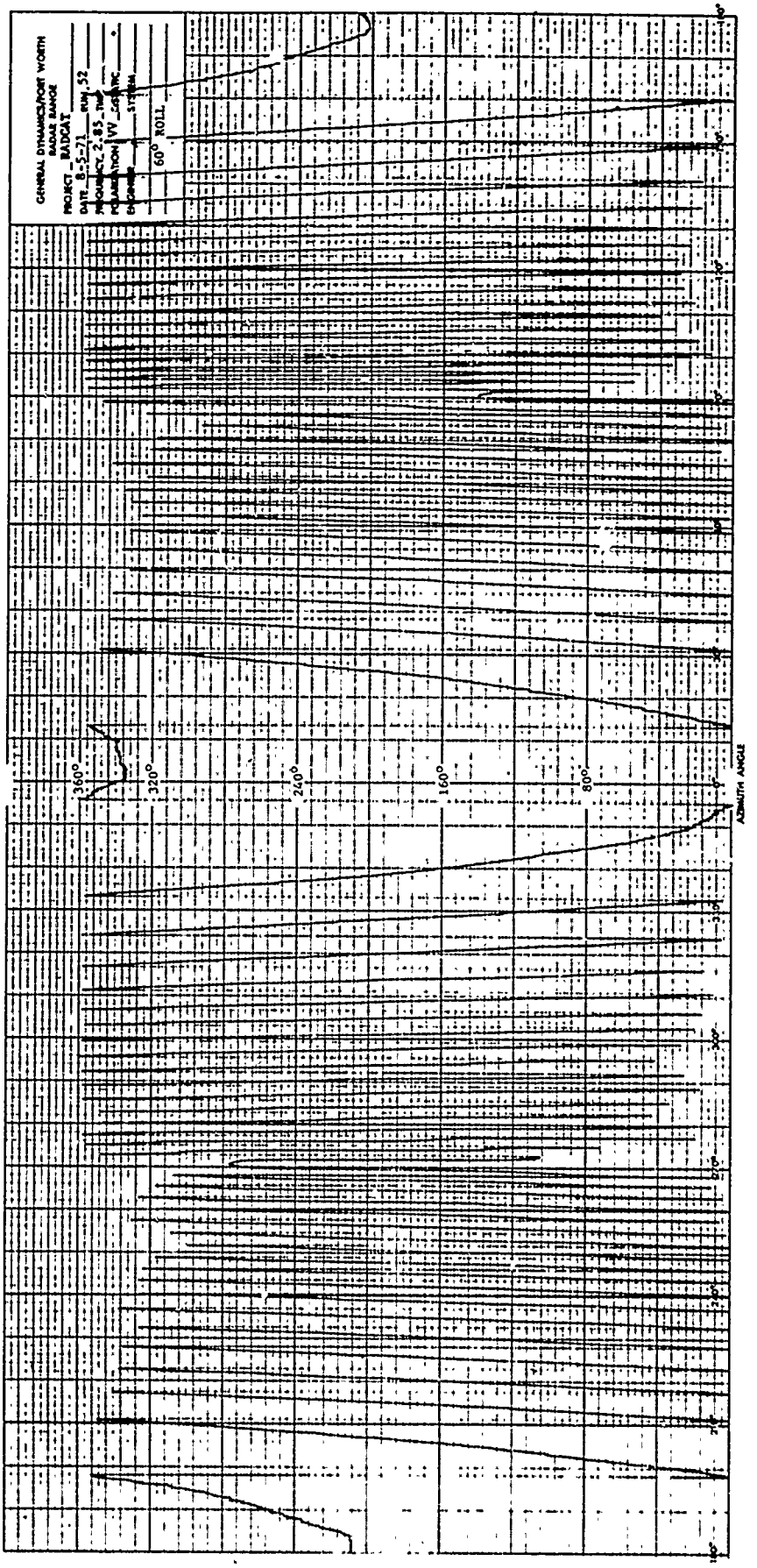

Fig. 2-27 VEHICLE 002 PHASE RESPONSE; S-BAND, VV POLARIZATION, 60-DEGREE ROLL

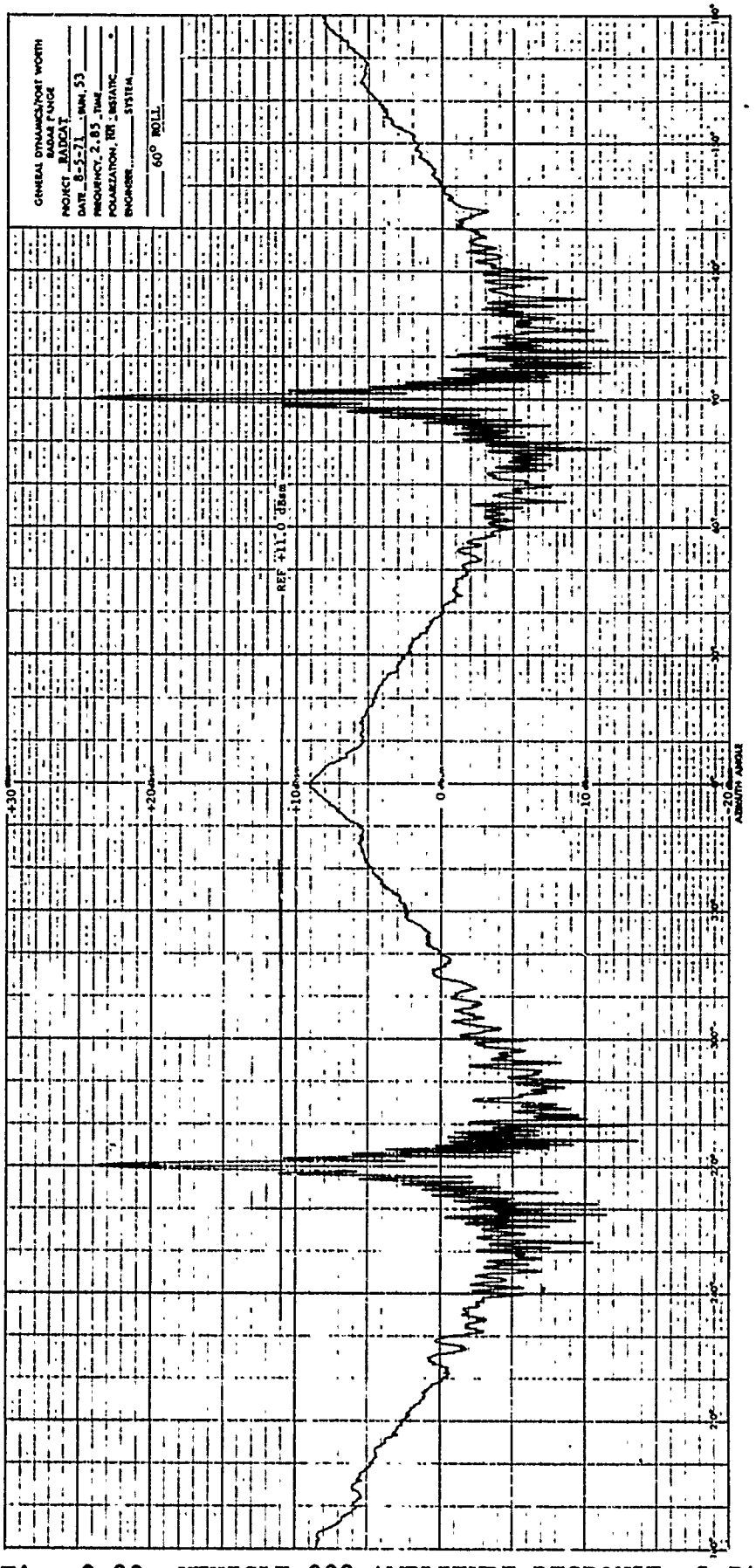

Fig. 2-28 VEHICLE 002 AMPLITUDE RESPONSE; S-BAND, HH POLARIZATION, 60-DEGREE ROLL

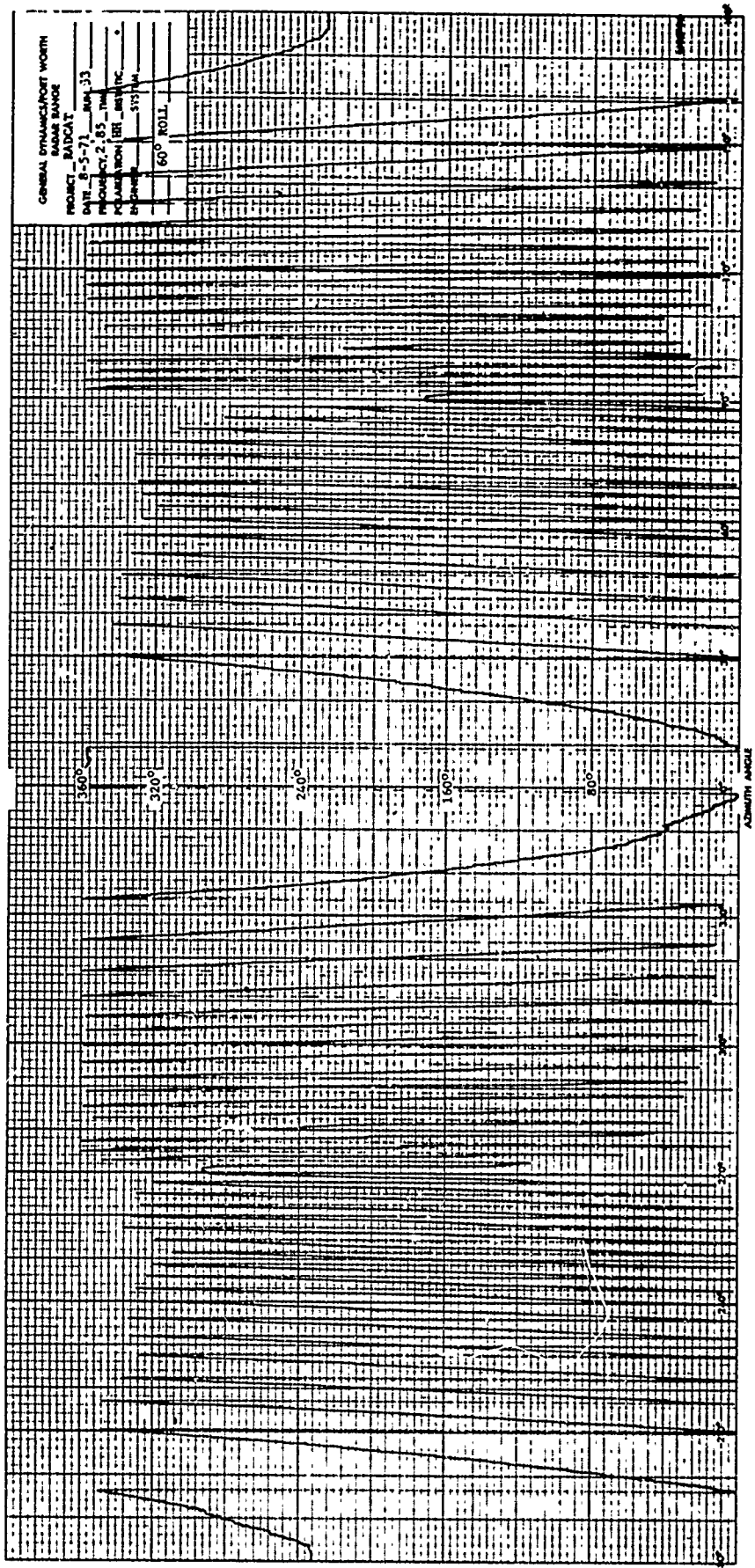

Fig. 2-29 VEHICLE 002 PHASE RESPONSE; S-BAND, HH POLARIZATION, 60-DEGREE ROLL

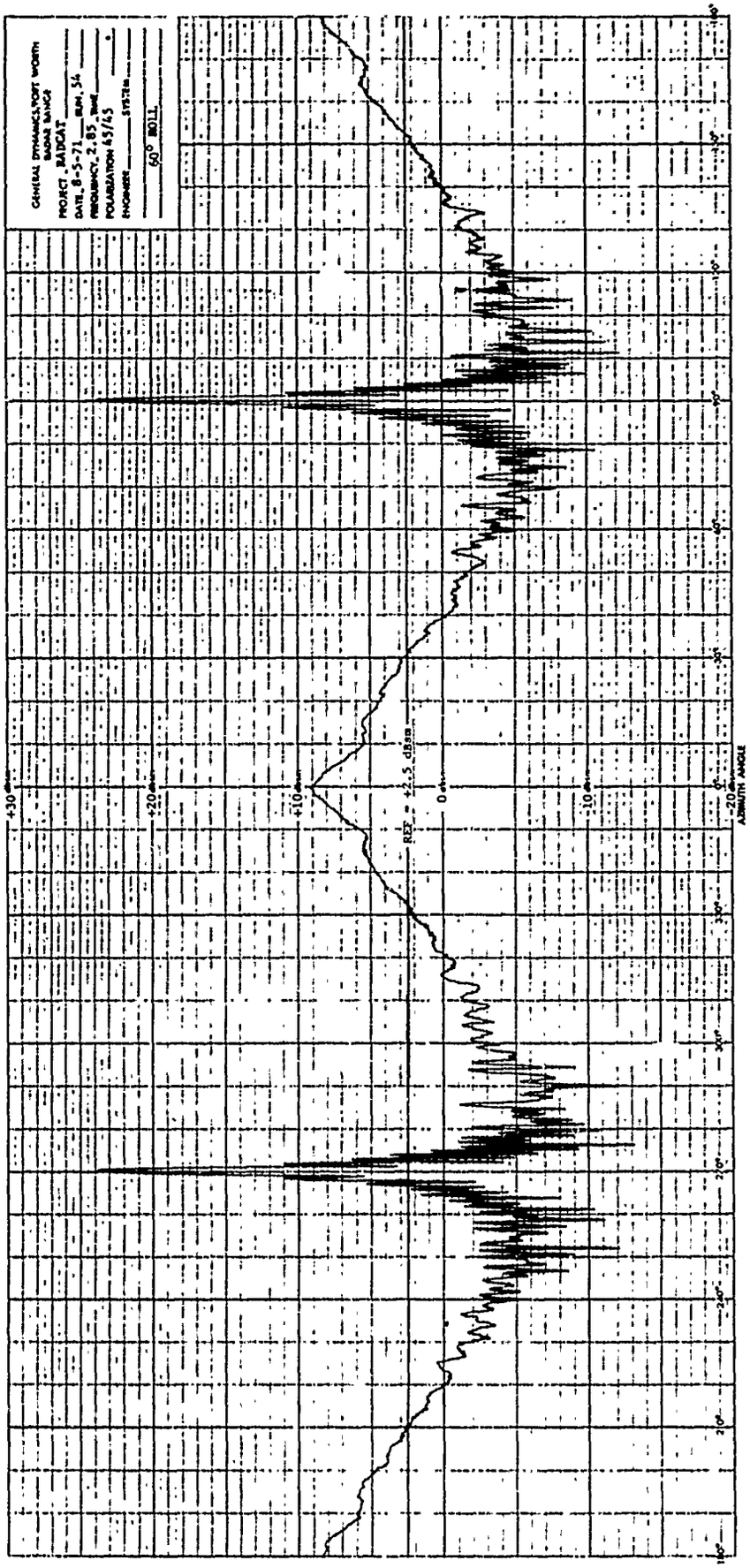

Fig. 2-30 VEHICLE 002 AMPLITUDE RESPONSE; S-BAND, $\pi/4$ $\pi/4$ POLARIZATION, 60-DEGREE ROLL

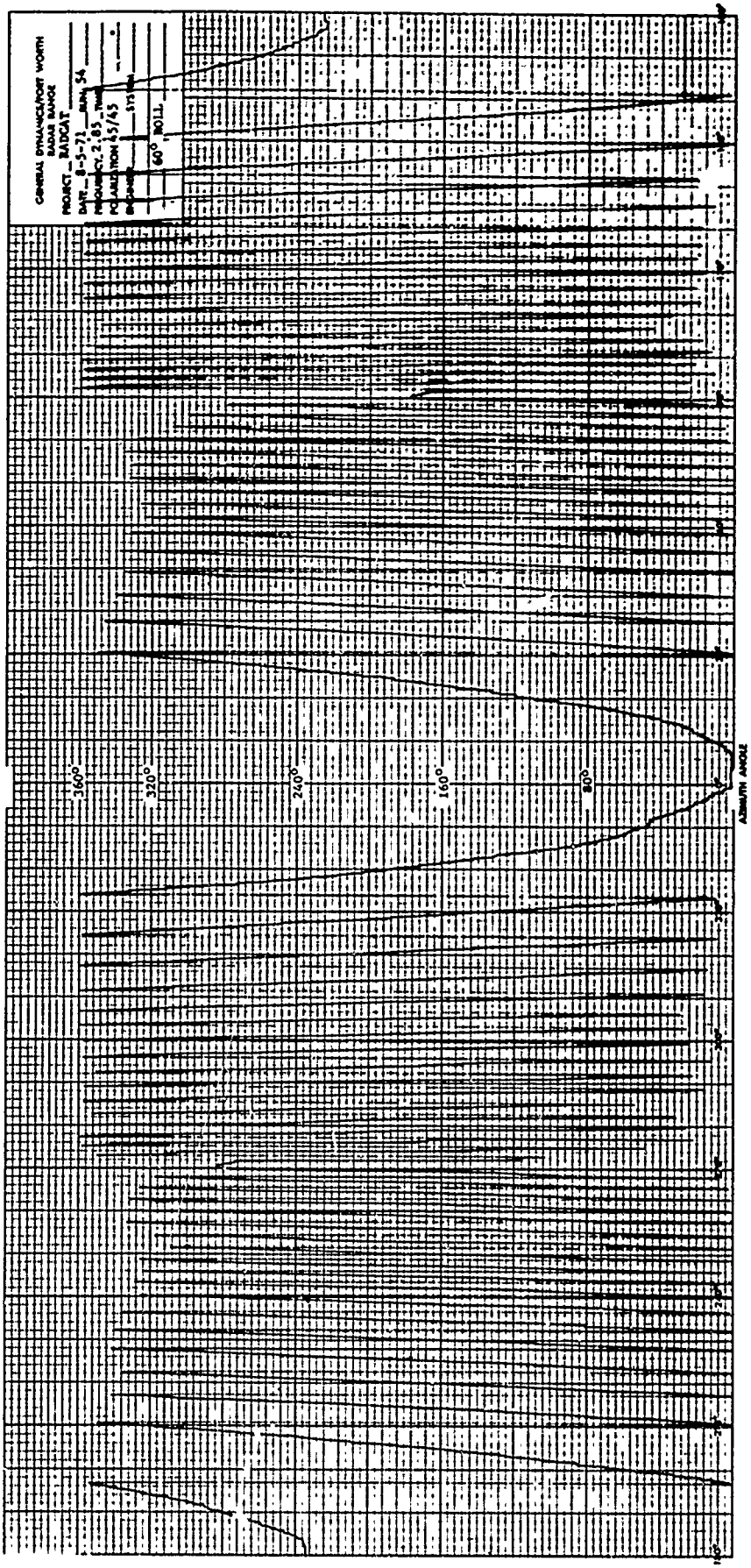

Fig. 2-31 VEHICLE 002 PHASE RESPONSE; S-BAND, $\pi/4$ $\pi/4$ POLARIZATION, 60-DEGREE ROLL

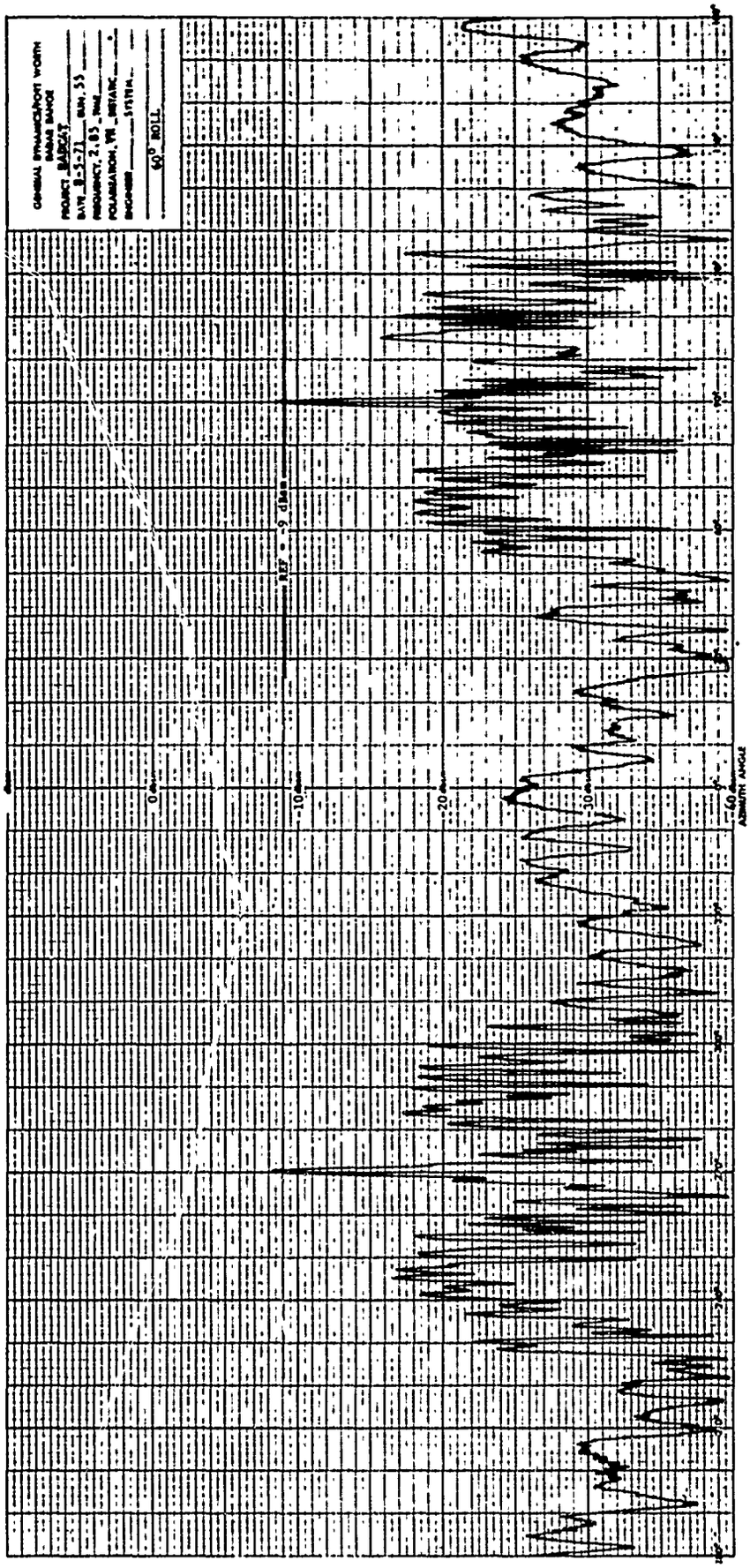

Fig. 2-32 VEHICLE 002 AMPLITUDE RESPONSE; S-BAND, VH POLARIZATION, 60-DEGREE ROLL

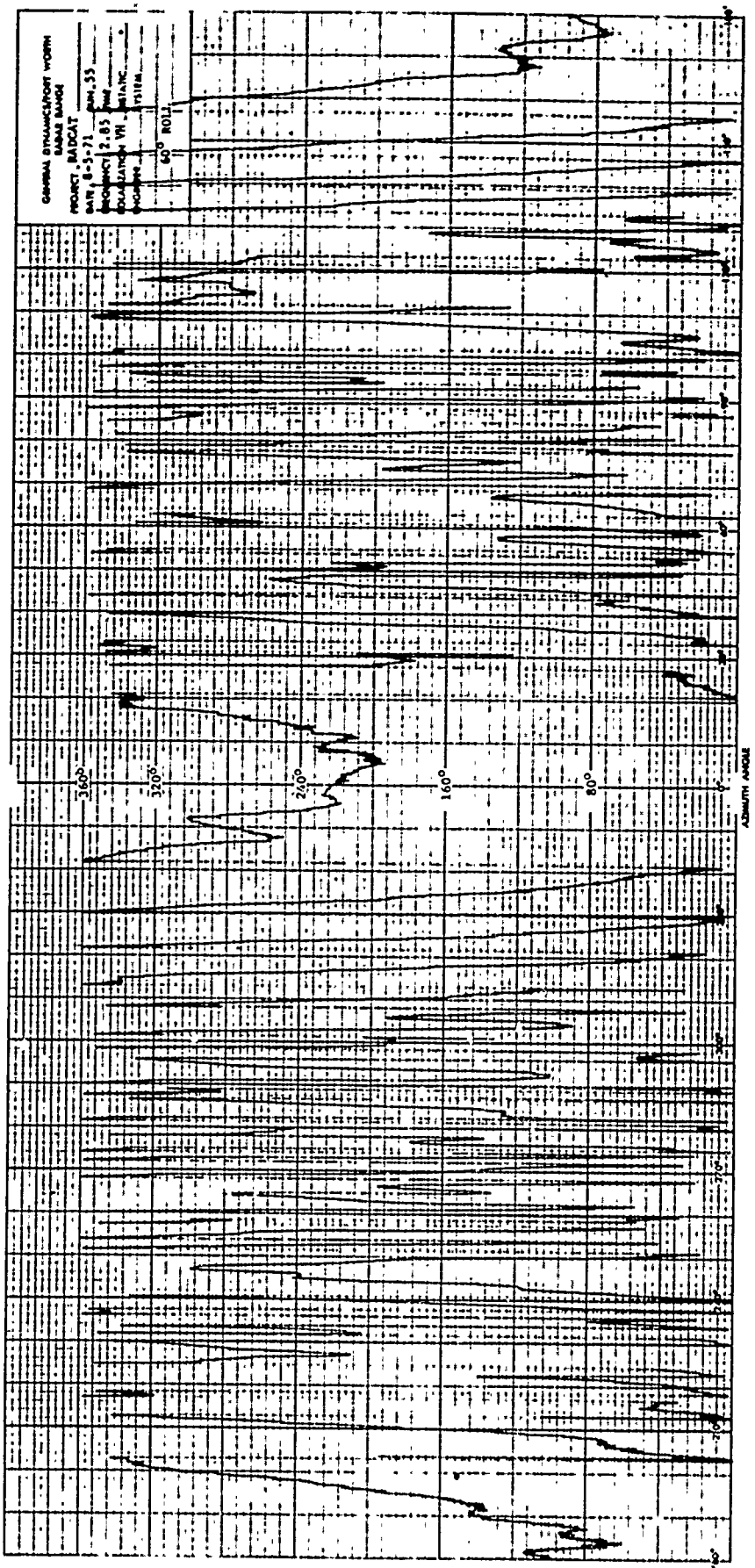

Fig. 2-33 VEHICLE 002 PHASE RESPONSE, S-BAND, VH POLARIZATION, 60-DEGREE ROLL

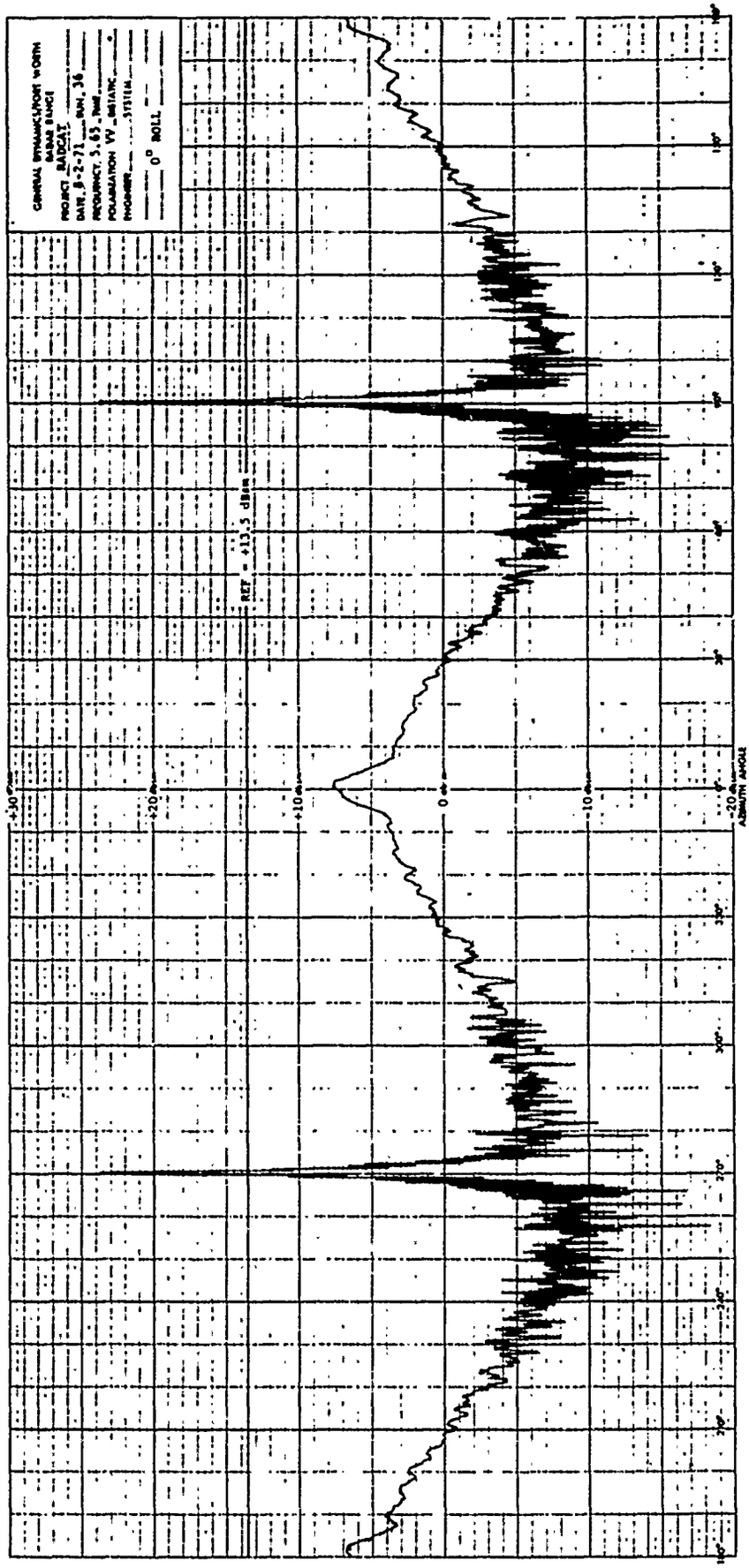

Fig. 2-34 VEHICLE 002 AMPLITUDE RESPONSE; C-BAND, VV POLARIZATION, 0-DEGREE ROLL

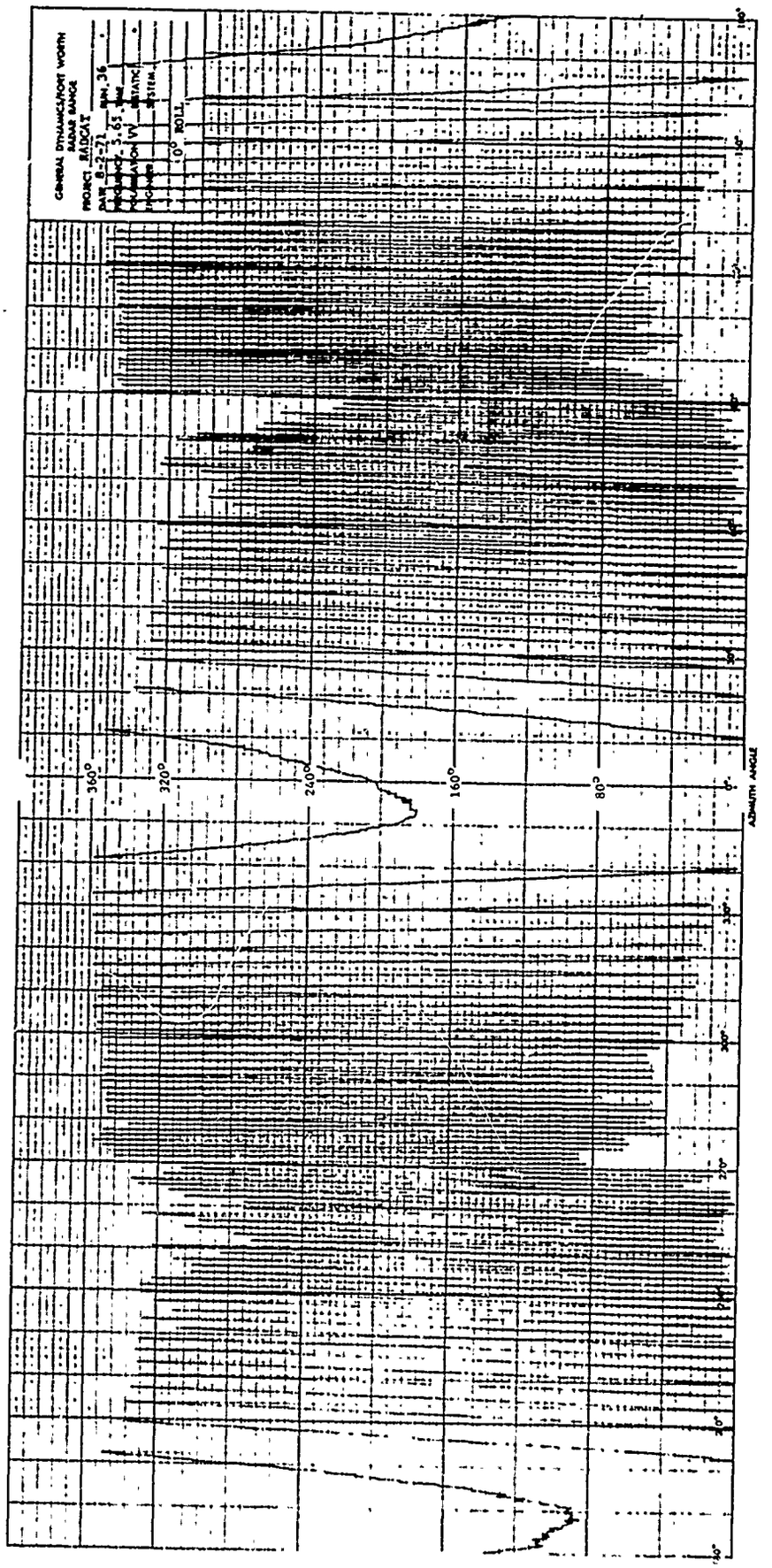

Fig. 2-35 VEHICLE 002 PHASE RESPONSE; C-BAND, VV POLARIZATION, 0-DEGREE ROLL

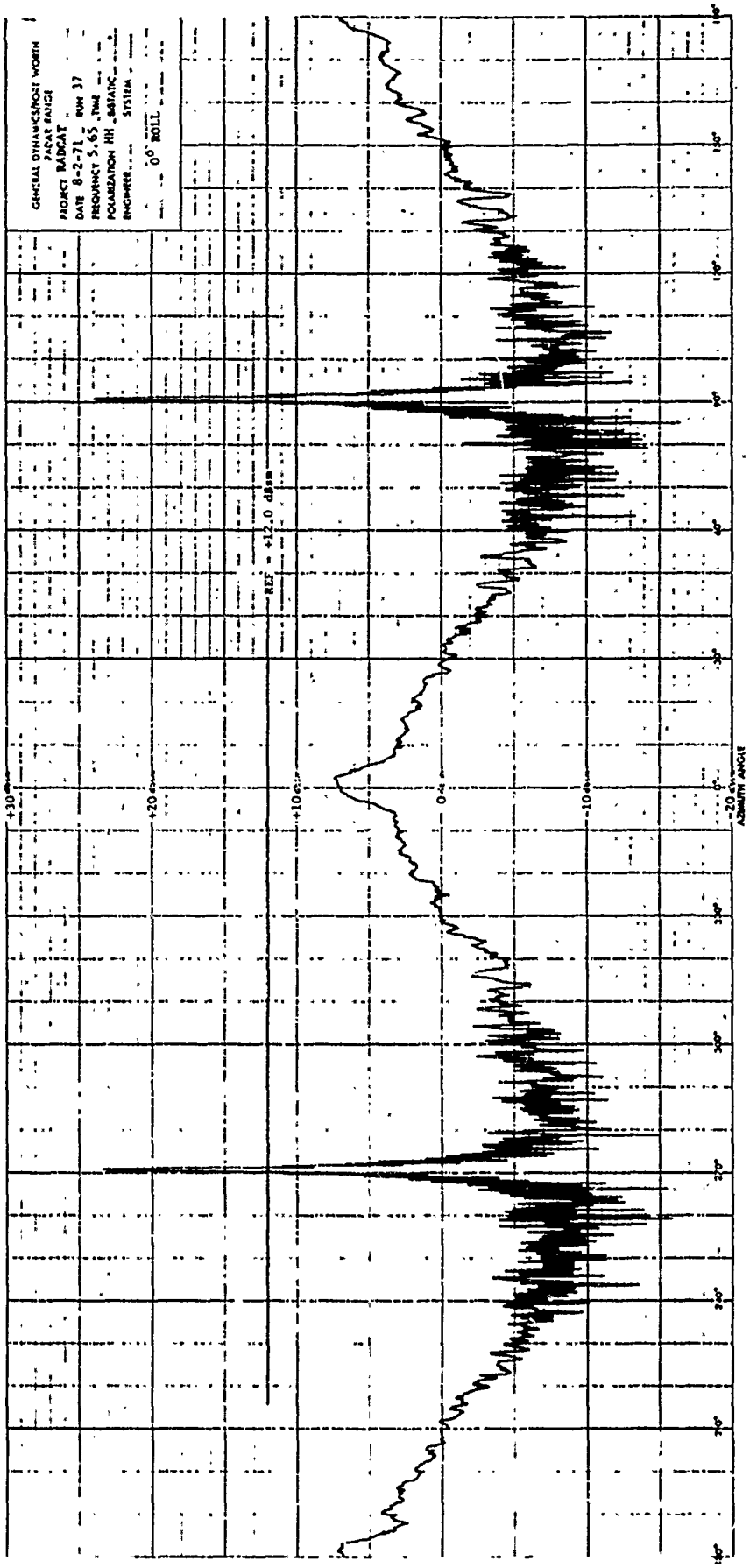

Fig. 2-36 VEHICLE 002 AMPLITUDE RESPONSE; C-BAND, HH POLARIZATION, 0-DEGREE ROLL

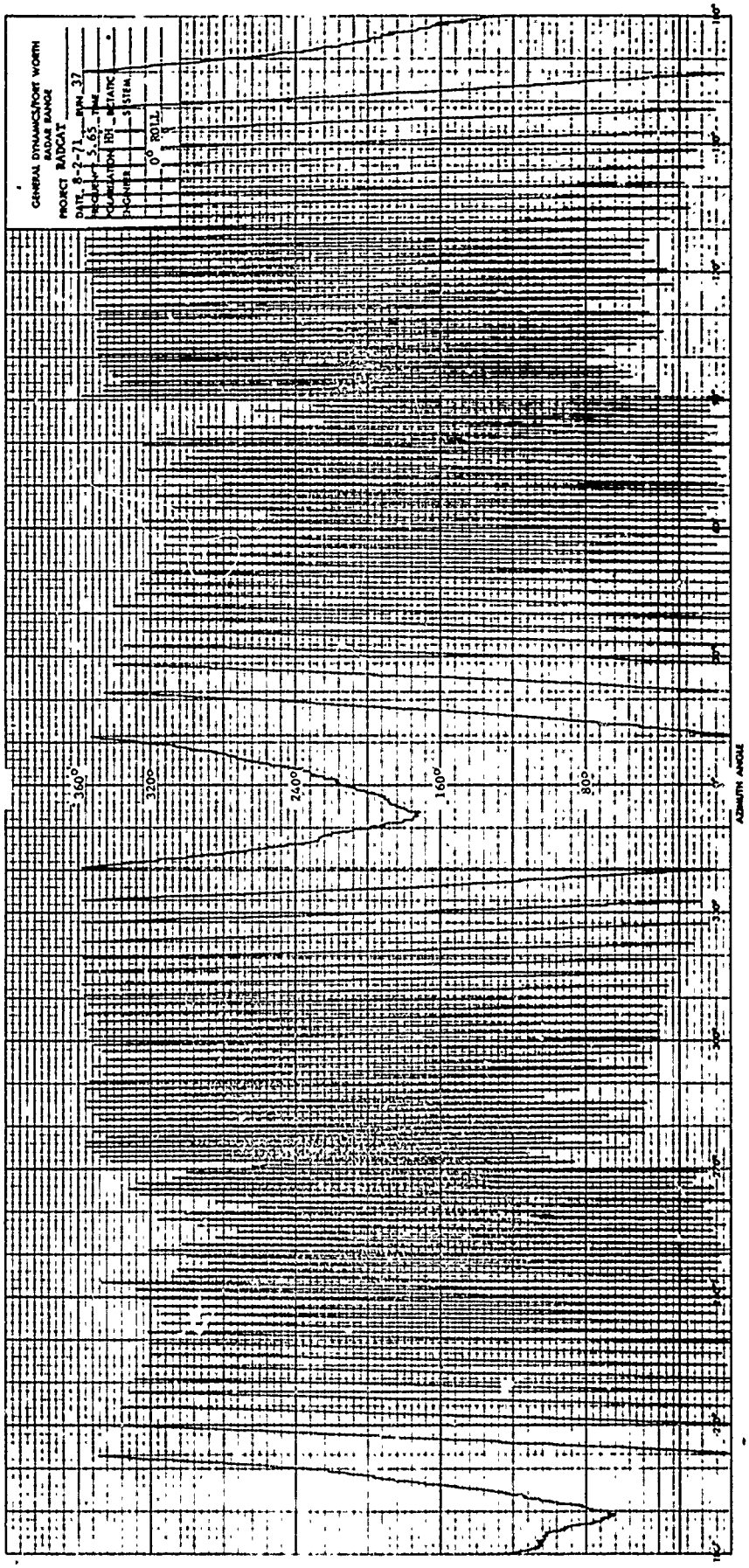

Fig. 2-37 VEHICLE 002 PHASE RESPONSE; C-BAND, HH POLARIZATION, 0-DEGREE ROLL

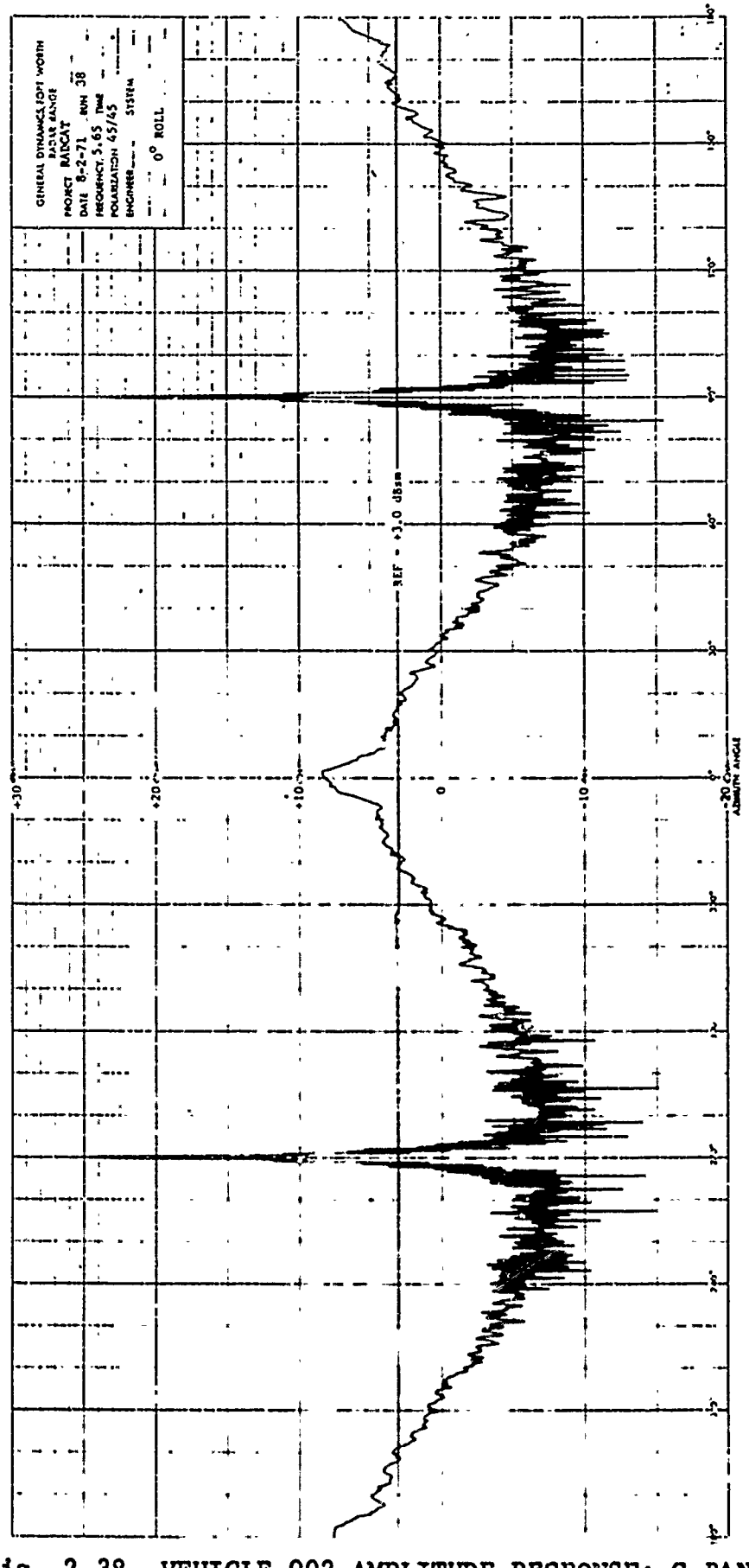

Fig. 2-38 VEHICLE 002 AMPLITUDE RESPONSE; C-BAND, $\pi/4$ $\pi/4$ POLARIZATION, 0-DEGREE ROLL

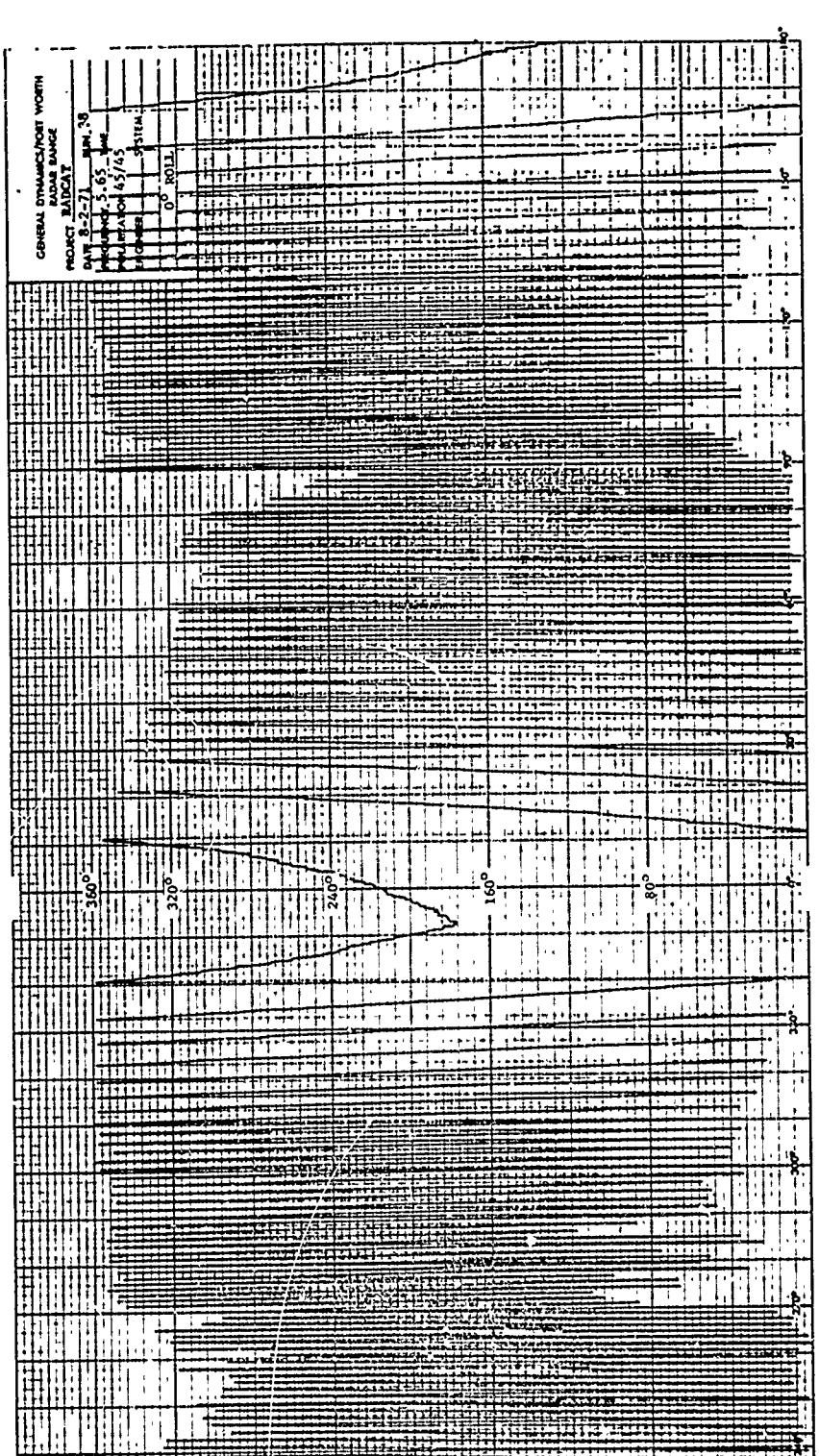

Fig. 2-39 VEHICLE 002 PHASE RESPONSE; C-BAND, $\pi/4$ $\pi/4$ POLARIZATION, 0-DEGREE ROLL

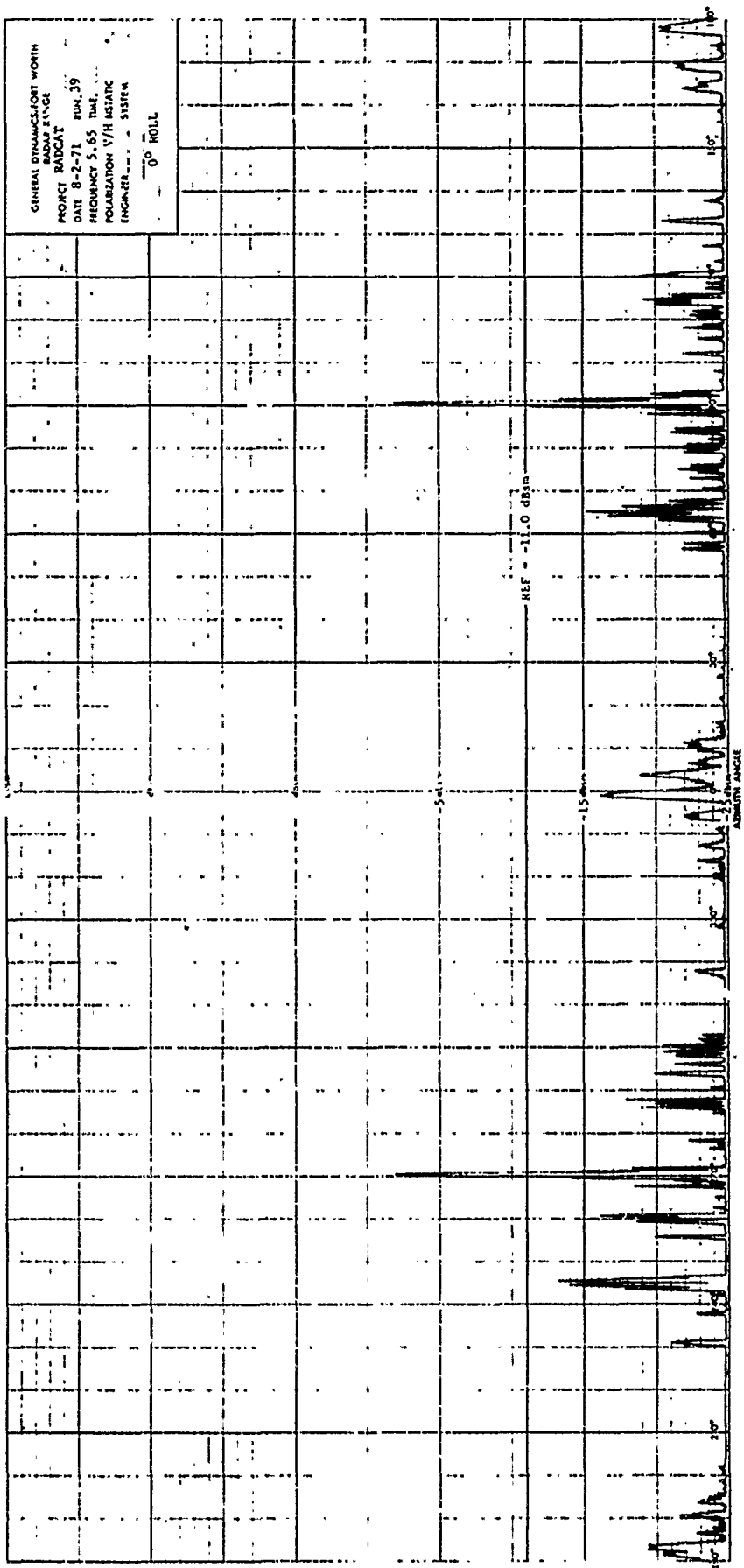

Fig. 2-40 VEHICLE 002 AMPLITUDE RESPONSE; C-BAND, VH POLARIZATION, 0-DEGREE ROLL

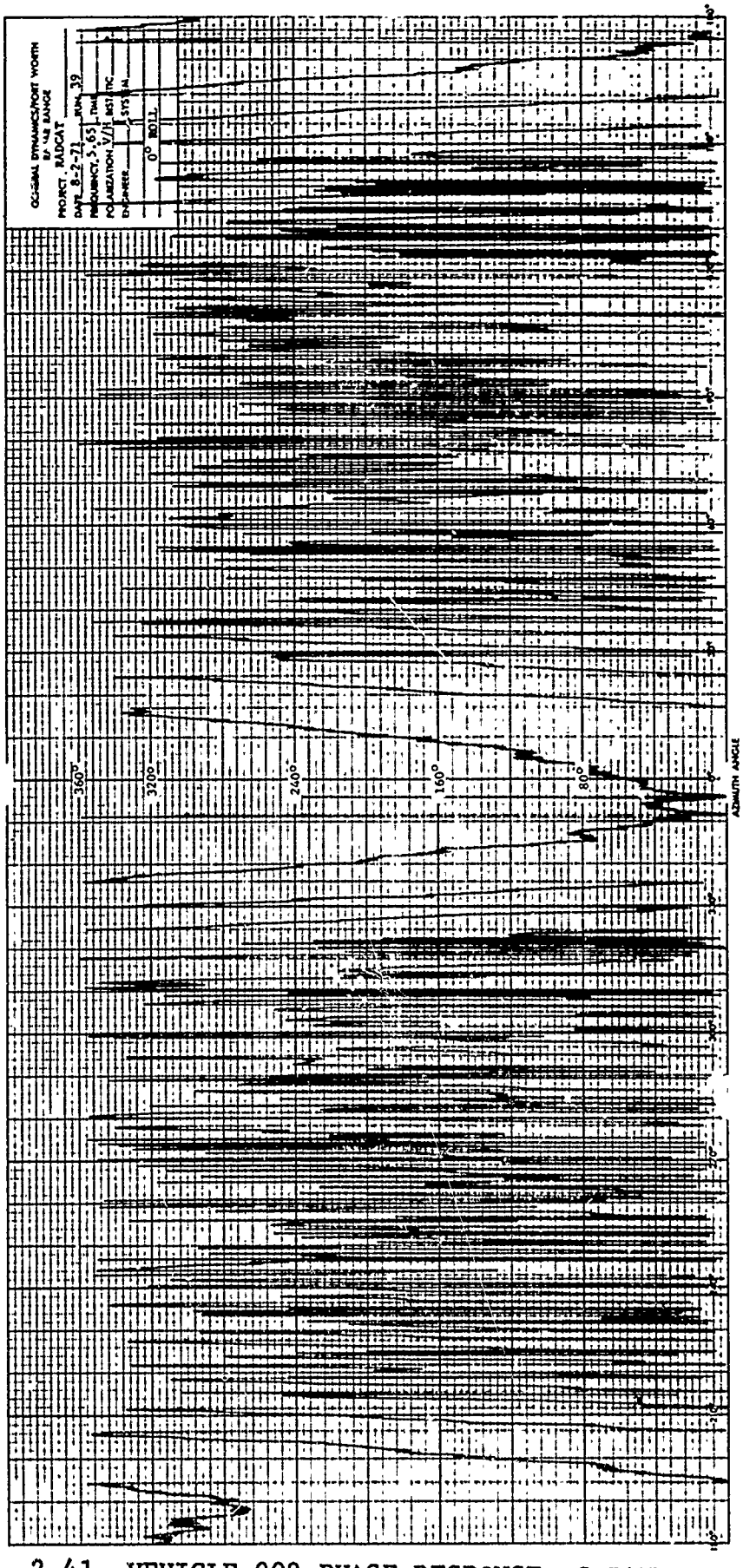

Fig. 2-41 VEHICLE 002 PHASE RESPONSE; C-BAND, VH POLARIZATION, 0-DEGREE ROLL

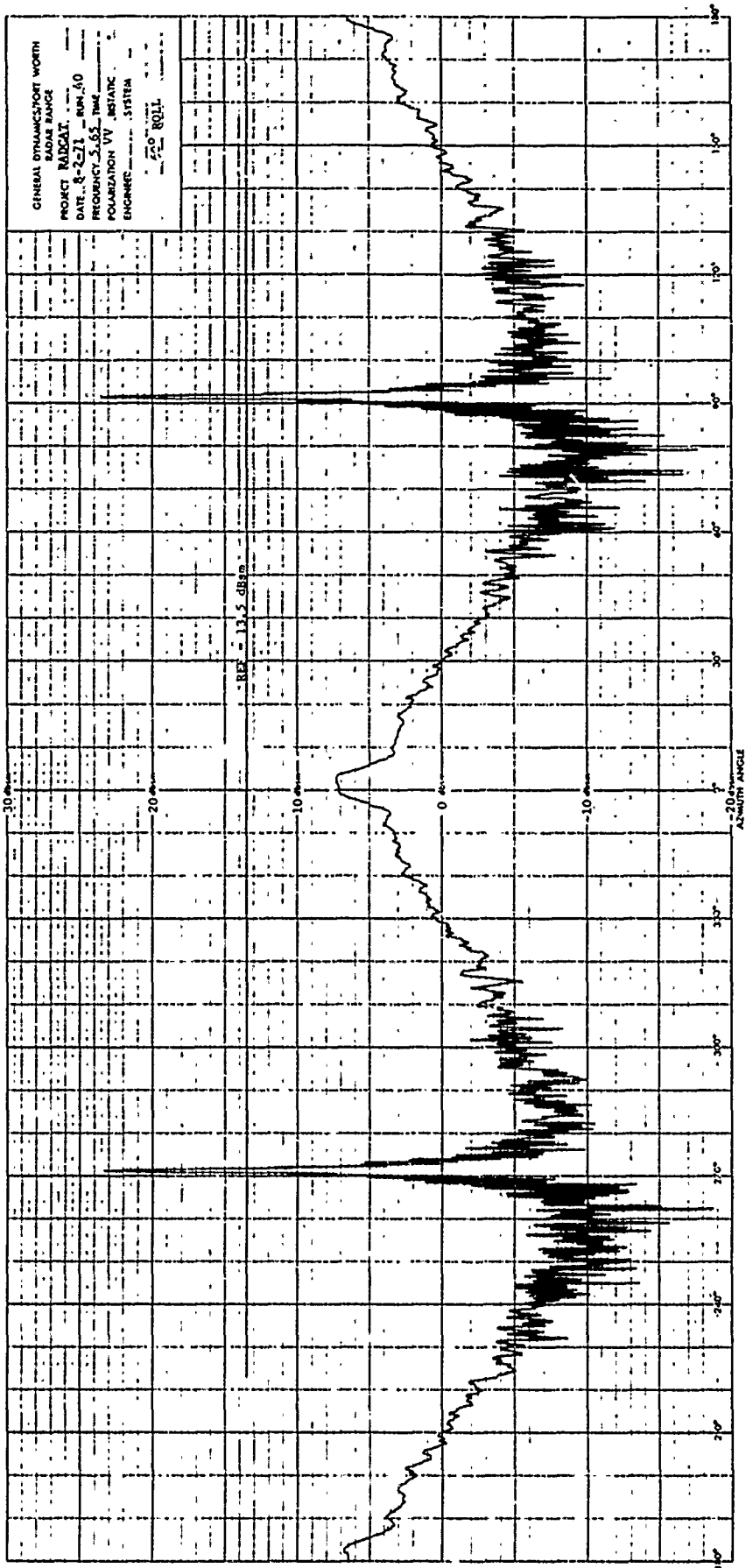

Fig. 2-42 VEHICLE 002 AMPLITUDE RESPONSE; C-BAND, VV POLARIZATION, 60-DEGREE ROLL

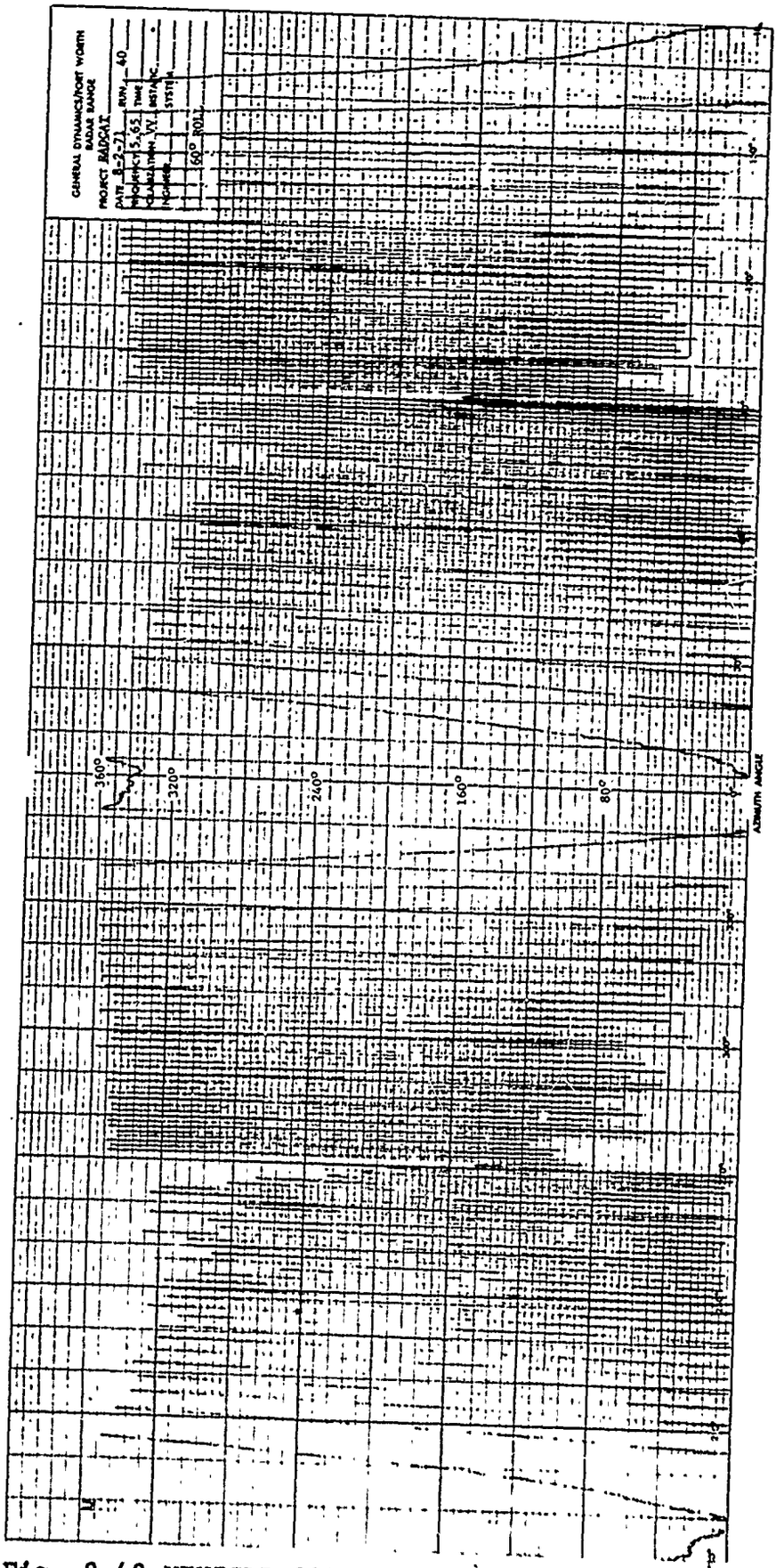

Fig. 2-43 VEHICLE 002 PHASE RESPONSE; C-BAND, VV POLARIZATION, 60-DEGREE ROLL

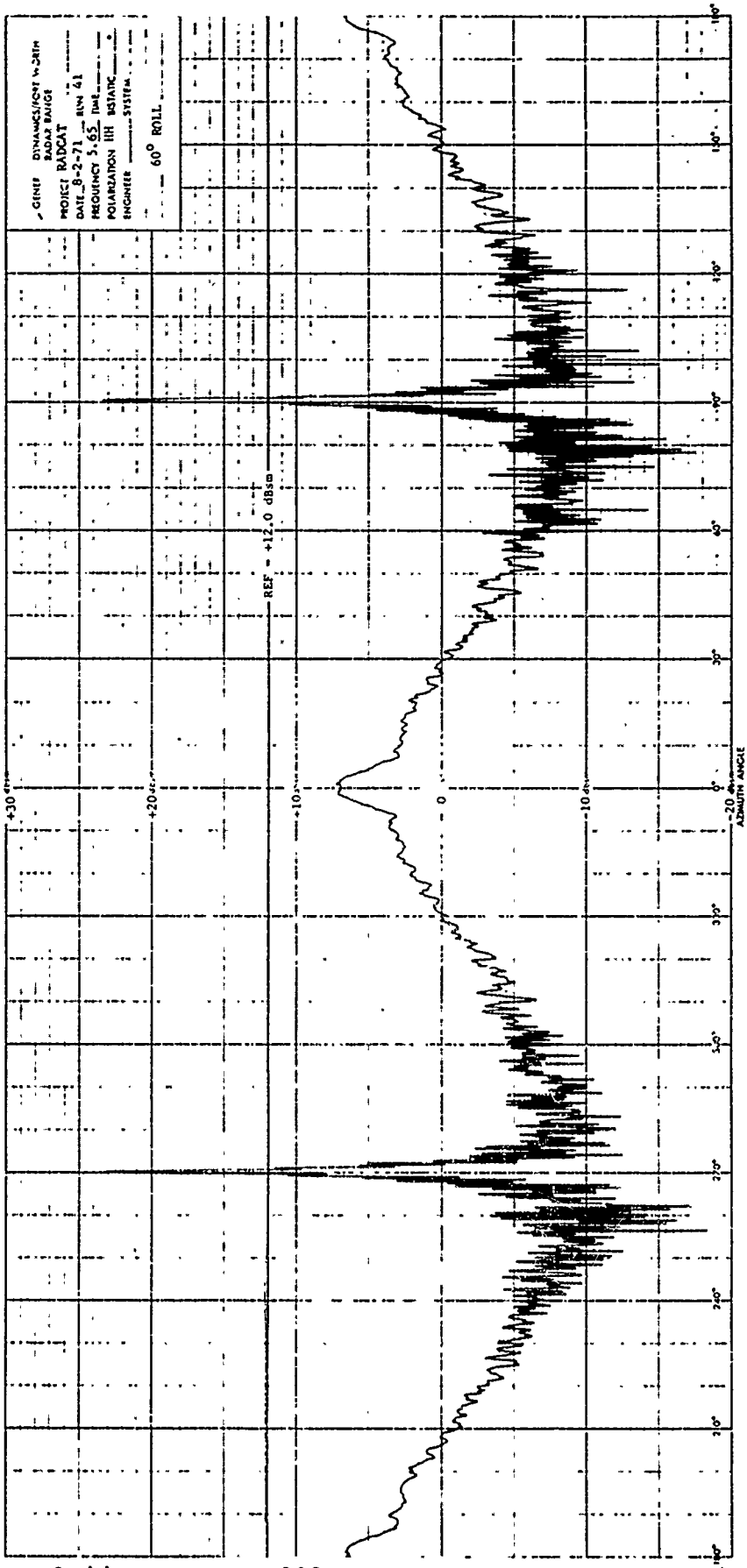

Fig. 2-44 VEHICLE 002 AMPLITUDE RESPONSE; C-BAND, HH POLARIZATION, 60-DEGREE ROLL

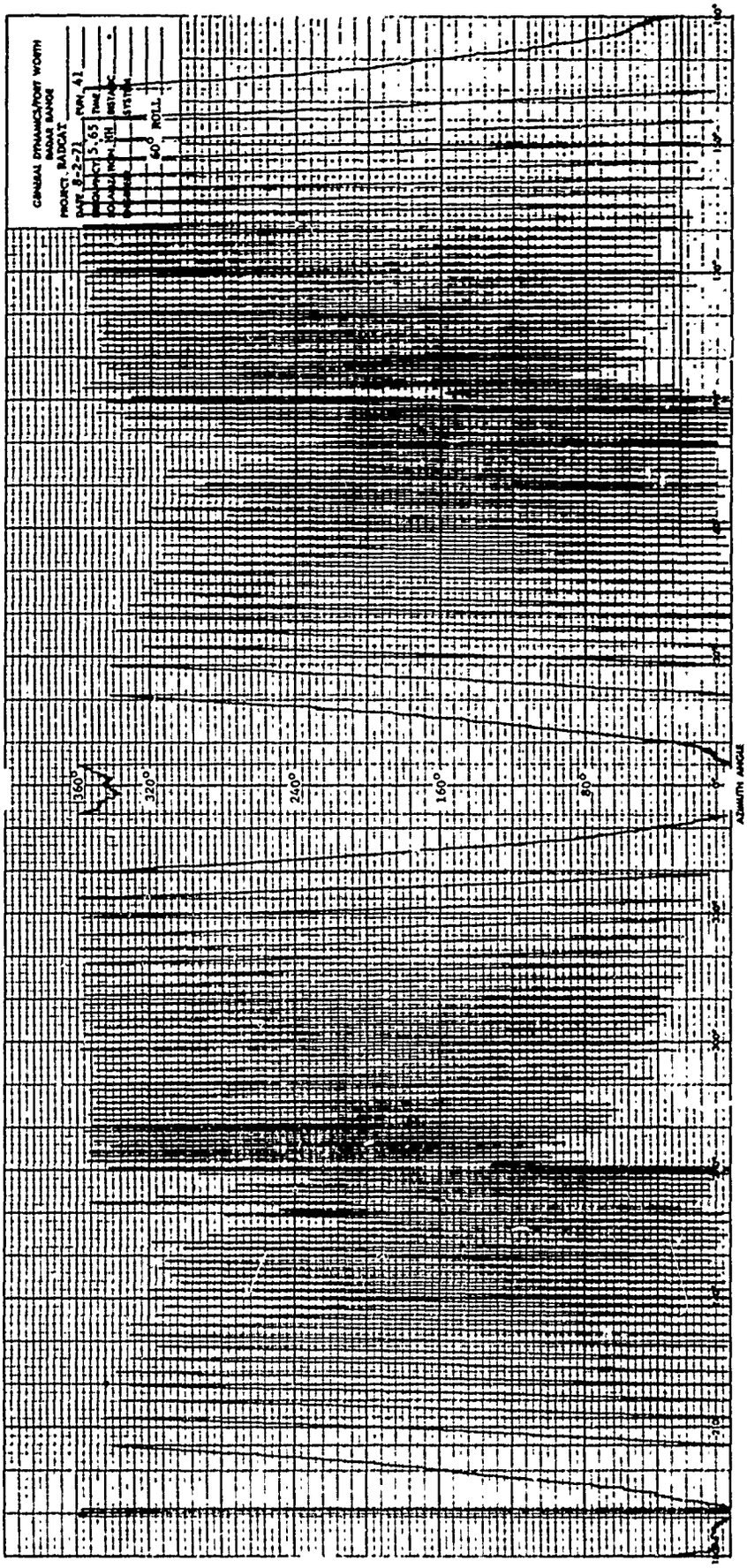

Fig. 2-45 VEHICLE 002 PHASE RESPONSE; C-BAND, HH POLARIZATION, 60-DEGREE ROLL

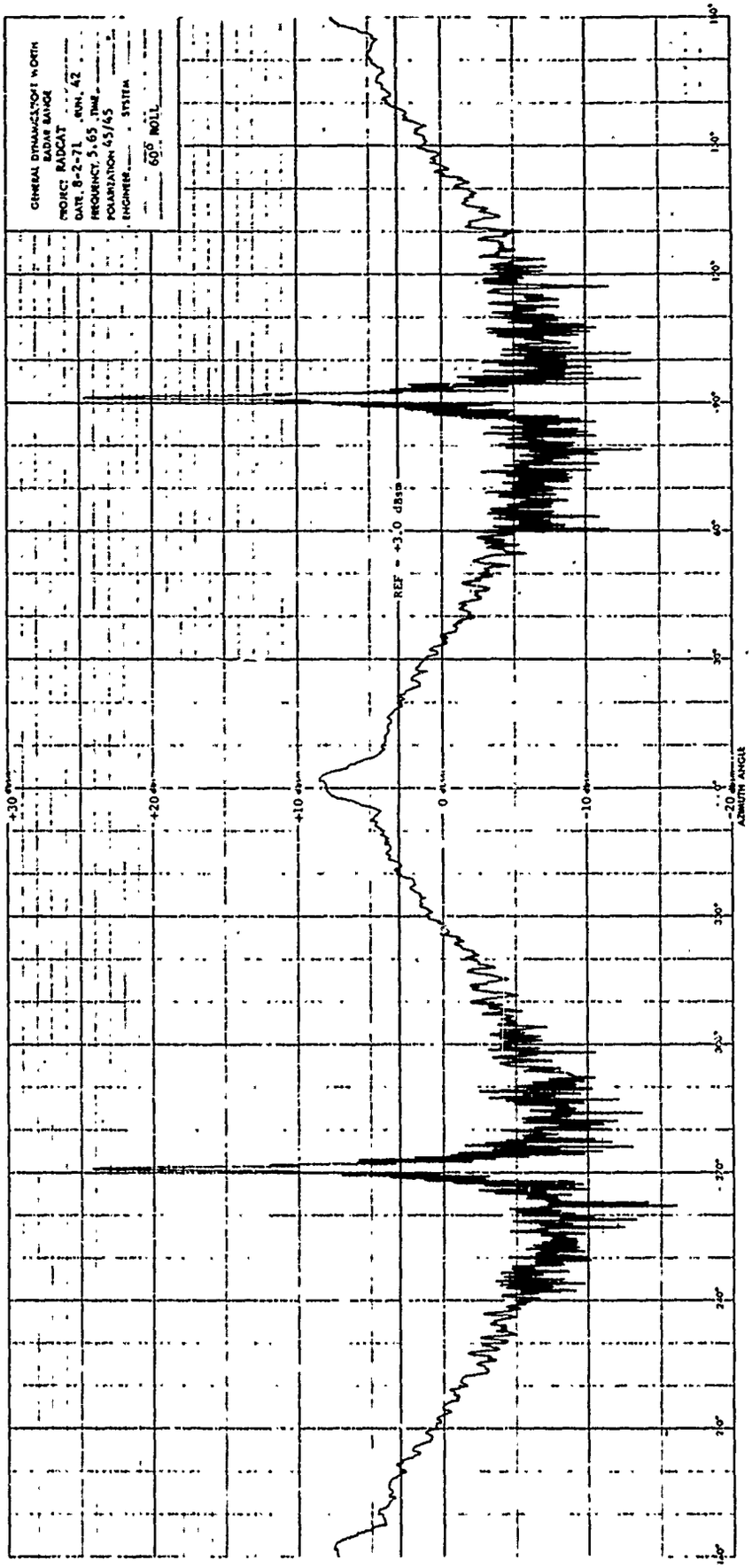

Fig. 2-46 VEHICLE 002 AMPLITUDE RESPONSE; C-BAND, $\pi/4$ $\pi/4$ POLARIZATION, 60-DEGREE ROLL

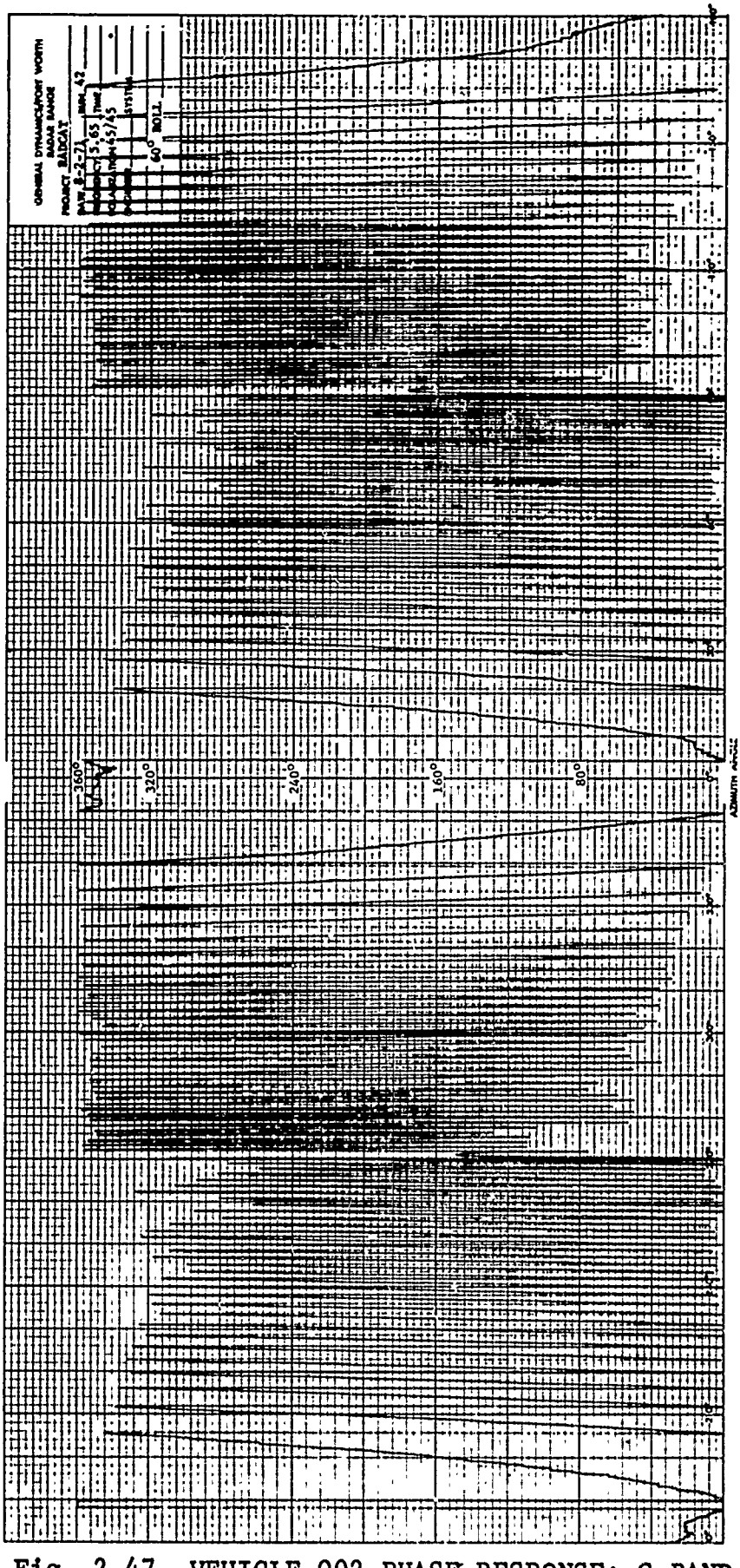

Fig. 2-47 VEHICLE 002 PHASE RESPONSE; C-BAND, $\pi/4$ $\pi/4$ POLARIZATION, 60-DEGREE ROLL

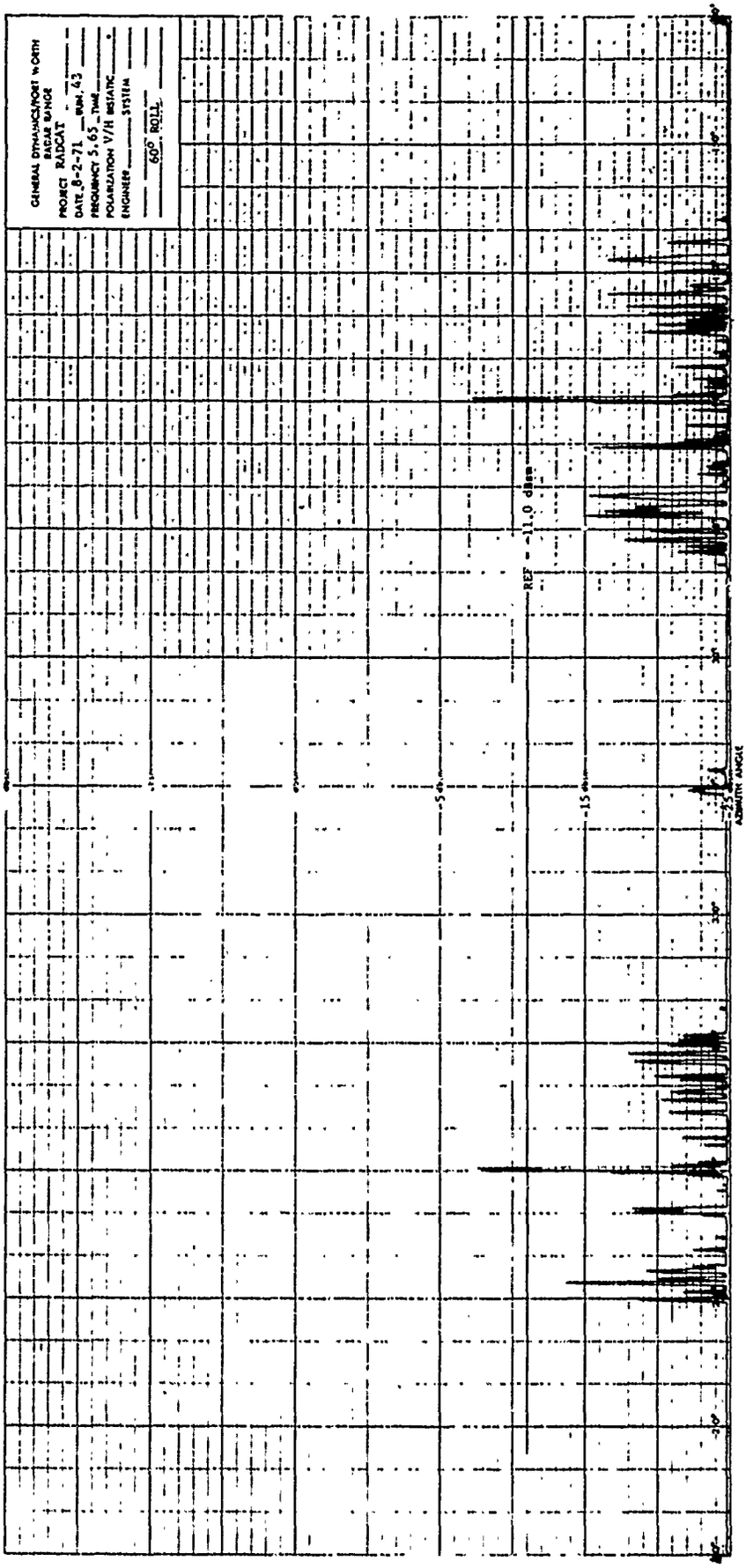

Fig. 2-48 VEHICLE 002 AMPLITUDE RESPONSE; C-BAND, VH POLARIZATION, 60-DEGREE ROLL

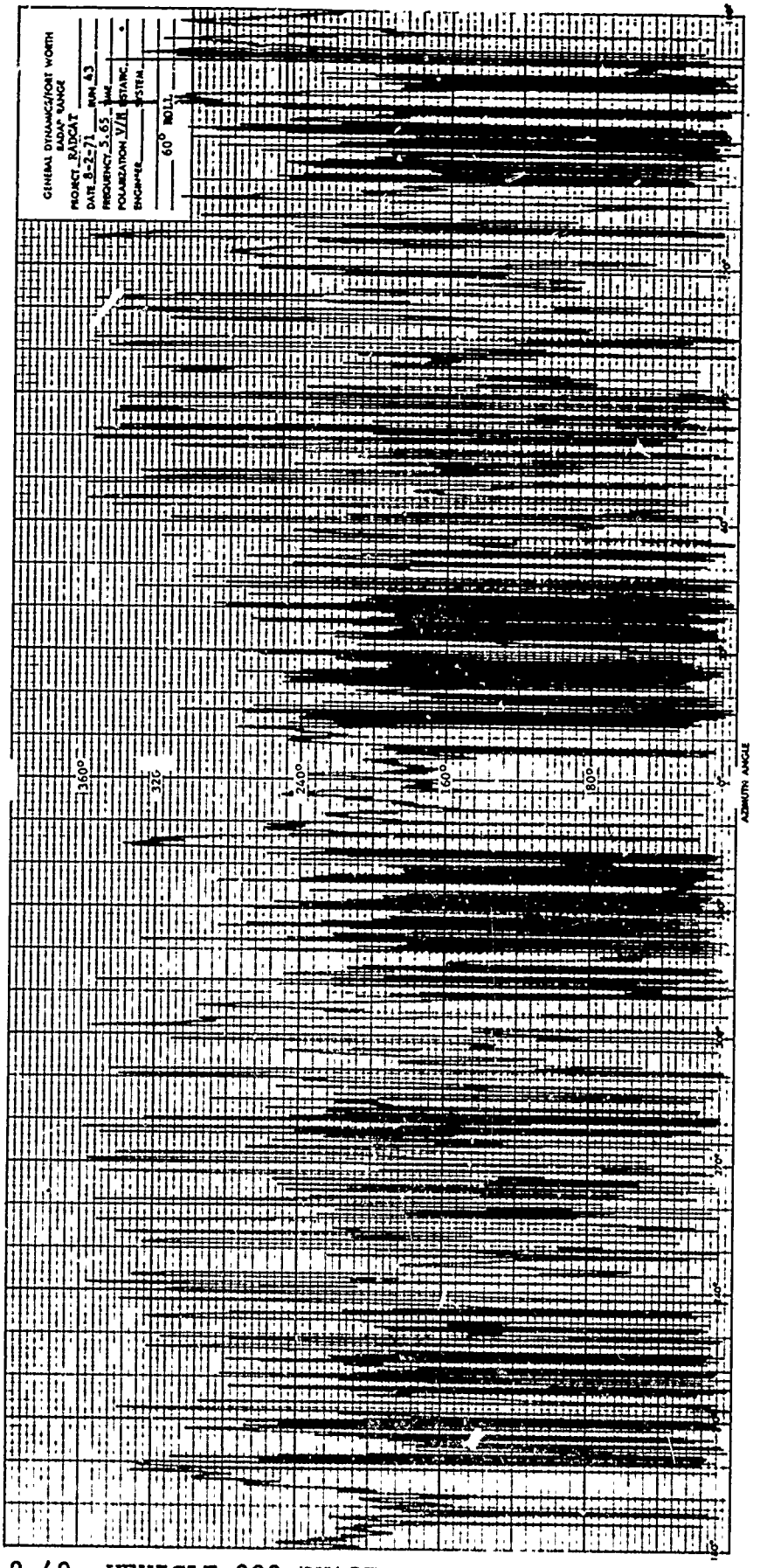

Fig. 2-49 VEHICLE 002 PHASE RESPONSE; C-BAND, VH POLARIZATION, 60-DEGREE ROLL

THIS PAGE INTENTIONALLY LEFT BLANK

2.3 SHORT-PULSE MEASUREMENTS

Coherent short-pulse measurements were performed at 5.65 gigahertz in accordance with the measurement matrix shown in Table 2.2. As noted in this matrix, the target response was recorded over a complete 0- to 90-degree aspect sector at both VV and HH polarization.

The readers attention is called to the sketch in Figure 2-50 which illustrates the aspect angle convention which is associated with the short-pulse recording system. Note in particular that 90-degrees aspect in the short-pulse recordings system corresponds to the 270-degree orientation as recorded by the long-pulse system (see Figure 2-1). The designations for 0-degree and 180-degree orientations are consistent between the two systems, and in each case the target orientation is changed by rotating in the clockwise direction. This difference in convention should be kept in mind when comparing the C-Band long-pulse and the short-pulse phase response which nulls slightly off of zero-degrees in aspect.

Figures 2-51 and 2-52 contain the peak C-band short-pulse amplitude response of vehicle 002 as measured at VV and HH polarization respsectively; data shown are calibrated in dBsm. In addto the peak return from the RADCAT vehicle, a scattered return from the back shadow boundary was observed at each polarization and has been plotted as σ_2 in each of these figures. The phase response (relative) corresponding to VV and HH polarization is shown in Figures 2-53 and 2-54 respectively.

The data illustrated in Figure 2-55 correspond to the peak S-band amplitude response as measured at VV and HH polarization. As a result of the relatively short pulse width which was achieved, the scattered return from the back shadow boundary was still resolvable. This return, labeled as σ_2 , is also presented in Figure 2-55 for comparison with the C-band response.

A complete listing of the calibrated short-pulse response may be found in Appendix C for both C-band and S-band measurements.

Table 2.2 RADCAT SHORT-PULSE MEASUREMENT MATRIX

FREQUENCY GHz	POLARIZATION	PITCH ANGLE (DEGREES)	ROLL ANGLE (DEGREES)	ASPECT ANGLE (DEGREES)	ASPECT INCREMENT (DEGREES)
5.65	VV, HH	0	0	0 TO 90	~1.0 (0° TO 85°) ~0.5 (85° TO 90°)
2.4	VV, HH	0	0	0 TO 90	~1.0 (0° TO 85°) ~0.2 (85° TO 90°)

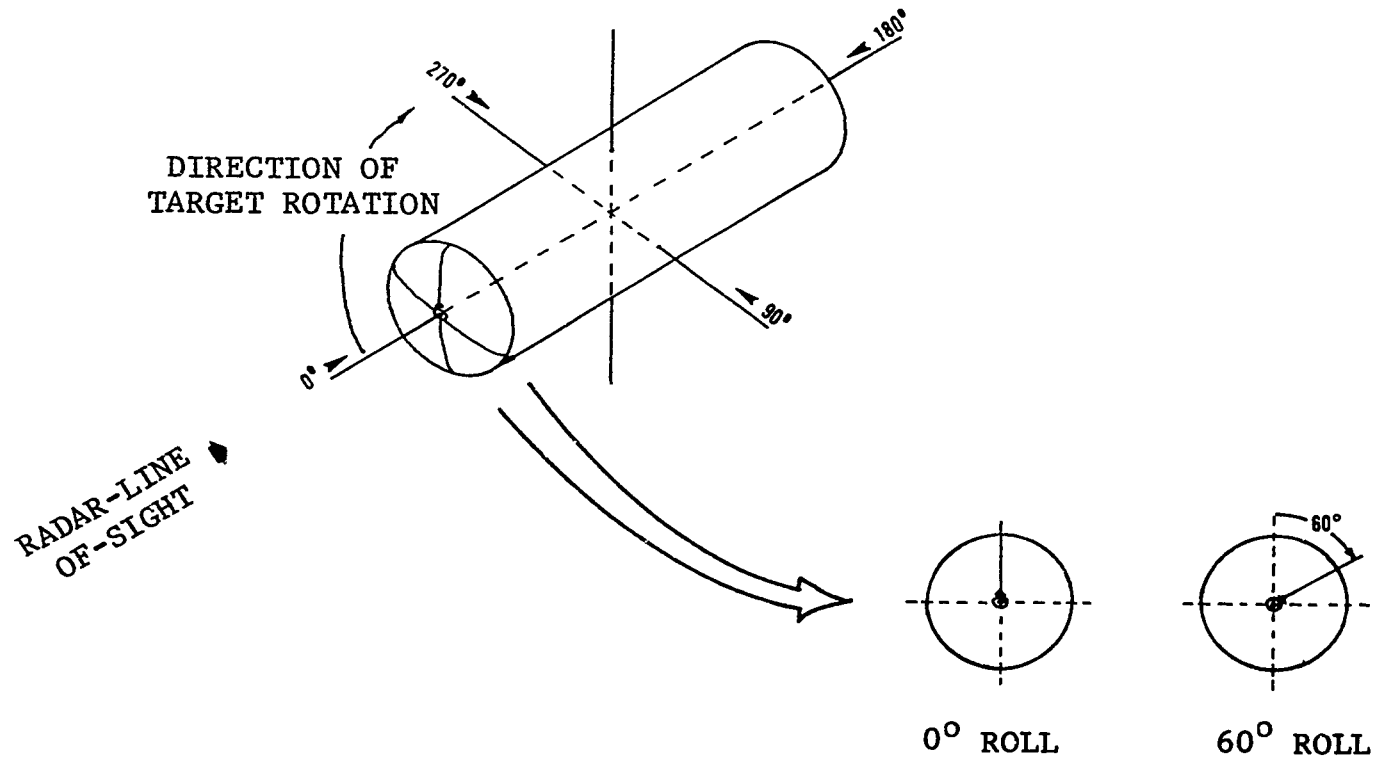

Fig. 2-50 TARGET ORIENTATION CONVENTION FOR SHORT-PULSE MEASUREMENTS

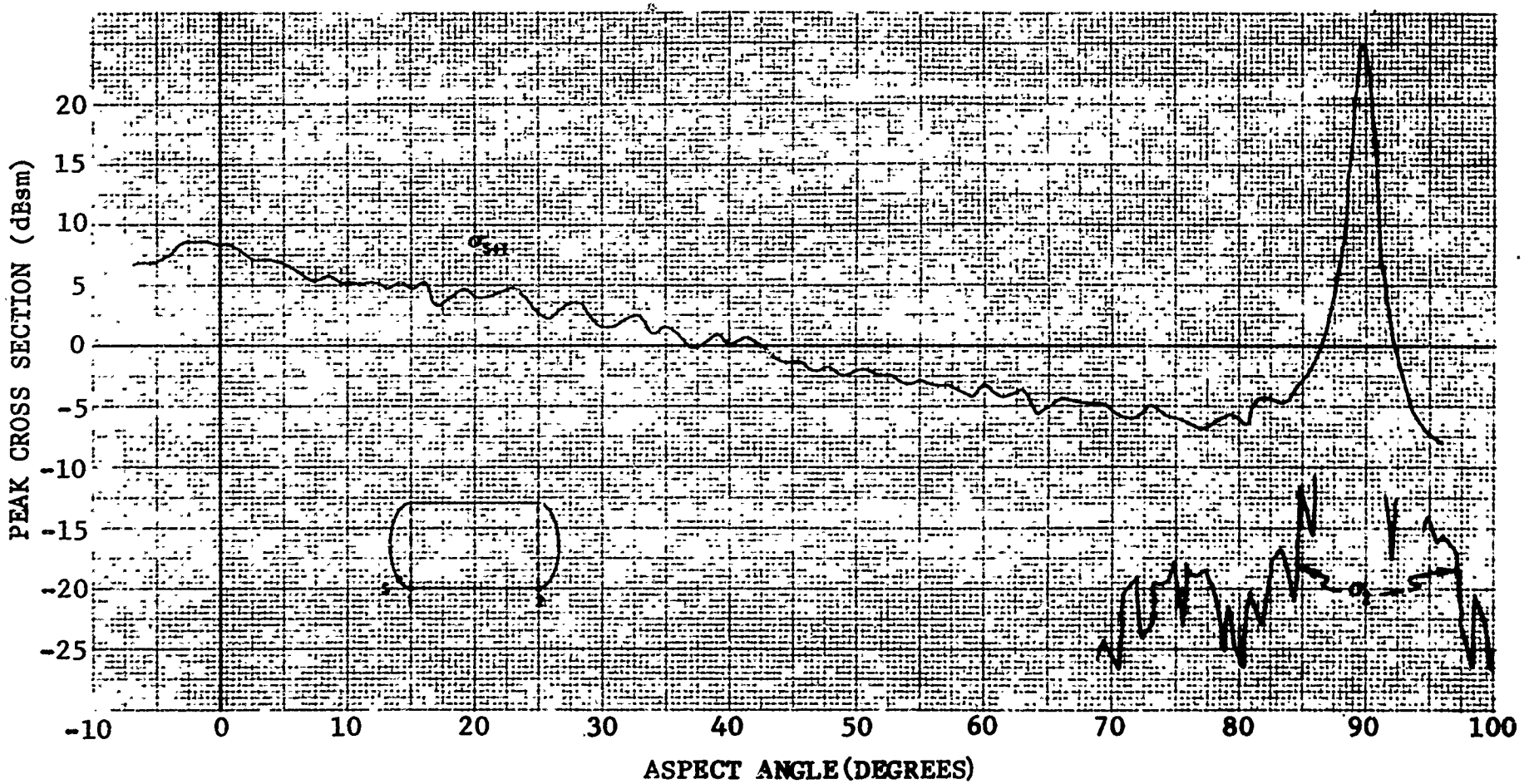

Fig. 2-51 VEHICLE 002 SHORT-PULSE AMPLITUDE RESPONSE; C-BAND, VV POLARIZATION, 0-DEGREE ROLL

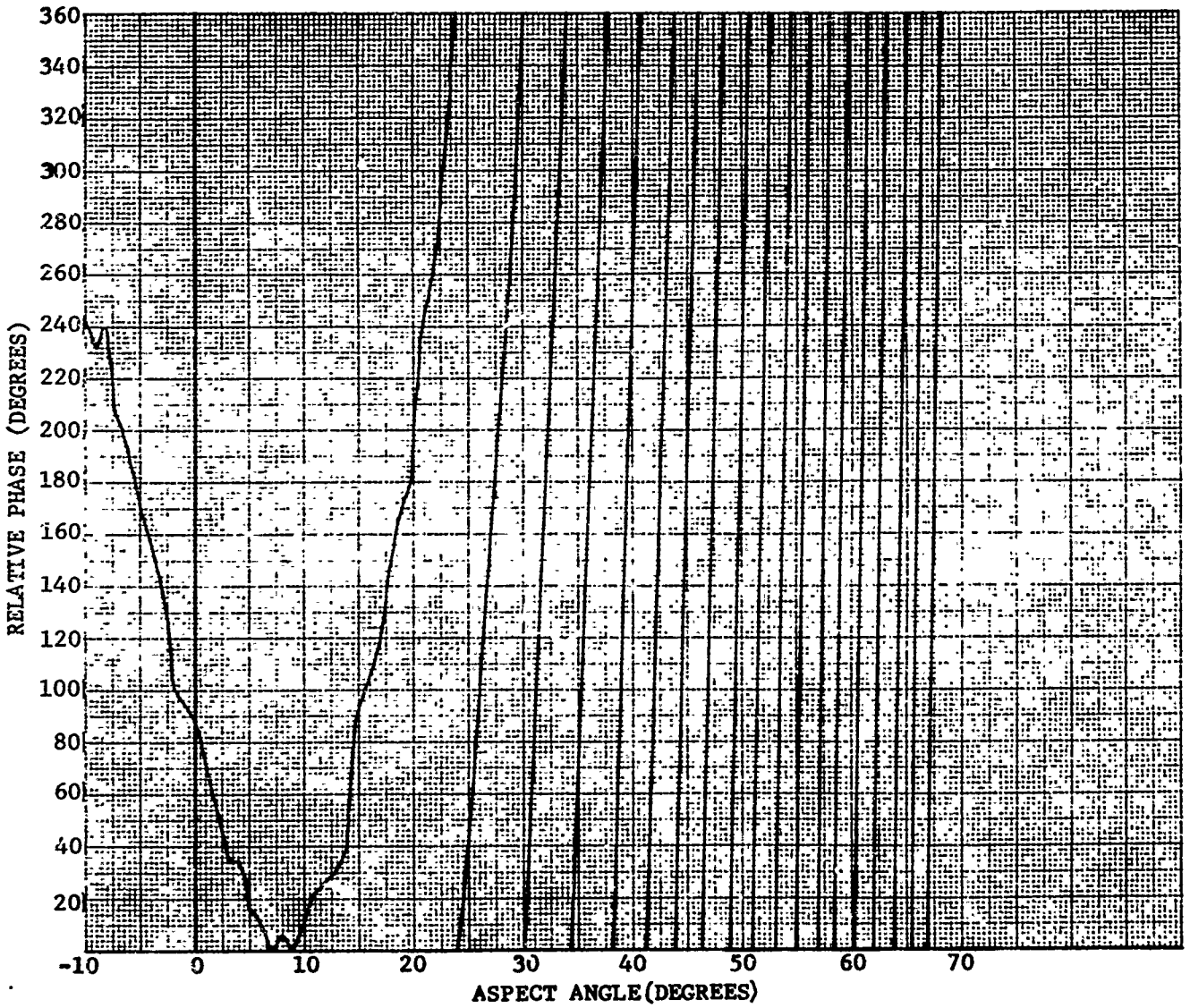

Fig. 2-52 VEHICLE 002 SHORT-PULSE PHASE RESPONSE; C-BAND, VV POLARIZATION, 0-DEGREE ROLL

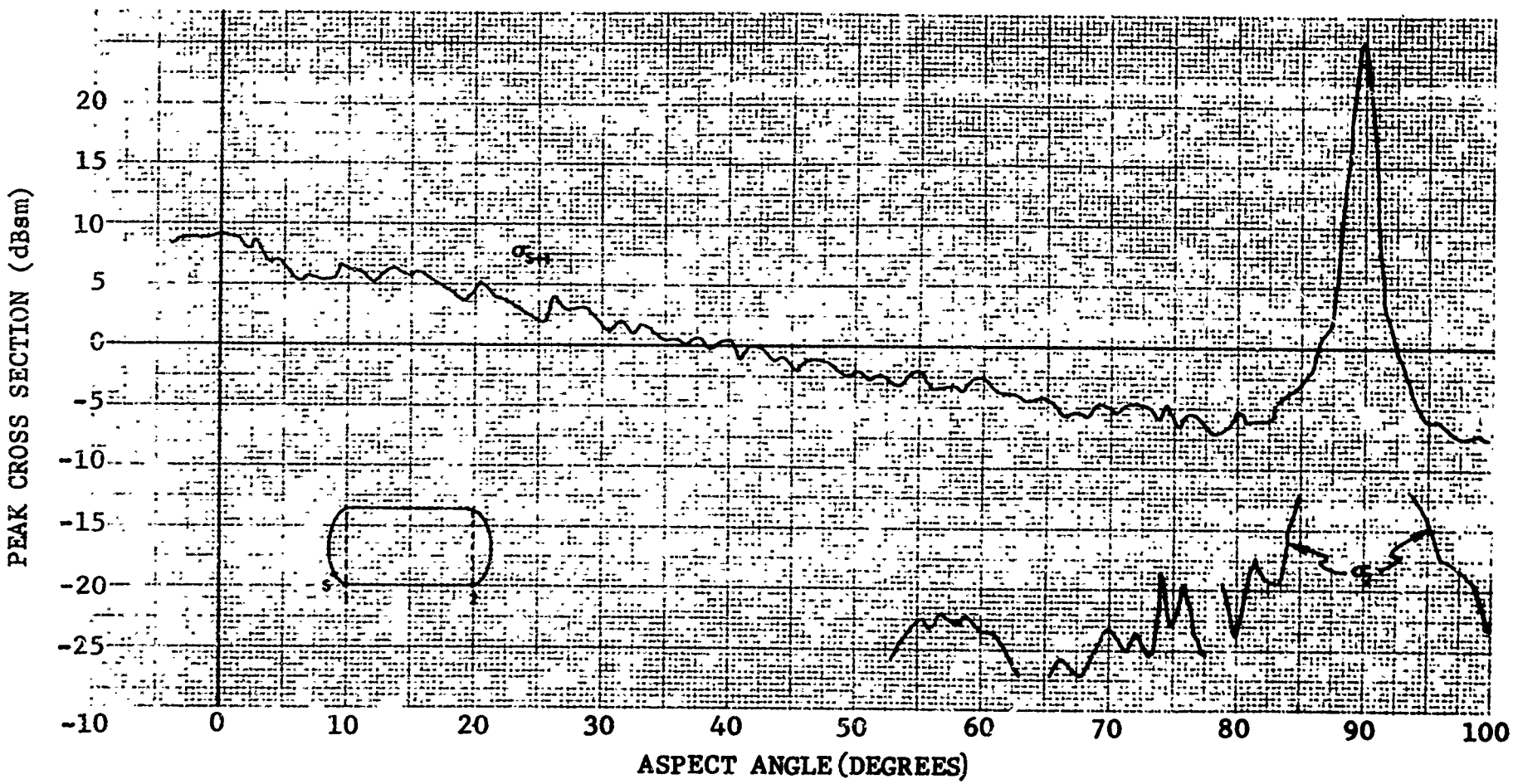

Fig. 2-53 VEHICLE 002 SHORT-PULSE AMPLITUDE RESPONSE; C-BAND, HH POLARIZATION, 0-DEGREE ROLL

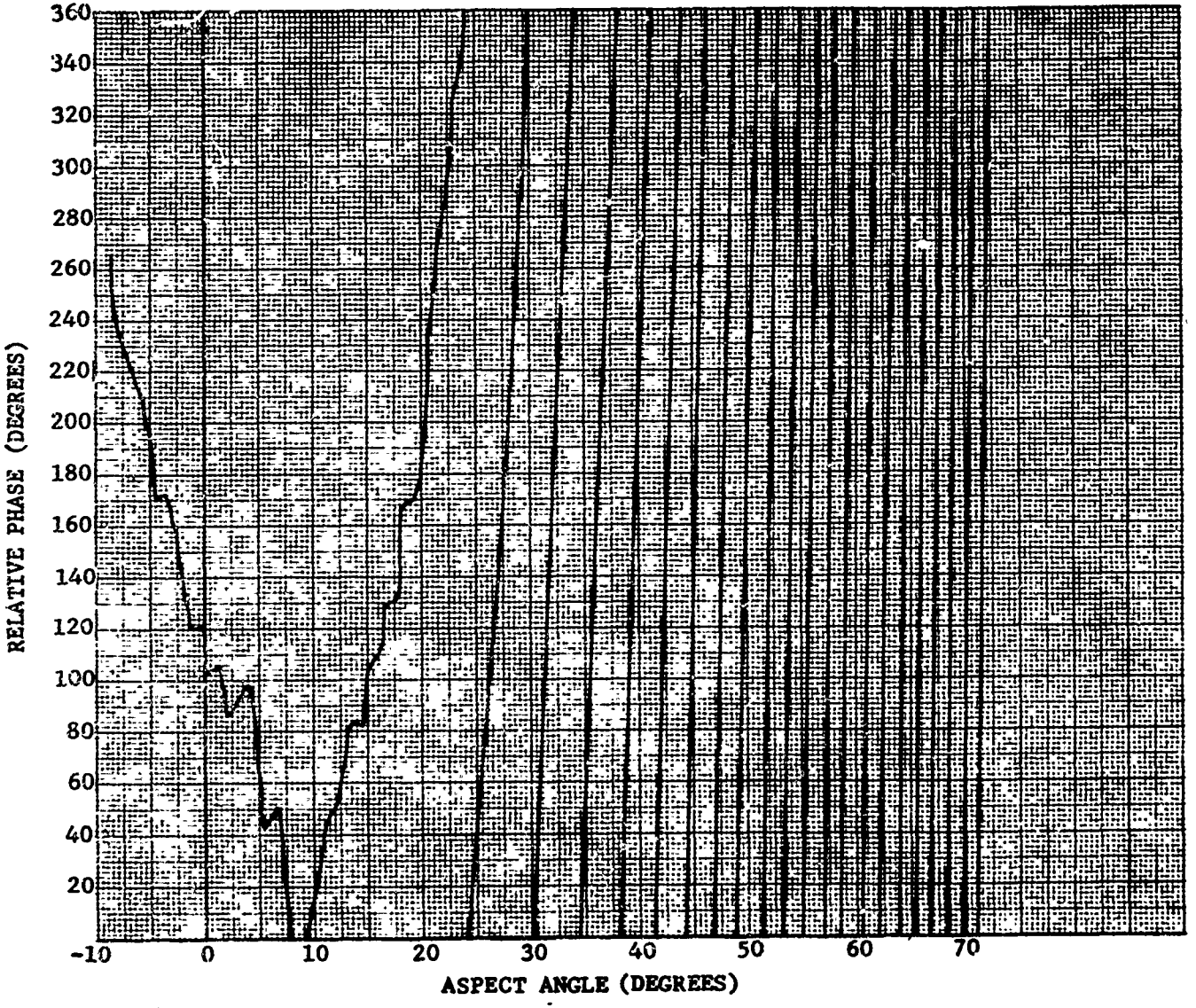

Fig. 2-54 VEHICLE 002 SHORT-PULSE PHASE RESPONSE; C-BAND HH POLARIZATION, 0-DEGREE ROLL

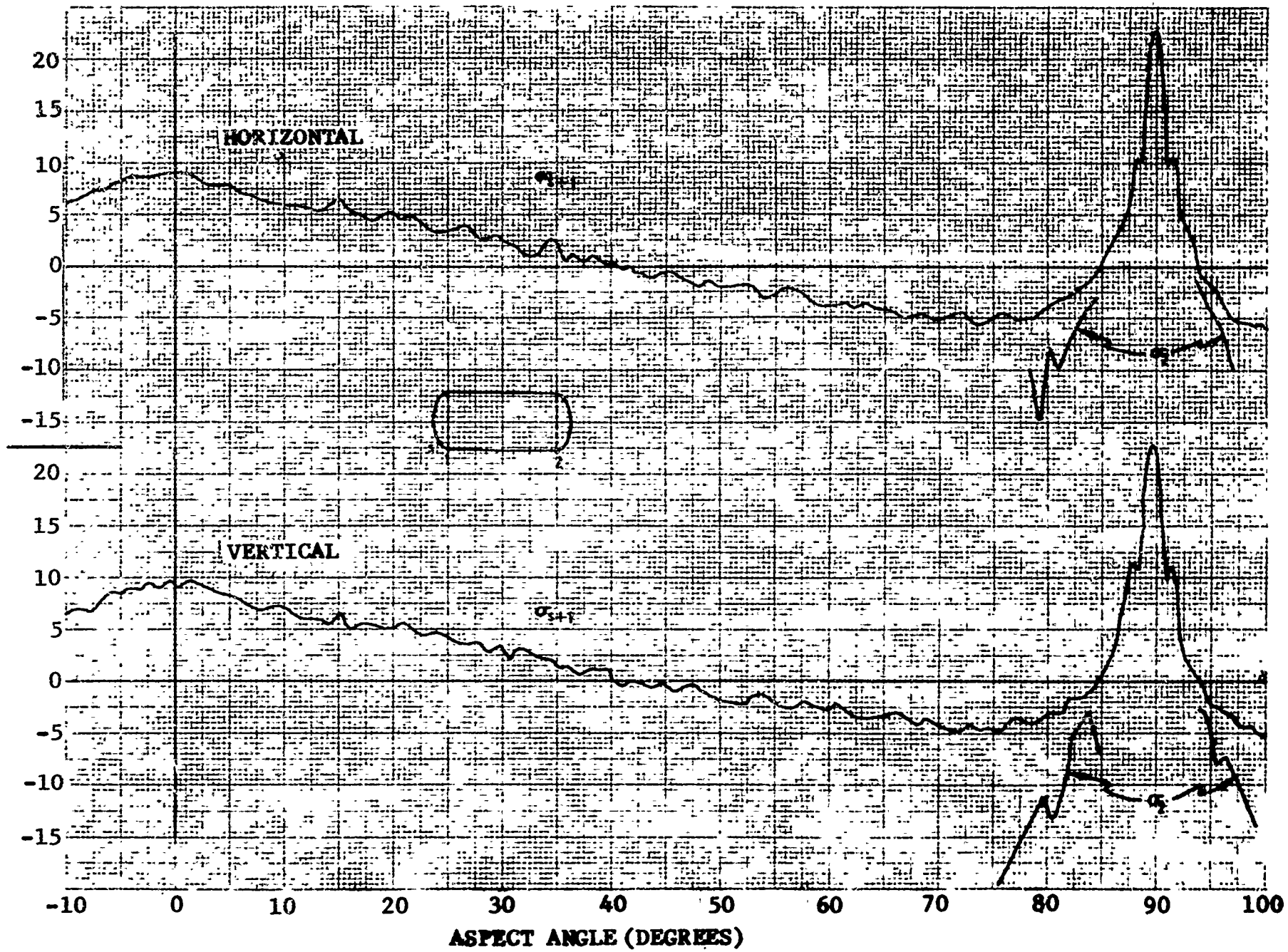

Fig. 2-55 VEHICLE 002 SHORT-PULSE RESPONSE; S-BAND

This page intensionally left blank

SECTION 3.
COMPARATIVE EXAMINATION OF RADCAT VEHICLE 002 RESPONSE

3.1 GENERAL

At the time measurements were initiated on vehicle 002, it was generally suspected that the radar cross section response from vehicle 002 might exhibit some differences in scattering from that of vehicle 001. It was, in fact, the objective of this program to acquire sufficient data on vehicle 002 to document any such difference in the scattered response between the first and second vehicle and to subsequently recommend the degree to which vehicle 001 measurement data could be utilized to represent the response from vehicle 002.

A comparison between the scattered response of vehicle 001 and vehicle 002 is presented in this section. In addition, a further comparison is made between the response from vehicle 002 and (1) the solution obtained from a Physical Optics approximation and (2) the measured response of a perfectly conducting 1/2-scale model of the RADCAT cylindrical target.

3.2 COMPARISON WITH SELECTED VEHICLE 001 SIGNATURES

3.2.1 L-Band Long-Pulse Measurements

Figures 3-1 and 3-2 contain the long-pulse response of vehicle 001 corresponding to a measurement frequency of 1.28 gigahertz at VV polarization for the cases of 0-degree and 60-degree target roll

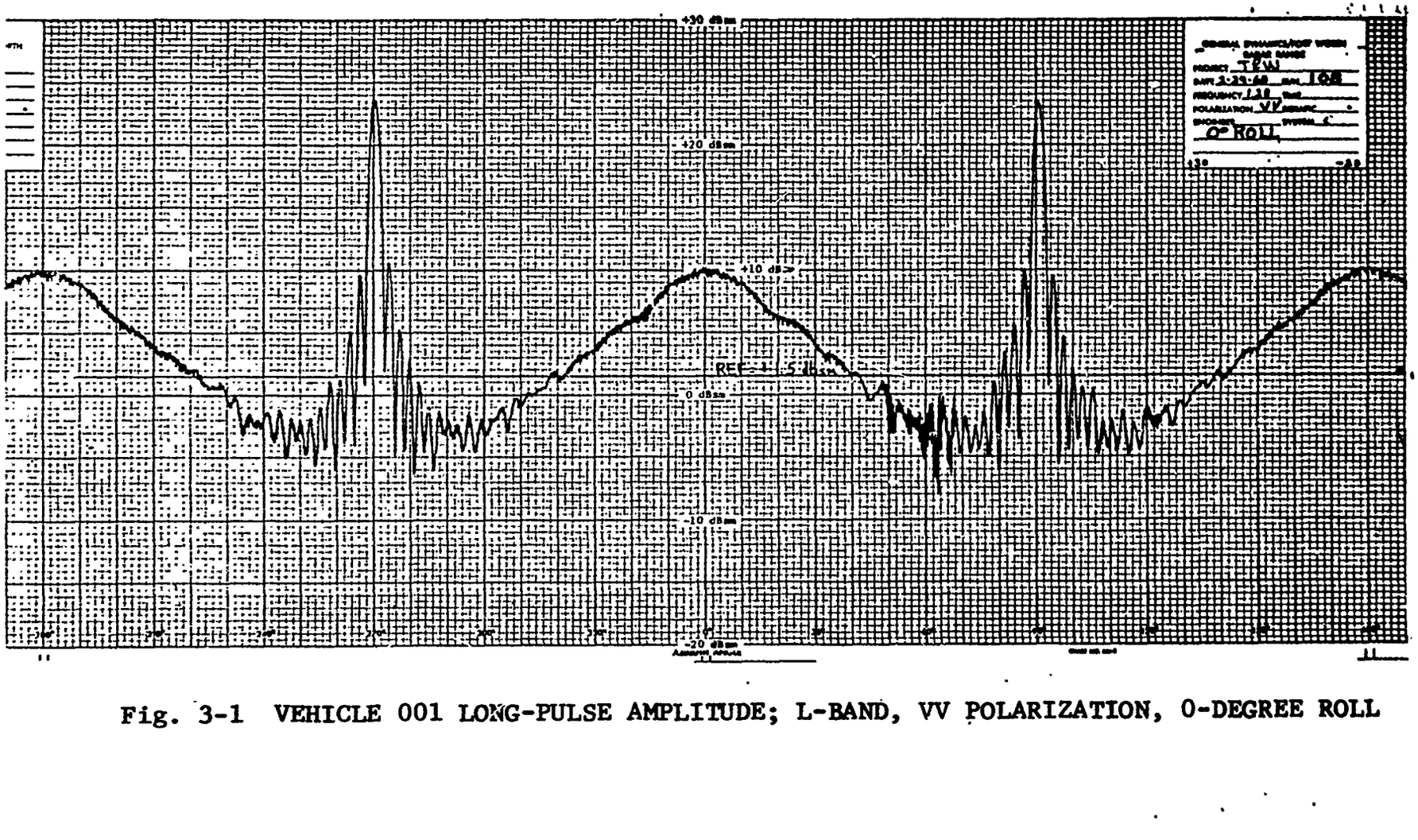

Fig. 3-1 VEHICLE 001 LONG-PULSE AMPLITUDE; L-BAND, VV POLARIZATION, 0-DEGREE ROLL

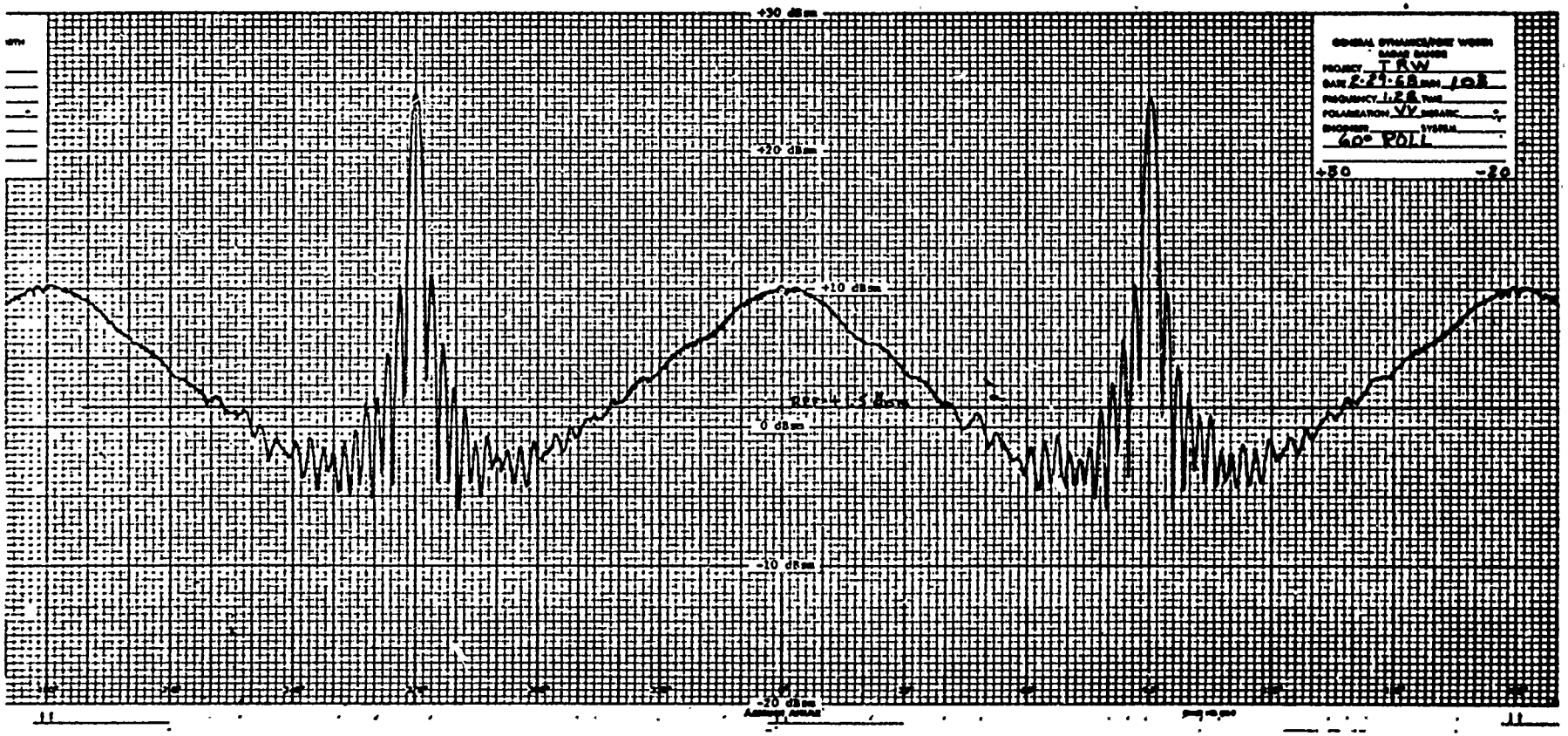

Fig. 3-2 VEHICLE 001 LONG-PULSE AMPLITUDE; L-BAND, VV POLARIZATION, 60-DEGREE ROLL

angles respectively. These data have been reproduced from a 1967 report which documented the RADCAT Vehicle 001 Measurement Program (Reference 1). The response of vehicle 002 measured under the same conditions is shown in Figure 3-3 and 3-4 for comparison. The phase response associated with the data contained in Figures 3-1 and 3-2 may be found in Appendix D along with the L-Band signatures acquired at HH, $\pi/4$ $\pi/4$, and VH polarizations. Similar data were presented in Section 2 for vehicle 002.

The following cross section levels are defined for ease in comparing the dominant scattering characteristics of vehicle 001 and 002.

$\sigma_{eo}(0^o)$: end-on cross section at 0-degrees in aspect

$\sigma_{eo}(180^o)$: end-on cross section at 180-degrees in aspect

$\sigma_{bs}(90^o)$: broadside cross section at 90-degrees in aspect

$\sigma_{bs}(270^o)$: broadside cross section at 270-degrees in aspect

$\sigma_{s1}(90^o)$: average of first sidelobe peaks near 90-degrees in aspect

$\sigma_{s1}(270^o)$: average of first sidelobe peaks near 270-degrees in aspect

$\bar{\sigma}_{eo}$: average end-on level

$\bar{\sigma}_{bs}$: average broadside level

$\bar{\sigma}_{s1}$: average first sidelobe level

Figure 3-5 contains a succession of averages of the above cross section levels for both vehicles. In Matrix 001(a) of Figure 3-5, a complete itemization is presented for each recorded end-on,

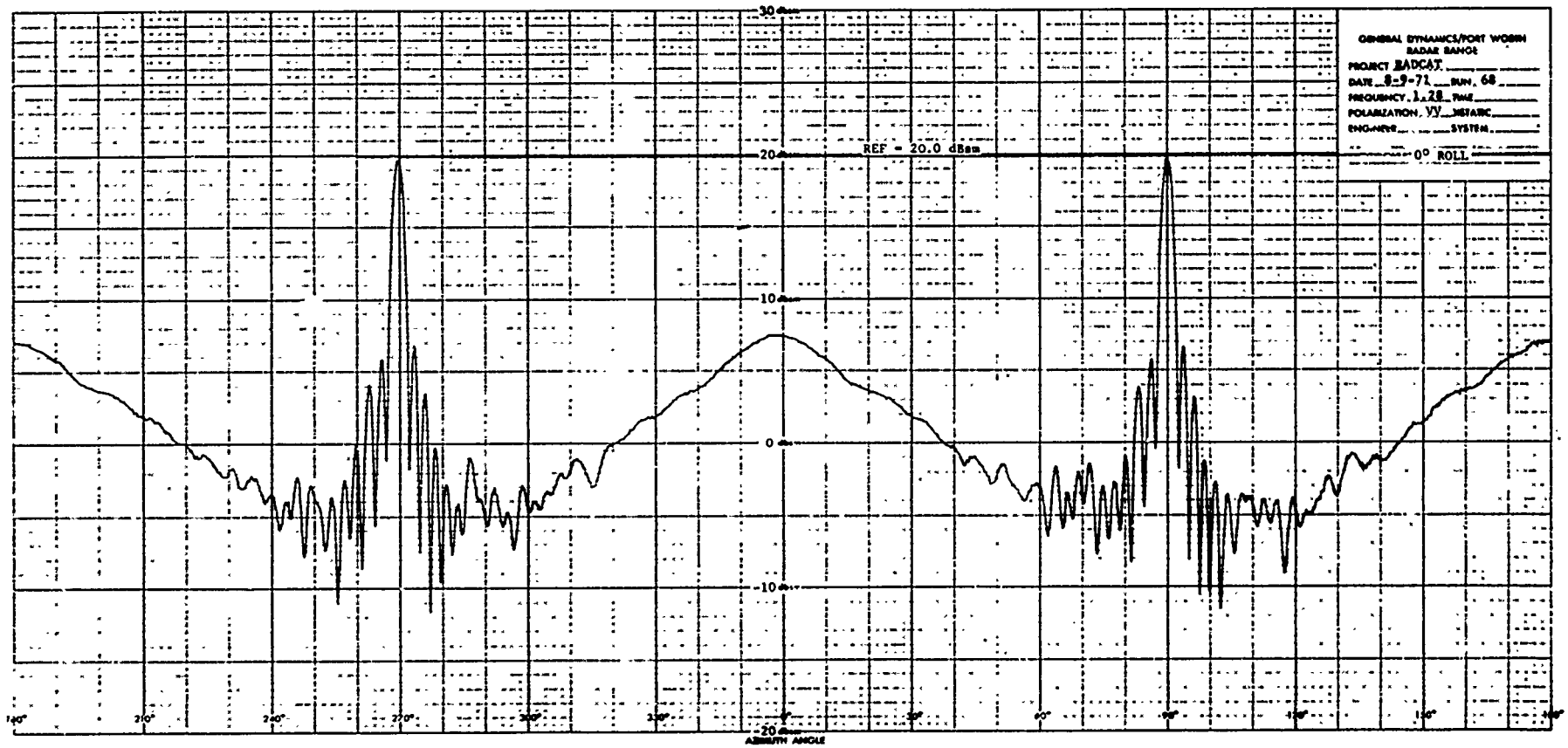

Fig. 3-3 VEHICLE 002 LONG-PULSE AMPLITUDE RESPONSE; L-BAND, VV POLARIZATION, 0-DEGREE ROLL

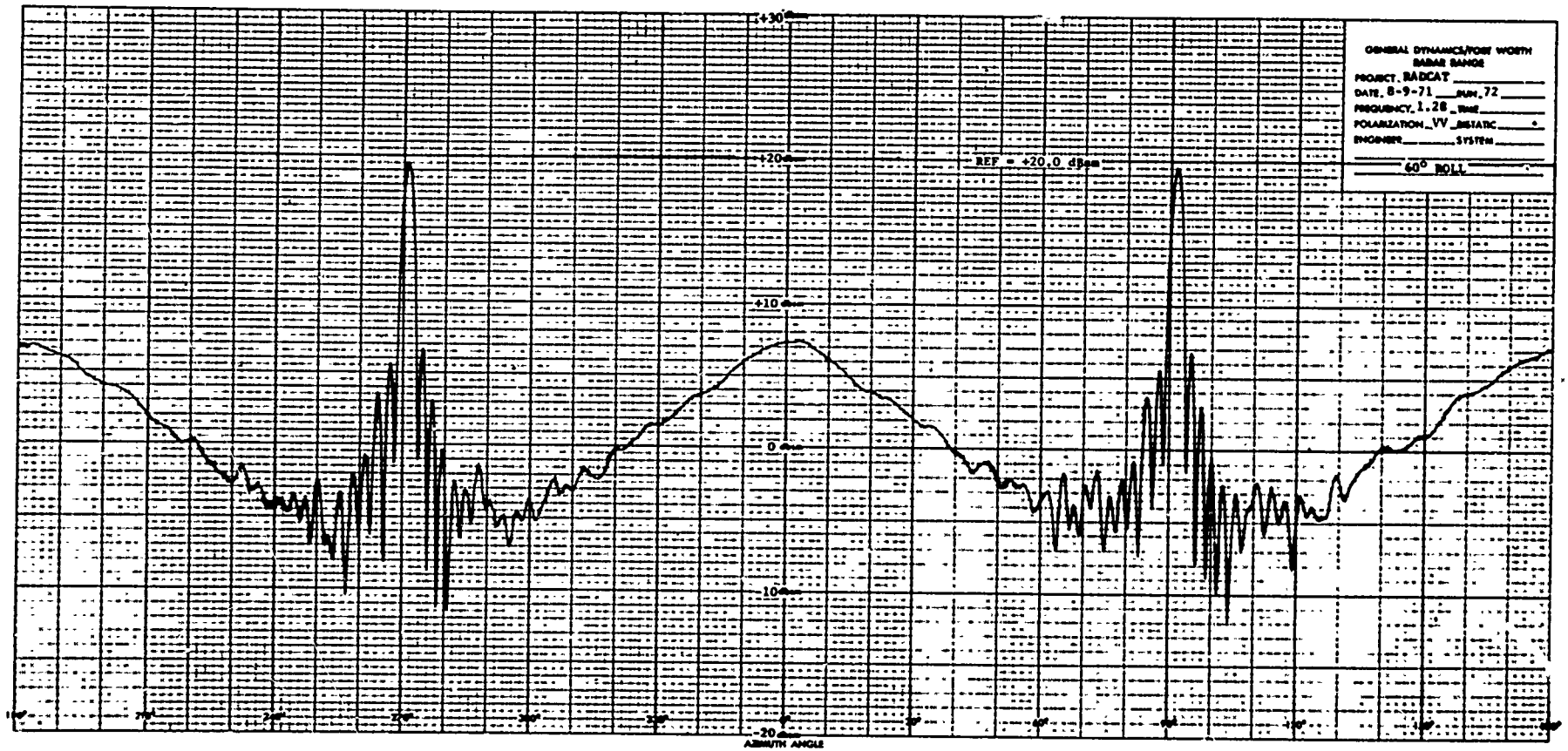

Fig. 3-4 VEHICLE 002 LONG-PULSE AMPLITUDE RESPONSE; L-BAND, VV POLARIZATION, 60-DEGREE ROLL

VEHICLE 001

MATRIX 001a

ROLL ANGLE	POLARIZATION	$\sigma(0^o)$	$\sigma(180^o)$	σ_{bs} (90°)	σ_{bs} (270°)	σ_{s1} (90°)	σ_{s1} (270°)
0°	VV	9.9	9.8	23.3	23.5	9.8	10.2
	HH	10.0	9.8	23.5	24.0	9.8	10.5
	¾ ¾	10.0	9.9	23.8	24.1	10.2	10.4
60°	VV	10.0	10.0	23.9	24.3	10.0	10.5
	HH	9.6	9.5	24.0	23.6	10.3	9.9
	¾ ¾	10.1	10.0	2-.1	24.1	10.3	10.4

MATRIX 001b

ROLL ANGLE	POLARIZATION	$\bar{\sigma}_{oo}$	$\bar{\sigma}_{bs}$	$\bar{\sigma}_{s1}$
0°	VV	9.85	23.4	10.0
	HH	9.9	23.75	10.15
	¾ ¾	9.95	23.95	10.3
60°	VV	10.0	24.1	10.25
	HH	9.55	23.8	10.1
	¾ ¾	10.05	24.1	10.35

MATRIX 001c

POLARIZATION	$\bar{\sigma}_{oo}$	$\bar{\sigma}_{bs}$	$\bar{\sigma}_{s1}$
VV	9.92	23.75	10.13
HH	9.7	23.77	10.12
¾ ¾	10.0	24.0	10.33

MATRIX 001d

$\bar{\sigma}_{oo}$	$\bar{\sigma}_{bs}$	$\bar{\sigma}_{s1}$
9.87	23.84	10.17

VEHICLE 002

MATRIX 002a

ROLL ANGLE	POLARIZATION	$\sigma(0^o)$	$\sigma(180^o)$	σ_{bs} (90°)	σ_{bs} (270°)	σ_{s1} (90°)	σ_{s1}(270°)
0°	VV	7.4	7.0	19.6	19.6	6.1	6.3
	HH	7.4	6.9	19.4	19.3	6.4	6.2
	¾ ¾	7.0	6.8	19.2	19.2	6.2	6.0
60°	VV	7.3	6.9	19.5	19.5	6.15	6.1
	HH	7.3	6.7	19.7	19.9	6.3	6.4
	¾ ¾	7.4	7.15	19.6	19.6	6.4	6.3

MATRIX 002b

ROLL ANGLE	POLARIZATION	$\bar{\sigma}_{oo}$	$\bar{\sigma}_{bs}$	$\bar{\sigma}_{s1}$
0°	VV	7.2	19.6	6.2
	HH	7.15	19.35	6.3
	¾ ¾	6.9	19.2	6.1
60°	VV	7.1	19.5	6.1
	HH	7.0	19.8	6.35
	¾ ¾	7.23	19.6	6.35

MATRIX 002c

POLARIZATION	$\bar{\sigma}_{oo}$	$\bar{\sigma}_{bs}$	$\bar{\sigma}_{s1}$
VV	7.15	19.55	6.15
HH	7.07	19.57	6.33
¾ ¾	7.06	19.4	6.22

MATRIX 002d

$\bar{\sigma}_{oo}$	$\bar{\sigma}_{bs}$	$\bar{\sigma}_{s1}$
7.09	19.51	6.23

Fig. 3-5 COMPARISON BETWEEN 001 AND 002 DOMINANT SCATTERING CHARACTERISTICS; L-BAND

broadside, and (first) sidelobe level such that each particular polarization and roll angle response is listed independently. Matrix 001(b) presents the average end-on, broadside, and sidelobe levels for each polarization and roll angle eliminated, and matrix 001(d) presents the average with polarization eliminated. A similar succession of data collapsing is presented for the L-Band response of vehicle 002.

The L-Band data illustrated in Figure 3-5 may be summarized as follows:

1) The dominant scattering characteristics of each vehicle are essentially independent of polarization (VV, HH, $\pi/4$ $\pi/4$)
2) The dominant scattering characteristics of each vehicle are essentially independent of roll angle
3) Vehicle 002 is characterized by a response at 0-degree aspect angle which is higher than that at 180-degree aspect angle by approximately 0.4 dBsm
4) The average end-on, broadside, and (first) sidelobe response of vehicle 001 exceeds that of vehicle 002 by 2.8, 4.3 and 3.9 dBsm respectively
5) The response from each vehicle is symmetric about either broadside orientation
6) The response from each vehicle is symmetric about either end-on orientation.

3.2.2 S-Band Long-Pulse Measurements

The signatures contained in Figure 3-6 and 3-7 correspond to the measured response of vehicles 001 and 002 respectively at a measured frequency of 2.85 gigahertz. The data in each figure represents the response at vertical polarization and 0-degree target roll angle. Reference to the signatures presented in Section 2 and Appendix D for the response at HH and $\pi/4$ $\pi/4$ polarization and the response at 60-degree target roll angle will reveal that the data contained in Figures 3-6 and 3-7 are typical for the two vehicles at S-band.

The S-band data presented in Figure 3-8 is of the same format as the L-band data in Figure 3-5. A summarization of the dominant scattering characteristics follows:

1) The dominant scattering characteristics of each vehicle are essentially independent of polarization(VV, HH, $\pi/4$ $\pi/4$)
2) The dominant scattering characteristics of each vehicle are essentially independent of roll angle.
3) Each vehicle is characterized by a response at 0-degree aspect angle which is higher than that measured at the 180-degree aspect angle by $\sim$ 0.9 dBsm in the case of vehicle 001 and $\sim$ 0.7 dBsm in the case of vehicle 002
4) The average end-on, broadside, and (first) sidelobe response of vehicle 001 exceeds that of vehicle 002 by 1.5, 2.7, and 1.8 dBsm, respectively

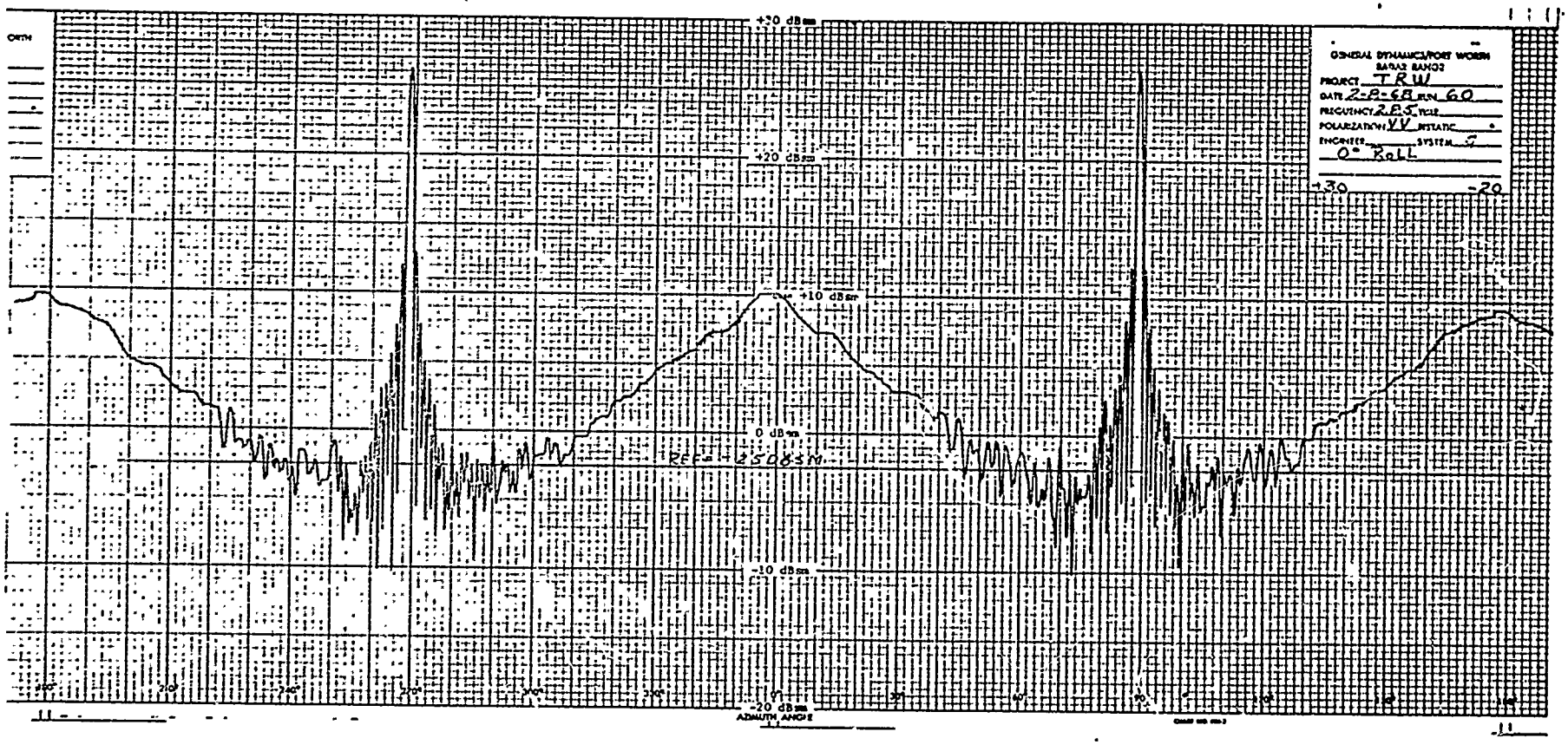

Fig. 3-6 VEHICLE 001 LONG-PULSE AMPLITUDE; S-BAND, VV POLARIZATION, 0-DEGREE ROLL

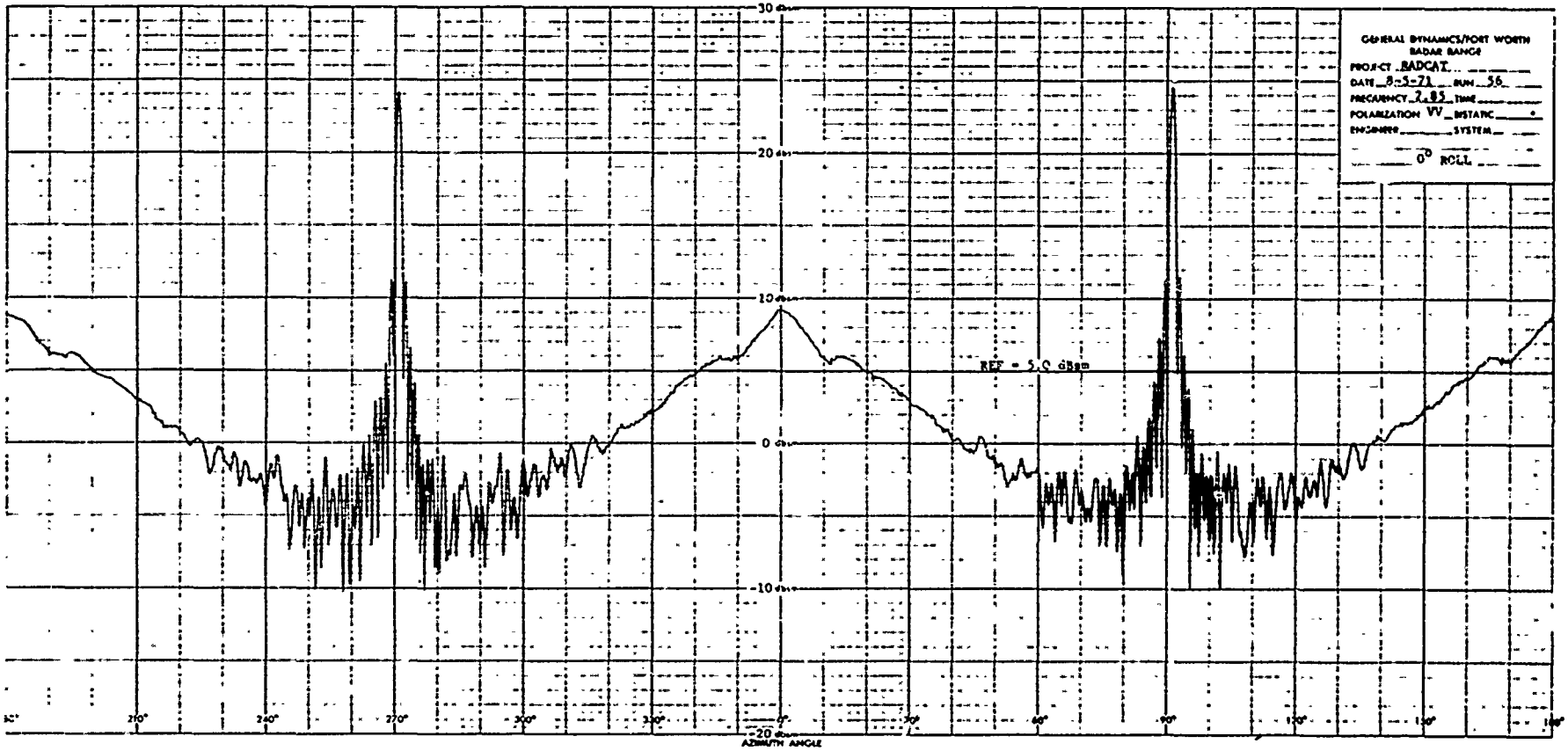

Fig. 3-7 VEHICLE 002 AMPLITUDE RESPONSE; S-BAND VV POLARIZATION, 0-DEGREE ROLL

VEHICLE 001

MATRIX 001a

ROLL ANGLE	POLARIZATION	$\sigma(0^o)$	$\sigma(180^o)$	$\sigma_{bs}(90^o)$	$\sigma_{bs}(270^o)$	$\sigma_{s1}(90^o)$	$\sigma_{s1}(270^o)$
0^o	VV	10.0	9.5	26.4	26.2	12.25	12.45
	HH	10.1	9.05	26.2	26.2	12.35	12.35
	$\pi/4$ $\pi/4$	10.5	9.5	26.6	26.6	12.85	13.05
60^o	VV	10.3	9.6	26.3	26.2	12.25	12.25
	HH	10.8	9.6	26.8	26.8	12.95	12.9
	$\pi/4$ $\pi/4$	10.8	9.9	26.8	26.8	13.0	13.15

MATRIX 001b

ROLL ANGLE	POLARIZATION	$\bar{\sigma}_{\perp\perp}$	$\bar{\sigma}_{\parallel\parallel}$	$\bar{\sigma}_{\perp\parallel}$
0^o	VV	9.75	26.3	12.35
	HH	9.6	26.2	12.35
	$\pi/4$ $\pi/4$	10.0	26.6	12.92
60^o	VV	9.95	26.25	12.25
	HH	10.2	26.8	12.95
	$\pi/4$ $\pi/4$	10.35	26.8	13.07

MATRIX 001c

POLARIZATION	$\bar{\sigma}_{\perp\perp}$	$\bar{\sigma}_{\parallel\parallel}$	$\bar{\sigma}_{\perp\parallel}$
VV	9.85	26.28	12.3
HH	9.9	26.5	12.65
$\pi/4$ $\pi/4$	10.17	26.7	13.0

MATRIX 001d

$\bar{\sigma}_{\perp\perp}$	$\bar{\sigma}_{\parallel\parallel}$	$\bar{\sigma}_{\perp\parallel}$
9.97	26.49	12.65

VEHICLE 002

MATRIX 002a

ROLL ANGLE	POLARIZATION	$\sigma(0^o)$	$\sigma(180^o)$	$\sigma_{bs}(90^o)$	$\sigma_{bs}(270^o)$	$\sigma_{s1}(90^o)$	$\sigma_{s1}(270^o)$
0^o	VV	9.2	8.7	24.5	24.1	11.45	11.2
	HH	8.6	7.8	23.7	23.5	10.75	10.7
	$\pi/4$ $\pi/4$	8.3	7.65	23.2	23.2	10.1	10.3
60^o	VV	9.1	8.4	23.9	23.9	10.85	11.0
	HH	9.0	8.25	23.9	23.7	10.75	11.0
	$\pi/4$ $\pi/4$	9.0	8.2	23.8	23.9	10.8	11.0

MATRIX 002b

ROLL ANGLE	POLRIZATION	$\bar{\sigma}_{\perp\perp}$	$\bar{\sigma}_{\parallel\parallel}$	$\bar{\sigma}_{\perp\parallel}$
0^o	VV	8.95	24.3	11.33
	HH	8.2	23.6	10.73
	$\pi/4$ $\pi/4$	7.95	23.2	10.2
60^o	VV	8.75	23.9	10.95
	HH	8.62	23.8	10.87
	$\pi/4$ $\pi/4$	8.6	23.8	10.9

MATRIX 002c

FOLARIZATION	$\bar{\sigma}_{\perp\perp}$	$\bar{\sigma}_{\parallel\parallel}$	$\bar{\sigma}_{\perp\parallel}$
VV	8.85	24.1	11.13
HH	8.41	23.7	10.8
$\pi/4$ $\pi/4$	8.28	23.5	10.55

MATRIX 002d

$\bar{\sigma}_{\perp\perp}$	$\bar{\sigma}_{\parallel\parallel}$	$\bar{\sigma}_{\perp\parallel}$
8.51	23.7	10.83

Fig. 3-8 COMPARISON BETWEEN 001 AND 002 DOMINANT SCATTERING CHARACTERISTICS; S-BAND

5) The response from each vehicle is symmetric about either broadside orientation

6) The response from only vehicle 002 is symmetric about either end-on orientation.

3.2.3 C-Band Long-Pulse Measurements

The signatures contained in Figures 3-9 and 3-10 correspond to the measured response of vehicles 001 and 002 respectively at a measurement frequency of 5.65 gigahertz. The data in each figure represents the response at vertical polarization and 0-degree target roll angle. Reference to Appendix D and the signatures presented in Section 2 will reveal that these data are typical for the two vehicles at C-band.

The C-band data presented in Figure 3-11 is of the same format as the S-band data in Figure 3-8. Summarization of the dominant scattering characteristics is as follows:

1) The dominant scattering characteristics of each vehicle are essentially independent of polarization (VV, HH, $\pi/4$ $\pi/4$)

2) The dominant scattering characteristics of each vehicle are essentially independent of roll angle

3) Each vehicle is characterized by a response at 0-degree aspect angle which is higher than that measured at the 180-degree aspect angle by $\sim$ 2.2dBsm in the case of vehicle 001, and by $\sim$ 0.7dBsm in the case of vehicle 002

4) The average end-on, broadside, and (first) sidelobe responds of vehicle 001 exceed the corresponding levels associated with vehicle 002 by 1.2, 4.5, and 2.7dBsm respectively.

5) The response from each vehicle is symmetric about either broadside orientation.

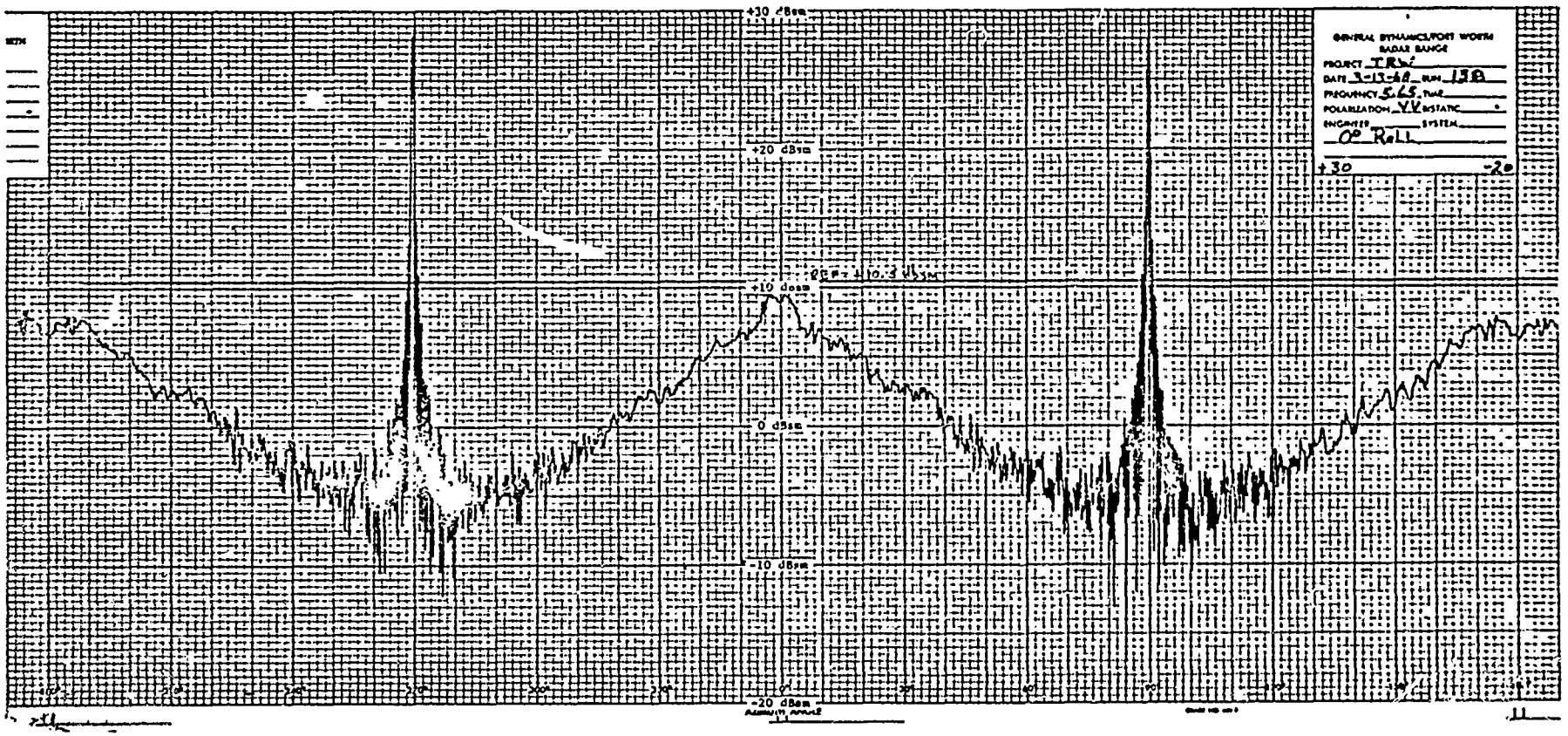

Fig. 3-9 VEHICLE 001 LONG-PULSE AMPLITUDE; C-BAND, VV POLARIZATION, 0-DEGREE ROLL

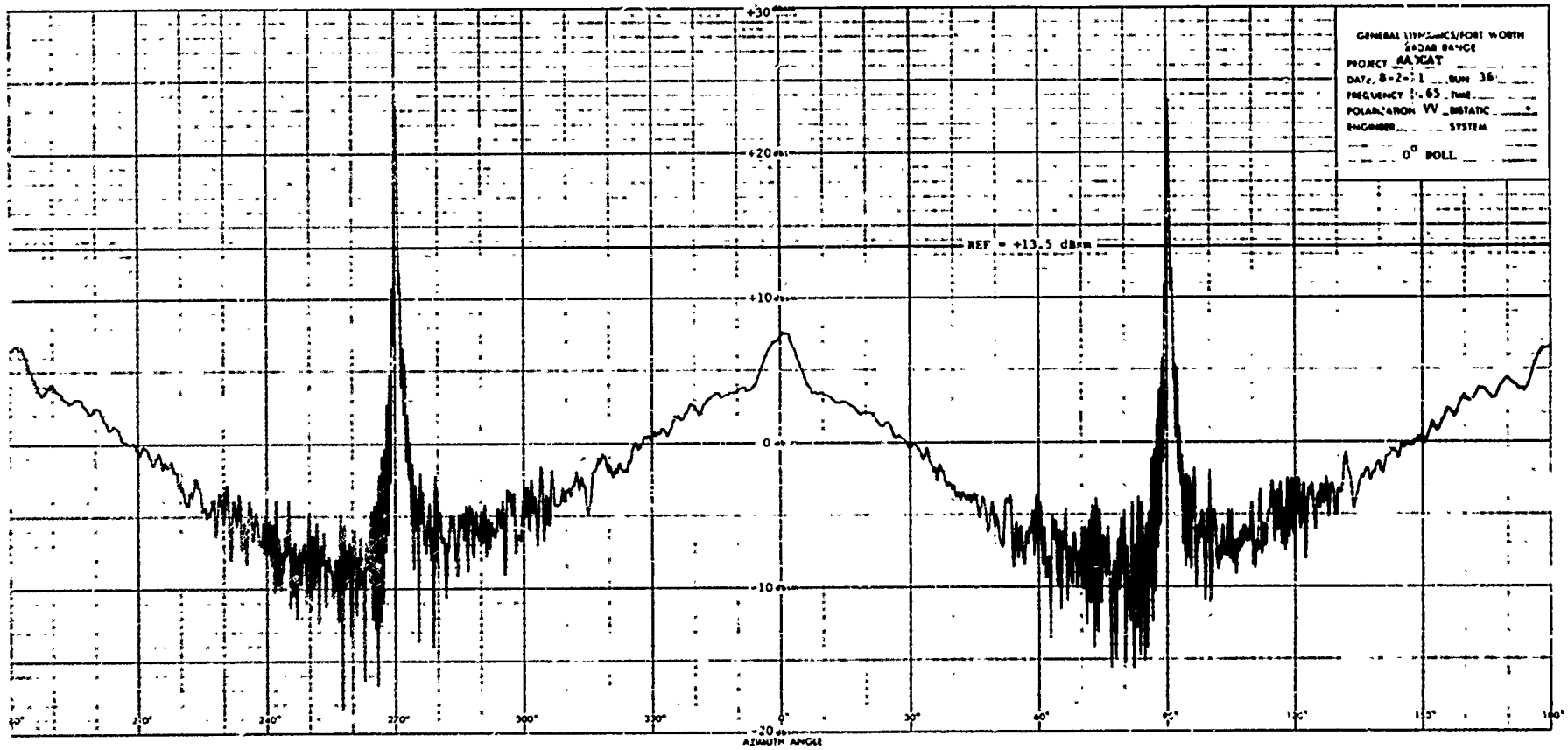

Fig. 3-10 VEHICLE 002 AMPLITUDE RESPONSE; C-BAND, VV POLARIZATION, 0-DEGREE ROLL

VEHICLE 001

MATRIX 001a

ROLL ANGLE	POLARIZATION	$\sigma(0^o)$	$\sigma(180^o)$	$\sigma_{bs}(90^o)$	$\sigma_{bs}(270^o)$	$\sigma_{s1}(90^o)$	$\sigma_{s1}(270^o)$
0^o	VV	9.2	7.2	28.0	28.2	13.75	13.95
	HH	9.4	7.4	28.0	28.0	14.0	13.8
	$\pi/4$ $\pi/4$	9.0	7.1	27.8	28.0	13.85	13.55
60^o	VV	9.6	7.0	27.4	27.6	13.7	14.2
	HH	10.2	7.4	27.8	27.9	13.8	14.7
	$\pi/4$ $\pi/4$	10.4	7.5	28.2	27.9	14.45	14.65

MATRIX 001b

ROLL ANGLE	POLARIZATION	$\bar{\sigma}_{vv}$	$\bar{\sigma}_{hh}$	$\bar{\sigma}_{ii}$
0^o	VV	8.2	28.1	13.95
	HH	8.4	28.0	13.9
	$\pi/4$ $\pi/4$	8.05	27.9	13.7
60^o	VV	8.3	27.5	13.95
	HH	8.4	28.0	14.25
	$\pi/4$ $\pi/4$	8.05	28.05	14.55

MATRIX 001c

POLARIZATION	$\bar{\sigma}_{vv}$	$\bar{\sigma}_{hh}$	$\bar{\sigma}_{ii}$
VV	8.25	27.6	13.90
HH	8.6	27.92	14.05
$\pi/4$ $\pi/4$	8.5	27.97	14.15

MATRIX 001d

$\bar{\sigma}_{vv}$	$\bar{\sigma}_{hh}$	$\bar{\sigma}_{ii}$
8.45	27.89	14.03

VEHICLE 002

MATRIX 002a

ROLL ANGLE	POLARIZATION	$\sigma(0^o)$	$\sigma(180^o)$	$\sigma_{bs}(90^o)$	$\sigma_{bs}(270^o)$	$\sigma_{s1}(90^o)$	$\sigma_{s1}(270^o)$
0^o	VV	7.5	6.7	23.6	23.8	11.5	11.35
	HH	7.2	6.9	23.9	23.4	11.75	11.0
	$\pi/4$ $\pi/4$	8.2	7.25	23.6	24.3	11.15	11.5
60^o	VV	7.2	6.65	23.5	23.4	11.6	10.75
	HH	7.1	6.55	23.4	23.2	10.95	11.0
	$\pi/4$ $\pi/4$	8.2	7.6	24.7	24.3	11.85	11.9

MATRIX 002b

ROLL ANGLE	POLARIZATION	$\bar{\sigma}_{vv}$	$\bar{\sigma}_{hh}$	$\bar{\sigma}_{ii}$
0^o	VV	7.1	23.7	11.42
	HH	7.05	23.65	11.37
	$\pi/4$ $\pi/4$	7.7	23.95	11.32
60^o	VV	6.87	23.45	11.25
	HH	6.77	23.3	10.97
	$\pi/4$ $\pi/4$	7.95	24.5	11.88

MATRIX 002c

POLARIZATION	$\bar{\sigma}_{vv}$	$\bar{\sigma}_{hh}$	$\bar{\sigma}_{ii}$
VV	7.02	23.57	11.33
HH	6.91	23.48	11.17
$\pi/4$ $\pi/4$	7.77	24.23	11.63

MATRIX 002d

$\bar{\sigma}_{vv}$	$\bar{\sigma}_{hh}$	$\bar{\sigma}_{ii}$
7.24	23.43	11.38

Fig. 3-11 COMPARISON BETWEEN 001 AND 002 DOMINANT SCATTERING CHARACTERISTICS; L-BAND

6) The response from only vehicle 002 is symmetric about either end-on orientation.

3.2.4 Comparison Overview

The data presented in Figures 3-5, 3-8, and 3-11 and their respective summaries have been consolidated in Table 3-1 for ease in interpretation. Pertinent entries in this table are related to (1) the sensitivity of the response of each vehicle to changes in polarization and roll angle, (2) the degree to which each separate vehicle exhibits pattern and amplitude symmetry about end-on and broadside orientations, and (3) the amount by which the dominant response characteristics of vehicle 001 exceed those of vehicle 002.

3.3 SUPPLEMENTARY COMPARISON THROUGH USE OF FULL-SCALE COMPUTED AND 1/2-SCALE MEASURED SIGNATURES

In addition to comparing the measured signatures of vehicle 002 with those of vehicle 001, it was desirable to establish a common denominator to which the response from each vehicle could be compared separately. Two sources of data were organized for this purpose. The computed response based on the use of physical optics formed one source of signatures for comparison with full scale perfectly conducting model of the RADCAT vehicle formed the second source. The measurements which were performed on the 1/2-scale model were conducted furing 1967 by General Dynamics under subcontract to TRW Systems (Reference 2).

Table 3.1 SUMMARY OF VEHICLE 001/002 COMPARISON

3-1a INDIVIDUAL PROPERTIES

FREQ GHz	VEHICLE	POLARIZATION SENSITIVITY	ROLL ANGLE SENSITIVITY	END-ON SYMMETRY		BROADSIDE SYMMETRY	
				PATTERN	$\Delta\sigma$(dBsm)	PATTERN	$\Delta\sigma$(dBsm)
1.28	001	NONE	NONE	YES	0	YES	0
	002	NONE	NONE	YES	0.4	YES	0
2.85	001	NONE	NONE	NO	0.9	YES	0
	002	NONE	NONE	YES	0.7	YES	0
5.65	001	NONE	NONE	NO	2.2	YES	0
	002	NONE	NONE	YES	0.7	YES	0

3-1b COMPARATIVE PROPERTIES

FREQUENCY GHz	AVERAGE END-ON RESPONSE	AVERAGE BROADSIDE RESPONSE	AVERAGE (FIRST) SIDELOBE RESPONSE
	VEHICLE 001 EXCEEDS VEHICLE 002 BY		
1.28	2.8 dBsm	4.3 dBsm	3.9 dBsm
2.85	1.5 dBsm	2.7 dBsm	1.8 dBsm
5.65	1.2 dBsm	4.5 dBsm	2.7 dBsm

Figures 3-12 through 3-14 contain the radar cross section amplitude and phase as computed by use of the physical optics radar approximation for frequencies of 1.28, 2.85, and 5.65 gigahertz respectively. Attention is called to the fact that $\epsilon^{+j\omega t}$ was used as the theoretical reference in computing the scattered phase whereas the measurement of scattered phase is based on the assumption of an $\epsilon^{-j\omega t}$ harmonic time-variation. As a consequence, the computed phase variations will appear reversed from those acquired through measurements. The reader is referred to Appendix E for details of the physical optics formulation.

Figures 3-15 through 3-17 contain the measured response (at VV polarization) of the 1/2-scale model of the RADCAT vehicle at frequencies of 2.56, 5.7, and 11.3 gigahertz respectively. With the addition of 6-dB to each signature illustrated, these data may be made to correspond to full scale signatures at 1.28, 2.85, and 5.65 gigahertz, respectively. A summarization is presented in Figure 3-18 of the end-on, broadside, and (first) side-lobe levels in a format consistent with that used for vehicles 001 and 002. Reference is made to Appendix F for the signatures of this model corresponding to measurements at HH and $\pi/4$ $\pi/4$ polarization.

Four significant observations may be made regarding the computed signatures and those corresponding to measurements performed on the perfectly conducting RADCAT model.

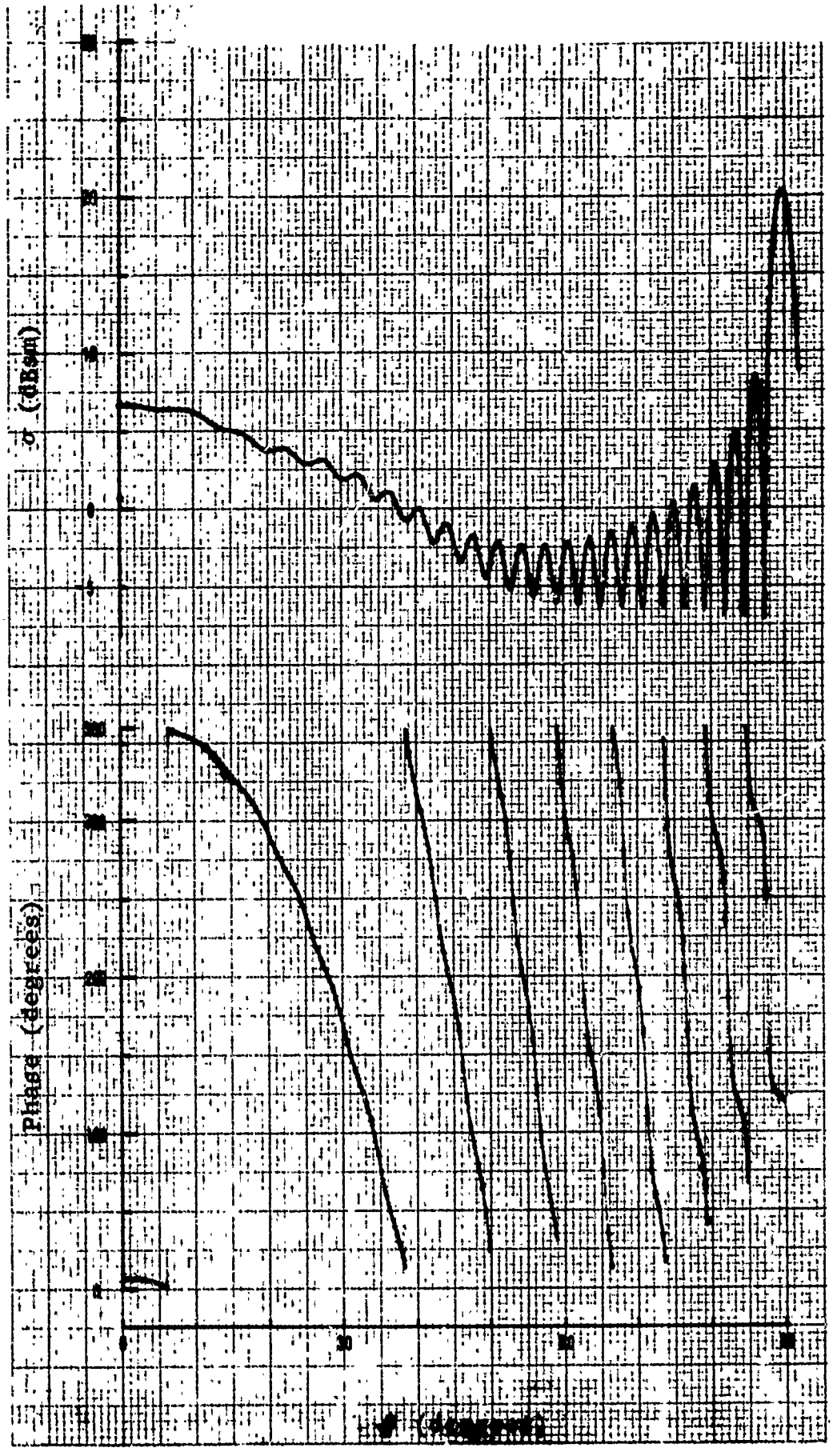

Fig. 3-12 COMPUTED LONG-PULSE RESPONSE: 1.28 GHz

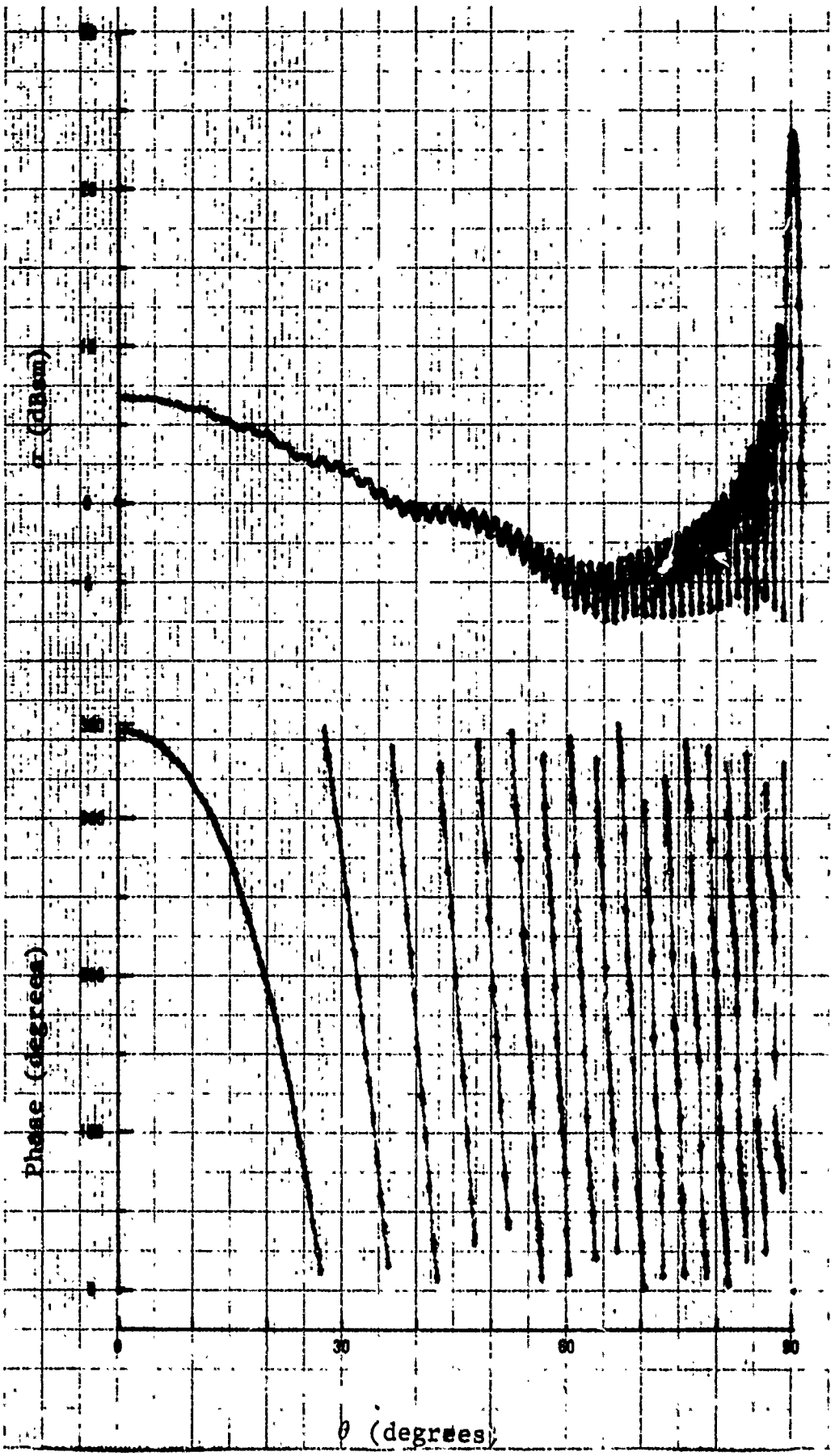

Fig. 3-13 COMPUTED LONG-PULSE RESPONSE; 2.85 GHz

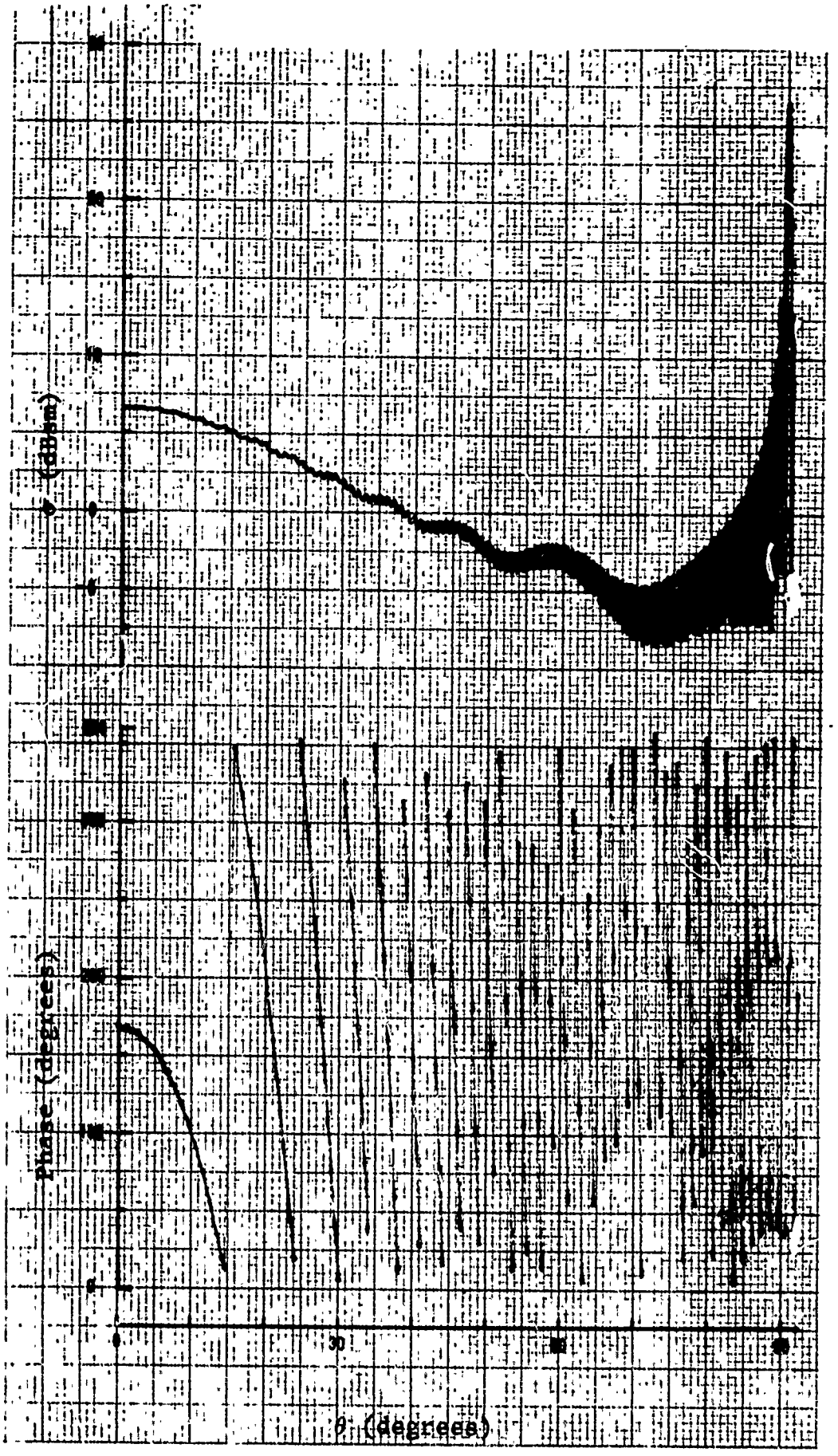

Fig. 3-14 COMPUTED LONG-PULSE RESPONSE; 5.65 GHz

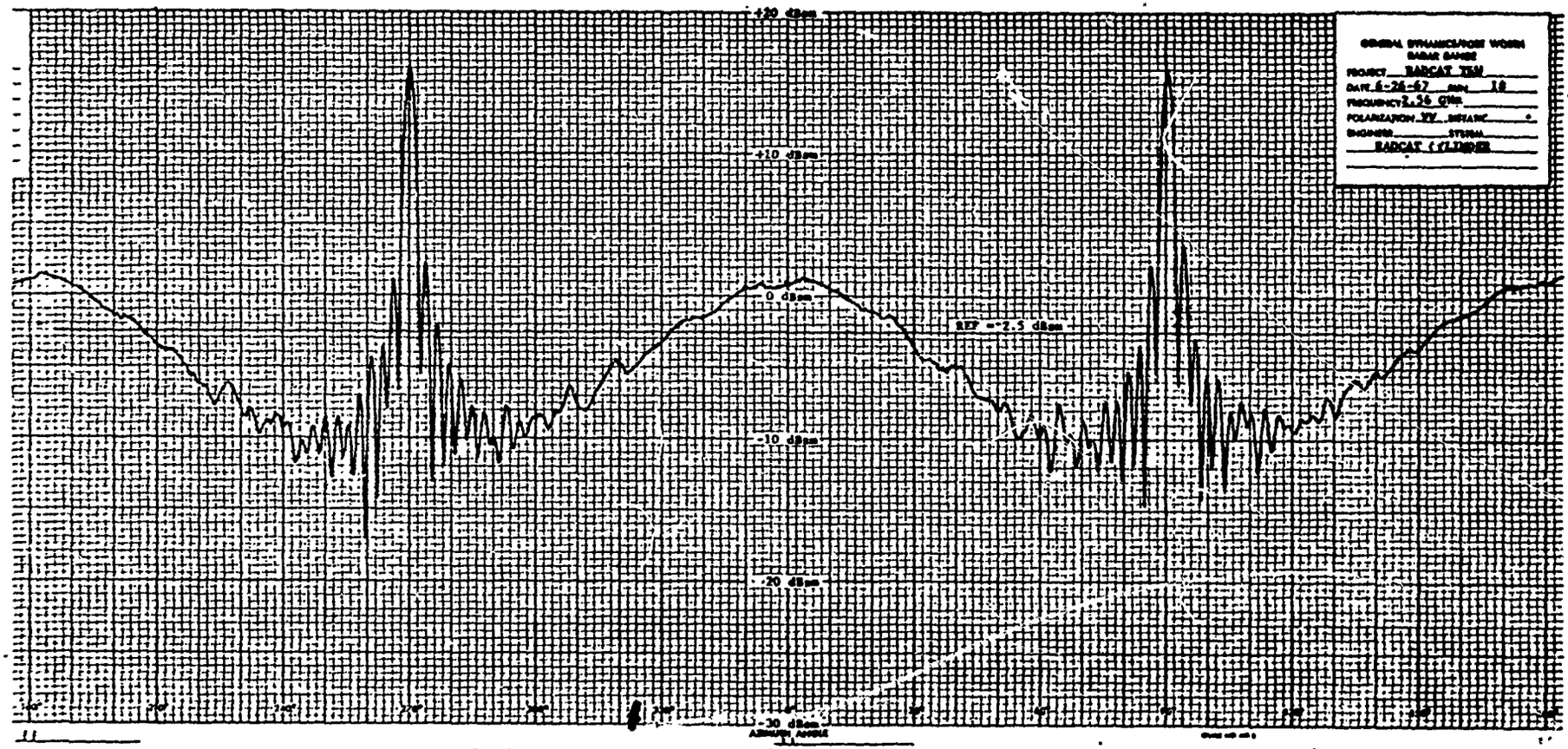

Fig. 3-15 HALF-SCALE MODEL MEASUREMENTS; S-BAND

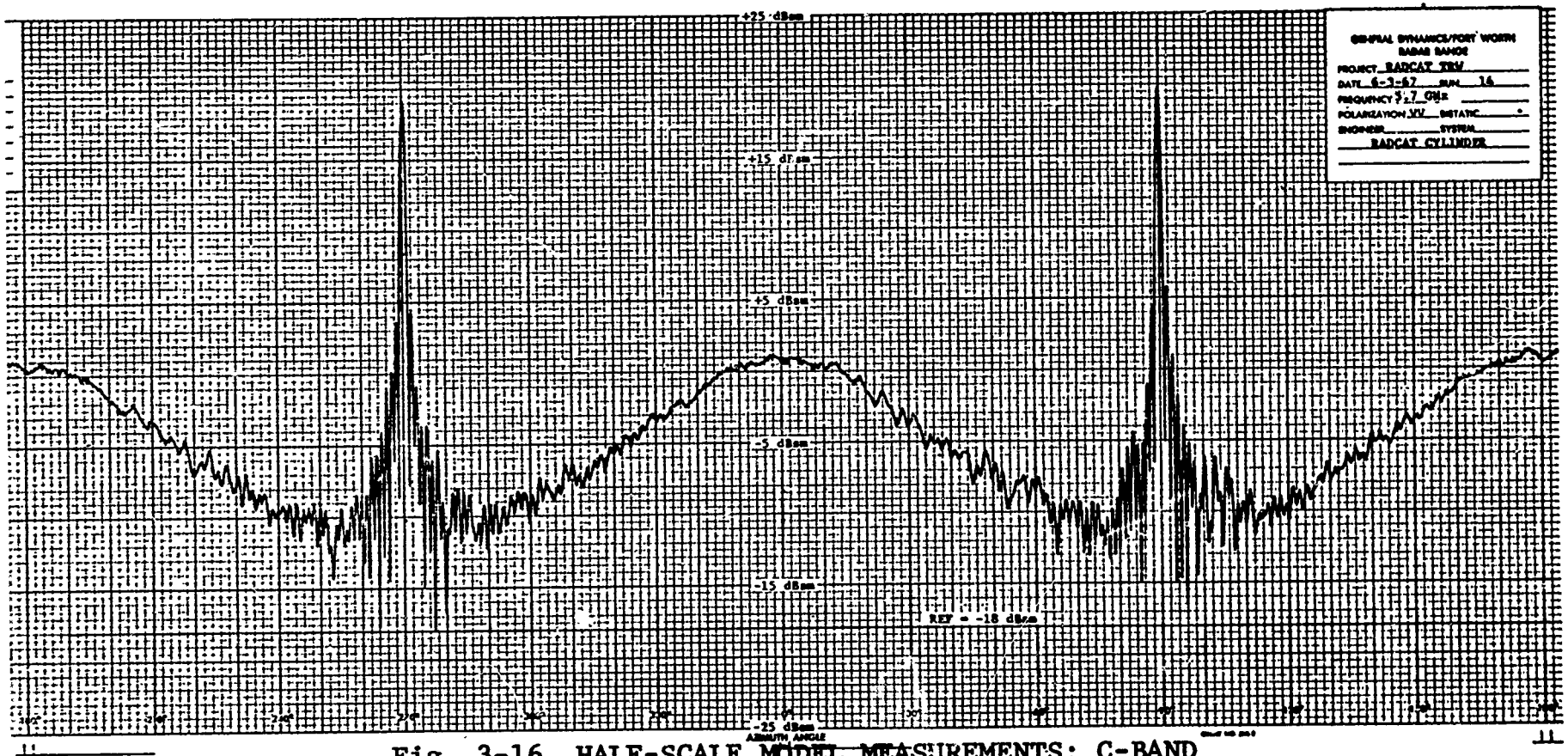

Fig. 3-16 HALF-SCALE MODEL MEASUREMENTS; C-BAND

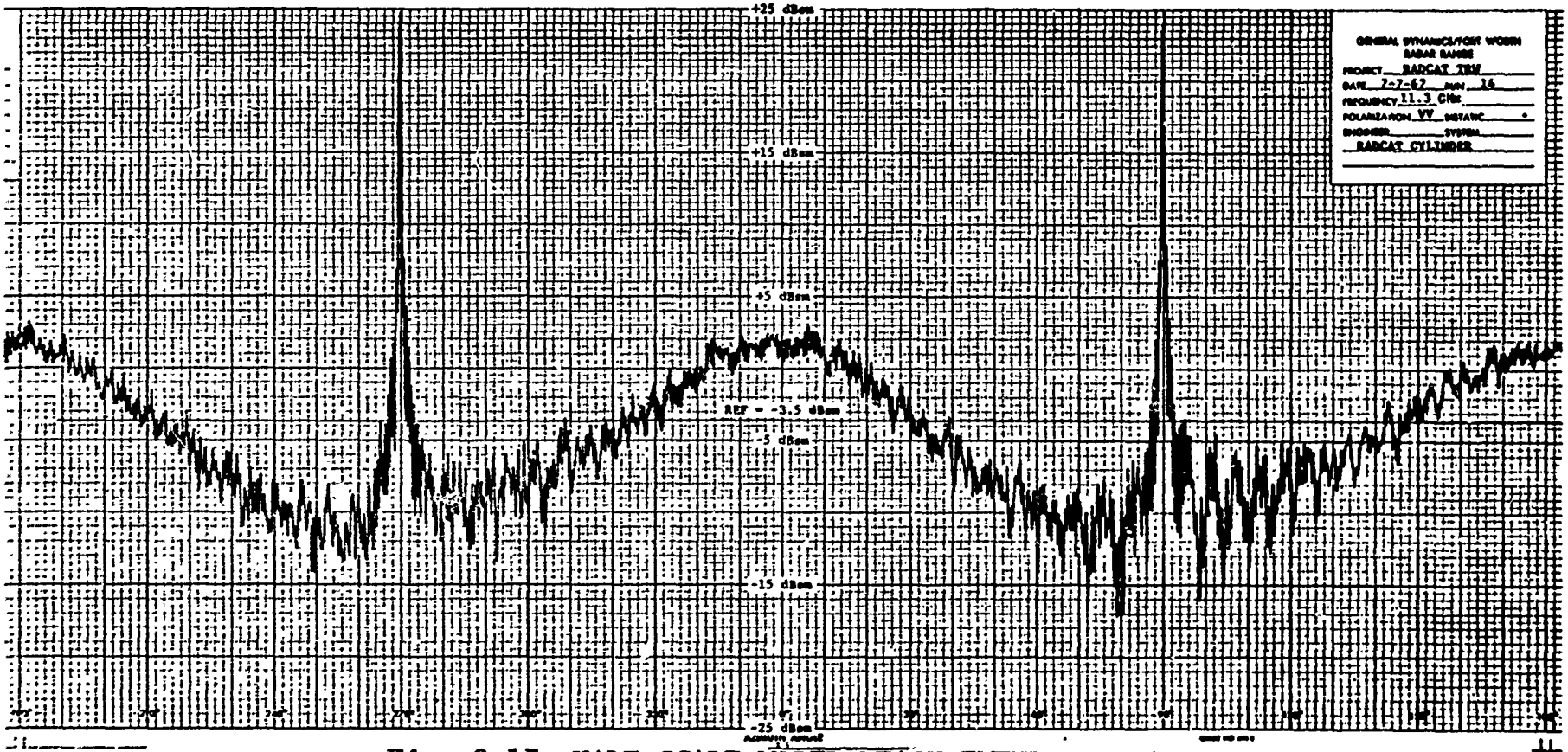

Fig. 3-17 HALF-SCALE MODEL MEASUREMENTS; X-BAND

FREQUENCY GHz	POLARIZATION	$\sigma(0^o)$	$\sigma(180^o)$	$\sigma_{bs}(90^o)$	$\sigma_{bs}(270^o)$	$\sigma_{s1}(90^o)$	$\sigma_{s1}(270^o)$
11.3	VV	1.5	1.5	24.0	24.6	8.1	7.0
	HH	0.4	0.2	23.0	23.0	6.5	5.5
	$\pi/4$ $\pi/4$	0.6	0.4	23.4	23.8	7.15	6.0
5.7	VV	0.6	0.6	19.8	19.2	4.9	3.5
	HH	0.6	0.6	19.7	19.5	5.2	4.5
	$\pi/4$ $\pi/4$	0.3	0.2	19.0	18.8	4.6	5.1
2.56	VV	0.8	1.1	16.0	16.0	2.9	1.7
	HH	1.5	1.5	16.6	16.8	3.3	2.2
	$\pi/4$ $\pi/4$	1.4	1.6	16.5	16.5	3.45	2.1

1/2-SCALE

FREQUENCY GHz	$\overline{\sigma}_{eo}$	$\overline{\sigma}_{bs}$	$\overline{\sigma}_{sl}$
11.3	0.76	23.6	6.71
5.7	0.48	19.33	4.63
2.56	1.31	16.4	2.61

FULL-SCALE

FREQUENCY GHz	$\overline{\sigma}_{eo}$	$\overline{\sigma}_{bs}$	$\overline{\sigma}_{sl}$
5.65	6.76	29.6	12.71
2.85	6.48	25.3	10.63
1.28	7.31	22.4	8.61

Fig. 3-18 SUMMARY OF 1/2-SCALE MODEL MEASUREMENTS

1) The measured end-on response is in excellent agreement with the calculated end-on response at all three frequencies. Inherent in this observation is the fact that the end-on return from the 2:1 oblate spheroidal cap is independent of frequency.

2) Neither the computed nor measured return from the aspect sector near end-on (0- to 40-degrees in aspect) exhibited any irregular lobing feature which might suggest complex scattering from this region.

3) The measured first sidelobe peak is in excellent agreement with the computed response with a maximum deviation of 1.1 dB occurring at 5.65 ghz.

4) Although only fair agreement exists between the measured and computed amplitude at broadside, the increase in the measured broadside amplitude with increase in measurement frequency is in very good agreement with the computed response. That is $\sigma_{bs}^{f_2} \approx \sigma_{bs}^{f_1} + 10\log(f_2/f_1)$

Figures 3-19 through 3-21 contain the L-, S-, and C-Band response of vehicle 001 at vertical polarization. The median cross section amplitude response of the scale model has been superimposed on each figure for comparison. Similar data for the case of vehicle 002 are shown in Figures 3-22 through 3-24 for comparison.

The reason for presenting the supplementary comparison between the RADCAT vehicles and (1) the calculated response based on physical

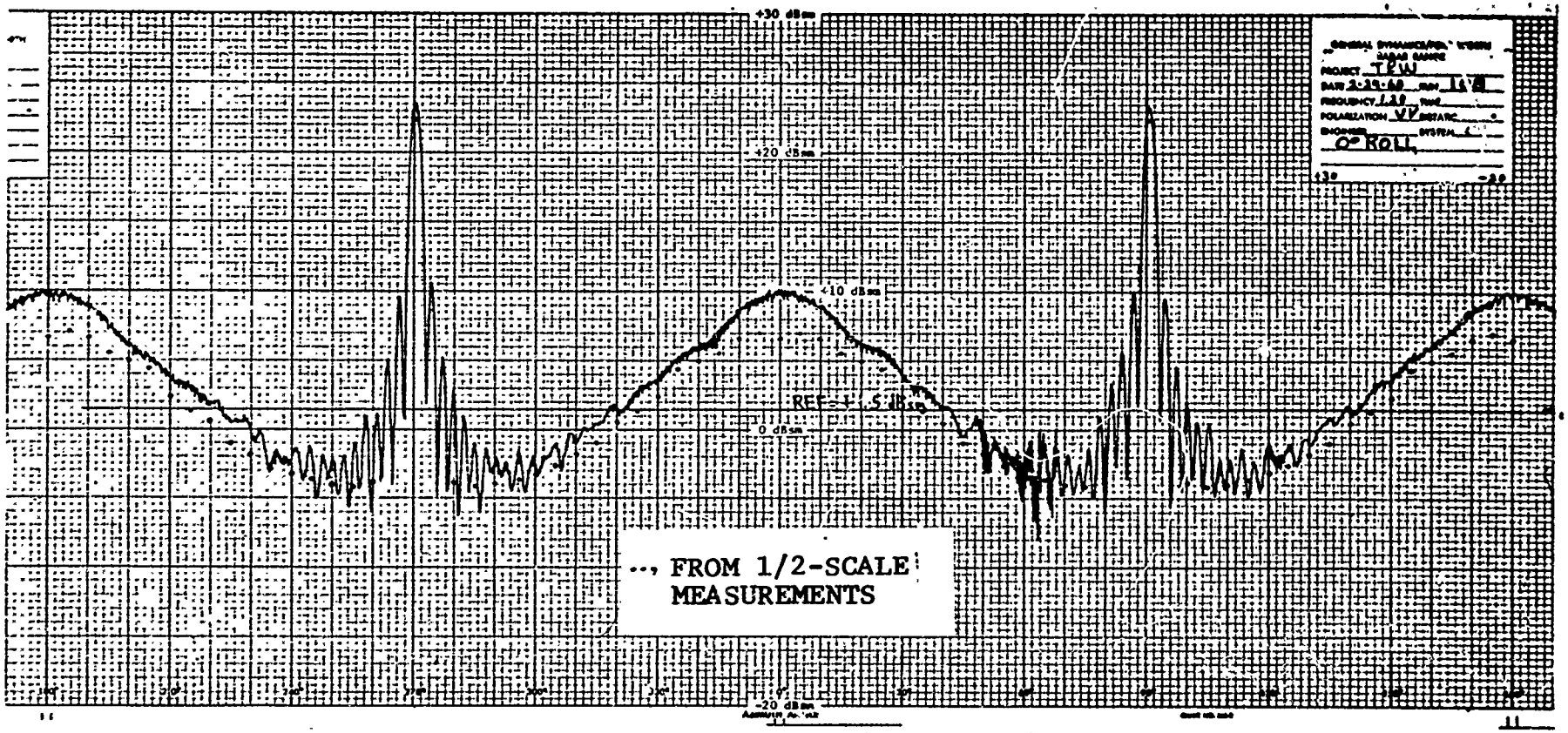

Fig. 3-19 COMPARISON BETWEEN VEHICLE 001 AND 1/2-SCALE MODEL MEASUREMENTS; L-BAND

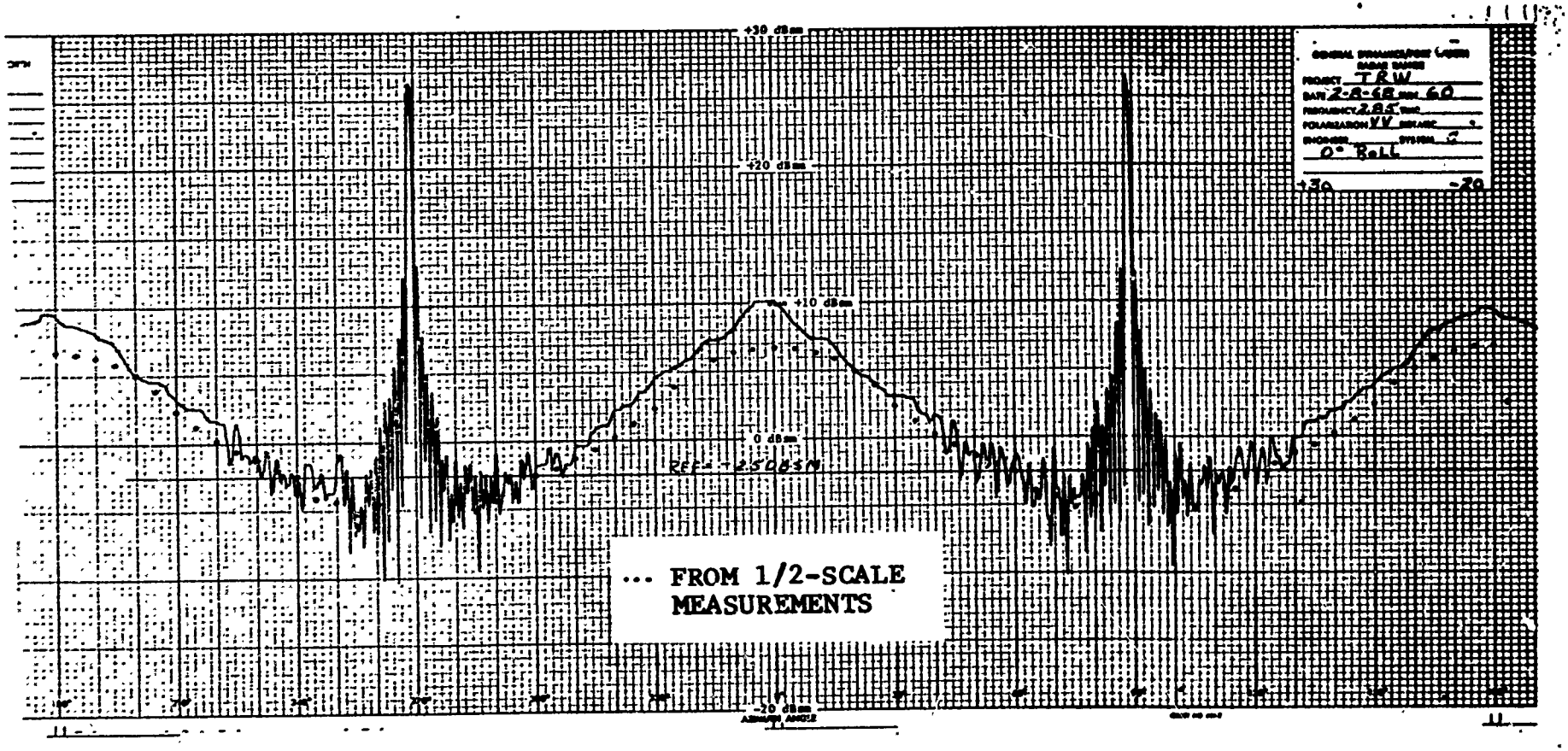

Fig. 3-20 COMPARISON BETWEEN VEHICLE 001 AND 1/2-SCALE MODEL MEASUREMENTS; S-BAND

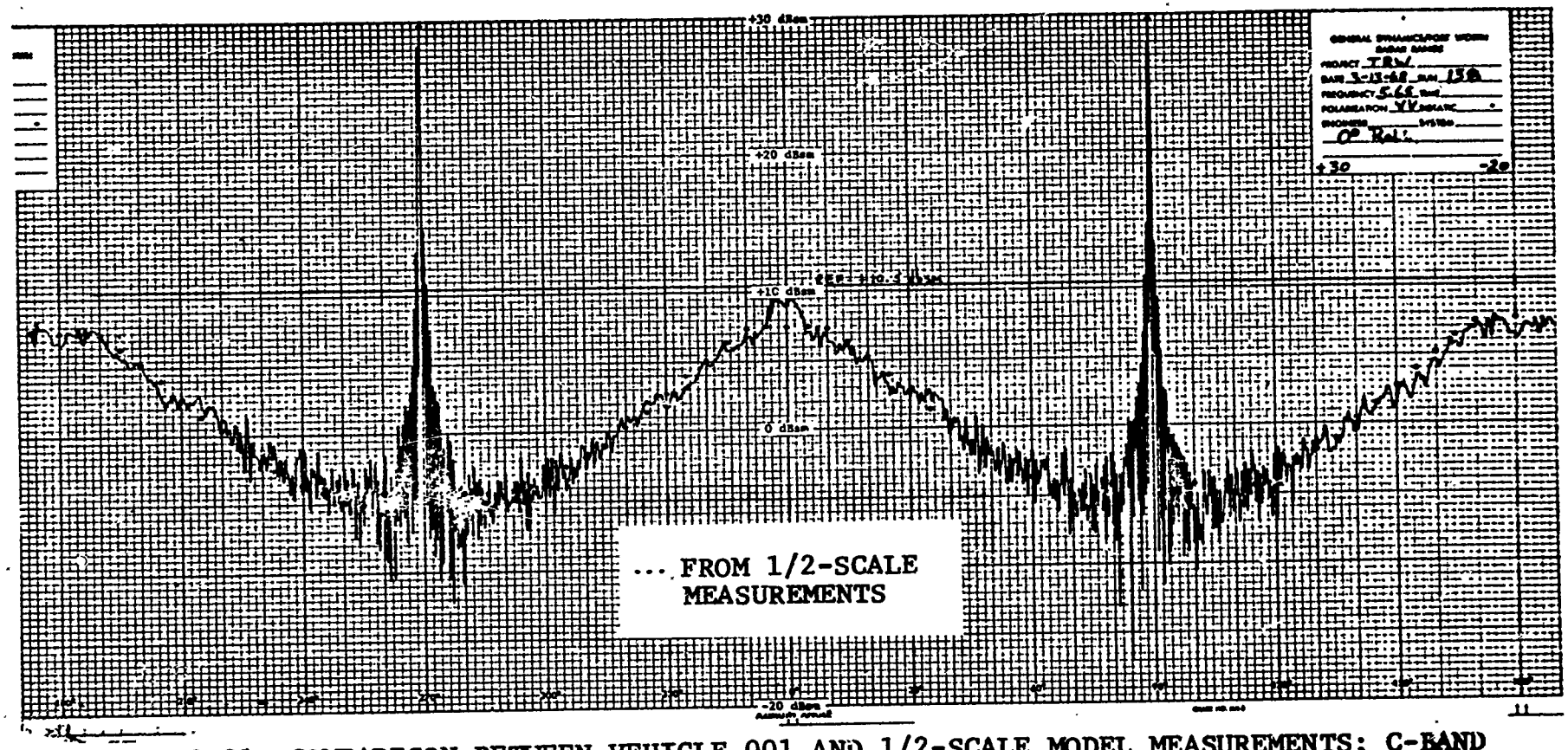

Fig. 3-21 COMPARISON BETWEEN VEHICLE 001 AND 1/2-SCALE MODEL MEASUREMENTS; C-BAND

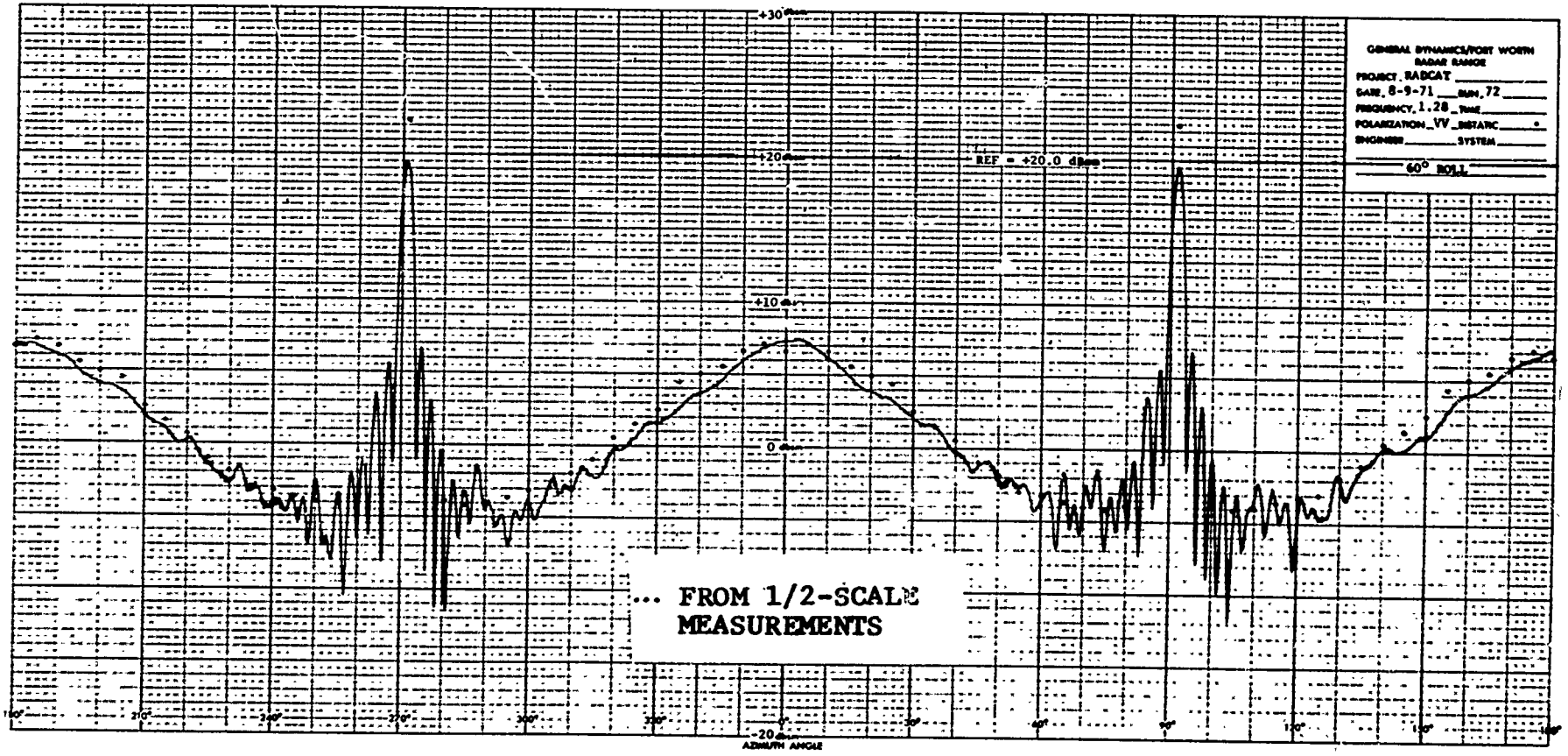

Fig. 3-22 COMPARISON BETWEEN VEHICLE 002 AND ½ SCALE MODEL MEASUREMENTS; L-BAND

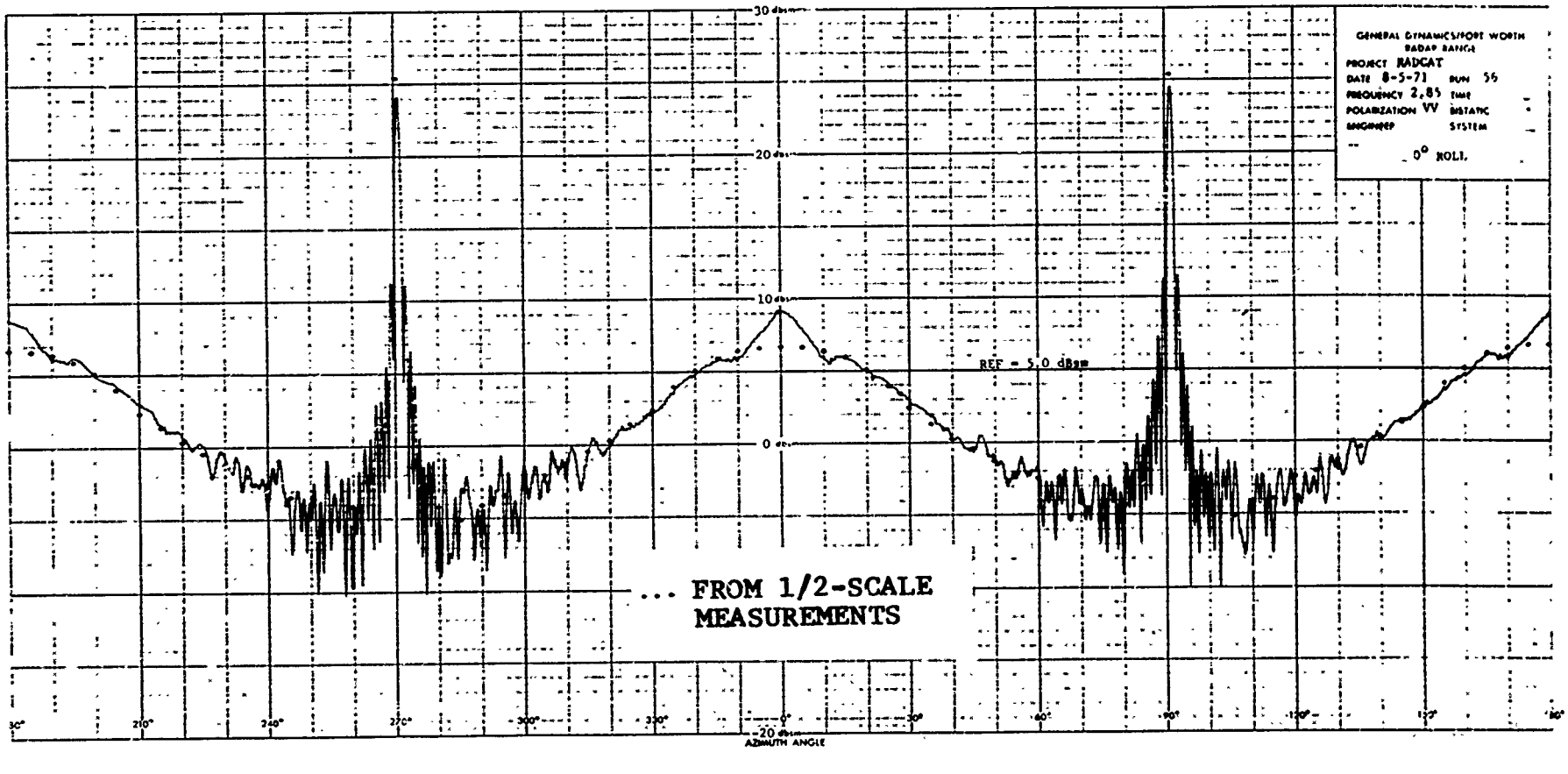

Fig. 3-23 COMPARISON BETWEEN VEHICLE 002 AND ½ SCALE MODEL MEASUREMENTS; S-BAND

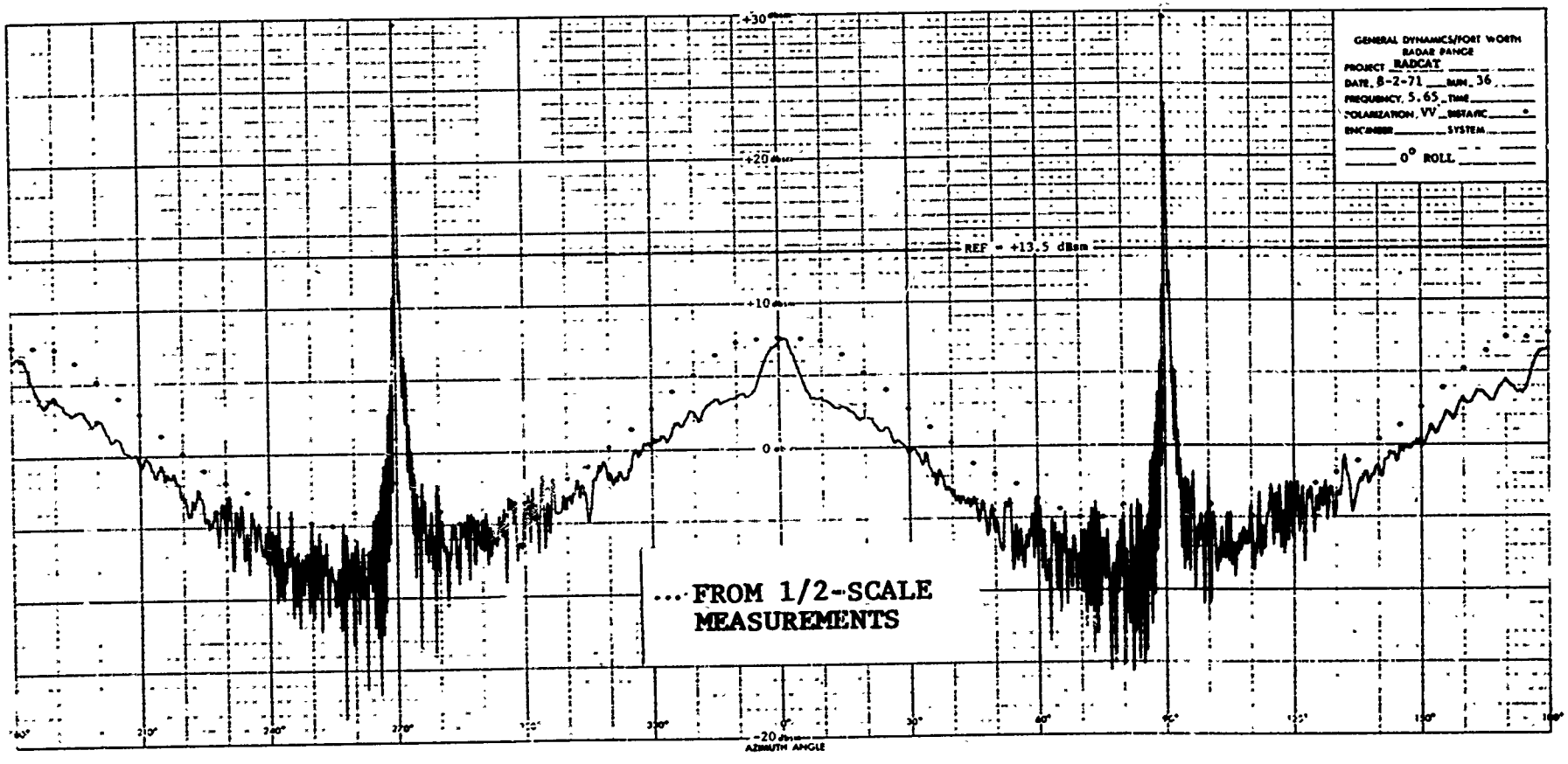

Fig. 3-24 COMPARISON BETWEEN VEHICLE 002 AND ½-SCALE MODEL MEASUREMENTS; C-BAND

optics and (2) the measured response of a perfectly conducting scale model of the RADCAT vehicle has been to call attention to a particular characteristic of the actual calibration targets which has repeatedly frustrated attempts to resolve differences in their radar cross section response. The characteristic referred to is the unusual frequency-dependent lobing pattern which is present within $\pm$ 15 degrees from nose-on. Whereas neither the computed response nor half-scale measurements exhibit this phenomenon, both, calibration targets do. In the case of vehicle 001, however, only one end exhibits the lobing which further frustrates a comparison between vehicles 001 and 002.

It was initially suspected that the small threaded hole at each end of the vehicle might be the cause of this variation. Measurements on vehicle 002 at C-Band failed to verify this assumption, however, when aluminum tape placed over the hole at one end of the target left the pattern lobing unaltered. The possibility of a response from the spheroid-cylinder joint of sufficient magnitude to cause the lobing was also eliminated as a result of its not being detected by use of the C-band short-pulse measurements.

With the above possibilities eliminated, it would appear that the dielectric and/or conductive coating is the contributive cause for the observed lobing phenomenon. The fact that vehicle 001 was measured within months of application of the coating while vehicle 002 was "on the shelf" for several years prior to measurement is

somewhat in support of this reasoning since vehicle 001 exhibited the highest radar cross section. The implementation here is that the electrical properties of the coating on vehicle 002 may have undergone a change as a result of outgassing, crystallization, etc., during the past several years. This would not explain why one end of each vehicle exhibits a higher cross-section than the opposite end. If one end received higher loads than the other end during structural testing, however, a slight flattening of one end would cause a larger radar cross section.

This page intensionally left blank

SECTION 4

CONCLUSIONS AND RECOMMENDATIONS

The following conclusions are based on comparisons made in Section 2 between the signatures of vehicle 001 and vehicle 002, as well as the comparisons between the signatures of each RADCAT vehicle and those of (1) a 1/2-scale model of the basic vehicle, and (2) the response computed using the physical optics formulation.

I) The radar cross section response from both vehicle 001 and vehicle 002 exhibits a lobing pattern near end-on aspect angles which was not exhibited by 1/2-scale model measurements nor predicted by computations. As a consequence, it may be concluded that the dielectric coating of the full-scale vehicle has a greater influence on its scattering characteristics than was originally expected.

II) RADCAT Vehicle 002 is better suited for use as a calibration target than was vehicle 001 due to its (identically) symmetrical response at either of its end-on orientations.

III) Although the radar cross section amplitude response of vehicle 002 is measurably less than that of vehicle 001, the two vehicles exhibit almost identical radar cross section patterns in the aspect sector defined by $-90^{o} \leq \theta \leq 90^{o}$. As a result, the signature library for

vehicle 001 could be made representative of the response from vehicle 002 with proper selection of a bias level to be applied to the vehicle 001 library.

IV) The high degree of similarity observed between the response of vehicle 002 at 0-degree roll angle and 60-degree roll angle is sufficient to characterize this vehicle as being insensitive to roll angle orientation. Note that for purposes of comparison a 360-degree rotation in azimuth at a 60-degree roll angle configuration is equivalent to a 180-degree rotation in azimuth at 60-degree roll and a 180-degree rotation in azimuth at 240-degree roll.

The following two recommendations are submitted for consideration. Since either recommendation would result in a data library suitable for radar cross section calibration, the particular choice of action must be based on convenience and compatibility with the overall RADCAT program.

V) As per item III, the existing data library for vehicle 001 could be utilized to represent the radar cross section characteristics of vehicle 002. Selection of a fixed bias level to be applied to these data however, would necessitate defining either the end-on region or the broadside region as most important.

VI) Although the volume of data (long-pulse) acquired on vehicle 002 during this program is but one-third that acquired previously on vehicle 001, it is considered quite adequate to describe its radar cross section scattering characteristics. It could, therefore, replace the existing signature library on vehicle 001 and thus serve unchanged as the source of calibration data.

APPENDIX A

RADAR SYSTEM DESCRIPTION

A.1 MEASUREMENTS SYSTEMS

Four separate radar systems were utilized during the performance of the program measurements. Coherent long-pulse radars were used to obtain L-band, S-band, and C-band amplitude and phase data. Short-pulse measurements were obtained through the use of a coherent C-band system which provided both amplitude and phase data on the RADCAT Vehicle.

A.1.1 Coherent, Long-Pulse Radar Systems

Each radar system is composed of instrumentation capable of obtaining long-pulse amplitude and phase measurements. Traveling wave amplifiers are used as transmitters for frequencies from 150 to 12,000 megahertz. The transmitting chain typically consists of a master oscillator followed by two stages of TWT amplification with an output of approximately one kilowatt.

As shown in Figure A-1, the received signal is mixed with a local oscillator signal to obtain a 60-megahertz IF signal. Following the IF amplifier is a range-gate circuit which allows only echos at the desired target range to be gated through the receiver. The gated pulses are detected and stretched in a boxcar circuit to provide an output voltage which is proportional to the strength of the echo signal.

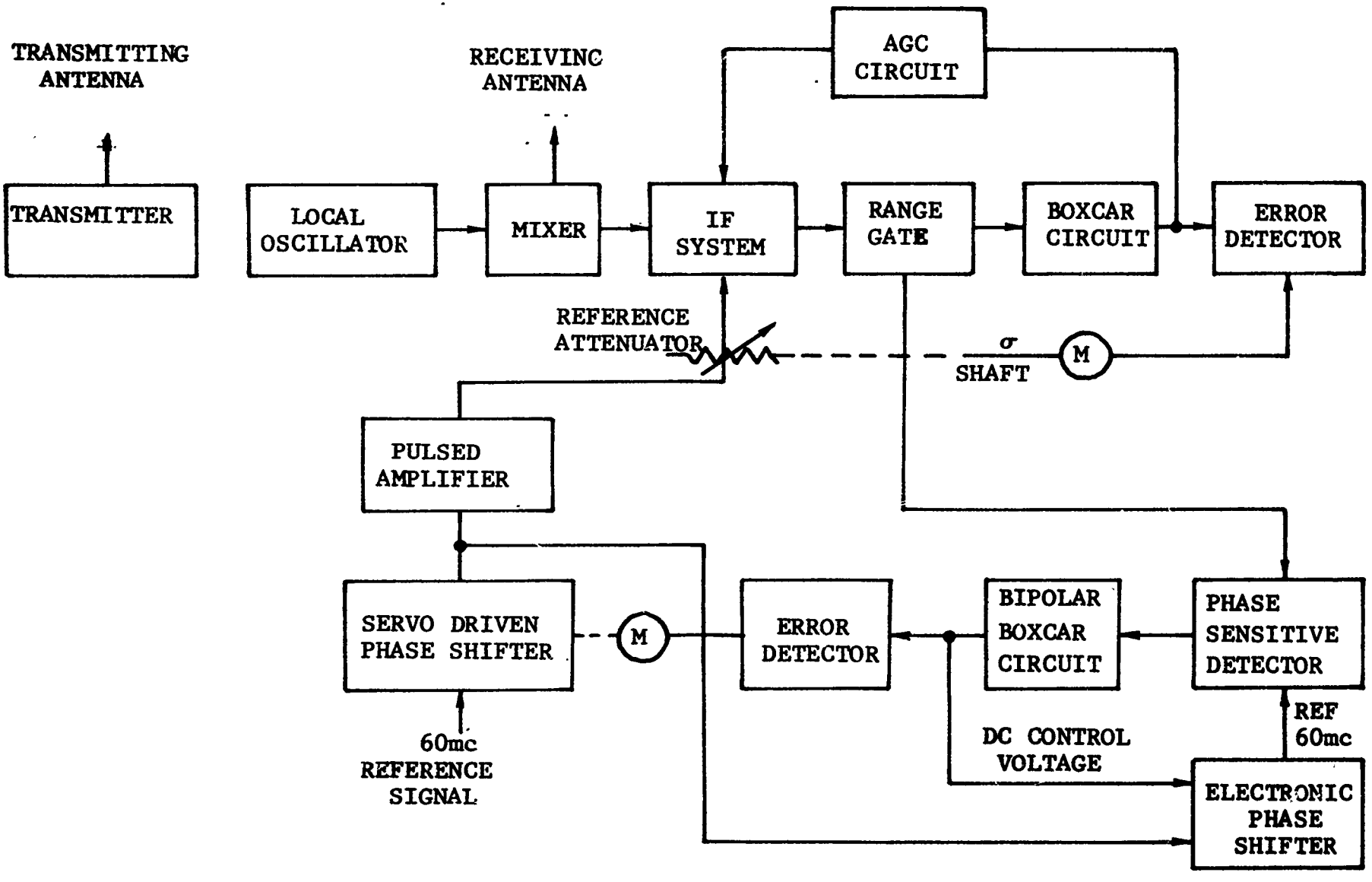

Fig. A-1 COHERENT LONG PULSE AMPLITUDE AND PHASE MEASURING SYSTEM

A standard, 60-megahertz, pulsed signal is injected into the IF system at a time sufficiently delayed after main bang that no target echos are received. This pulsed signal is fed through a precision, servo-driven attenuation to the input of the IF system. The range gate and boxcar circuits act on this pulsed signal in the same way as they act on the target echo signal. The resultant output of the boxcar circuit is a rectangular wave if the amplitude of the echo is not equal to the amplitude of the reference signal. The amplitude of the rectangular wave is proportional to the difference between the amplitudes of the echo and the standard signals.

This rectangular wave is fed to an error detector circuit in which it is demodulated and used to generate a correction voltage that is proportional to the amplitude difference between the echo and the standard signals. This correction voltage is fed to the servo motor which drives the precision reference attenuator until the amplitudes of the standard and target echo signals are equal. When the servo system is balanced, as a result of this action, the shaft position of the reference attenuator represents an accurate indication of the received signal. Use of this technique avoids the nonlinearities of AGC recording systems and the instabilities of CW systems and provides a linear,

accurate means of measuring radar cross section directly in decibels referenced to one square meter over a dynamic range of 50 dB. Potentiometers and digital shaft encoders are connected to the referenced attenuator drive shaft to permit the analog and digital readout of the radar cross section (sigma).

A.1.2 Coherent, Short-Pulse Radar Systems

The Fort Worth facility has conducted numerous short-pulse measurement programs which have demonstrated the value of high-resolution measurements in isolating dominant sources of scattering. The Fort Worth facility currently operates short-pulse radars at UHF-, S-, C-, and X-band. The measurement system described in the following paragraphs corresponds to the existing C-band capability which was utilized during this program to obtain coherent short-pulse data on the RADCAT Vehicle.

A block diagram of the C-band short-pulse system is shown in Figure A-2. The transmitted waveform is generated by modulating the output of a stable microwave source with a pulse duration of approximately 0.8 nanoseconds. The waveform is amplified by a 60 dB gain 1 KW output TWT. Depending upon the polarization requirements, either one or two offset parabolic antenna are utilized to avoid the multiple reflections associated with most antennas. A circulator is normally used

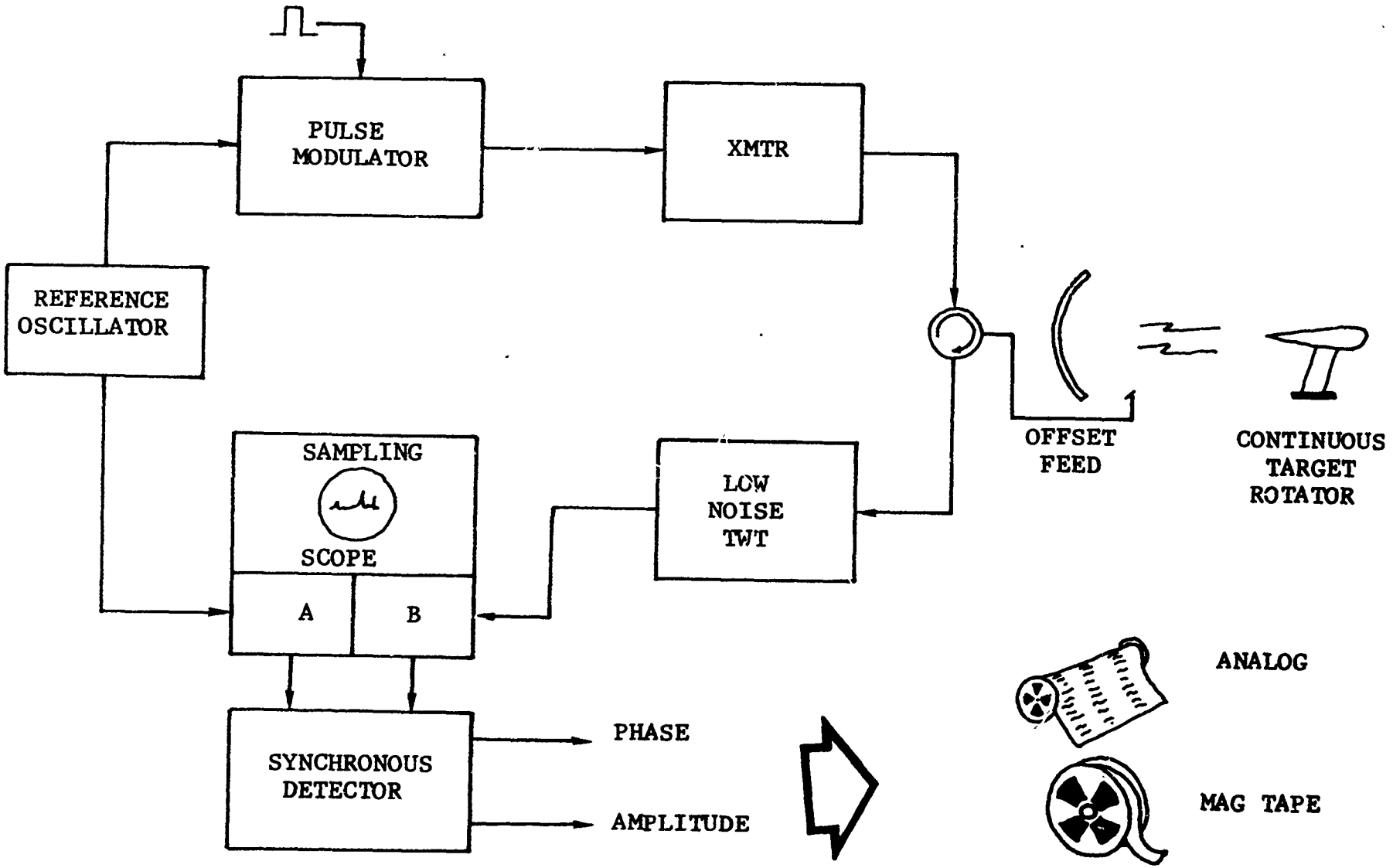

Fig. A-2 BLOCK DIAGRAM OF C-BAND SHORT-PULSE SYSTEM

to separate the transmit and receive signals if a single antenna is utilized. The receiver consists of a wideband low noise TWT and dual-channel C-band sampling oscilloscope. The two channels of the sampling scope obtain nearly simultaneous samples of the C-band reference oscillator output and received waveform. Alternate transmitted pulses are received and sampled coincident with the RF reference shifted by 90 degrees in order to obtain the quadrature component. The sampling scope provides output samples at the PRF rate that are separated into in-phase and quadrature components. These components are derived from the sample data by a correlation processor. The output is also envelope detected to form an output linear with input voltage. These data corresponding to range, amplitude, in-phase, and quadrature components are recorded simultaneously on an analog strip chart and digital magnetic tape. A typical target signature obtained at a fixed aspect angle will be digitized over a 40 ns (20 foot) interval at less than 0.1 ns intervals. Thus, the fine structure of the received signature is retained. A typical amplitude signature on the strip chart recorder is shown in Figure A-3. This signature was obtained through use of the X-band system. The recorded X-band waveform is typically 0.6 ns wide at the 3-dB point and has no time sidelobes above -27 dB. The system dynamic range is typically 20 dB on the

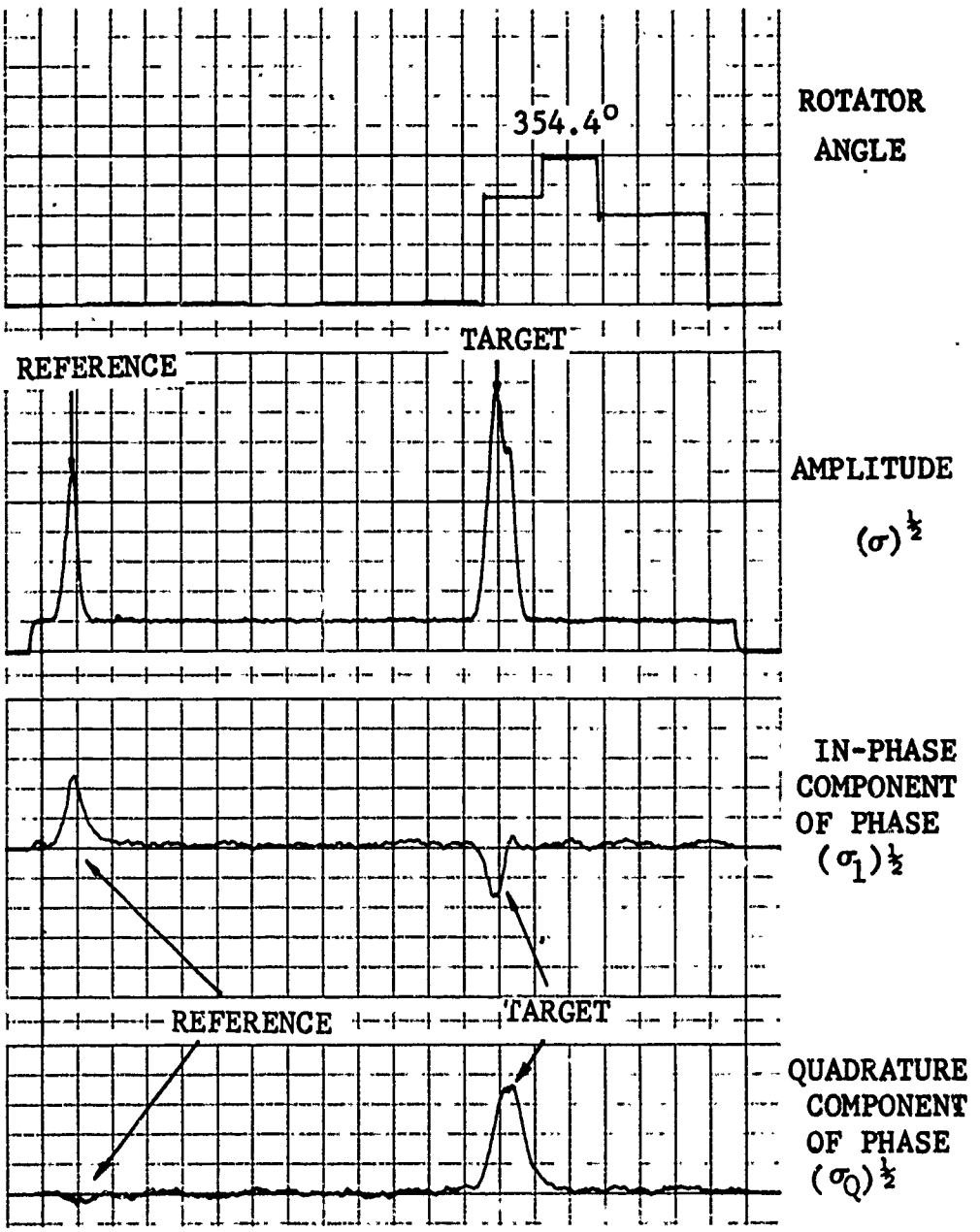

Fig. A-3 TYPICAL SHORT-PULSE ANALOG SIGNATURE

envelope detected data and approximately 30 dB for the coherent channels. Measurements obtained at successive attenuation levels provide a means of achieving an essentially unlimited dynamic range of measurements.

A.2 CALIBRATION

The radar cross section data obtained from measurements must be calibrated in order to determine the absolute magnitude to the cross section. The calibration procedure established at the Fort Worth facility is based on the use of an accurate reference level derived from a target of known cross section. During all measurement programs, precision spheres are used as the primary standard to establish system calibration.

To calibrate the long-pulse radar system, a standard, precision sphere is positioned in the radar beam at the location which will be subsequently occupied by the unknown target. The range gate is then positioned over the return from the sphere, and the values of cross section are recorded as the sphere is rotated 360 degrees in azimuth. The range gate is then positioned over the return from a corner reflector which is installed at a range which is not included in the target range gate. The return from this reflector is recorded on the same plot as the return from the sphere. The cross section level of the corner reflector is then

assigned a value in dB relative to one square meter based on its relationship to the cross section of the sphere. When the sphere is subsequently replaced by the target of interest, the return from the corner reflector is used to calibrate the system. Each measurement is subsequently calibrated through a comparison with the cross section level of the corner reflector. A comparison is made just prior to and immediately after the target measurement in order to ensure that there is no short-term drift in the radar system. The corner reflector calibration is checked on a daily basis by replacing the standard sphere for comparison. This ensures that there is no long-term drift in the amplitude and phase response of the system.

An extensive calibration procedure is utilized to insure the validity of all short-pulse data. A calibration of amplitude and phase linearity, time-base stability (range accuracy) and RCS are recorded on magnetic tape prior to and following each measurement sequence. The calibration also includes a documentation of pulse shape, time sidelobes, and the absolute value of RCS by measurements performed on a large (frequency insensitive) sphere. Field probes and system stability are verified periodically. In addition, a delayed sample of the transmitted waveform is injected into the receiver near the leading portion of each recorded range gate to serve

as amplitude, phase and range reference, thus providing an essentially closed loop operation.

Calibration of the short-pulse radar system requires the establishment of (1) a time reference, (2) a system phase and amplitude reference, and (3) acceptable pulse-width and time sidelobe characteristics. The time base is established through the use of an ultra stabel one-gHz reference oscillator. Appropriate system parameters are commonly adjusted to provide a 2-nanosecond time interval (1-foot in range) per centimeter on an analog strip chart recorder. A precision sphere positioned in the main beam at the location which will subsequently be occupied by the target is utilized as the primary calibration standard; and a dipole, located near the target region, or an injected signal serves as the secondary reference for use during the acquisition of actual target data.

The system amplitude response is determined by recording, in 1-dB attenuated increments, the return from the reference sphere. These data and subsequent recordings of the returns at VV and HH polarizations from the precision sphere and the secondary reference (both of which are simultaneously positioned within the same range gate) are sufficient to calibrate the dipole reference. System phase linearity is determined by thirty-six recordings of the

sphere return. Each recording is made after an incremental change of ten degrees has been introduced manually through use of a precision phase shifter.

A.3 MEASUREMENT PROCEDURES

The Fort Worth facility has extensive experience in obtaining high quality RCS measurements data. A measurements procedure has been established to ensure that quality is obtained from both long- and short-pulse systems.

Prior to pre-calibration, a number of detailed set-up procedures are followed to obtain accurate signature measurements from the long-pulse system. These include:

1. Adjustment of the antenna heights and pointing direction to obtain maximum sensitivity and sufficiently uniform field amplitude and phase across the volume to be occupied by the target
2. Adjustment of the target rotator so that the target motion in the radar beam is in accordance with the desired orientations
3. Use of all possible means to reduce the cross section of the target support, the target rotator, and the other back-scattering mechanisms which might be located in the target range gate.

The antenna heights are adjusted so that the target is located in the first lobe of the radar interference pattern. An initial height estimate is obtained from the relation

$$H_A = R\lambda/4H_T$$

where

H_A = antenna height

H_T = target height

R = range to target

λ = wavelength at the measurement frequency

Final adjustment is achieved by maximizing the return from a calibration target which is located at the position which is subsequently occupied by the target.

The uniformity of the field in the target area is determined by raising a calibration probe (usually a sphere or corner reflector) through the region where the target will be located and recording the signal return as a function of the height of the probe.

The tilt angle of the rotator is adjusted so that the radar cross section levels of both sides of a flat plate are identical. Use of this action assures that the target will rotate in the plane of the radar beam, which generally is not exactly parallel to the ground.

The background cross section may be reduced (1) by tuning the support column by means of small changes in

frequench so that the reflections from the front and back of the column cancel (if this technique is acceptable) or (2) by physically changing the column size. The column may also be tilted to obtain a very low background over most aspect angles. Specular returns from columns are generally positioned so that they correspond to the region of largest target cross section.

A typical short-pulse measurement procedure includes all aspects of the set-up procedures utilized in preparing for long-pulse measurements as well as (1) pre-calibration, (2) target mounting, (3) target measurement, and (4) post calibration.

The performance characteristics of the short-pulse system and the data parameters are documented during the pre-calibration phase by recording a reference 1-gHz time-base signal as well as the amplitude, phase, and pulse-shape characteristics measured through use of a large sphere which is mounted on the styrofoam target support. All parameter tolerances are defined and evaluated under operational conditions, i.e., through use of a mounted calibration target. When vertical and horizontal polarizations are utilized, calibration of radar cross section is accomplished by relating the known radar cross section of the

sphere to the stationary reference return which is positioned near the leading edge of the range gate.

When cross-polarization is utilized, the calibration of radar cross section is referenced to the radar cross section of a dipole which is mounted at a tilt angle of 45 degrees. The radar cross section of this dipole is identical in vertical, horizontal, and cross-polarization. The calibrated reference return is recorded near the beginning of each and every sweep in a data run in order to provide a range, phase, and RCS standard at each aspect angle. A delayed sample of the transmitted waveform is utilized at higher attenuation levels instead of the dipole.

APPENDIX B

BACKGROUND AND CALIBRATION MEASUREMENTS

The data presented in this appendix correspond to pertinent long-pulse and short-pulse system calibration measurements which were performed prior to measurement of RADCAT Vehicle 002.

The analog plots shown in Figure B-1 through B-30 contain background and calibration data which were acquired prior to long-pulse target measurements. Data related to the waveform characteristics of the C-band and S-band short-pulse measurement systems are shown in Figures B-31 through B-35.

PROJECT RADCAT
DATE RUN 22
FREQUENCY 5.65
POLARIZATION VV&HH

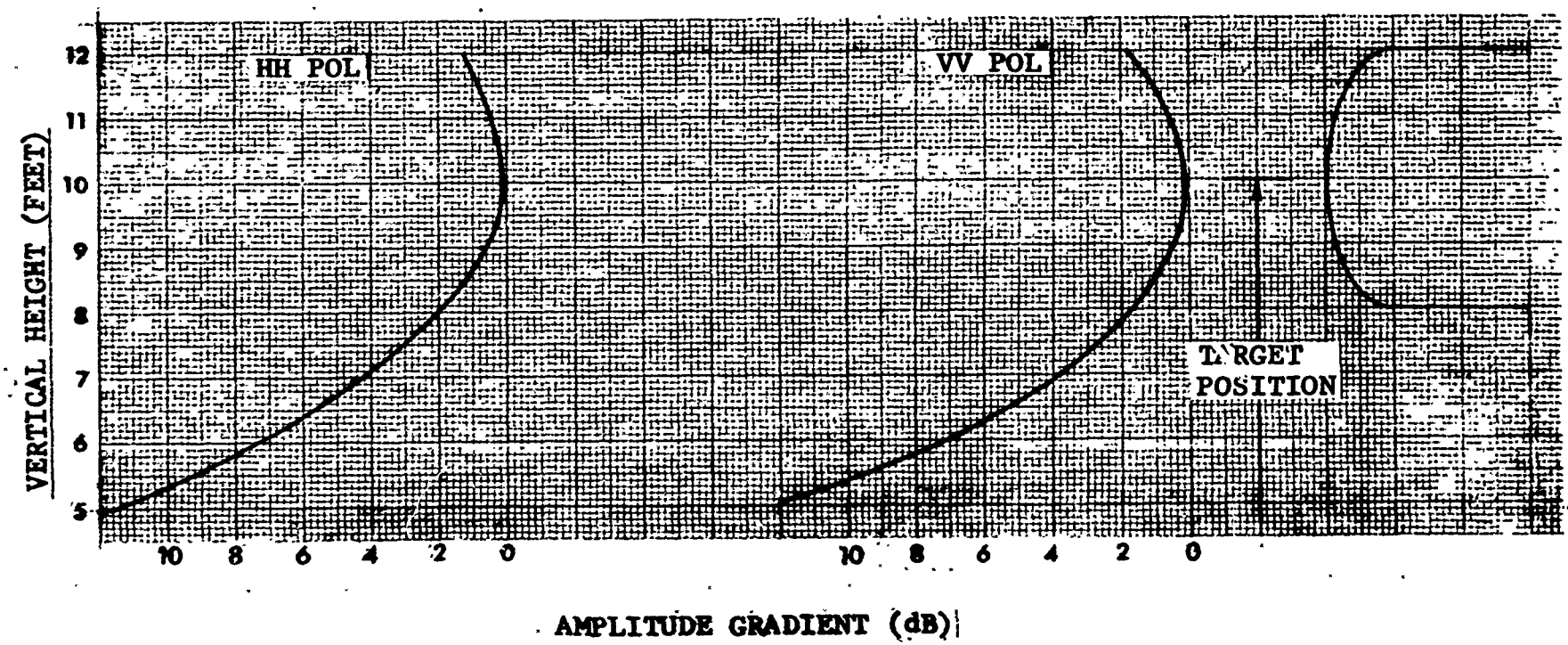

Fig. B-1 HORIZONTAL FIELD PROBE; LONG-PULSE, C-BAND

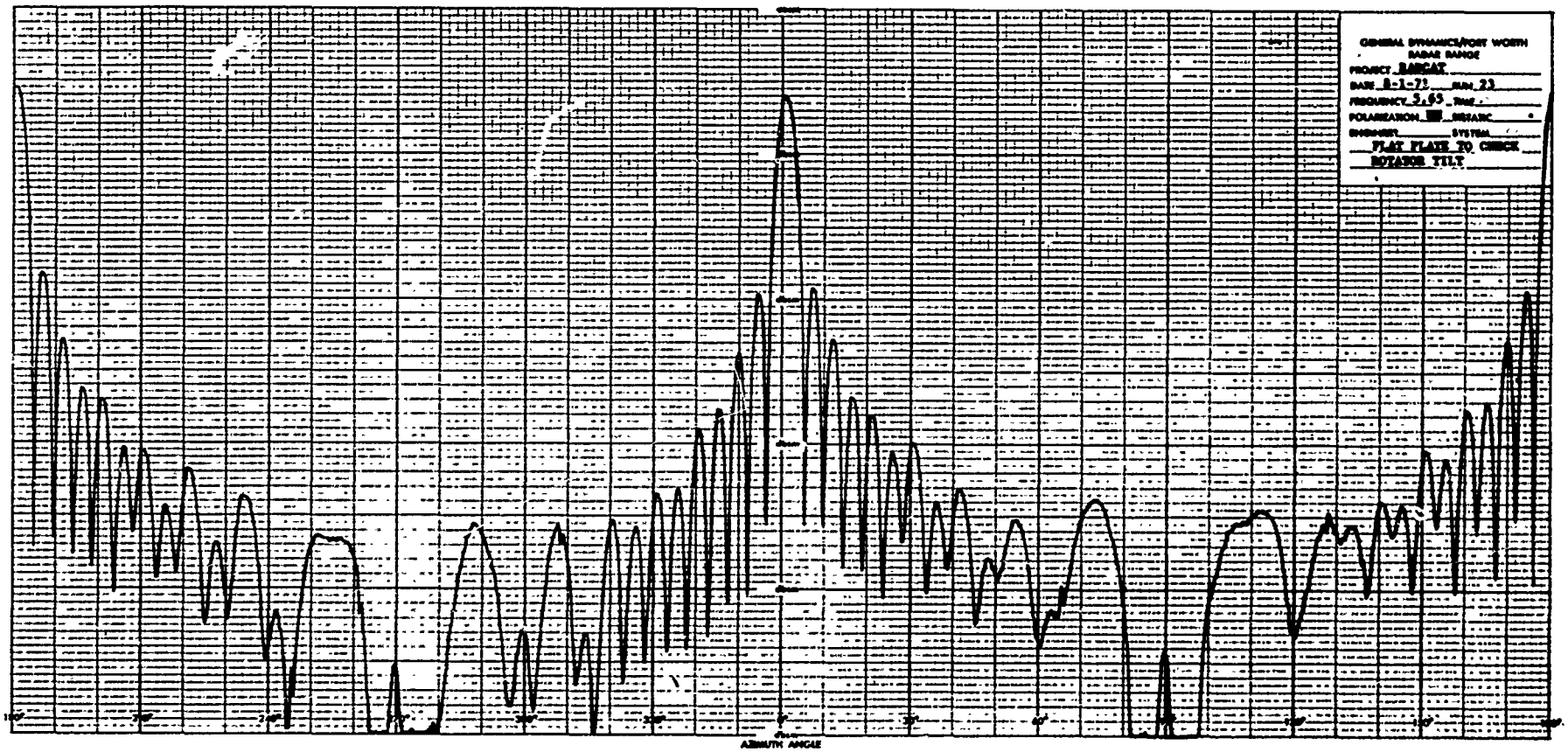

Fig. B-2 FLAT PLATE RESPONSE, C-BAND

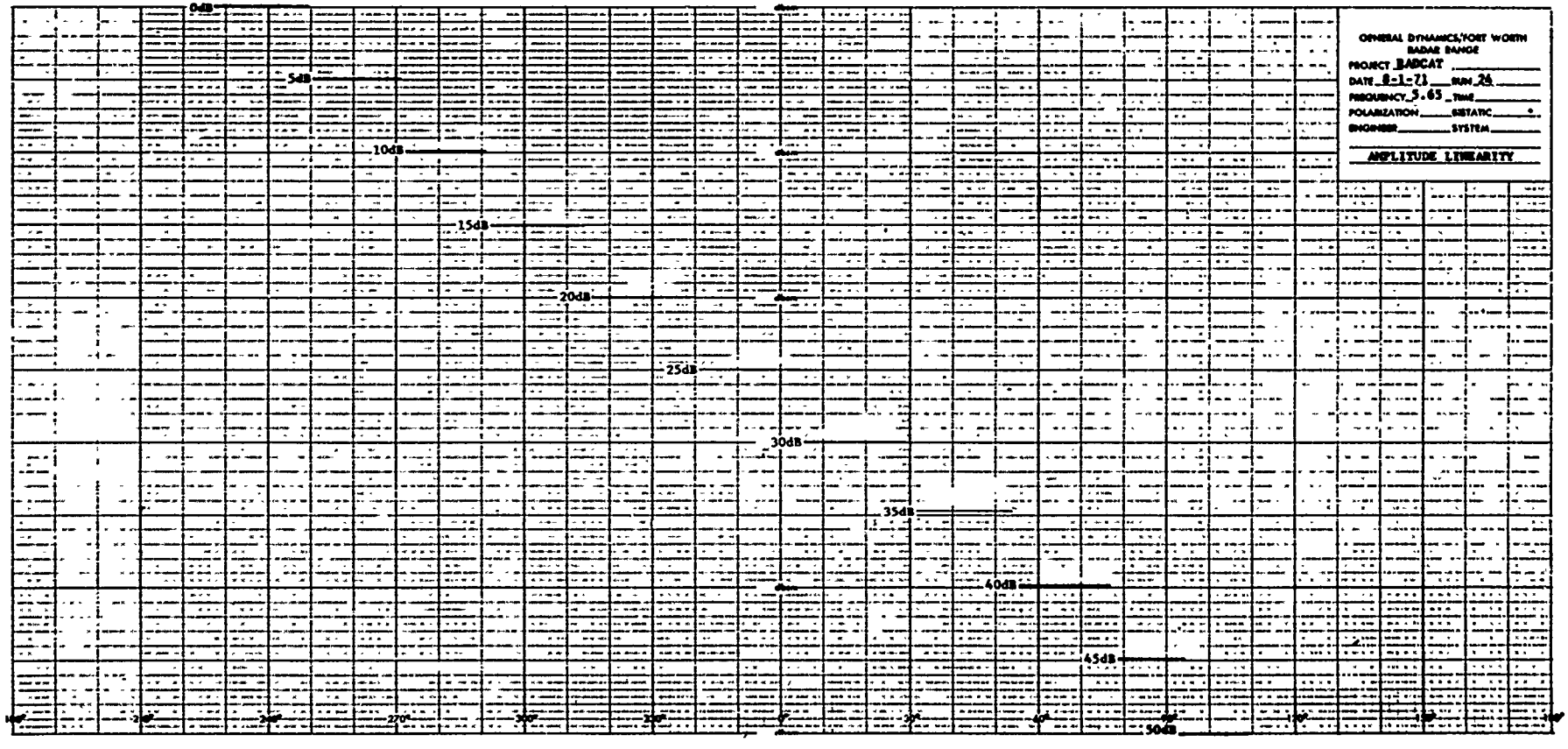

Fig. B-3 AMPLITUDE LINEARITY, C-BAND

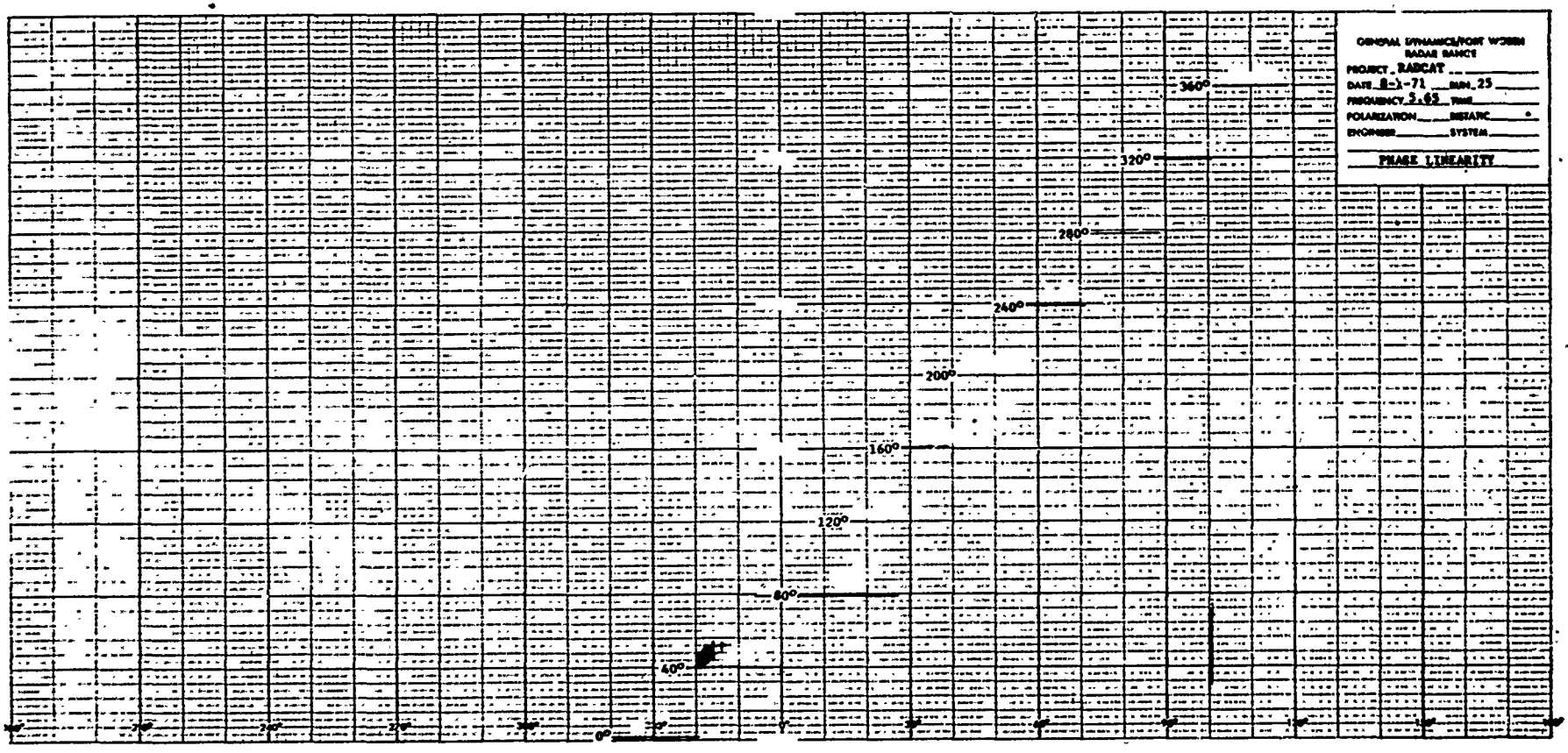

Fig. B-4 PHASE LINEARITY, C-BAND

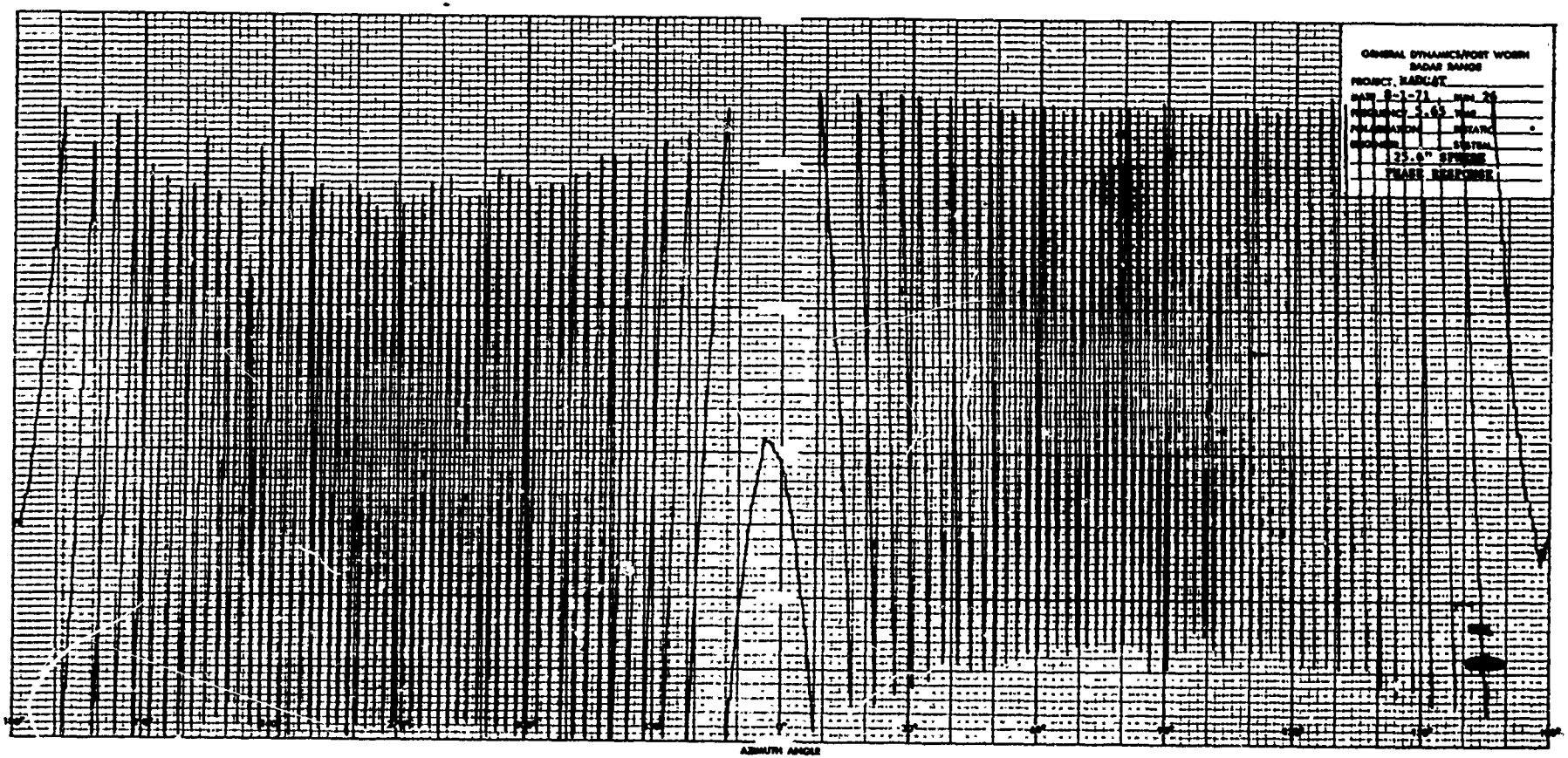

Fig. B-5 CALIBRATION SPHERE PHASE RESPONSE, C-BAND

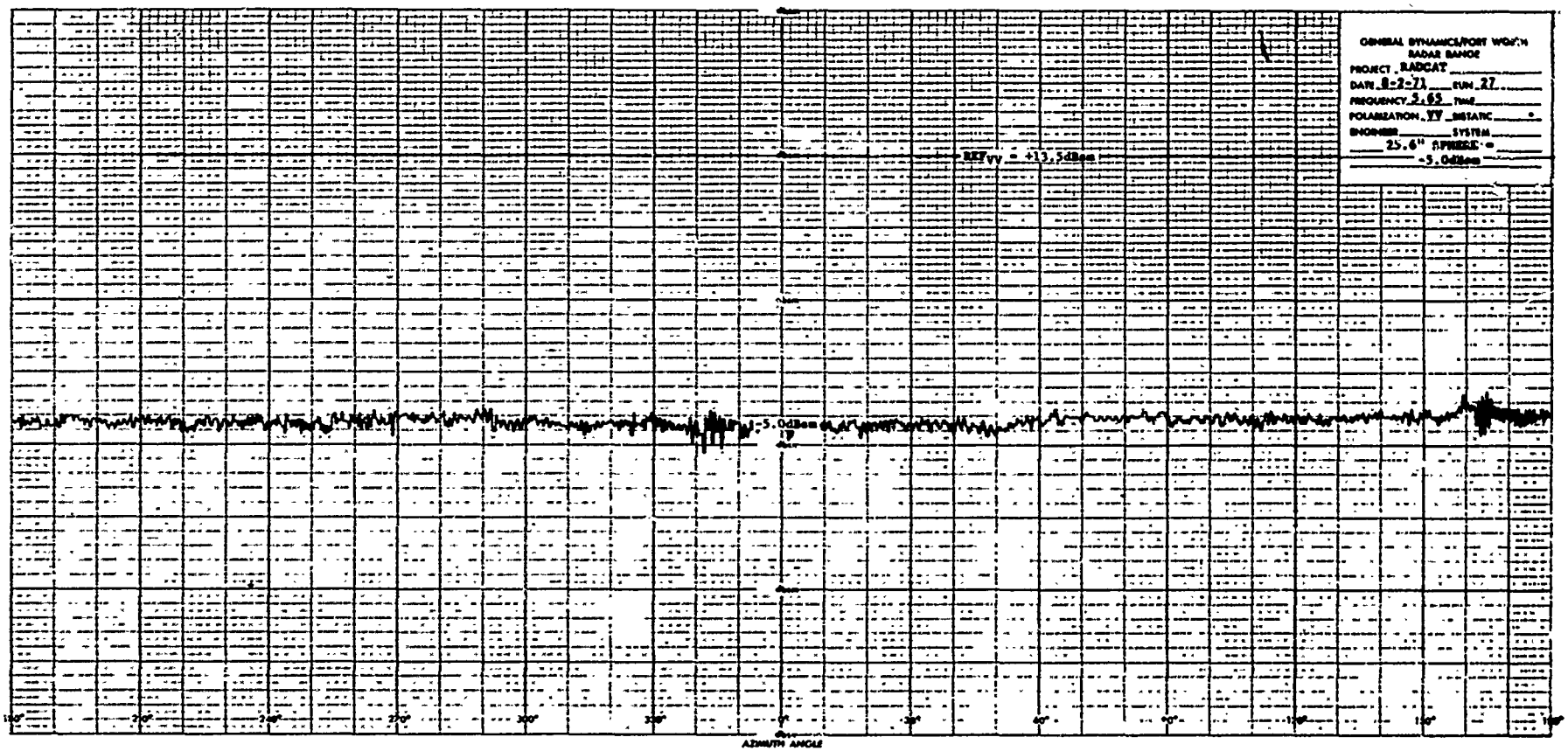

Fig. B-6 AMPLITUDE CALIBRATION, VV POLARIZATION, C-BAND

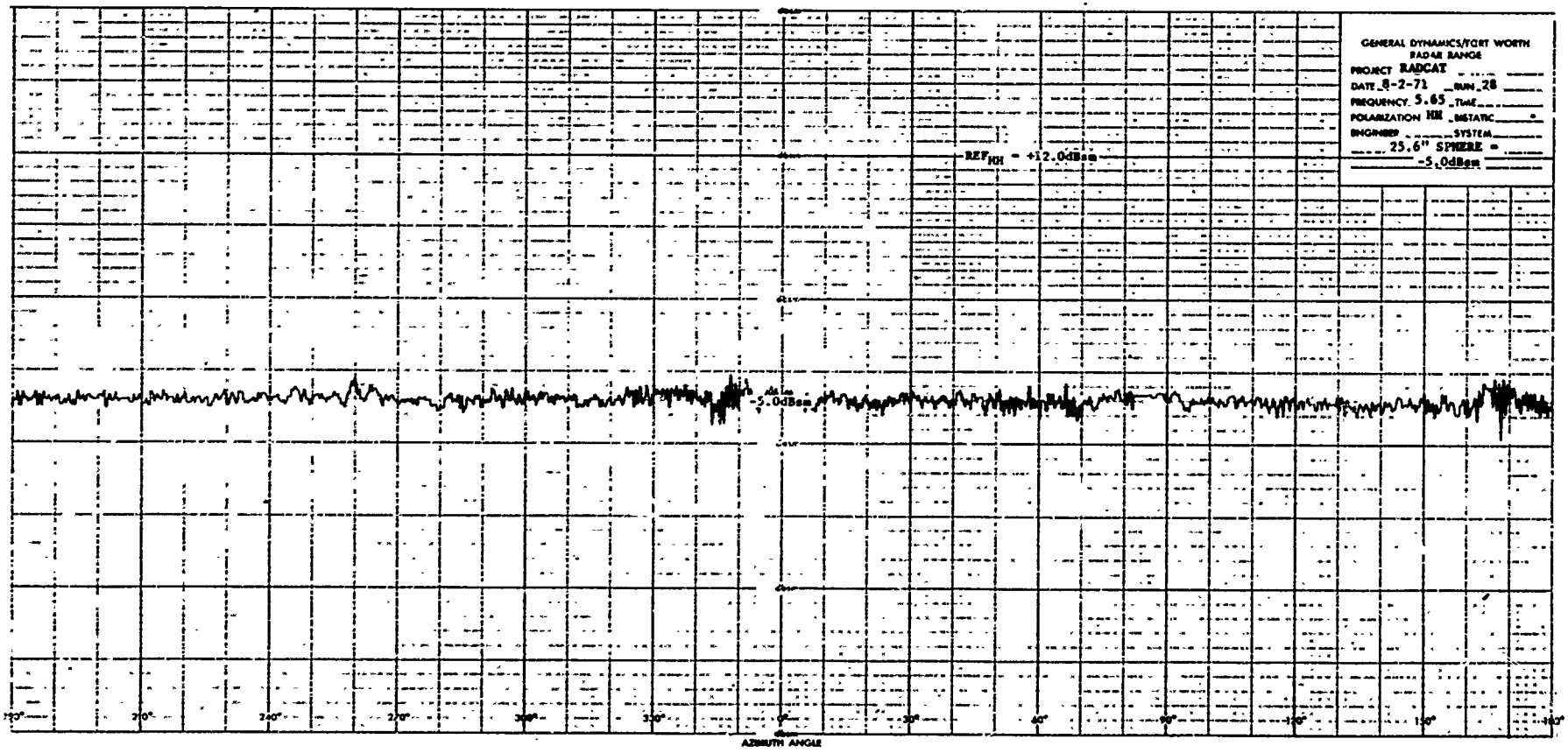

Fig. B-7 AMPLITUDE CALIBRATION, HH POLARIZATION, C-BAND

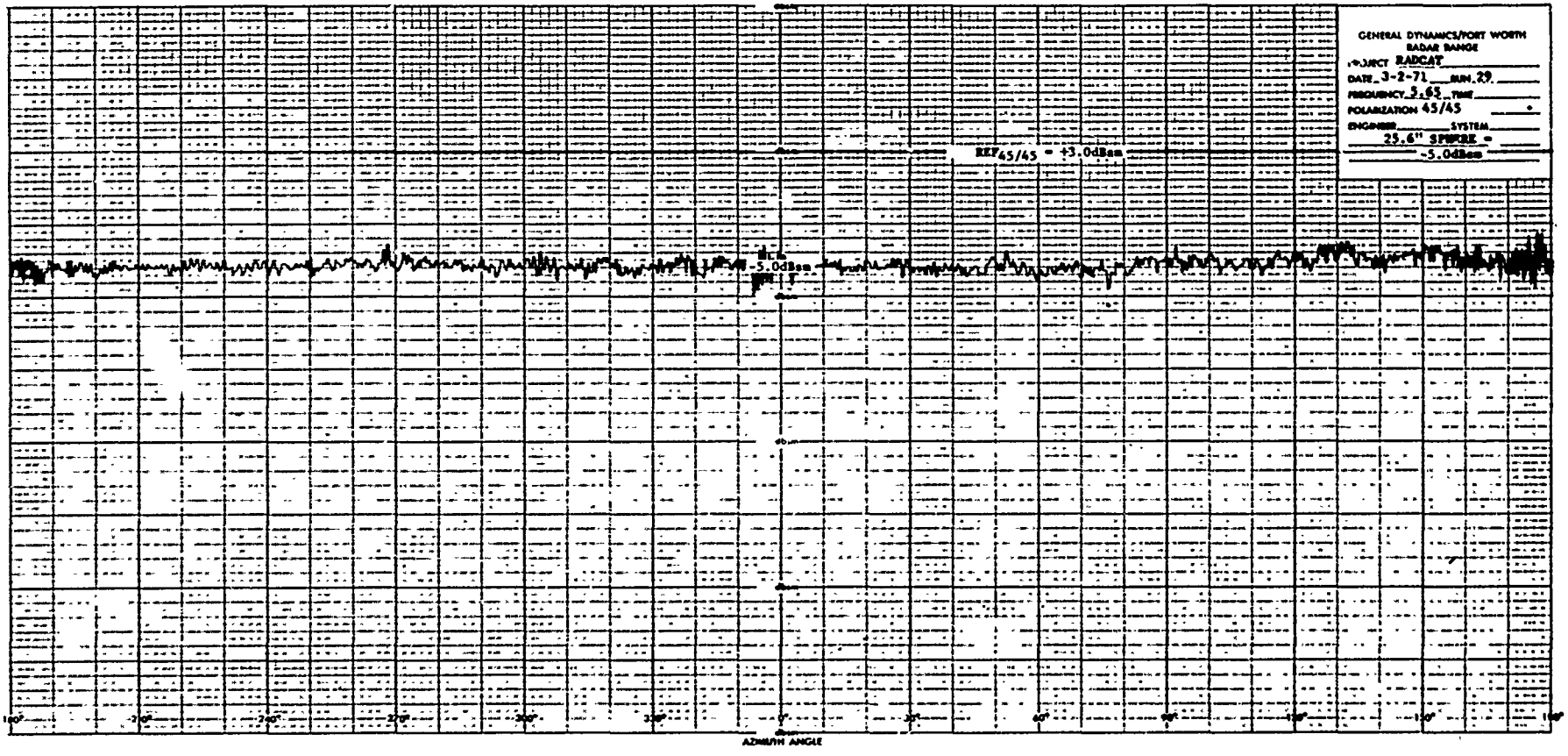

Fig. B-8 AMPLITUDE CALIBRATION, 45/45 POLARIZATION, C-BAND

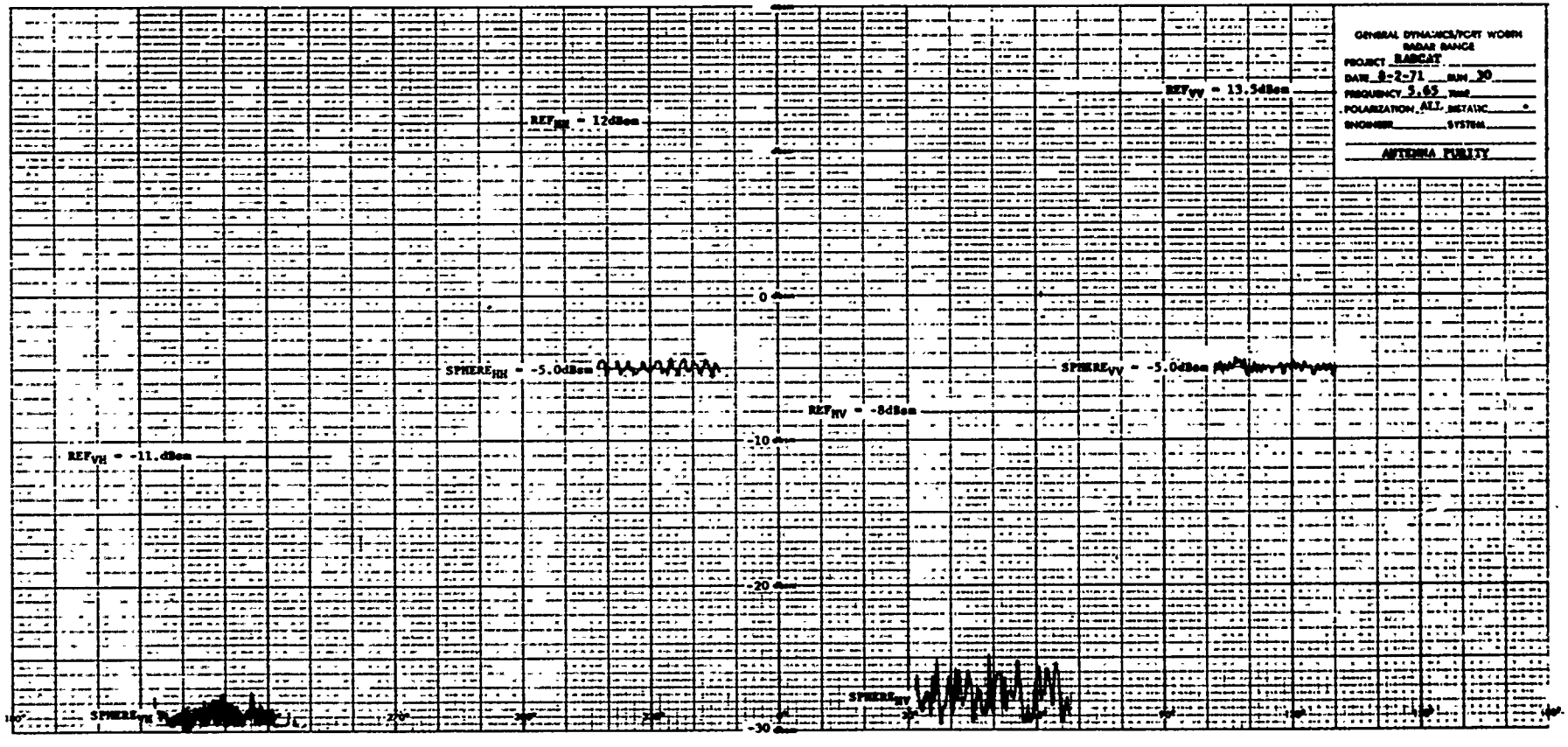

Fig. B-9 ANTENNA PURITY, C-BAND

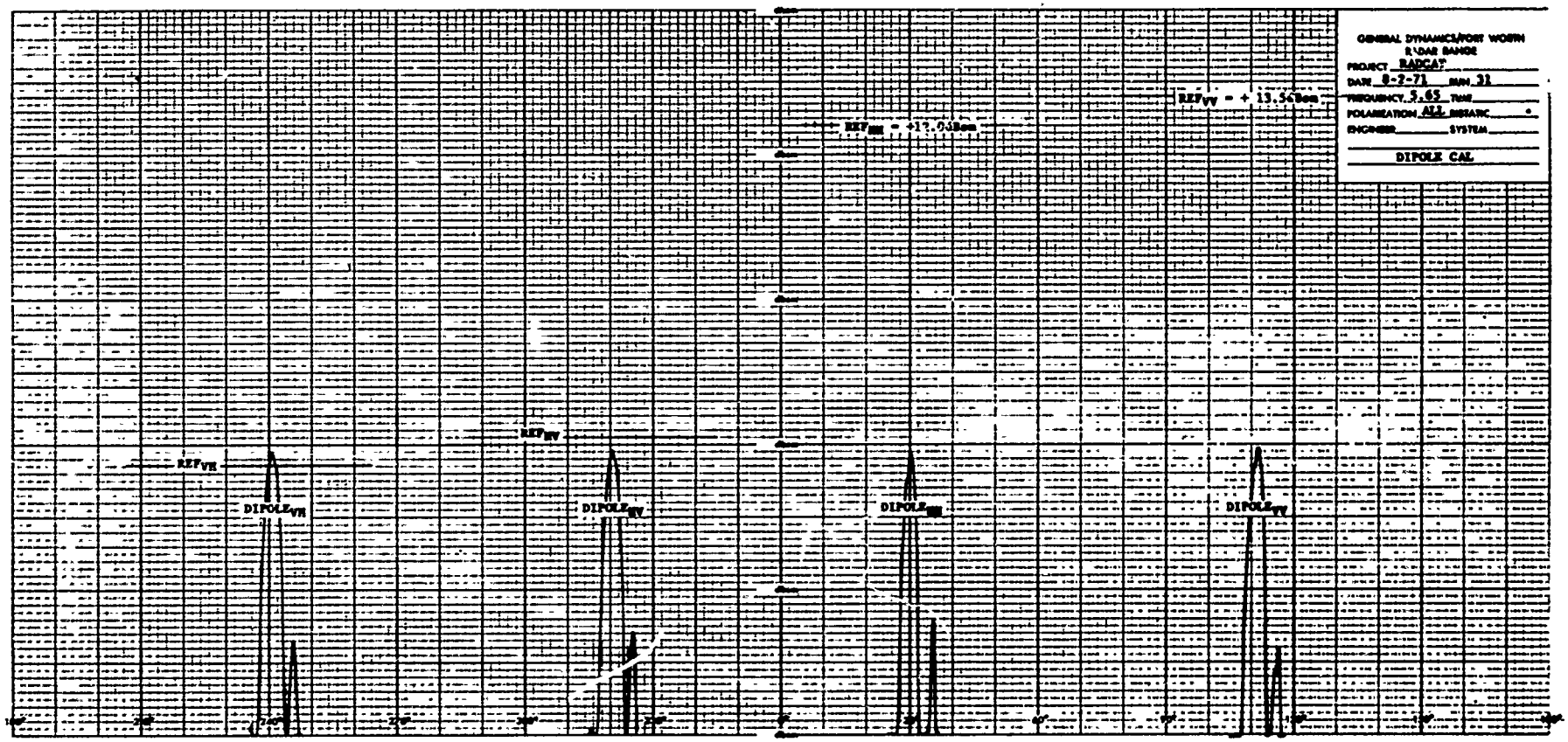

Fig. B-10 DIPOLE CALIBRATION, C-BAND

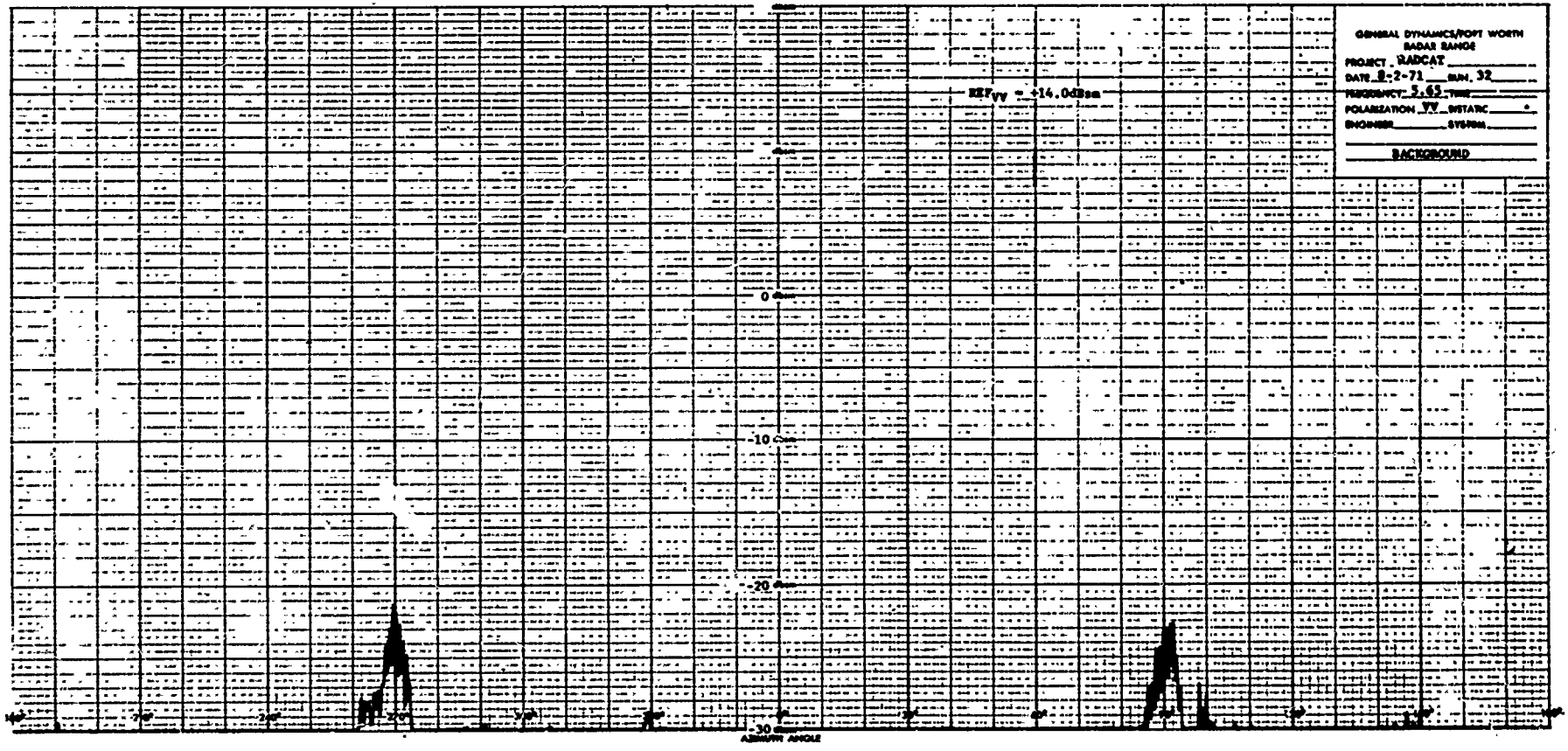

Fig. B-11 BACKGROUND, VV POLARIZATION, C-BAND

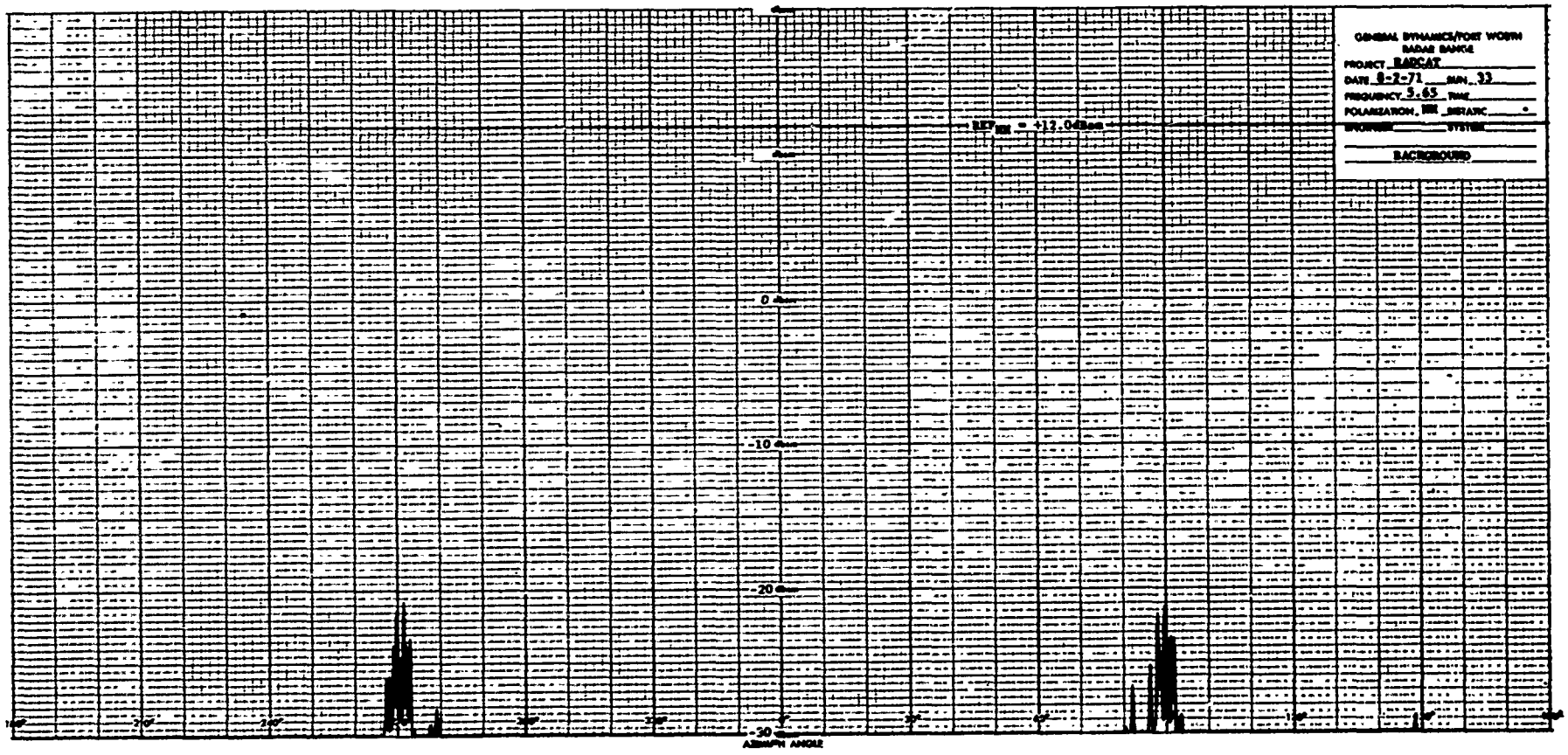

Fig. B-12 BACKGROUND, HH POLARIZATION, C-BAND

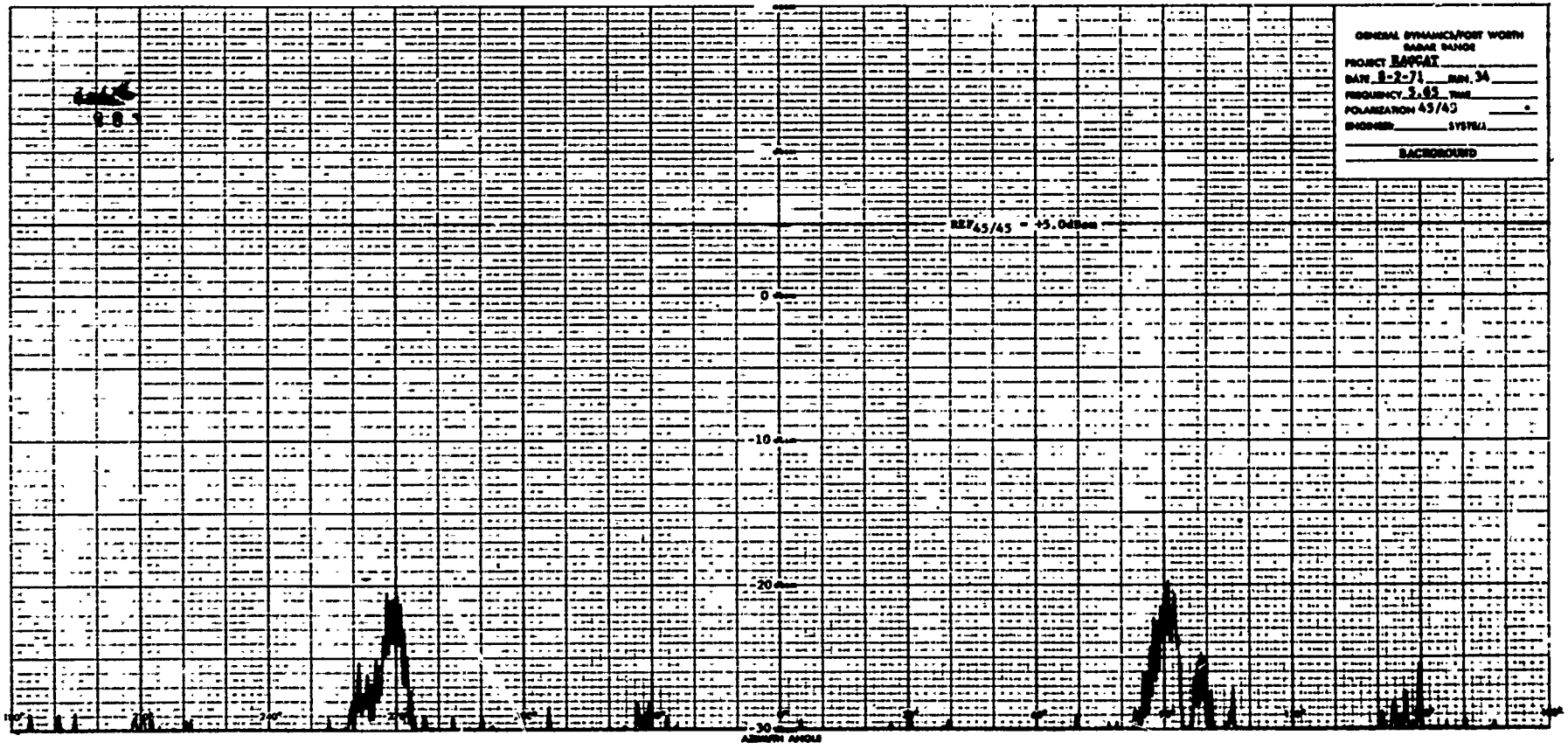

Fig. B-13 BACKGROUND, 45/45 POLARIZATION, C-BAND

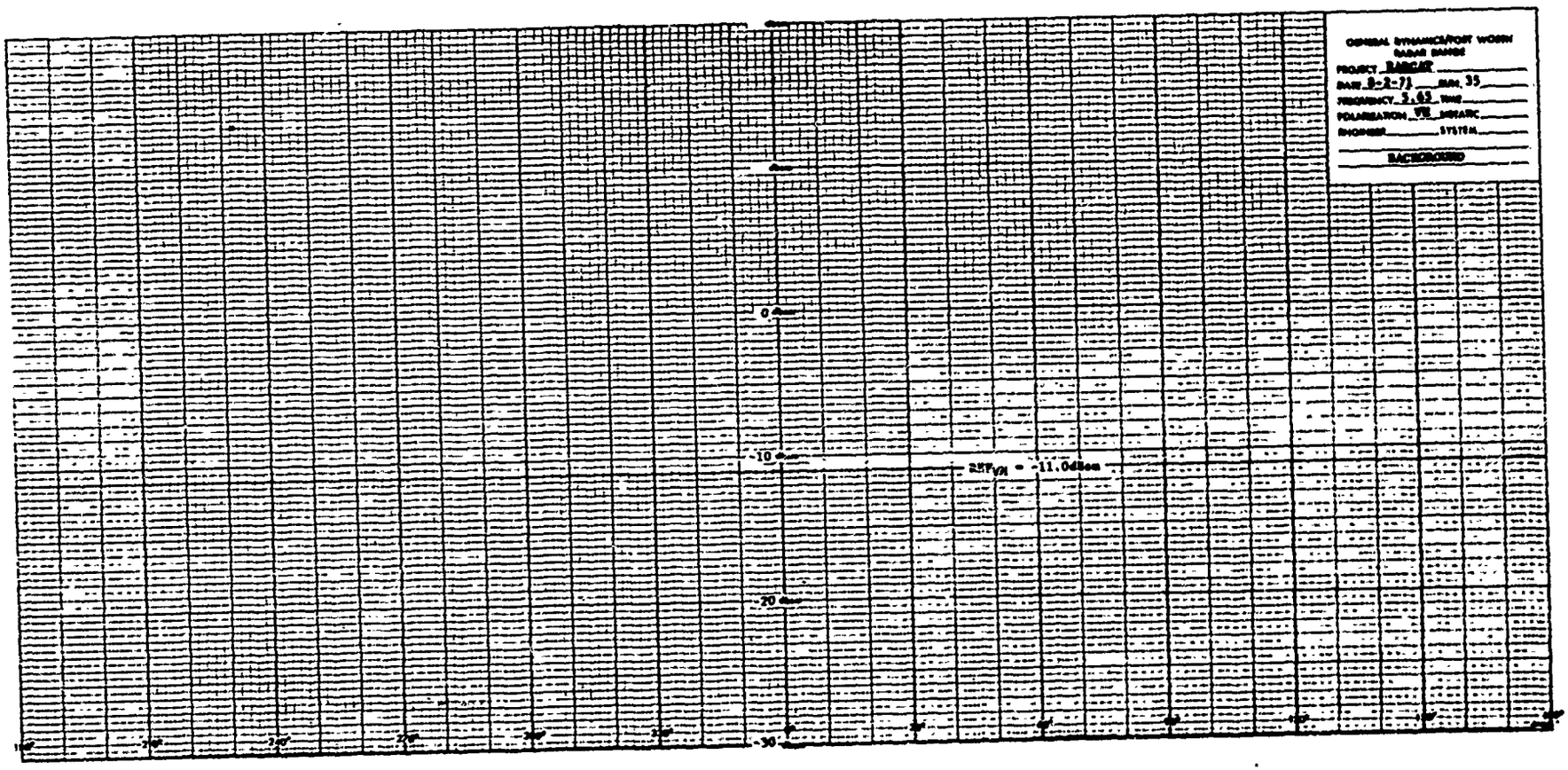

Fig. B-14 BACKGROUND, V/H POLARIZATION, C-BAND

PROJECT RADCAT
DATE RUN 44
FREQUENCY 2.85
POLARIZATION VV&HH

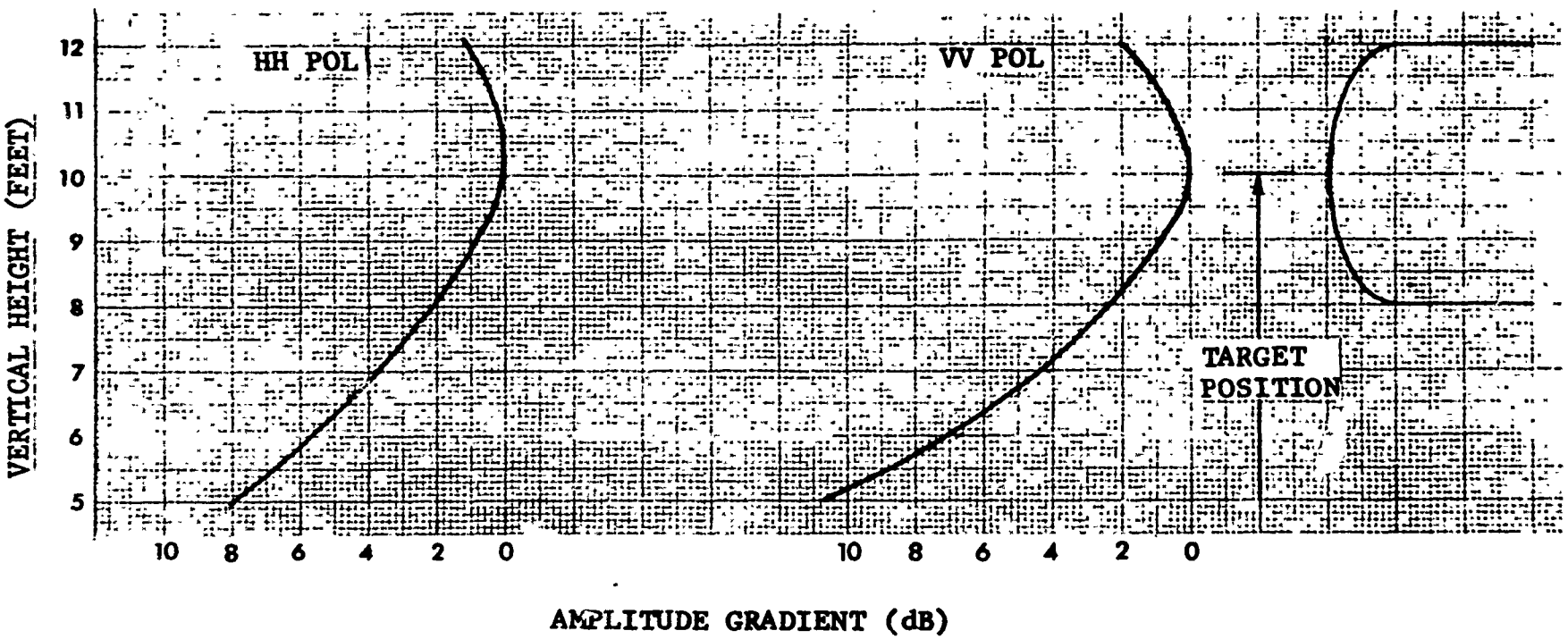

Fig. B-15 HORIZONTAL FIELD PROBE, LONG-PULSE, S-BAND

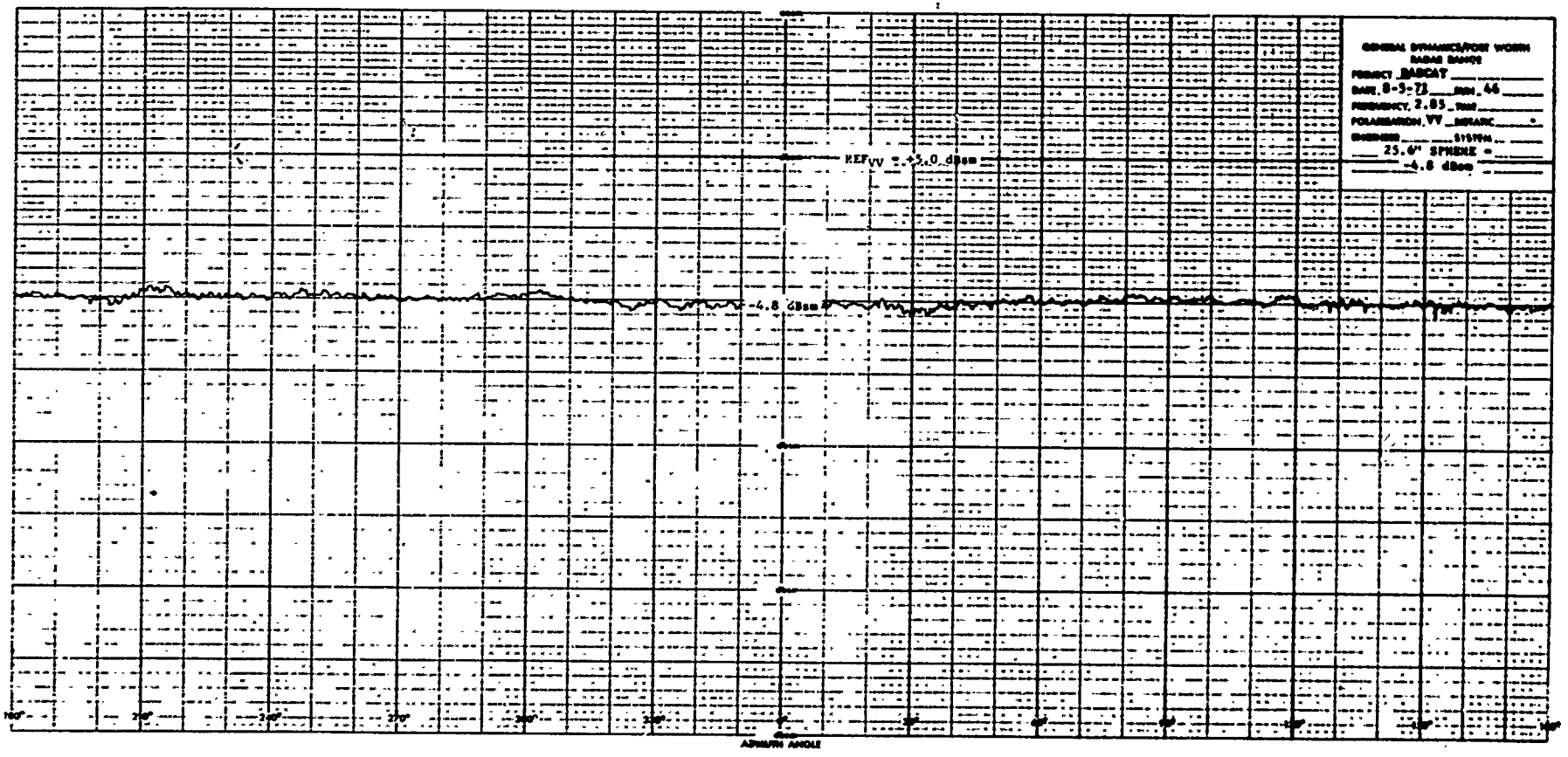

Fig. B-16 AMPLITUDE CALIBRATION, VV POLARIZATION, S-BAND

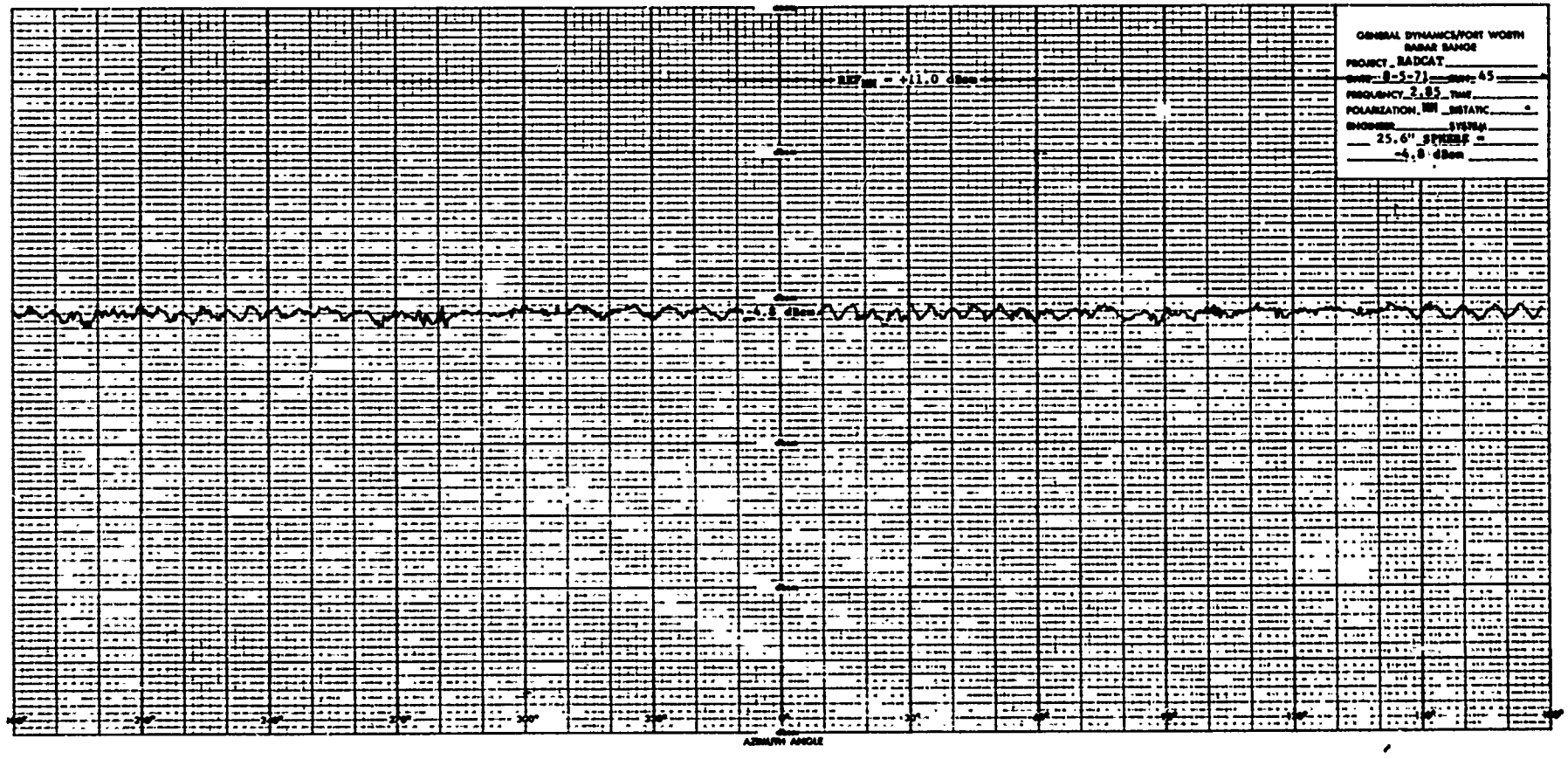

Fig. B-17 AMPLITUDE CALIBRATION, HH POLARIZATION, S-BAND

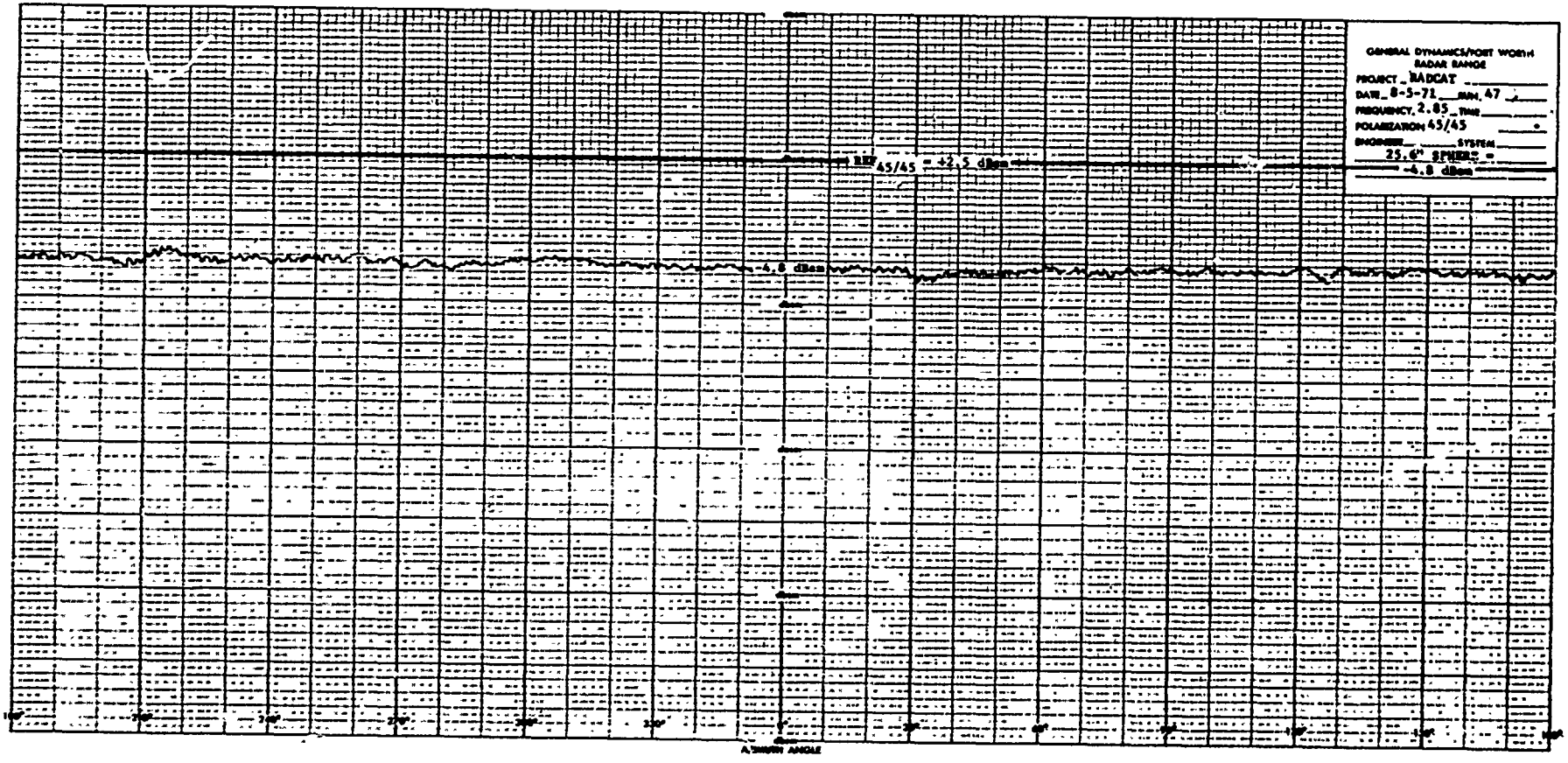

Fig. B-18 AMPLITUDE CALIBRATION, 45/45 POLARIZATION, S-BAND

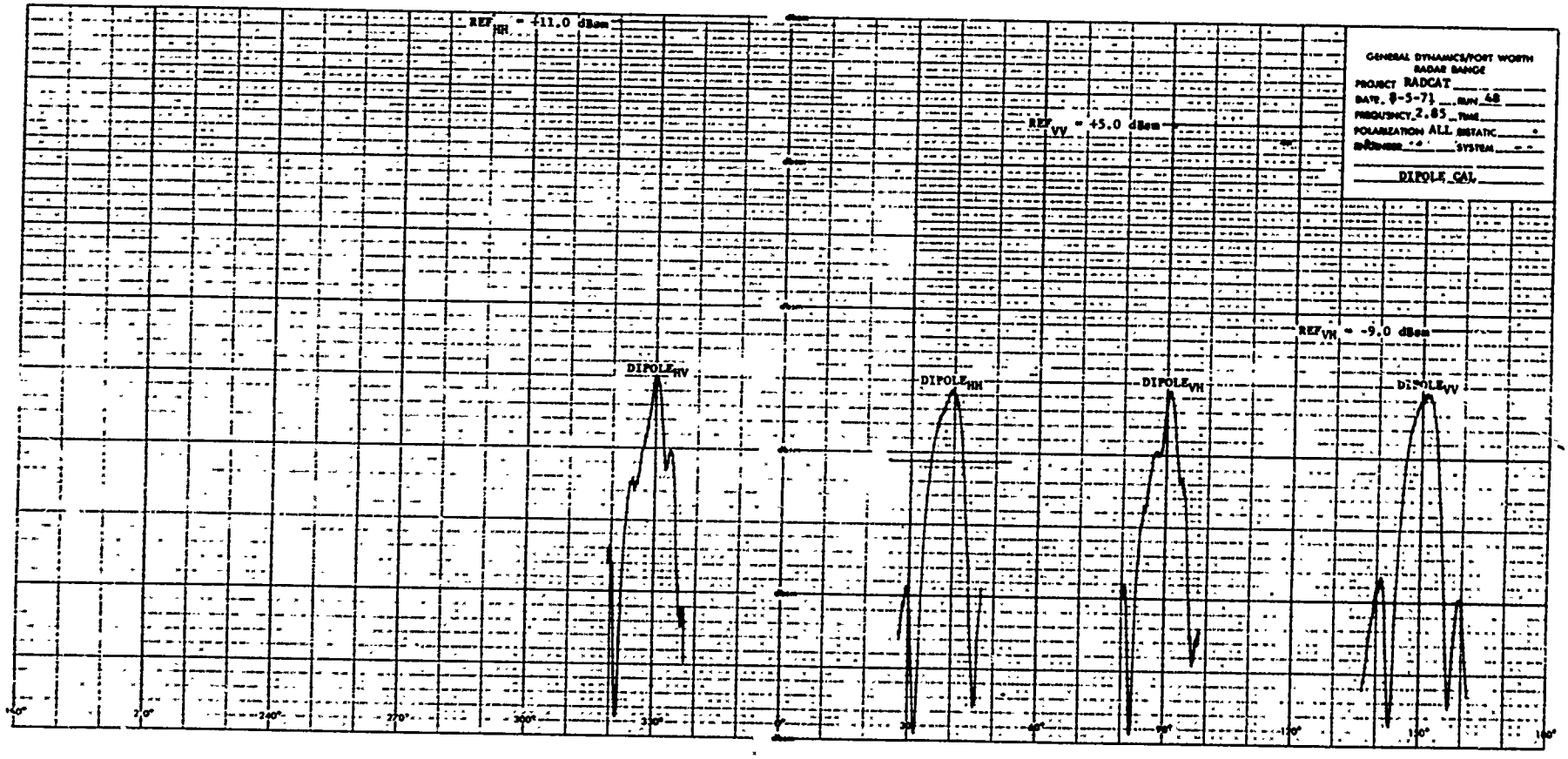

Fig. B-19 DIPOLE CALIBRATION, S-BAND

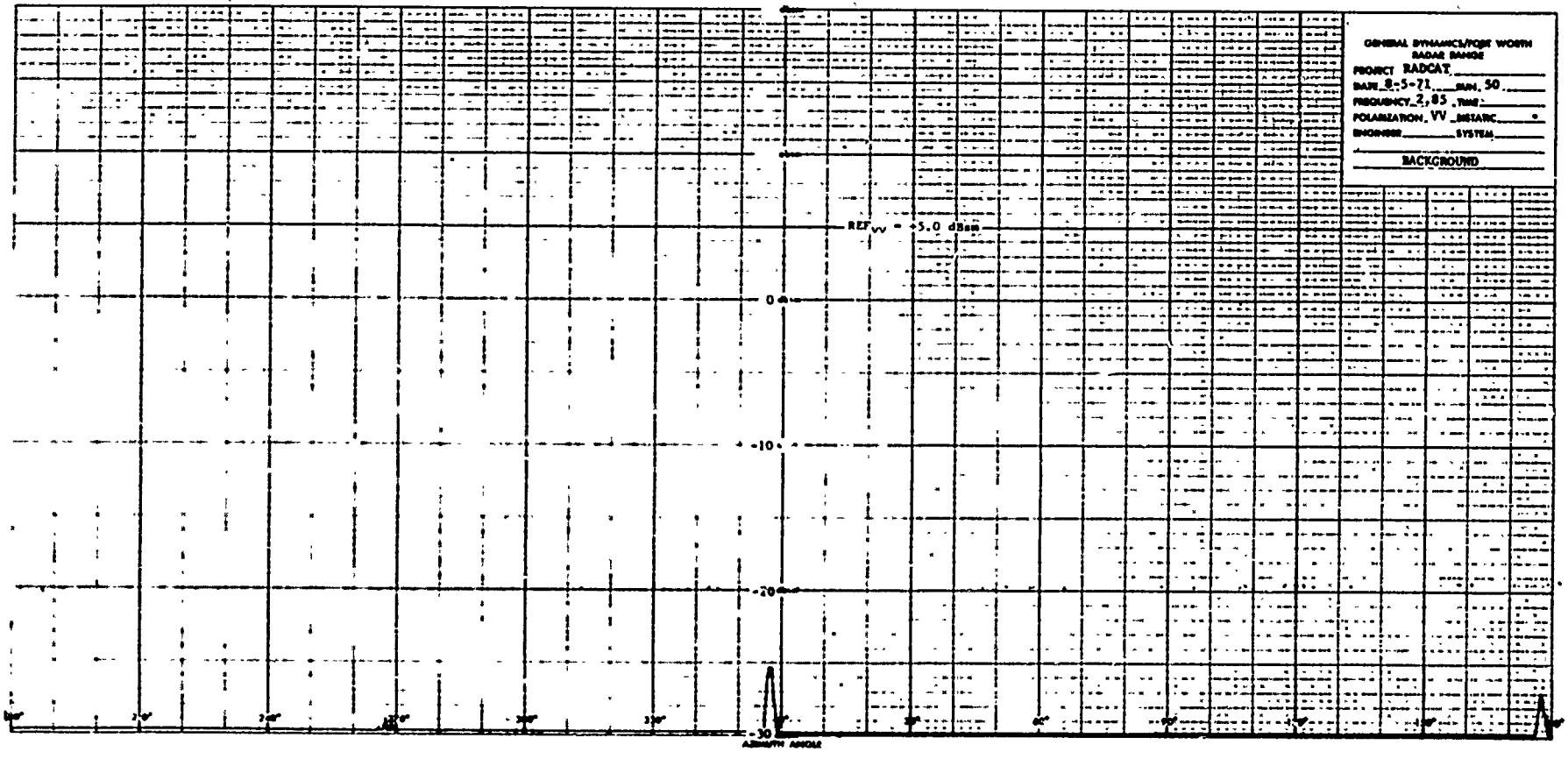

Fig. B-20 BACKGROUND, VV POLARIZATION, S-BAND

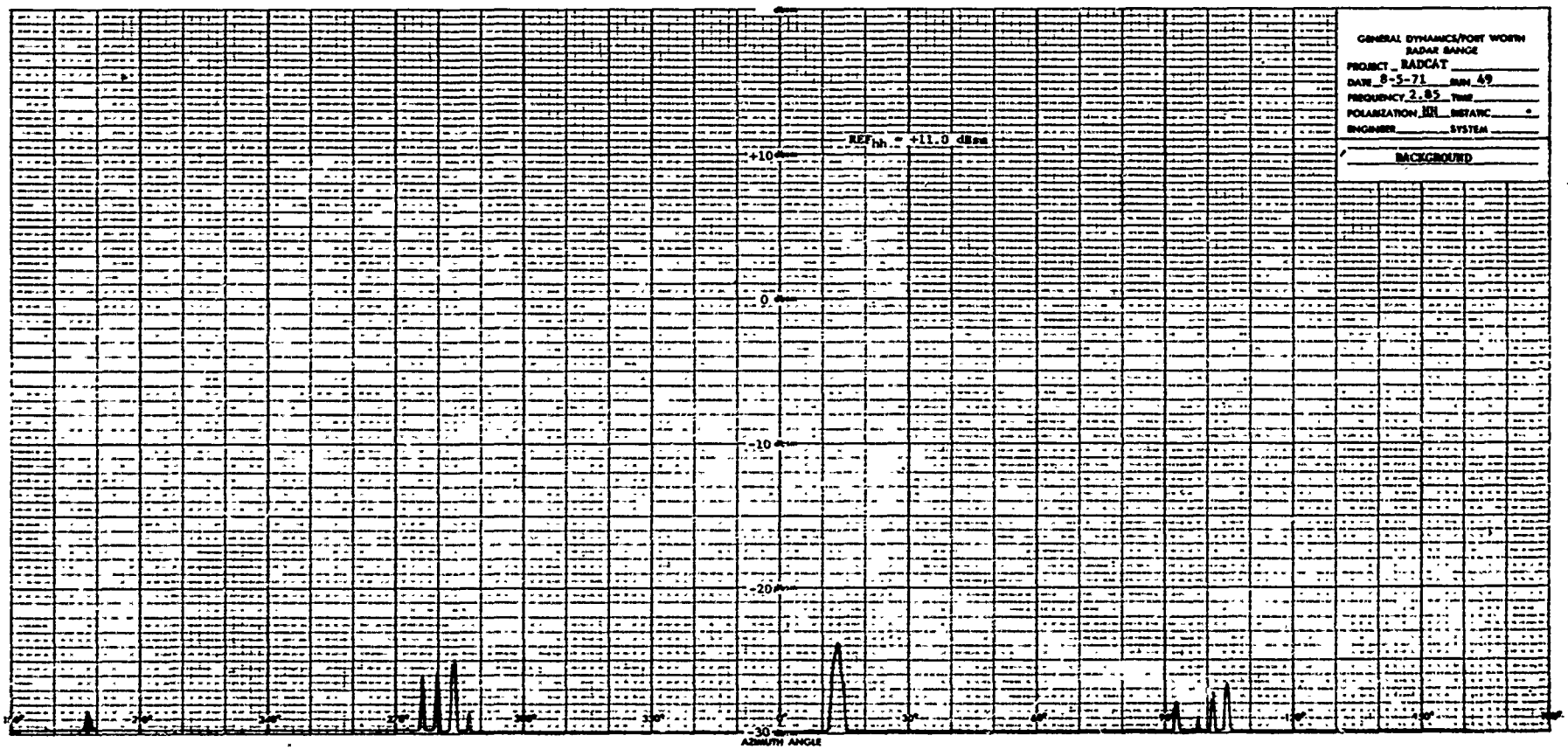

Fig. B-21 BACKGROUND, HH POLARIZATION, S-BAND

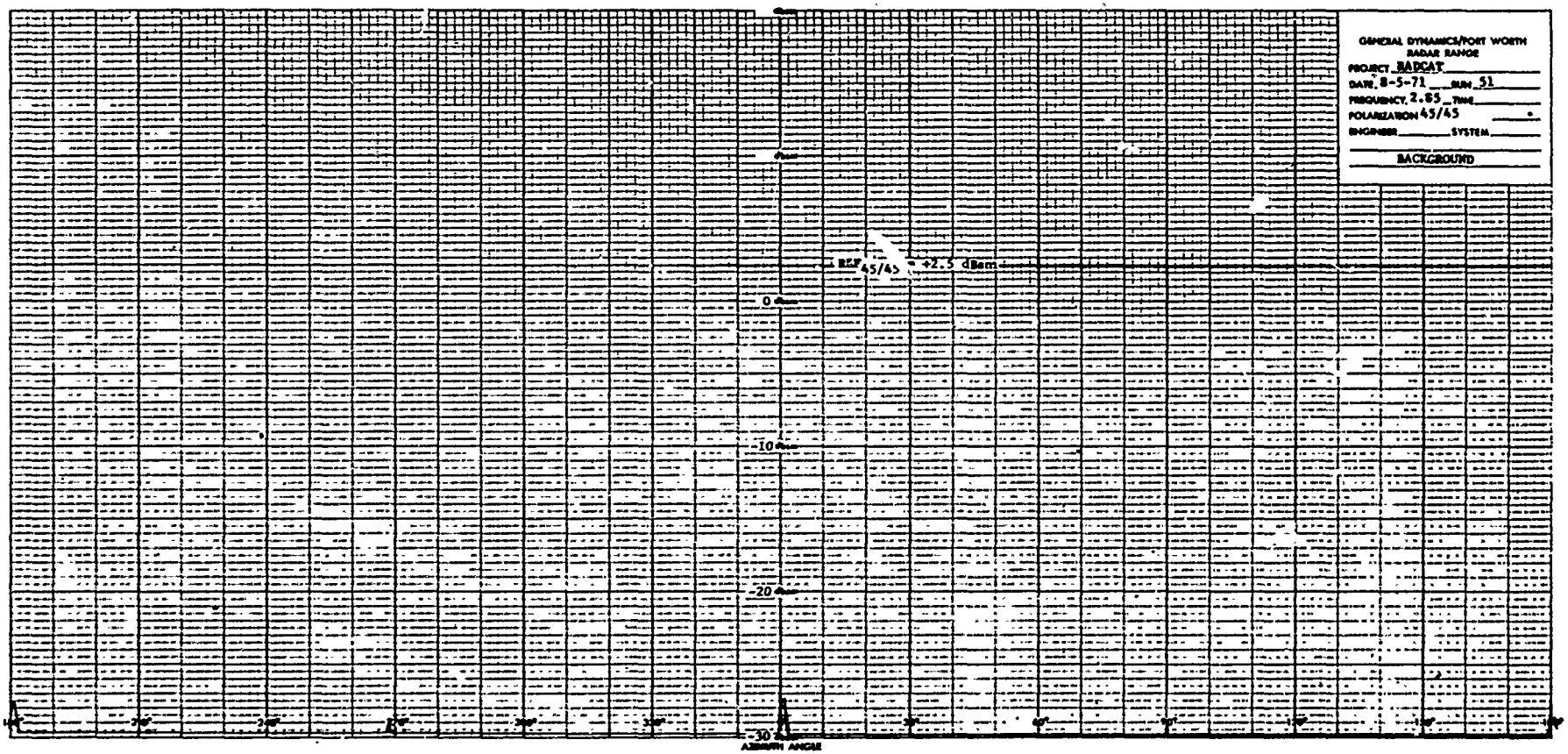

Fig. B-22 BACKGROUND, 45/45 POLARIZATION, S-BAND

PROJECT RADCAT
DATE RUN 60
FREQUENCY 1.28
POLARIZATION VV&HH

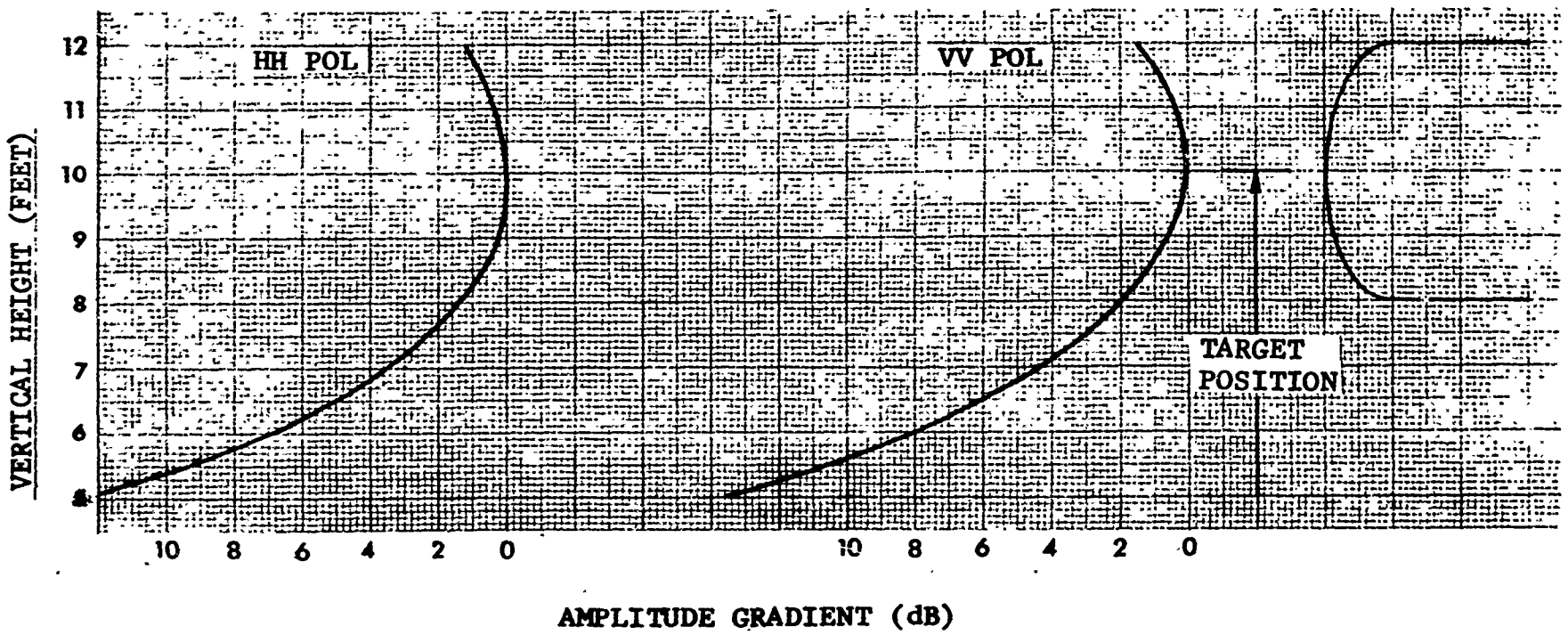

Fig. 3B-23 HORIZONTAL FIELD PROBE. LONG-PULSE, L-BAND

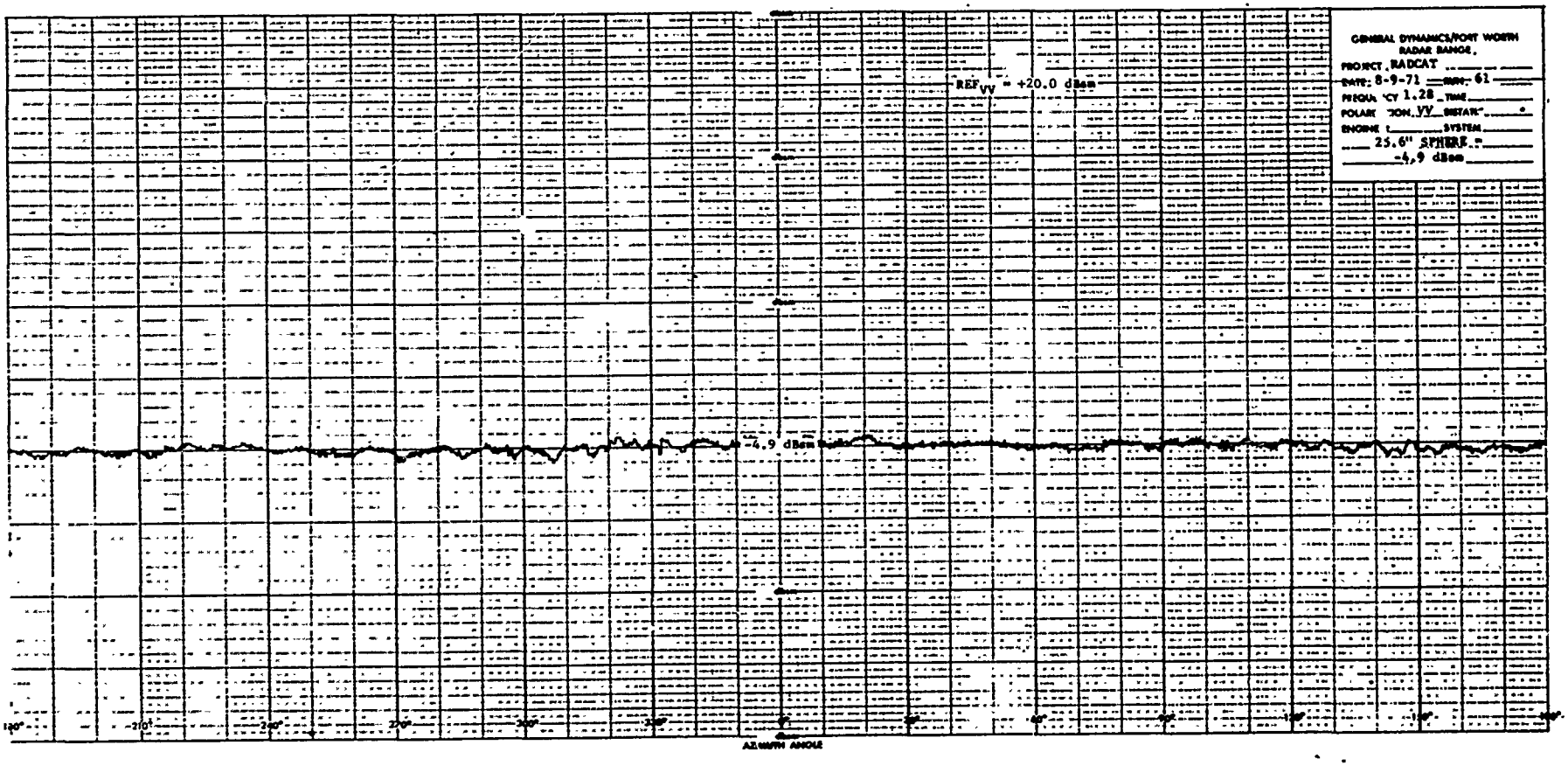

Fig. B-24 AMPLITUDE CALIBRATION, VV POLARIZATION, L-BAND

4

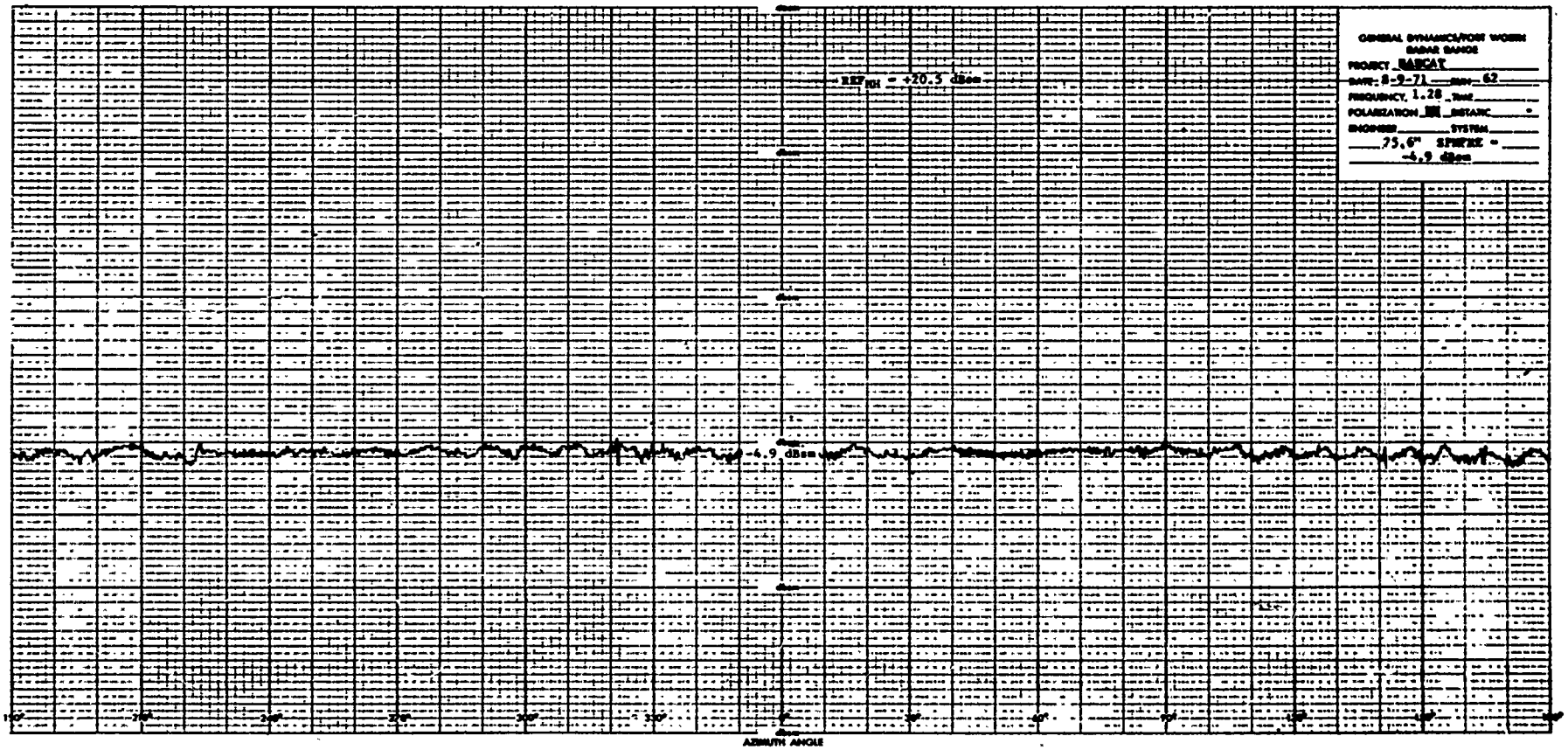

Fig. B-25 AMPLITUDE CALIBRATION, HH POLARIZATION, L-BAND

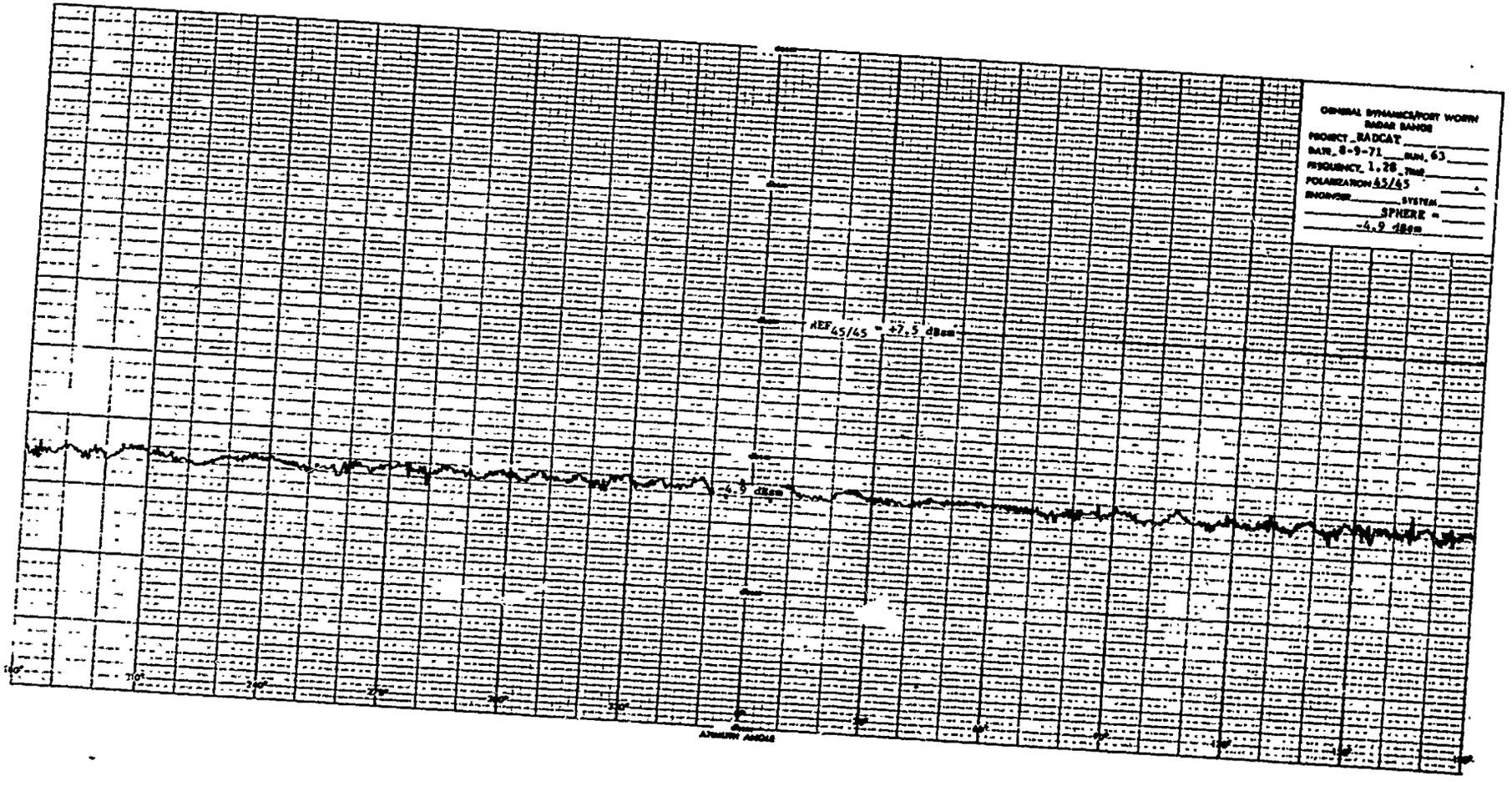

Fig. B-26 AMPLITUDE CALIBRATION, 45/45 POLARIZATION, L-BAND

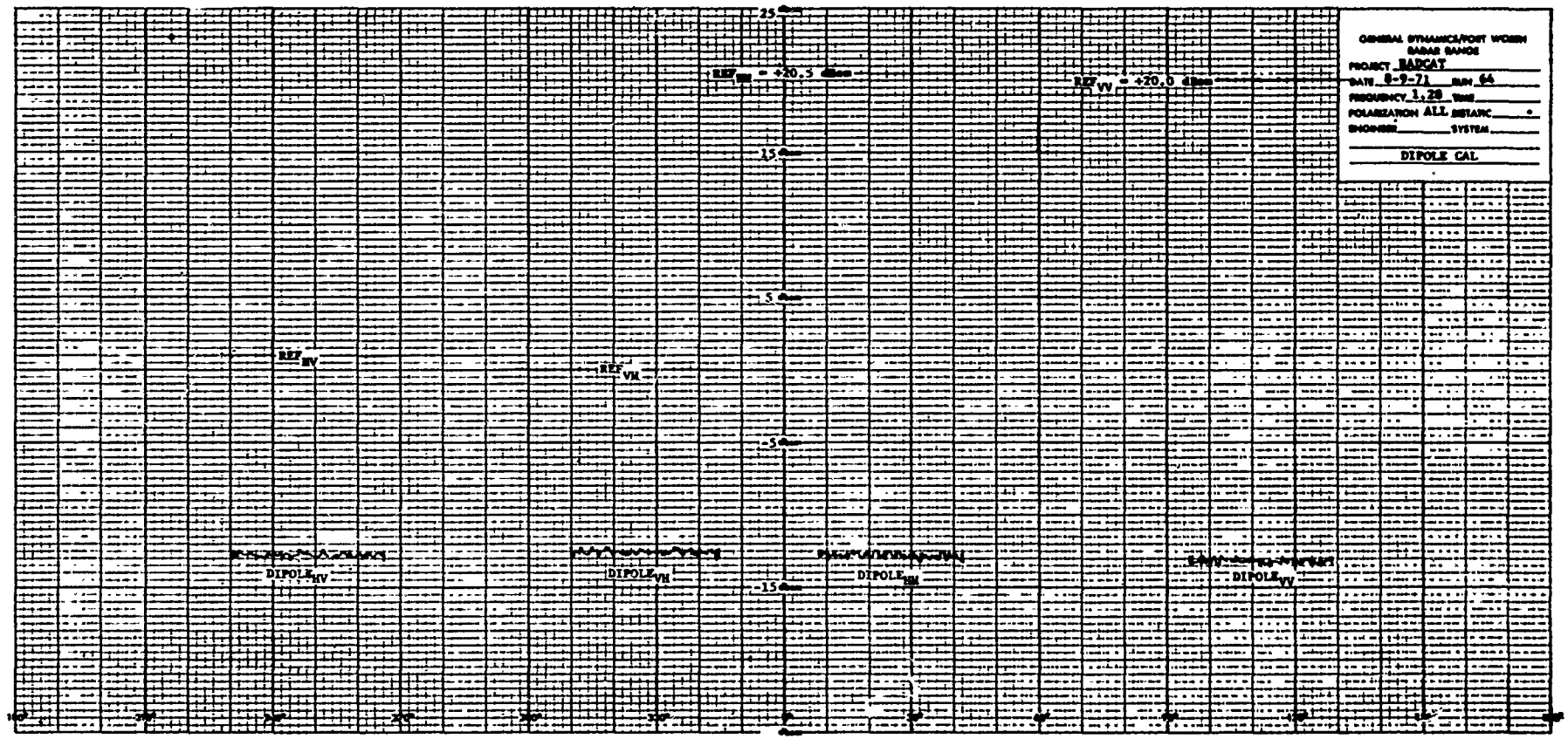

Fig. B-27 DIPOLE CALIBRATION, L-BAND

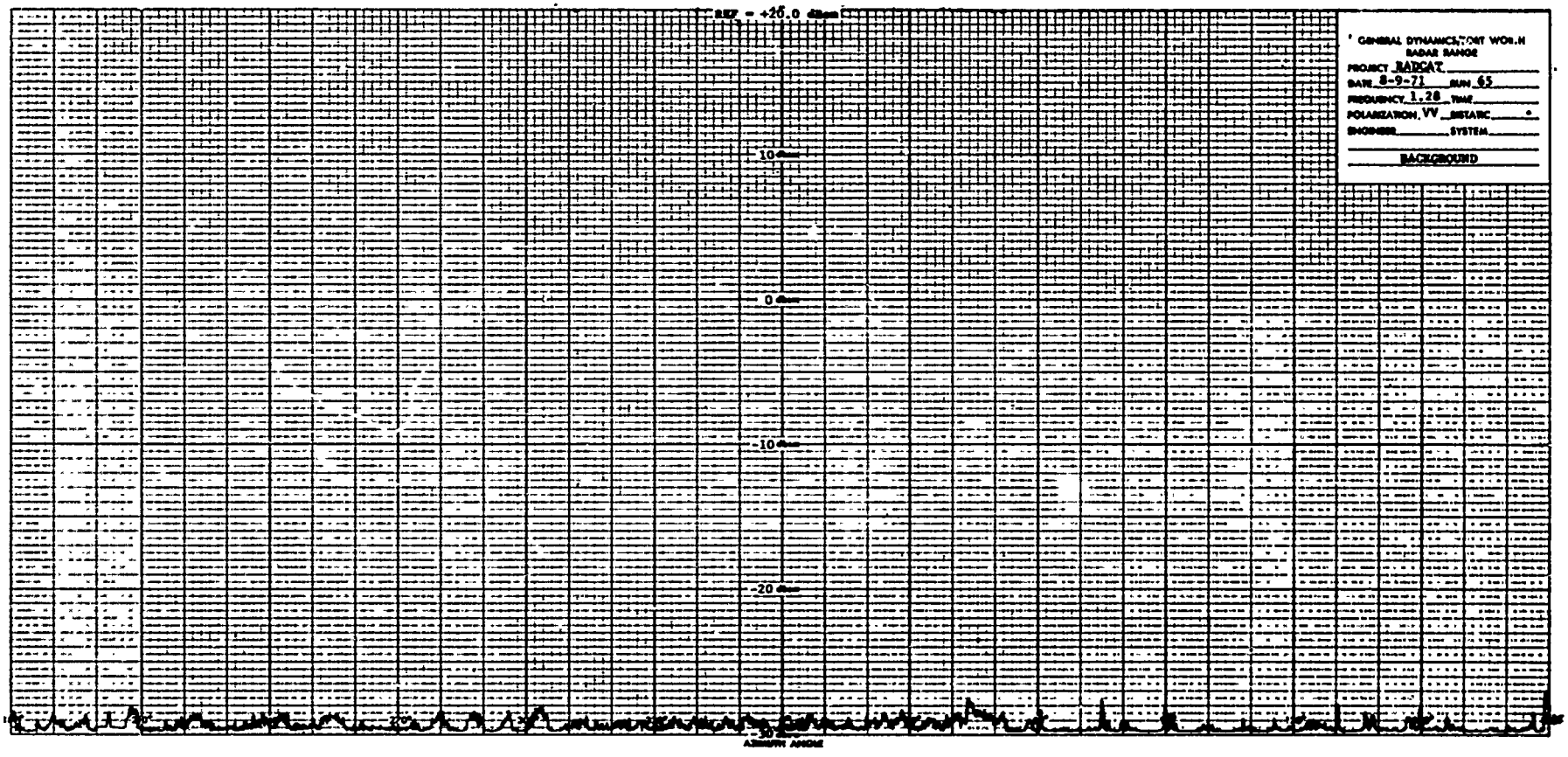

Fig. B-28 BACKGROUND, VV POLARIZATION, L-BAND

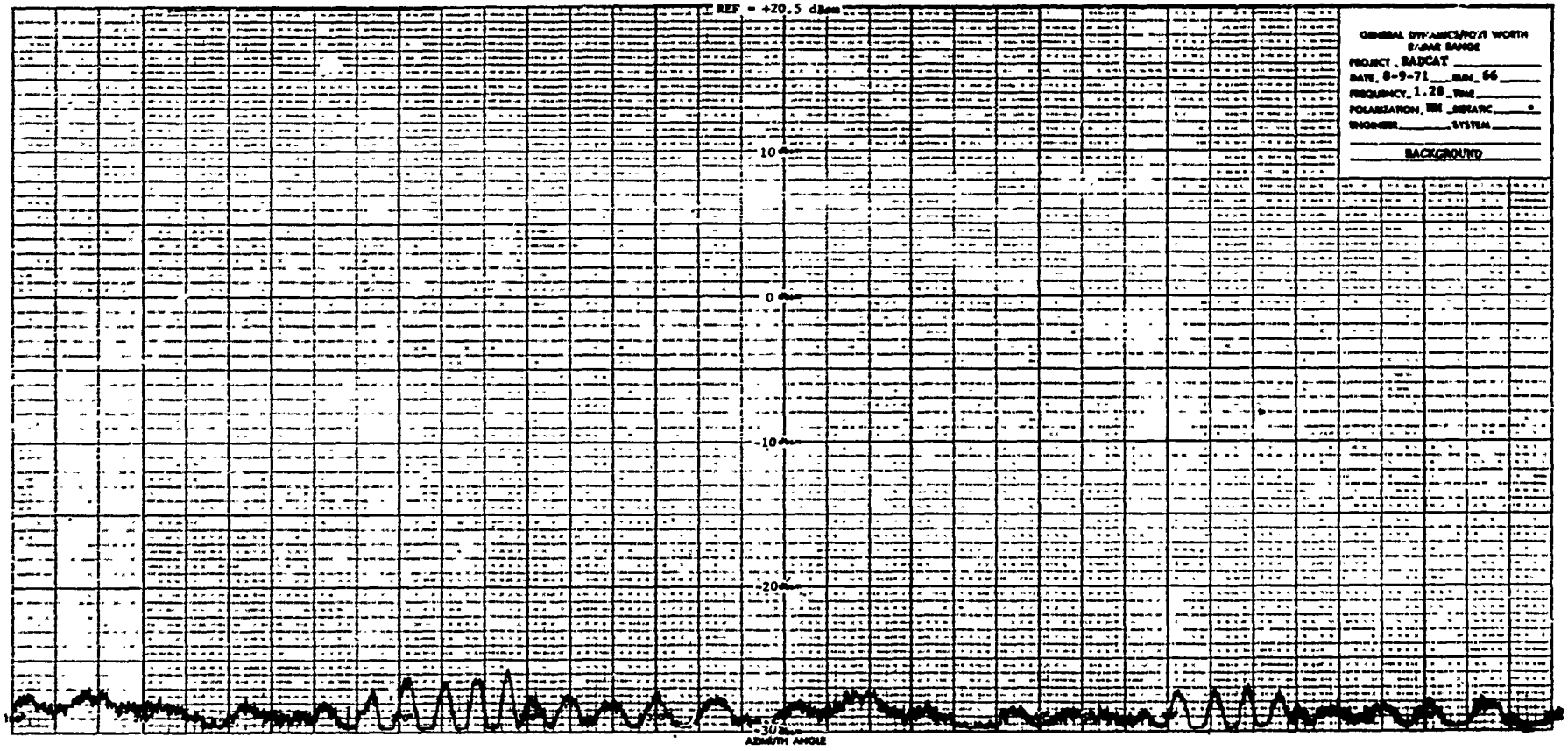

Fig. B-29 BACKGROUND, HH POLARIZATION, L-BAND

27

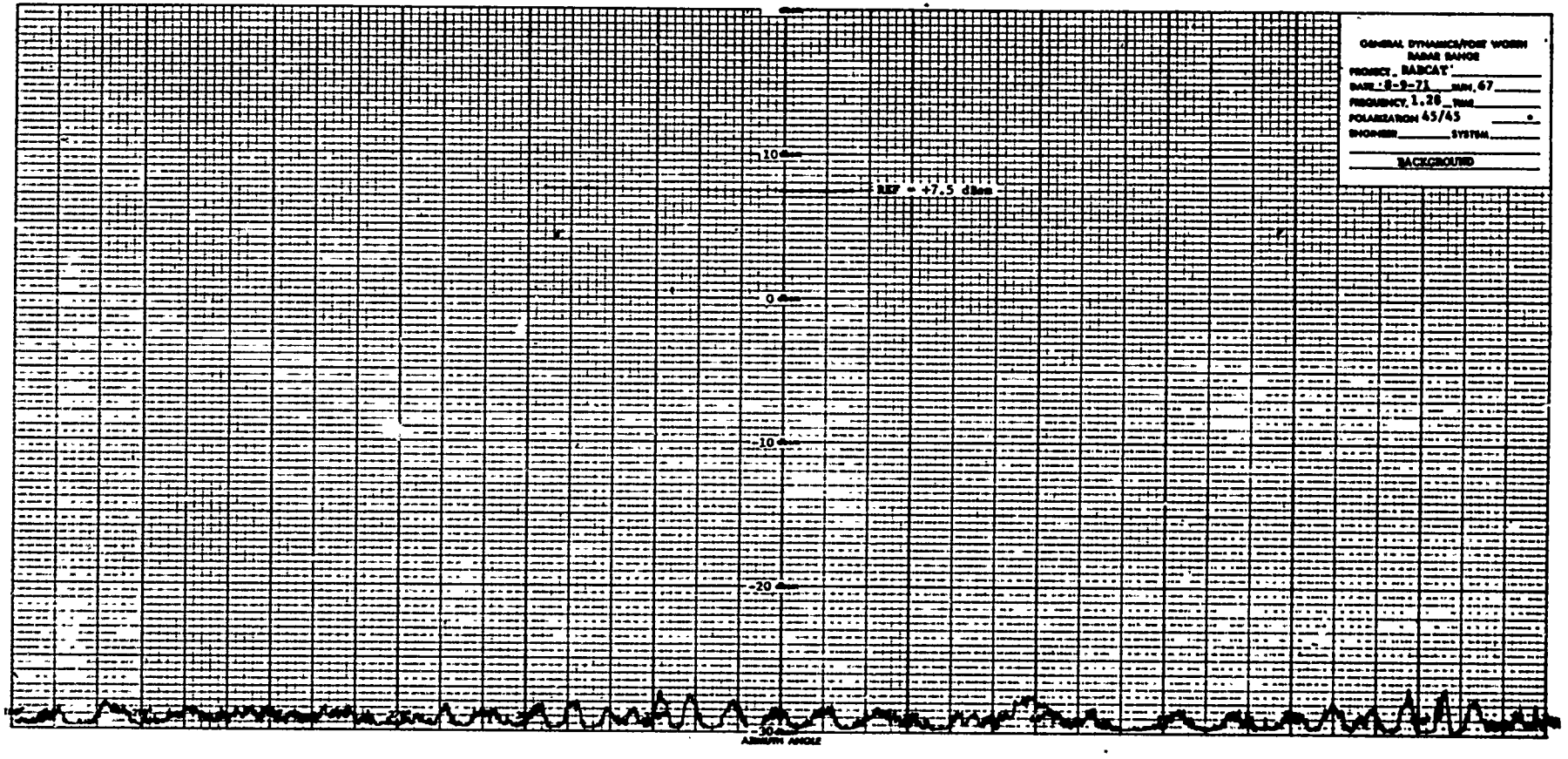

Fig. B-30 BACKGROUND, 45/45 POLARIZATION, L-BAND

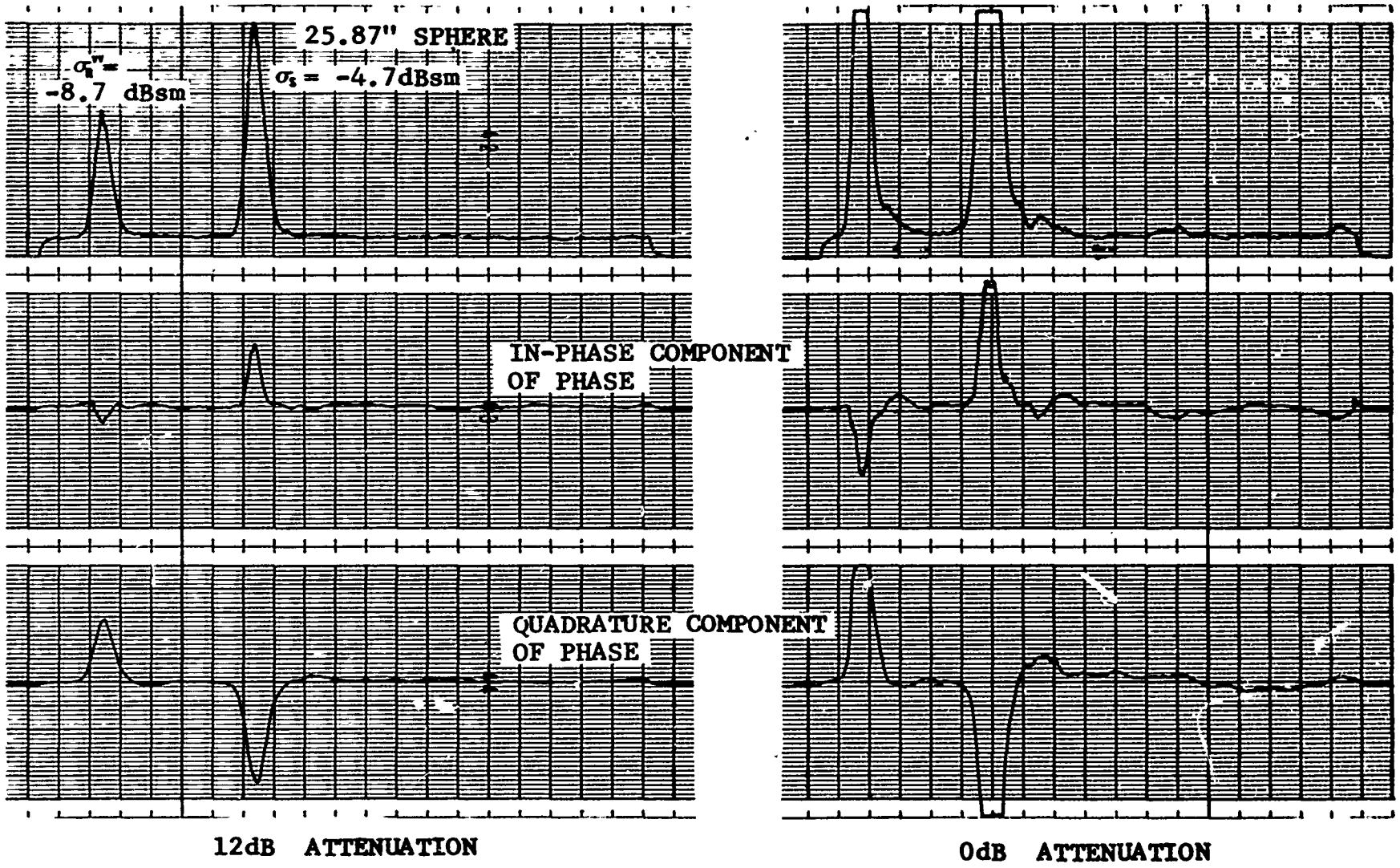

Fig. B-31 C-BAND PULSE SHAPE AND TIME SIDELOBES (VV POLARIZATION)

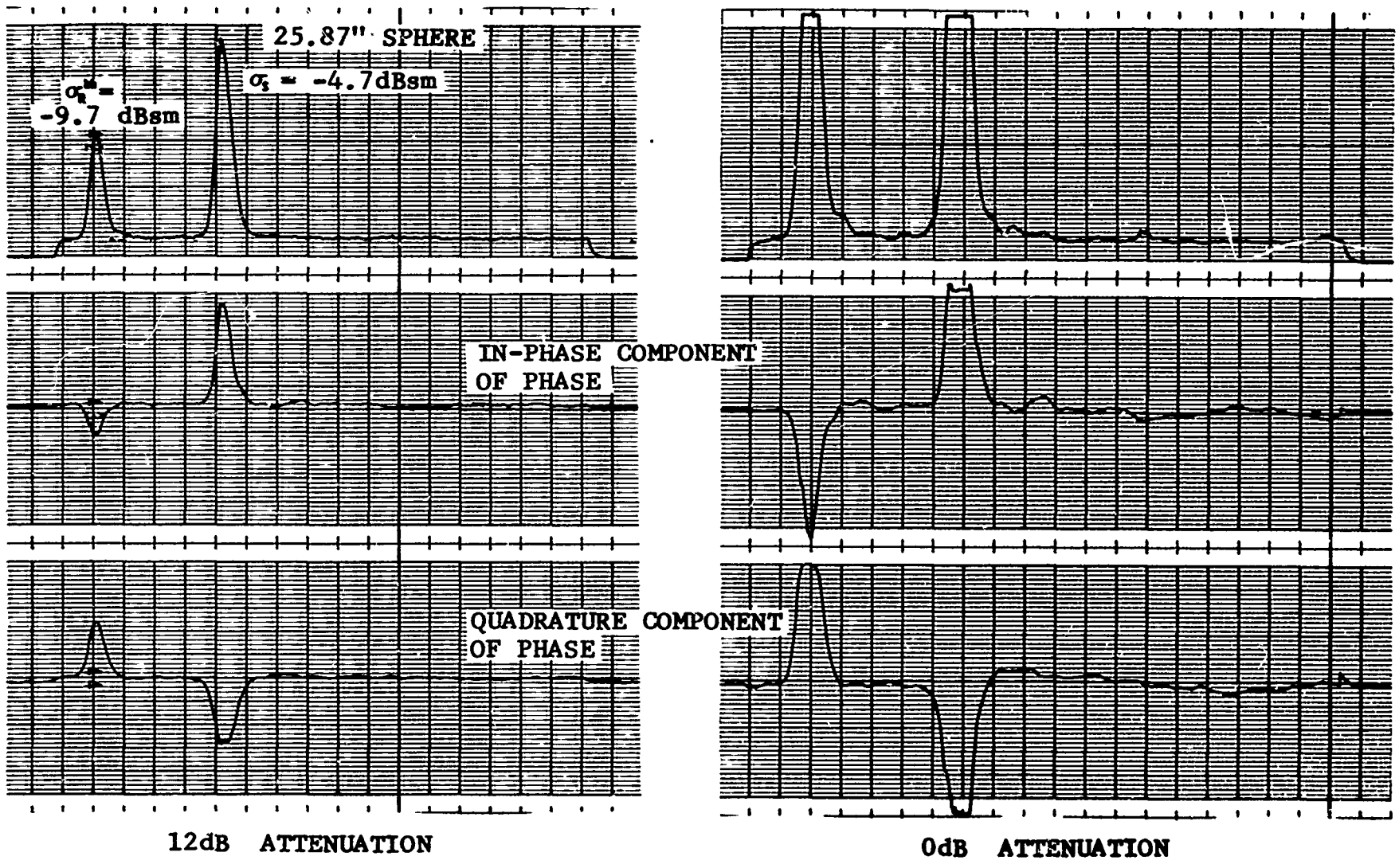

Fig. B-32 C-BAND PULSE SHAPE AND TIME SIDELOBES (HH POLARIZATION)

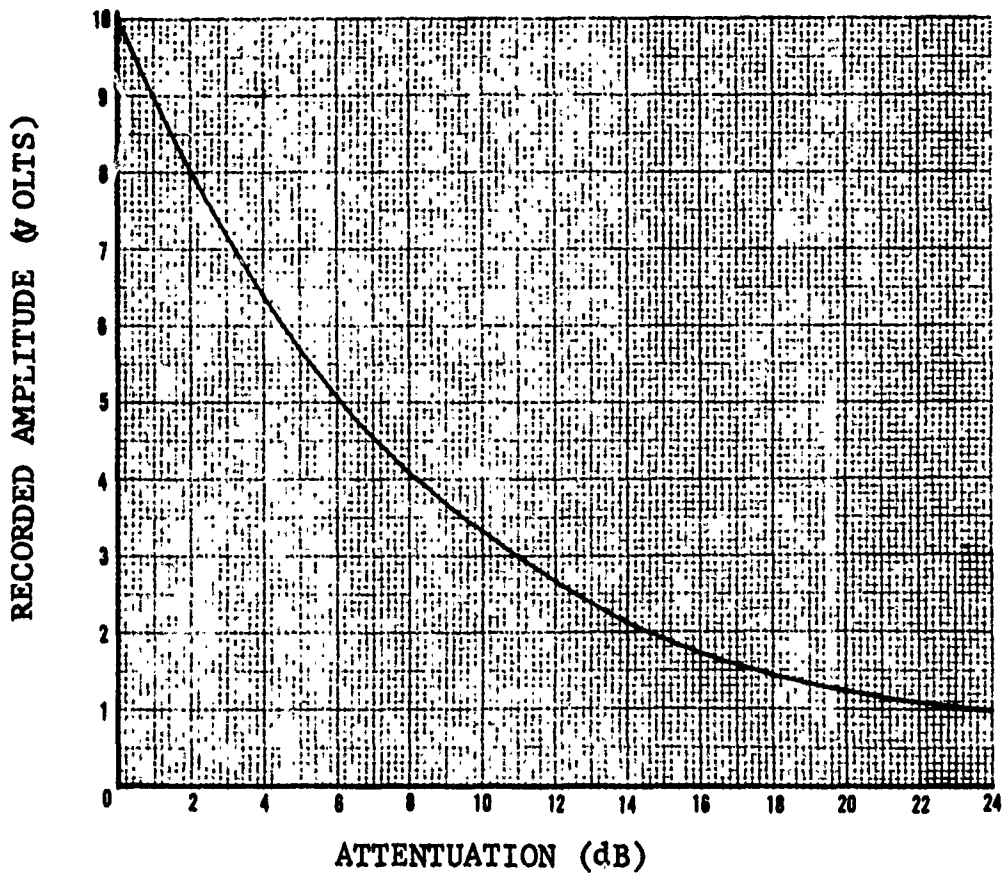

Fig. B-33 C-BAND SHORT-PULSE SYSTEM LINEARITY

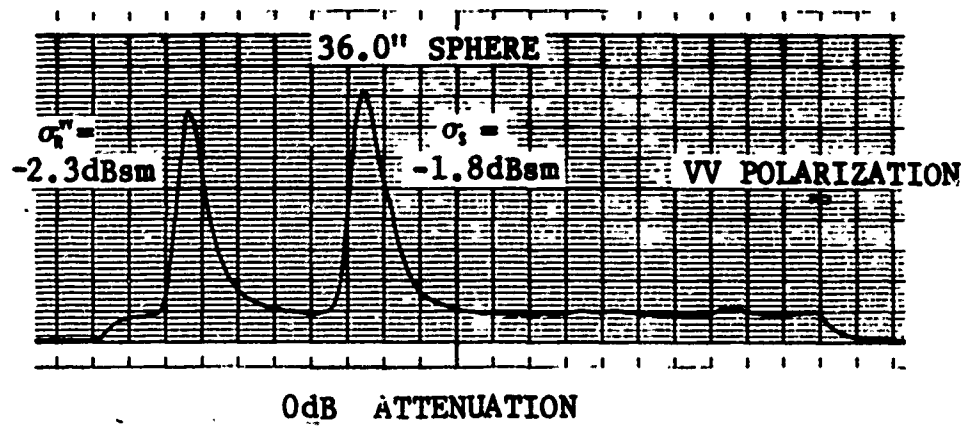

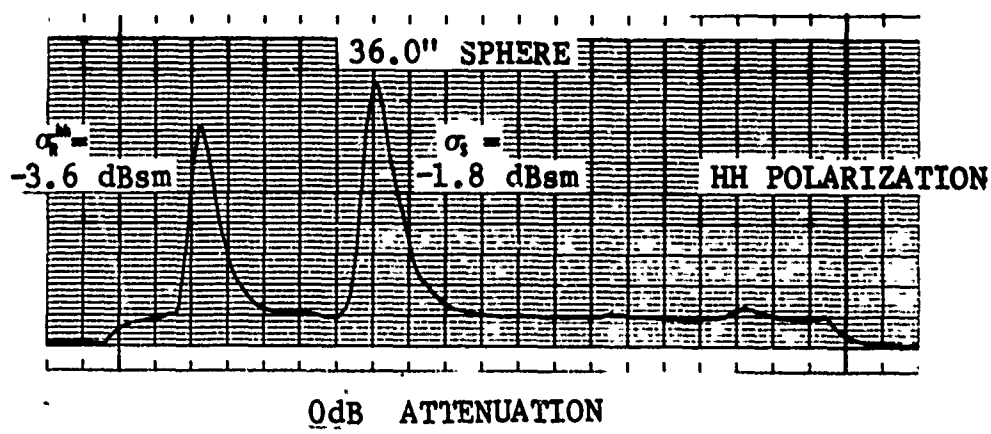

Fig. B-34 S-BAND PULSE SHAPE

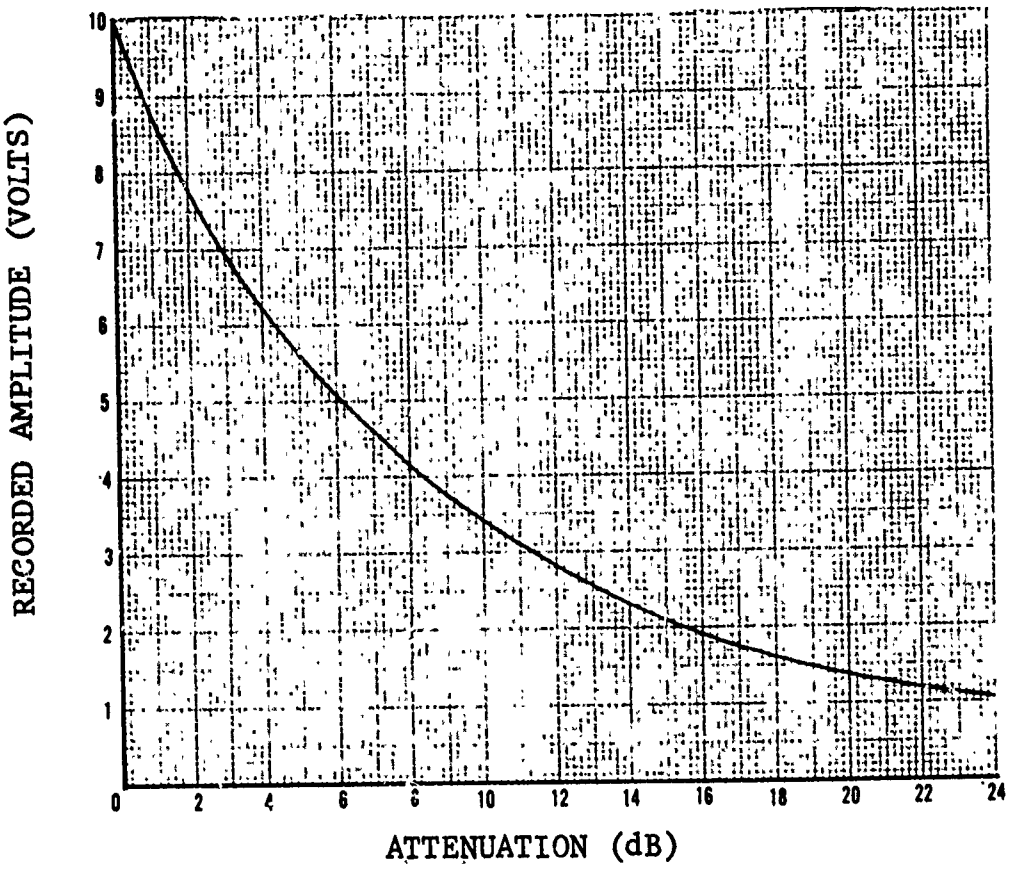

Fig. B-35 S-BAND SHORT-PULSE SYSTEM LINEARITY

APPENDIX C

DATA LISTING FOR SHORT-PULSE MEASUREMENTS

The data contained in this appendix correspond to the calibrated peak radar cross section response of RADCAT Vehicle 002 as measured through the use of this Division's C-band and S-band short-pulse radar systems. The peak amplitudes observed at each measurement aspect angle have been calibrated in dBsm; the corresponding relative phase (C-band only) has been calibrated in degrees, module 2π.

In the listings that follow, θ designates the aspect angle orientation of the vehicle, σ designates the peak radar cross section amplitude response, and ϕ designates the phase response.

C.1 C-Band Coherent Short-Pulse Response; VV Polarization

θ(deg)	σ(dBsm)	ϕ(deg)
0.8	8.6	94.0
1.8	7.8	85.5
2.8	7.2	65.1
3.7	7.2	50.9
4.6	7.1	34.0
5.5	6.9	34.0
6.3	6.2	15.5
7.4	5.4	10.3
8.3	5.9	0.0
9.4	5.5	6.0
10.4	5.5	0.5
11.3	5.4	10.3
12.3	5.4	22.2
13.3	5.0	25.1
14.3	5.4	30.6
15.2	4.7	37.8
16.2	5.3	84.5
17.2	3.2	99.8
18.2	4.1	112.5
19.3	4.8	145.3
20.2	3.9	165.1
21.3	4.1	179.5
22.3	4.5	237.0
23.2	4.9	251.5

θ(deg)	σ(dBsm)	ϕ(deg)
26.2	2.5	19.7
27.2	3.5	78.3
28.4	3.6	150.0
29.4	2.0	205.1
30.7	1.4	271.0
31.8	2.4	357.8
32.8	2.6	104.0
33.8	1.2	173.0
34.9	1.8	271.0
35.9	1.1	9.2
37.0	-0.1	104.0
38.1	0.0	197.7
39.1	1.1	328.0
40.2	0.0	66.0
41.3	-1.0	34.0
42.4	0.2	346.8
43.5	-0.7	128.0
44.7	-1.4	258.5
45.8	-1.1	14.0
46.8	-2.0	249.6
47.8	-1.6	346.5
48.8	-2.3	137.0
49.9	-1.9	348.0
51.0	-1.9	92.0

θ(deg)	σ(dBsm)	ϕ(deg)
53.9	-3.2	344.9
54.9	-2.9	97.5
56.0	-3.2	304.0
57.1	-3.2	118.2
58.1	-3.5	343.0
59.0	-4.3	155.8
60.1	-3.2	336.1
61.1	-4.3	154.5
62.1	-4.3	75.0
63.1	-3.6	319.9
64.1	-4.7	119.0
65.1	-5.0	350.5
66.1	-4.3	34.0
67.1	-4.7	124.0
68.0	-4.7	298.5
69.1	-4.7	149.3
70.1	-5.5	34.0
71.1	-5.9	304.0
72.2	-5.9	160.0
73.1	-4.8	
74.3	-5.6	22.2
75.3	-5.9	325.0
76.4	-6.6	242.0
77.4	-6.9	127.2

θ (deg)	σ (dBsm)	ϕ (deg)
80.5	- 6.6	271.0
81.5	- 4.3	174.4
82.6	- 4.3	112.0
83.7	- 4.7	57.0
84.7	- 3.2	352.3
85.7	- 2.0	317.1
86.7	0.8	209.2
87.7	5.6	161.5
83.0		61.8
88.6	11.1	
89.1	19.0	
89.2		104.0
89.5	22.0	
89.8	24.8	
90.0	24.6	
90.3	20.9	102.0
90.6	19.4	
90.9	15.3	
91.1	11.1	
91.3	7.2	311.1
92.0	1.8	125.3
92.5		173.5
92.7	- 1.8	261.2
93.7	- 5.6	294.1
95.0	- 7.2	164.1

Table C-2 C-BAND COHERENT SHORT-PULSE RESPONSE;
HH POLARIZATION (Sheet 1 of 2)

θ(deg)	σ(dBsm)	ϕ(deg)	θ(deg)	σ(dBsm)	ϕ(deg)	θ(deg)	σ(dBsm)	ϕ(deg)
-3.6	8.6	172.0	15.9	6.1	109.1	35.7	0.6	134.2
-2.8	8.9	161.0	16.7	5.3	129.7	36.7	0.4	218.5
-2.0	8.9	135.4	17.5	5.2	129.7	37.7	0.9	323.8
-1.3	8.9	120.5	18.2	4.5	167.0	38.3	0.0	49.0
-0.2	9.4	120.5	19.1	3.9	168.2	39.2	0.3	120.8
0.5	9.1	102.2	19.8	4.7	176.9	40.1	0.6	210.0
1.4	9.0	105.5	20.7	5.2	225.0	40.9	-1.0	325.6
2.1	7.9	86.0	21.5	4.0	270.3	41.8	0.0	84.0
2.9	8.7	91.0	22.3	4.0	285.6	42.8	-0.2	185.8
3.8	6.8	98.0	23.0	4.4	323.5	43.7	-1.3	300.0
4.7	7.3	89.5	23.9	2.8	350.3	44.4	-1.0	58.3
5.3	6.3	42.1	24.8	3.3	33.7	45.3	-2.0	130.6
6.3	5.3	49.5	25.5	2.9	85.5	46.0	-1.1	289.7
7.0	5.9	51.2	26.3	4.2	115.3	46.9	-1.0	28.0
7.8	5.3	358.0	27.2	2.9	62.7	47.9	-1.1	164.5
8.7	5.7	357.0	28.0	3.2	215.0	48.7	-2.0	309.0
9.5	6.7	7.5	28.8	3.2	289.8	49.5	-2.3	109.0
10.2	6.4	21.9	29.8	2.3	348.2	50.3	-1.9	237.0
11.2	6.4	43.4	30.5	1.4	49.6	51.2	-2.6	0.5
12.0	5.3	50.0	31.5	2.1	101.0	52.0	-2.2	136.5
12.7	5.9	76.6	32.3	1.1	197.5	52.8	-2.9	323.5
13.5	6.5	82.5	33.2	1.9	286.5	53.7	-3.0	89.0
14.3	6.0	80.4	34.0	1.4	350.6	54.2	-2.3	215.2
15.0	5.7	101.8	34.9	0.6	70.0	55.1	-2.0	41.0

Table C-2 C-BAND COHERENT SHORT-PULSE RESPONSE; HH POLARIZATION (Sheet 2 of 2)

ϑ(deg)	σ(dBsm)	ϕ(deg)
55.8	-3.4	168.2
56.7	-3.3	323.3
57.7	-3.2	220.3
58.4	-3.7	0.0
59.2	-2.6	212.5
60.0	-2.6	312.1
60.9	-3.7	91.1
61.7	-3.7	275.2
62.3	-3.7	103.5
63.0	-4.3	197.5
63.9	-4.3	48.8
64.7	-4.3	255.5
65.5	-4.8	70.0
66.3	-5.8	258.0
67.0	-5.2	85.3
67.9	-5.7	323.5
68.8	-4.8	85.3
69.7	-4.8	16.0
70.3	-5.3	180.9
71.2	-4.7	100.3

θ(deg)	σ(dBsm)	ϕ(deg)
72.0	-4.8	237.0
72.9	-4.8	83.5
73.7	-5.9	312.5
74.5	-4.8	112.8
75.2	-6.5	321.0
76.1	-5.4	185.1
75.9	-5.4	88.6
77.8	-6.8	328.5
78.5	-7.0	149.2
79.3	-6.3	357.3
80.0	-5.1	237.0
80.7	-6.0	108.0
81.6	-5.9	0.0
82.4	-5.9	254.6
83.3	-4.3	212.5
84.1	-3.7	28.0
84.9	-2.9	286.7
85.7	-1.8	150.6
86.5	0.6	81.6
87.4	2.0	350.1

θ(deg)	σ(dBsm)	ϕ(deg)
88.2	8.9	245.2
89.0	19.0	41.5
89.4	21.6	116.8
89.7	23.7	132.5
89.9	25.3	140.0
90.0	24.9	175.5
90.2	22.1	139.0
90.5	19.8	95.0
90.7	19.0	75.5
90.9	16.9	37.0
91.0	11.6	0.0
91.5	4.2	161.5
92.3	1.1	314.6
93.2	-1.8	83.4
94.0	-4.2	164.0
94.8	-5.9	0
95.7	-6.0	97.2
96.4	-6.7	294.0
97.2	-7.0	7.0

Table C-3 S-BAND SHORT-PULSE RESPONSE;
VV POLARIZATION (Sheet 1 of 2)

θ(deg)	σ(dBsm)	θ(deg)	σ(dBsm)	θ(deg)	σ(dBsm)	θ(deg)	σ(dBsm)
-9.9	6.6	12.3	6.2	35.3	1.25	57.7	-1.9
-8.7	7.2	13.3	6.05	36.2	2.1	58.8	-2.4
-7.7	6.9	14.2	5.55	37.2	0.75	59.8	-2.8
-6.6	7.9	15.2	6.6	38.2	1.2	60.7	-2.3
-5.8	8.6	16.2	5.1	39.1	1.05	61.6	-3.1
-4.9	8.5	17.2	5.65	40.1	1.40	62.5	-3.4
-4.1	8.9	18.2	5.65	41.0	-0.4	63.5	-3.55
-3.2	9.1	19.1	5.2	41.9	+0.2	64.4	-3.4
-2.3	9.5	20.1	5.2	43.0	-0.2	65.3	-3.35
-1.3	9.2	21.1	5.7	43.9	-0.5	66.3	-3.15
-0.4	9.8	22.0	4.85	44.8	-0.1	67.2	-3.85
0.4	9.2	22.9	4.45	45.8	-1.0	68.1	-4.15
1.4	9.9	24.0	4.7	46.7	-0.6	69.0	-3.75
2.3	9.5	24.9	4.45	47.6	-0.35	69.9	-4.3
3.2	9.0	25.9	3.75	48.6	-1.15	71.0	-4.7
4.1	8.7	26.8	3.5	49.5	-1.4	71.9	-0.75
5.0	8.4	27.8	3.85	50.4	-1.8	72.8	-4.35
5.6	8.2	28.7	2.7	51.4	-1.8	73.8	-4.65
6.8	7.45	29.7	3.4	52.3	-2.2	74.7	-4.55
7.7	6.75	30.7	2.15	53.2	-1.3	75.6	-4.7
8.6	7.25	31.6	3.2	54.1	-1.1	76.6	-3.8
9.5	7.2	32.5	2.8	54.9	-1.9	77.5	-3.5
10.5	7	33.4	2.3	55.7	-2.4	78.5	-4.0
11.4	6.87	34.3	2.3	56.8	-2.6	79.5	-3.55

Table C-3 S-BAND SHORT-PULSE RESPONSE;
VV POLARIZATION (Sheet 2 of 2)

θ(deg)	σ(dBsm)
80.4	-3.0
81.3	-3.0
82.2	-1.5
83.1	-1.5
84.0	-0.8
85.0	0.1
85.8	2.5
86.7	5.1
87.6	10.1
87.9	10.92
88.0	10.57
88.1	10.57
88.2	11.07
88.3	10.92
88.4	11.27
88.5	11.47

θ(deg)	σ(dBsm)
88.6	13.87
88.7	14.87
88.8	16.27
88.9	18.02
89.0	19.12
89.1	19.77
89.2	21.02
89.3	21.57
89.4	22.27
89.5	22.37
89.6	22.77
89.7	22.87
89.8	22.77
89.9	22.77
90.0	22.47

θ(deg)	σ(dBsm)
90.1	22.57
90.2	21.27
90.3	20.87
90.4	19.27
90.5	17.57
90.6	15.67
90.7	14.67
90.8	12.72
90.9	11.07
91.0	9.67
91.1	10.07
91.2	10.07
91.3	10.92
91.4	11.07
91.5	10.57

θ(deg)	σ(dBsm)
91.6	11.07
91.7	10.07
91.8	9.67
91.9	8.57
92.0	6.47
92.1	5.22
92.2	4.0
93.1	1.25
94.0	0.35
94.9	-2.3
95.9	-3.35
96.8	-3.05
97.7	-4.5
98.9	-4.1
99.7	-5.35

Table C-4 S-BAND SHORT-PULSE RESPONSE; HH POLARIZATION (Sheet 1 of 2)

θ(deg)	σ(dBsm)	θ(deg)	σ(dBsm)	θ(deg)	σ(dBsm)	θ(deg)	σ(dBsm)
-9.8	6.4	13.3	5.4	34.8	2.6	55.8	-1.9
-8.7	6.7	41.2	6.05	35.7	0.65	56.7	-2.15
-7.8	7.2	15.1	6.55	36.5	1.45	57.7	-2.6
-6.8	7.5	16.1	5.4	37.4	0.6	58.6	-3.6
-5.8	8.2	17.0	5.0	38.4	1.2	59.5	-3.6
-4.9	8.35	17.9	4.4	39.2	0.5	60.4	-3.6
-3.9	8.75	18.8	4.9	40.1	0.3	61.3	-3.45
-3.0	8.65	19.7	5.25	41.0	-0.2	62.1	-3.95
-1.9	8.7	20.6	4.6	41.8	-0.6	63.1	-3.6
-1.0	9.0	21.5	4.8	42.7	-0.6	64.0	-4.05
0.1	9.15	22.4	4.4	43.6	-1.0	64.9	-3.95
0.9	9.0	23.3	3.45	44.5	-0.5	65.8	-4.45
1.9	8.6	24.2	3.35	45.4	-0.4	66.7	-4.9
2.9	7.9	25.1	3.55	46.3	-1.0	67.6	-4.65
3.9	7.95	26.0	3.7	47.2	-1.4	68.4	-4.6
4.8	7.9	26.8	4.0	47.9	-1.8	69.3	-5.15
5.9	7.2	27.7	2.75	48.9	-1.45	70.2	-5.0
6.8	7.05	28.5	2.7	49.8	-1.8	71.1	-4.6
7.7	6.5	29.4	2.9	50.7	-1.9	72.0	-4.3
8.8	6.2	30.3	2.3	51.6	-1.7	73.0	-5.5
9.7	6.1	31.2	2.1	52.5	-1.75	73.9	-5.4
10.6	5.95	32.1	1.2	53.3	-2.0	74.8	-4.8
11.5	5.95	33.0	1.2	54.1	-3.1	75.7	-4.45
12.4	5.5	33.9	2.6	54.9	-2.5	76.6	-4.95

Table C-4 S-BAND SHORT-PULSE RESPONSE;
HH POLARIZATION (Sheet 2 of 2)

θ (deg)	σ(dBsm)
77.5	-4.9
78.4	-4.95
79.3	-4.05
80.2	-3.9
81.0	-3.25
81.9	-2.9
82.8	-2.45
83.7	-1.45
84.6	-0.8
85.2	1.9
86.1	3.1

θ(deg)	σ(dBsm)
86.9	4.6
87.8	9.87
88.0	10.57
88.2	10.57
88.3	10.32
88.5	11.87
88.8	15.97
89.0	18.42
89.2	20.72
89.4	21.42

θ(deg)	σ(dBsm)
89.6	22.87
89.8	22.87
89.9	22.57
90.1	21.97
90.3	19.12
90.5	17.67
90.7	14.02
90.8	10.07
91.0	10.07
91.2	10.57

θ(deg)	σ(dBsm)
91.4	10.57
91.6	10.32
91.8	9.87
91.9	5.05
92.8	3.1
93.7	0.75
94.5	-1.12
95.4	-3.2
96.2	-4.1
97.1	-5.0

This page intensionally left blank

APPENDIX D

VEHICLE 001 LONG-PULSE SIGNATURES

The signatures contained in this appendix correspond to the long-pulse amplitude and phase response of Vehicle 001 at zero-degree and sixty-degree target roll angle orientation. Measurements performed at L-band, S-band, and C-band frequencies and transmitter/receiver polarizations of V/V, H/H, $\pi/4/\pi/4$, and V/H are presented herein. These data have been reproduced from an earlier report which documented the measurements performed on Vehicle 001 (Reference 1). The readers attention is called to the title block appearing in the upper right-hand corner of each analog trace for pertinent measurement parameters.

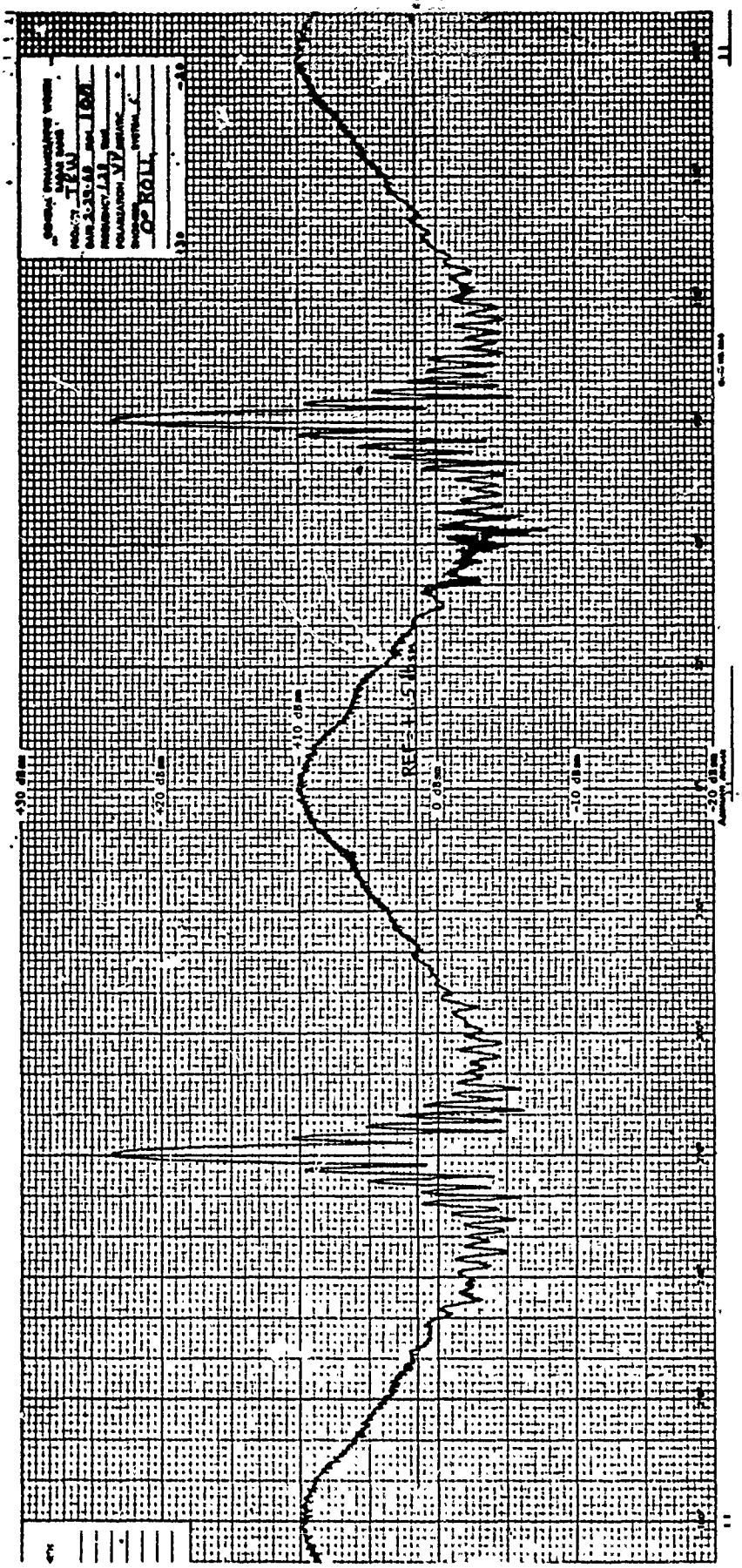

Fig. D-1 VEHICLE 001 AMPLITUDE RESPONSE; L-BAND, VV POLARIZATION, 0-DEGREE ROLL

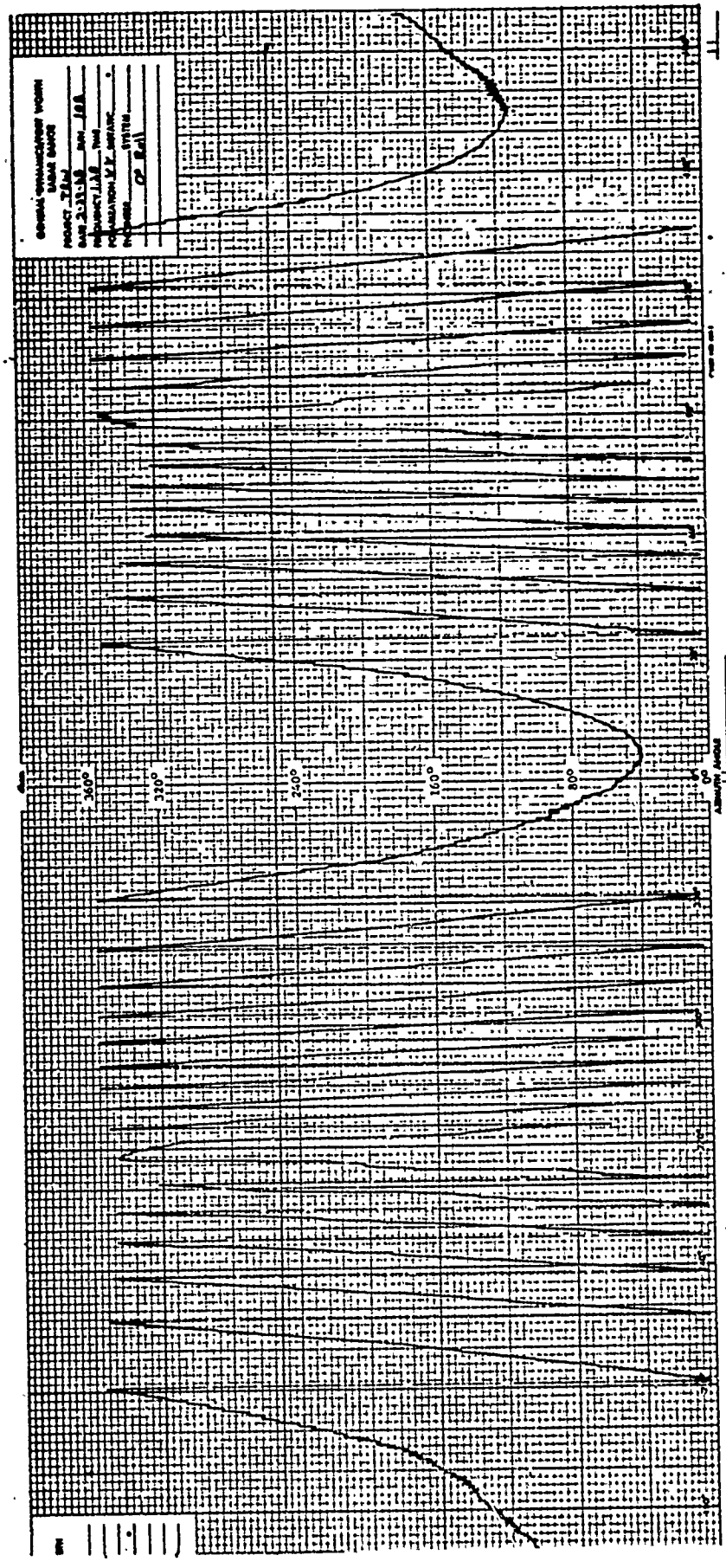

Fig. D-1 VEHICLE 001 PHASE RESPONSE; L-BAND, VV POLARIZATION, 0-DEGREE ROLL

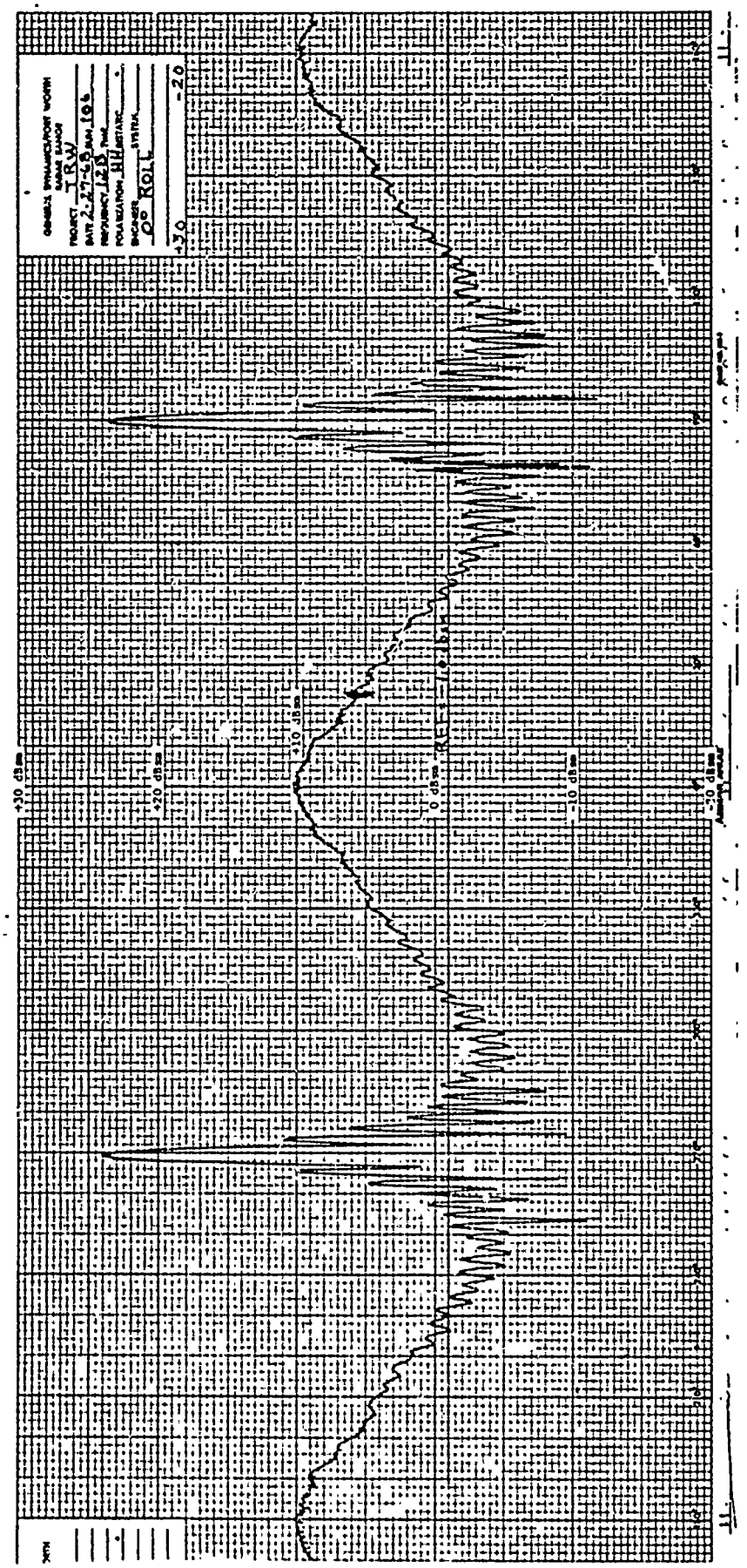

Fig. D-3 VEHICLE 001 AMPLITUDE RESPONSE; L-BAND, HH POLARIZATION, 0-DEGREE ROLL

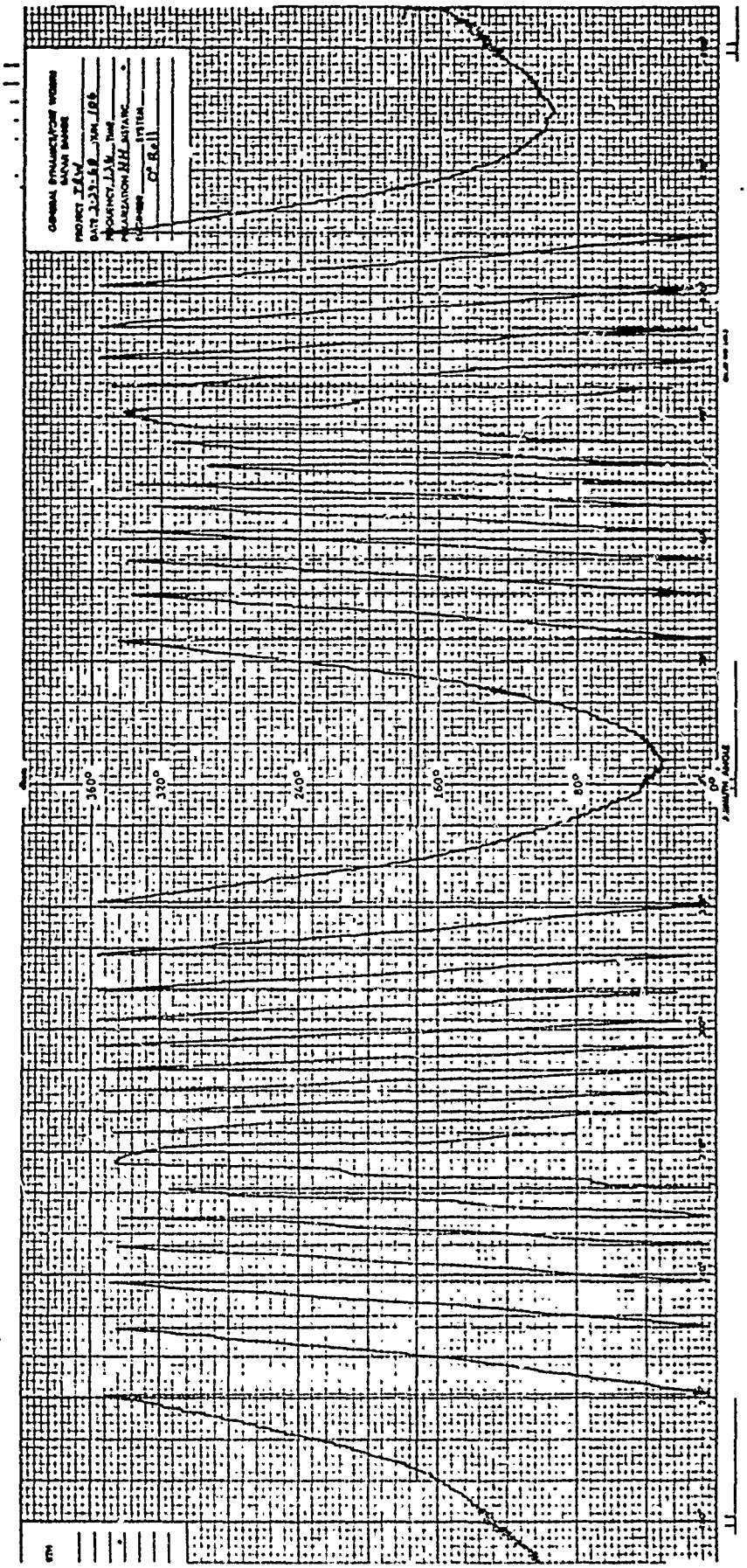

Fig. D-4 VEHICLE 001 PHASE RESPONSE; L-BAND, HH POLARIZATION, 0-DEGREE ROLL

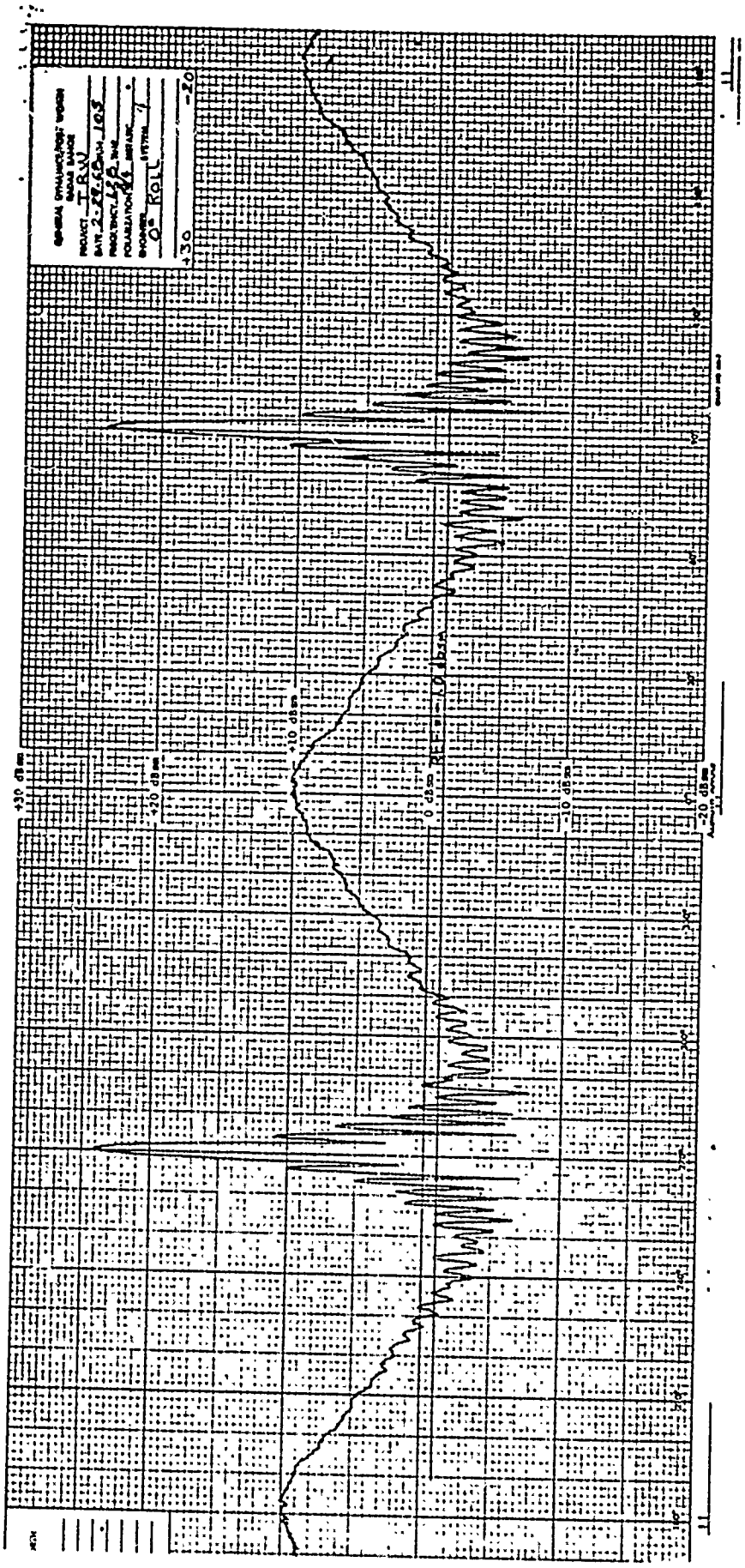

Fig. D-5 VEHICLE 001 AMPLITUDE RESPONSE; L-BAND, $\pi/4$ $\pi/4$ POLARIZATION, 0-DEGREE ROLL

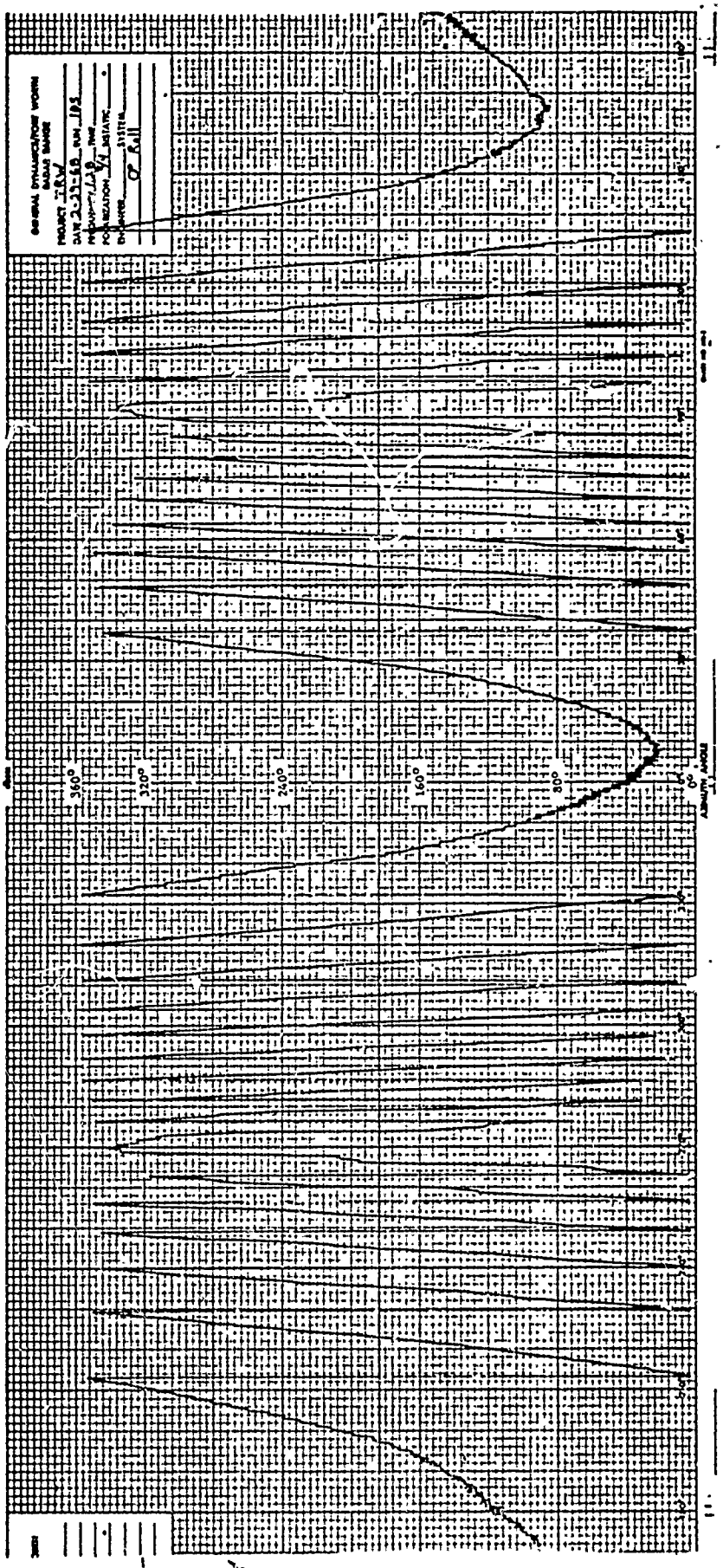

Fig. D-6 VEHICLE 001 PHASE RESPONSE; L-BAND, $\pi/4$ $\pi/4$ POLARIZATION, 0-DEGREE ROLL

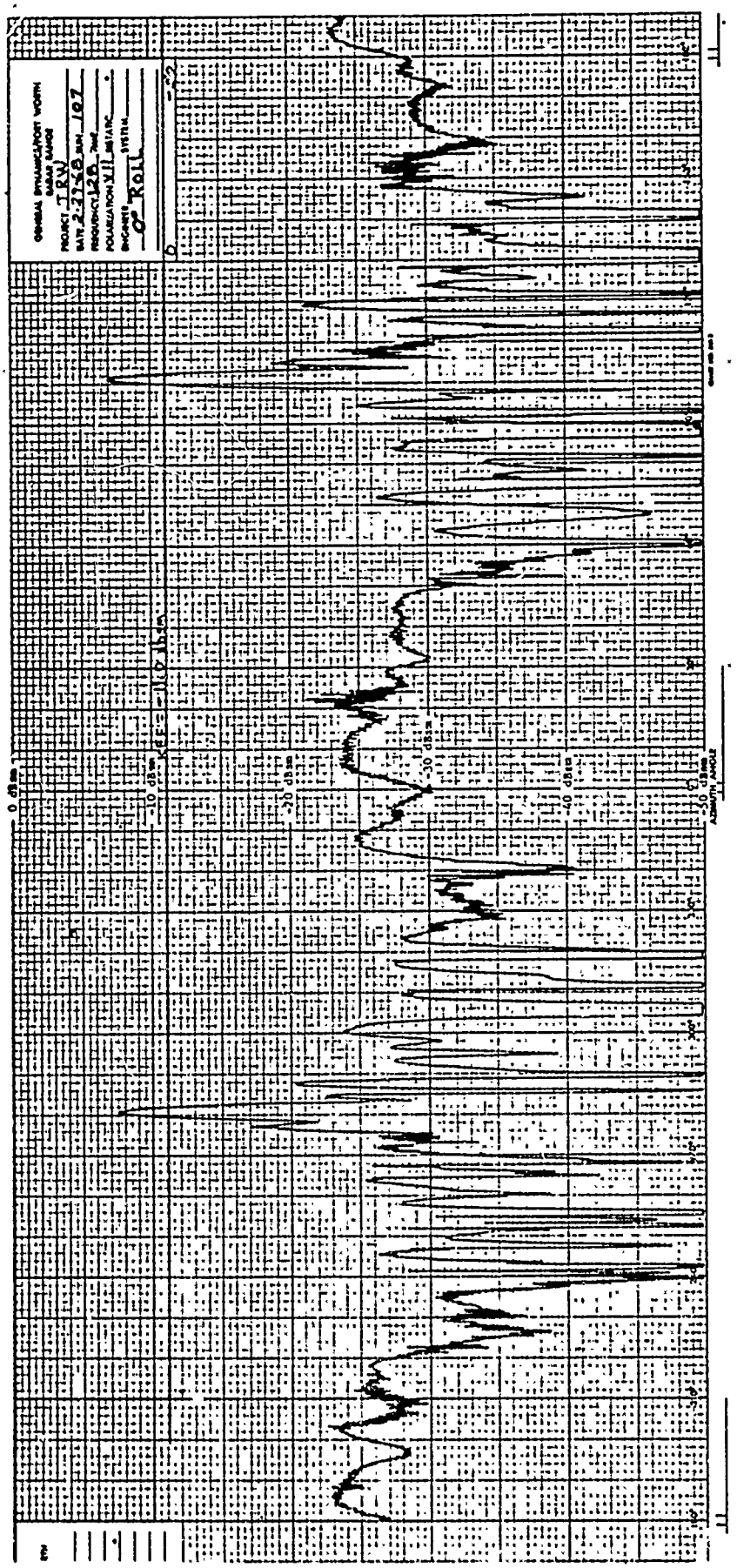

Fig. D-7 VEHICLE 001 AMPLITUDE RESPONSE; L-BAND, VH POLARIZATION, 0-DEGREE ROLL

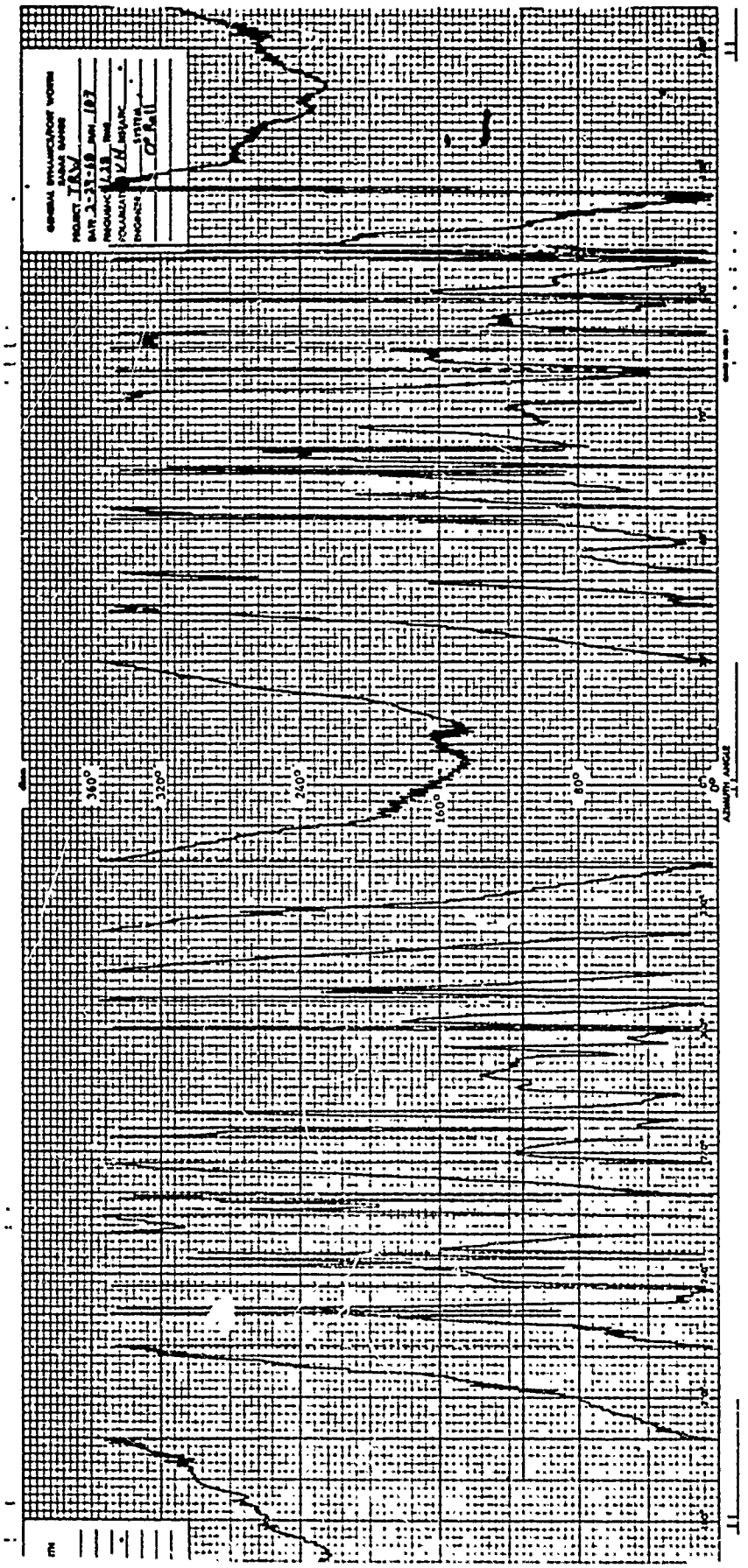

Fig. D-8 VEHICLE 001 PHASE RESPONSE; L-BAND, VH POLARIZATION, 0-DEGREE ROLL

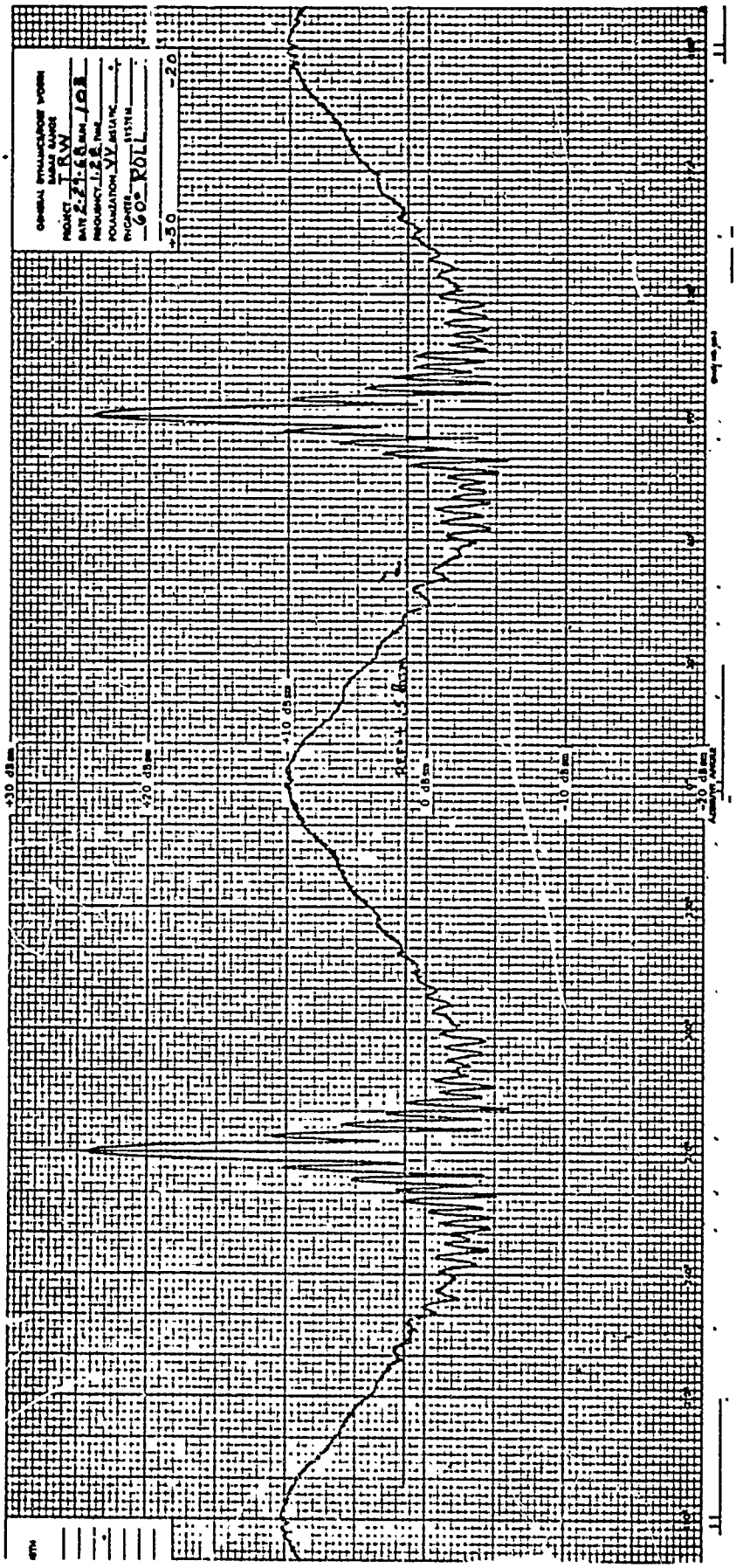

Fig. D-9 VEHICLE 001 AMPLITUDE RESPONSE; L-BAND, VV POLARIZATION, 60-DEGREE ROLL

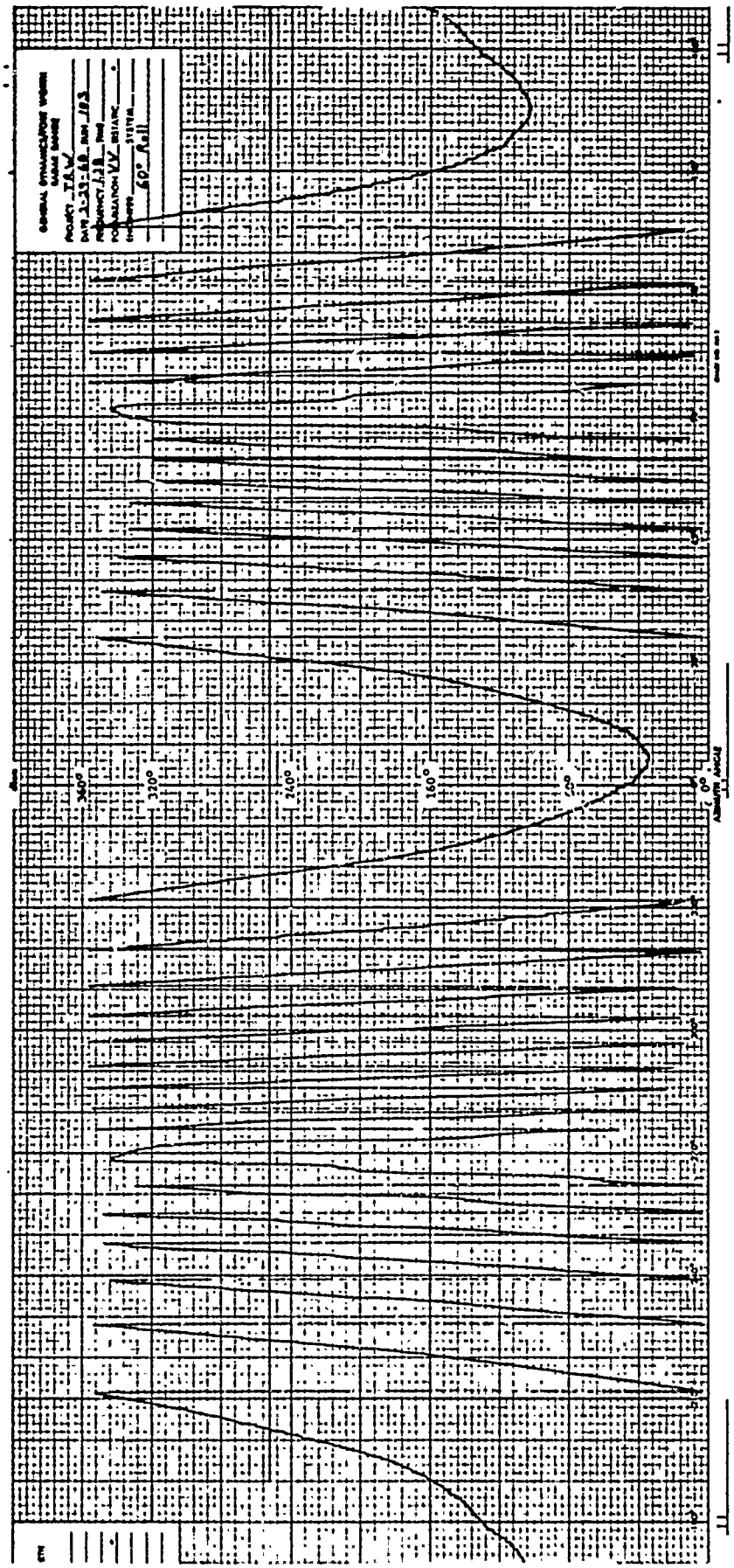

Fig. D-10 VEHICLE 001 PHASE RESPONSE; L-BAND, VV POLARIZATION, 60-DEGREE ROLL

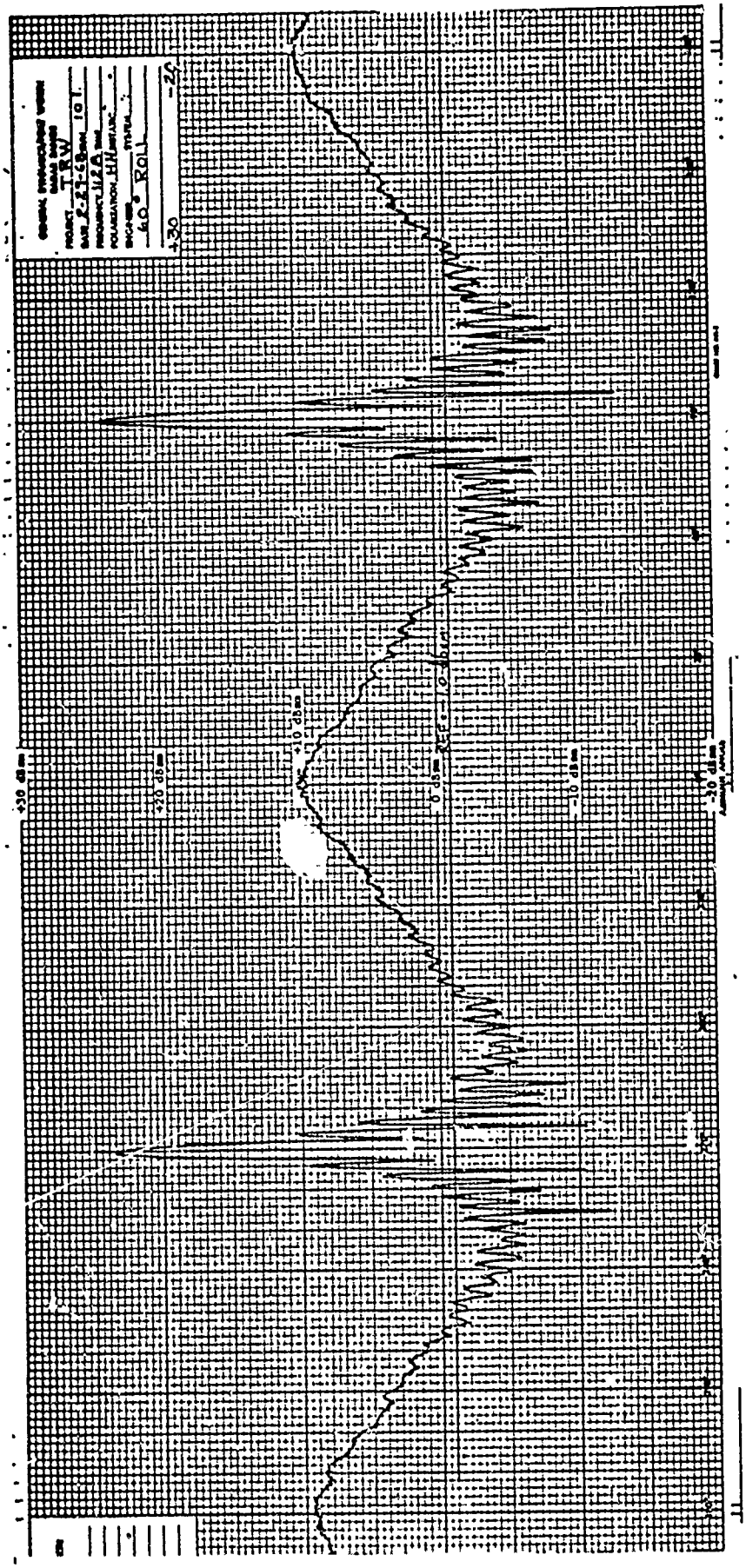

Fig. D-11 VEHICLE 001 AMPLITUDE RESPONSE; L-BAND, HH POLARIZATION, 60-DEGREE ROLL

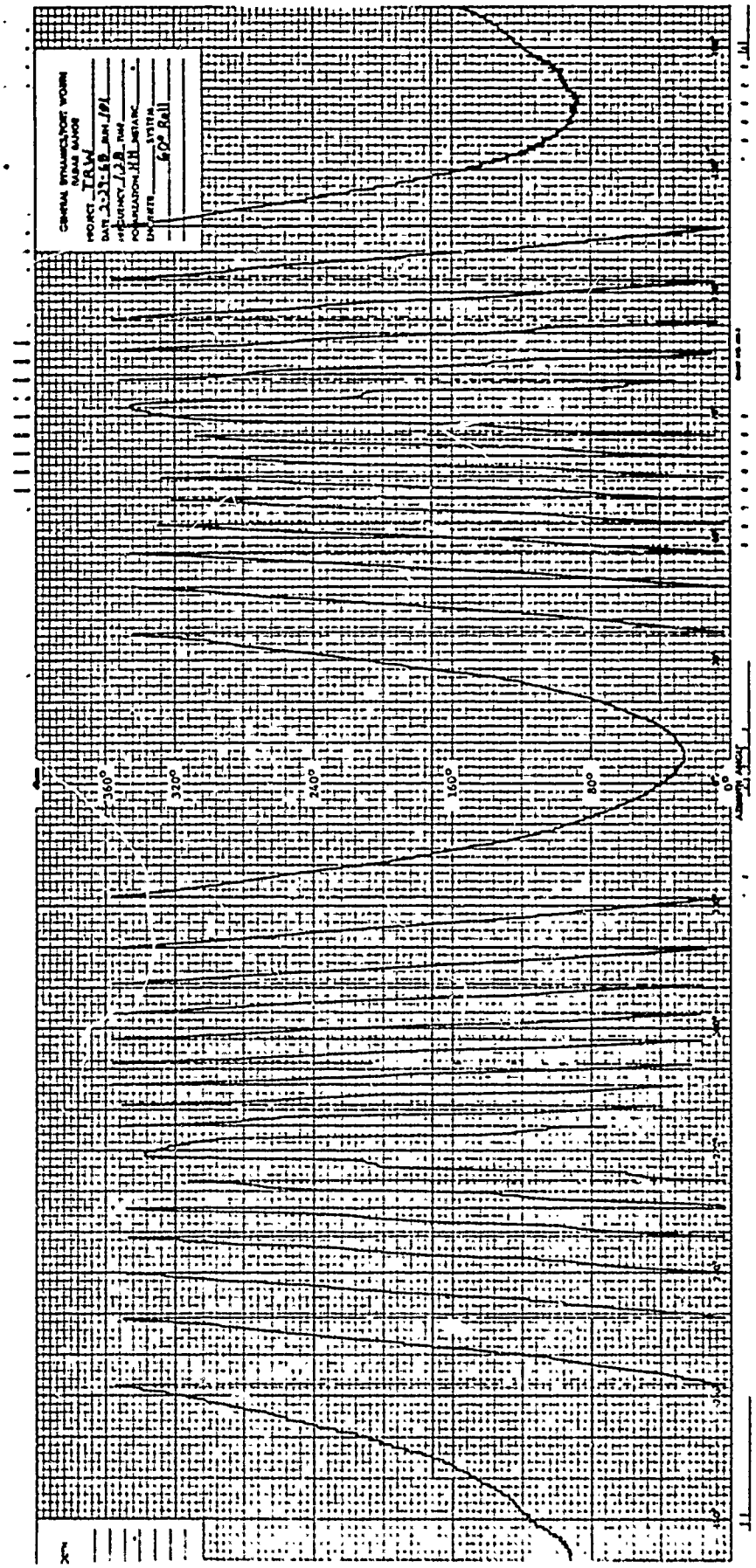

Fig. D-12 VEHICLE 001 PHASE RESPONSE; L-BAND, HH POLARIZATION, 60-DEGREE ROLL

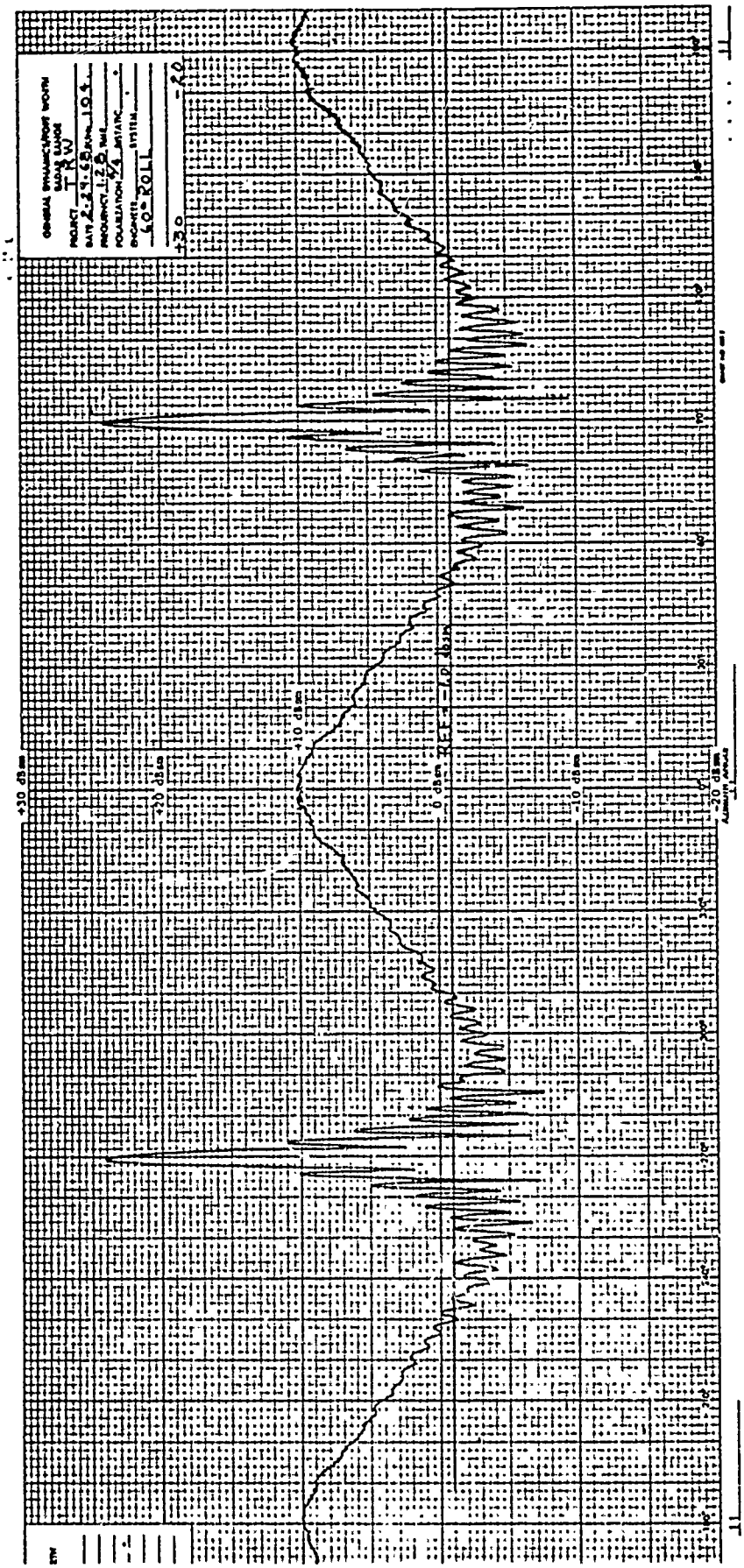

Fig. D-13 VEHICLE 001 AMPLITUDE RESPONSE; L-BAND, $\pi/4$ $\pi/4$ POLARIZATION, 60-DEGREE ROLL

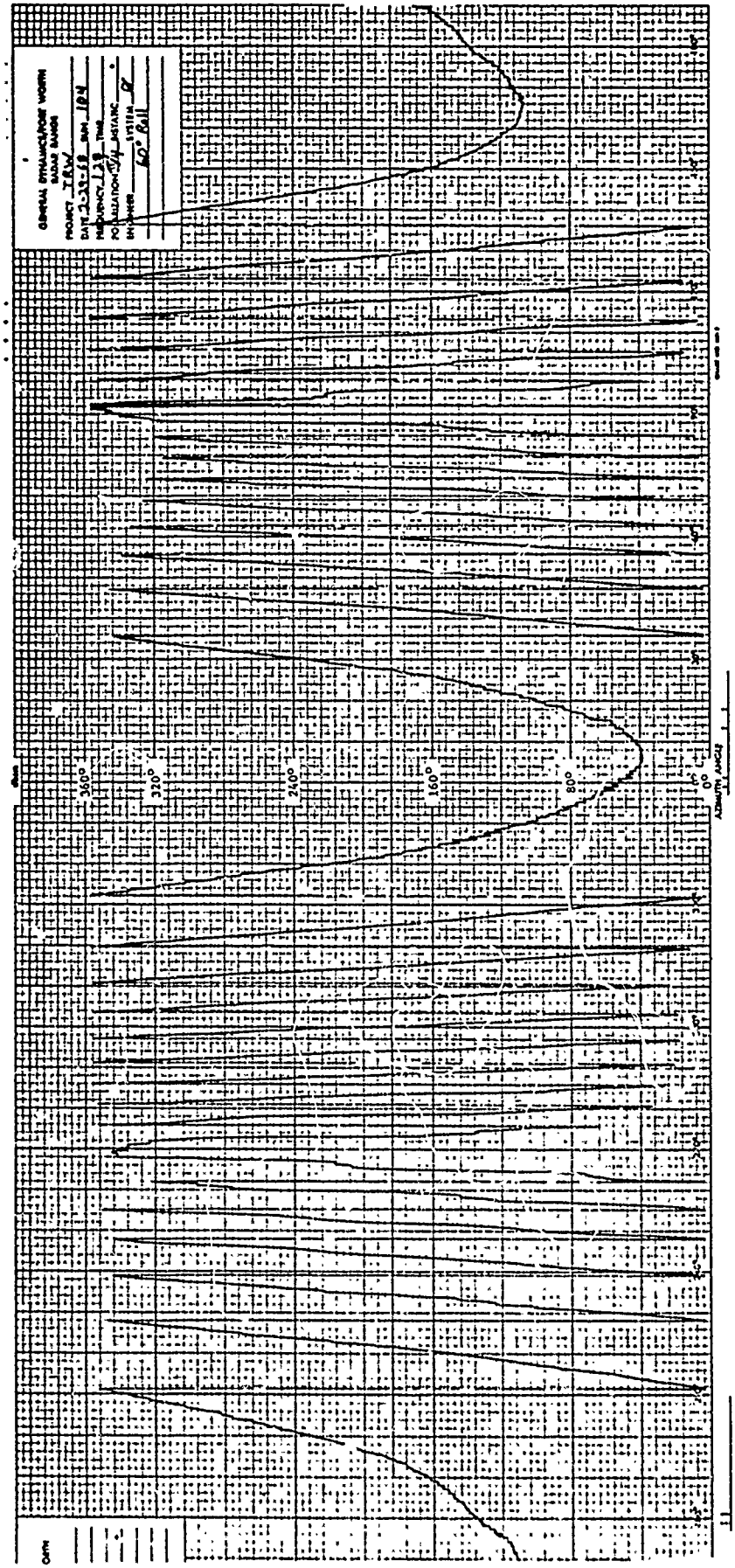

Fig. D-14 VEHICLE 001 PHASE RESPONSE; L-BAND, $\pi/4$ $\pi/4$ POLARIZATION, 60-DEGREE ROLL

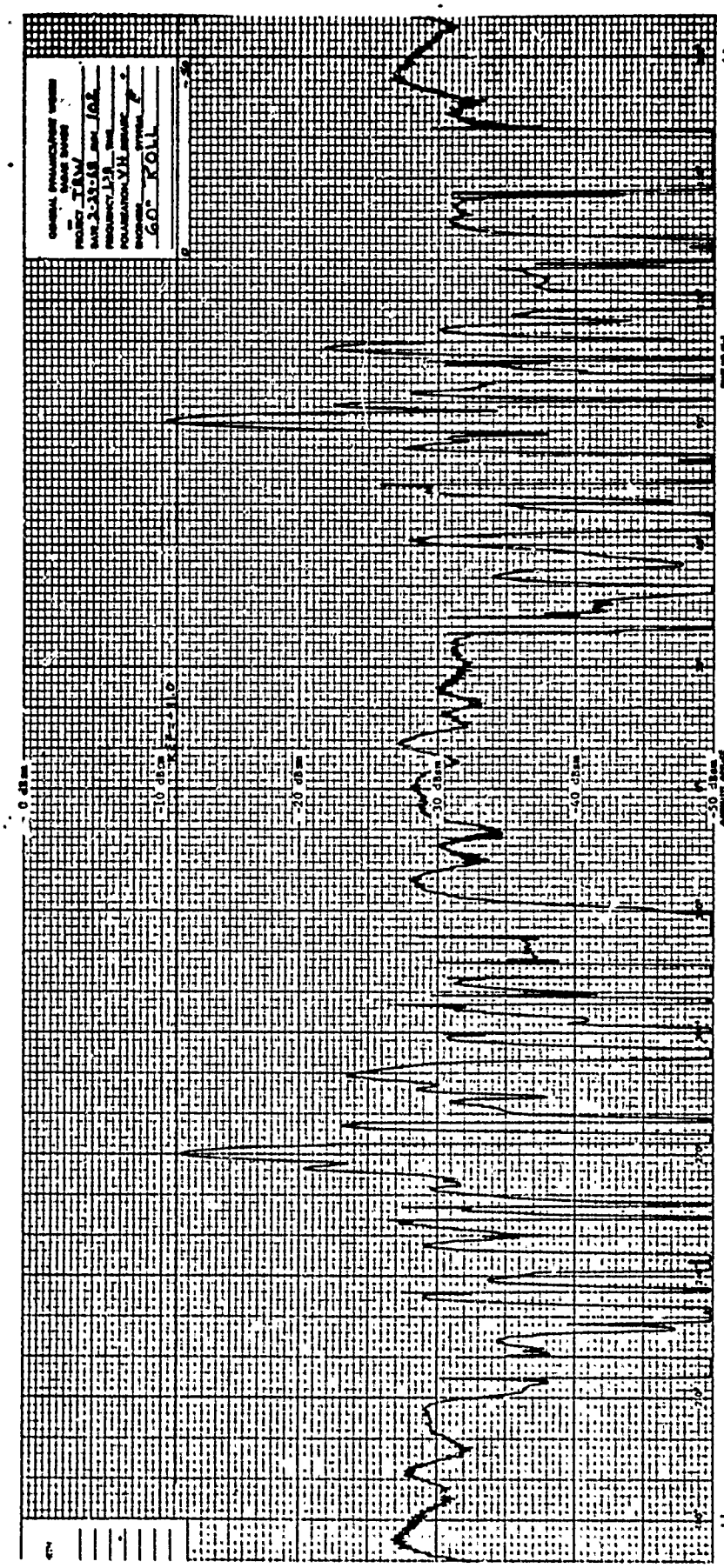

Fig. D-15 VEHICLE 001 AMPLITUDE RESPONSE; L-BAND, VH POLARIZATION, 60-DEGREE ROLL

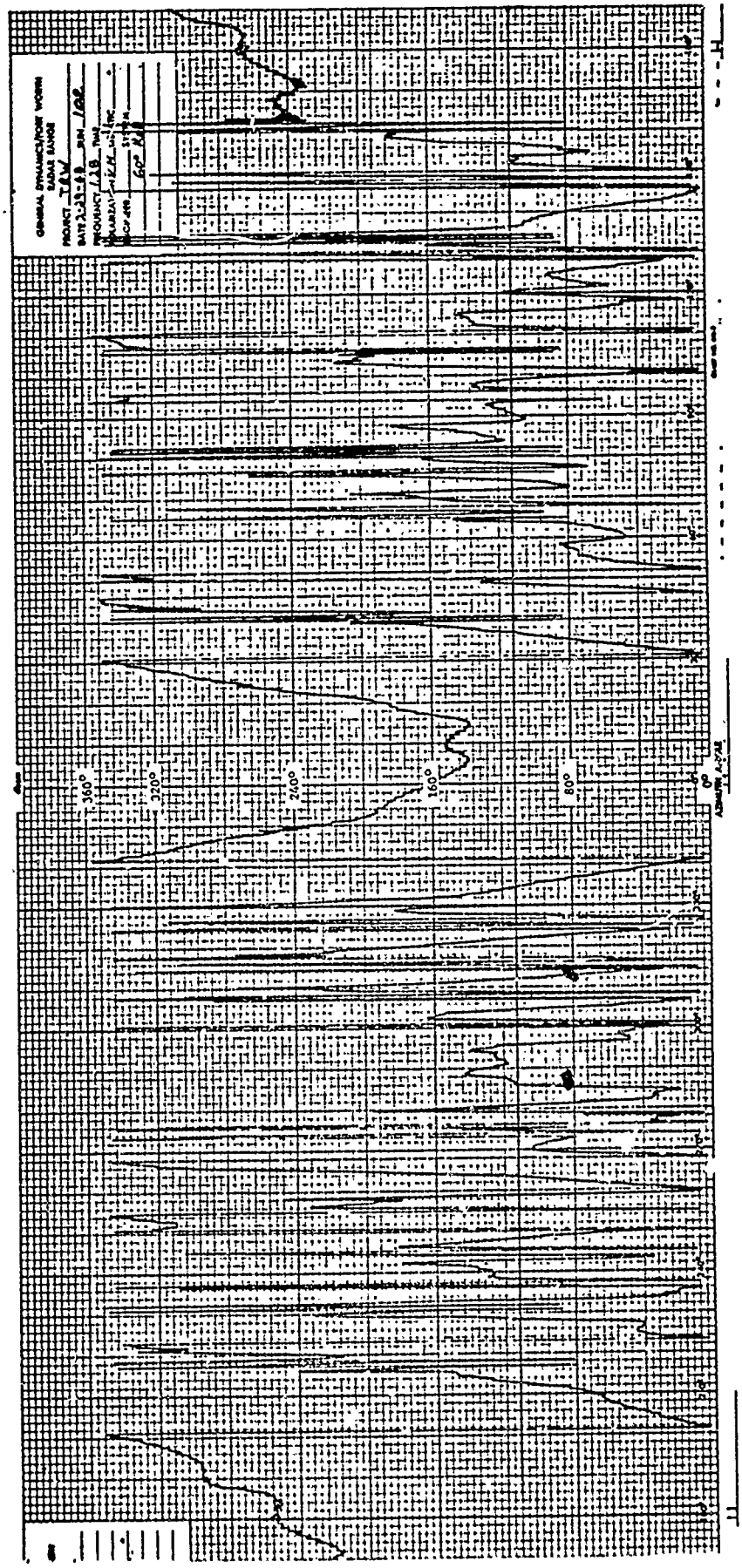

Fig. D-16 VEHICLE 001 PHASE RESPONSE; L-BAND, VH POLARIZATION, 60-DEGREE ROLL

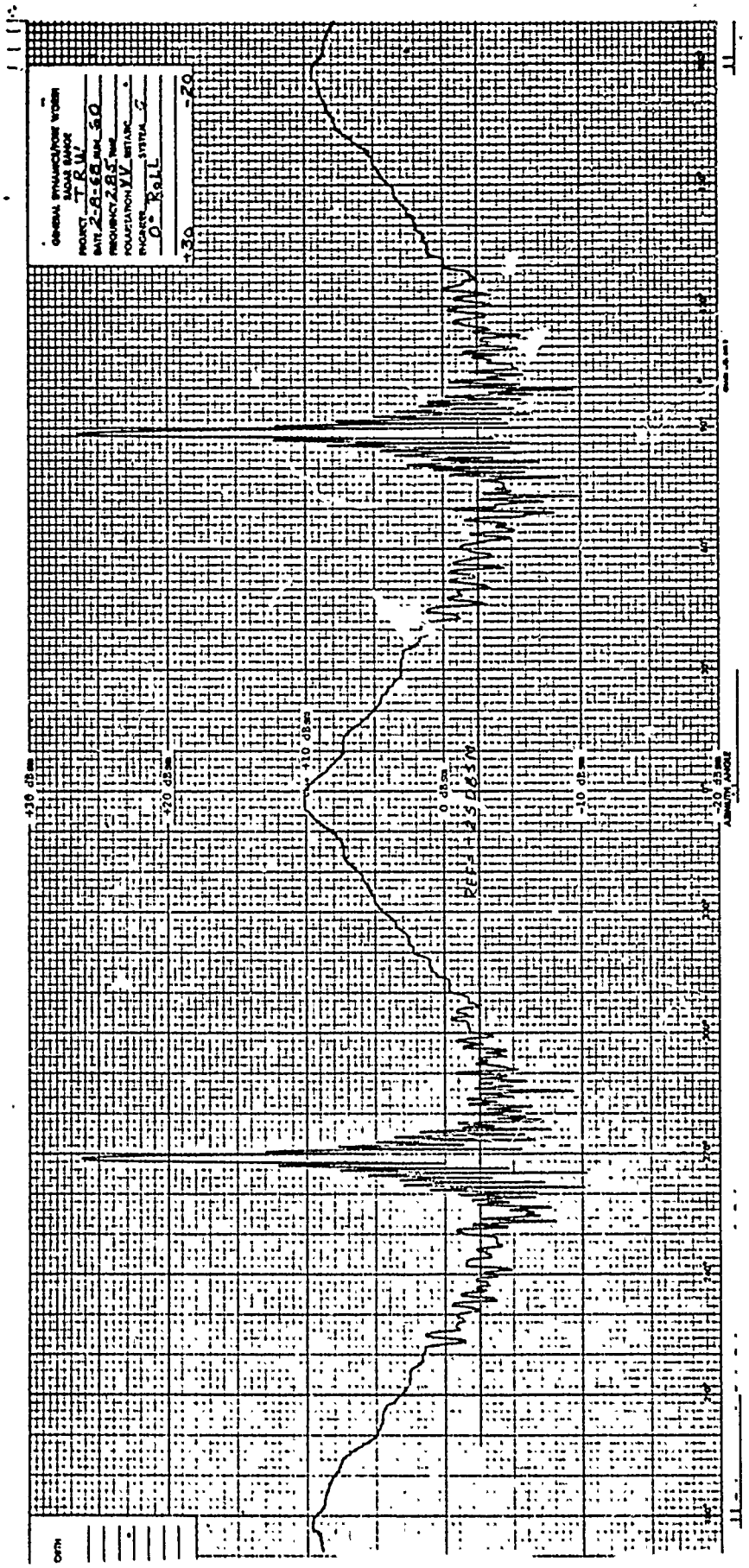

Fig. D-17 VEHICLE 001 AMPLITUDE RESPONSE; S-BAND, VV POLARIZATION, 0-DEGREE ROLL

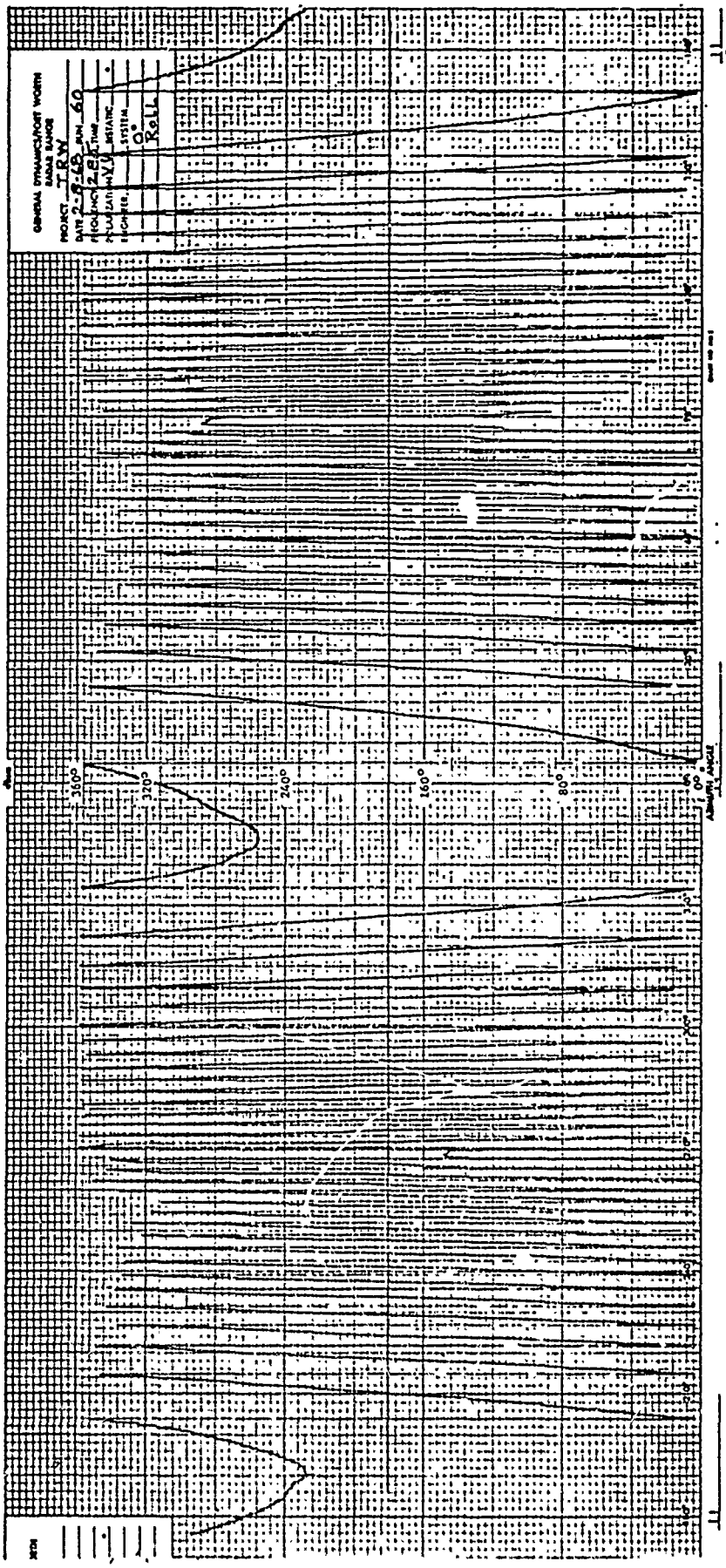

Fig. D-18 VEHICLE 001 PHASE RESPONSE; S-BAND, VV POLARIZATION, 0-DEGREE ROLL

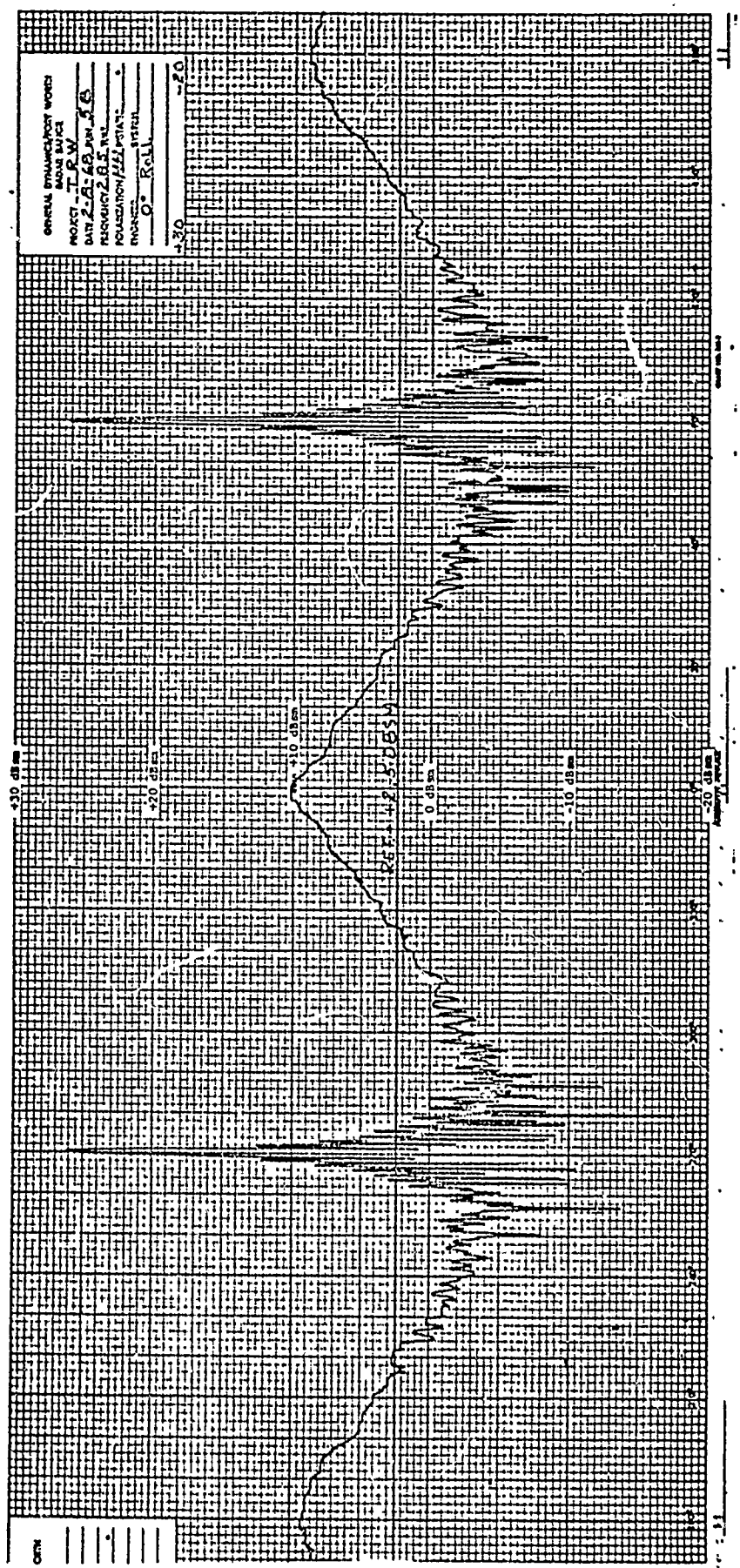

Fig. D-19 VEHICLE 001 AMPLITUDE RESPONSE; S-BAND, HH POLARIZATION, 0-DEGREE ROLL

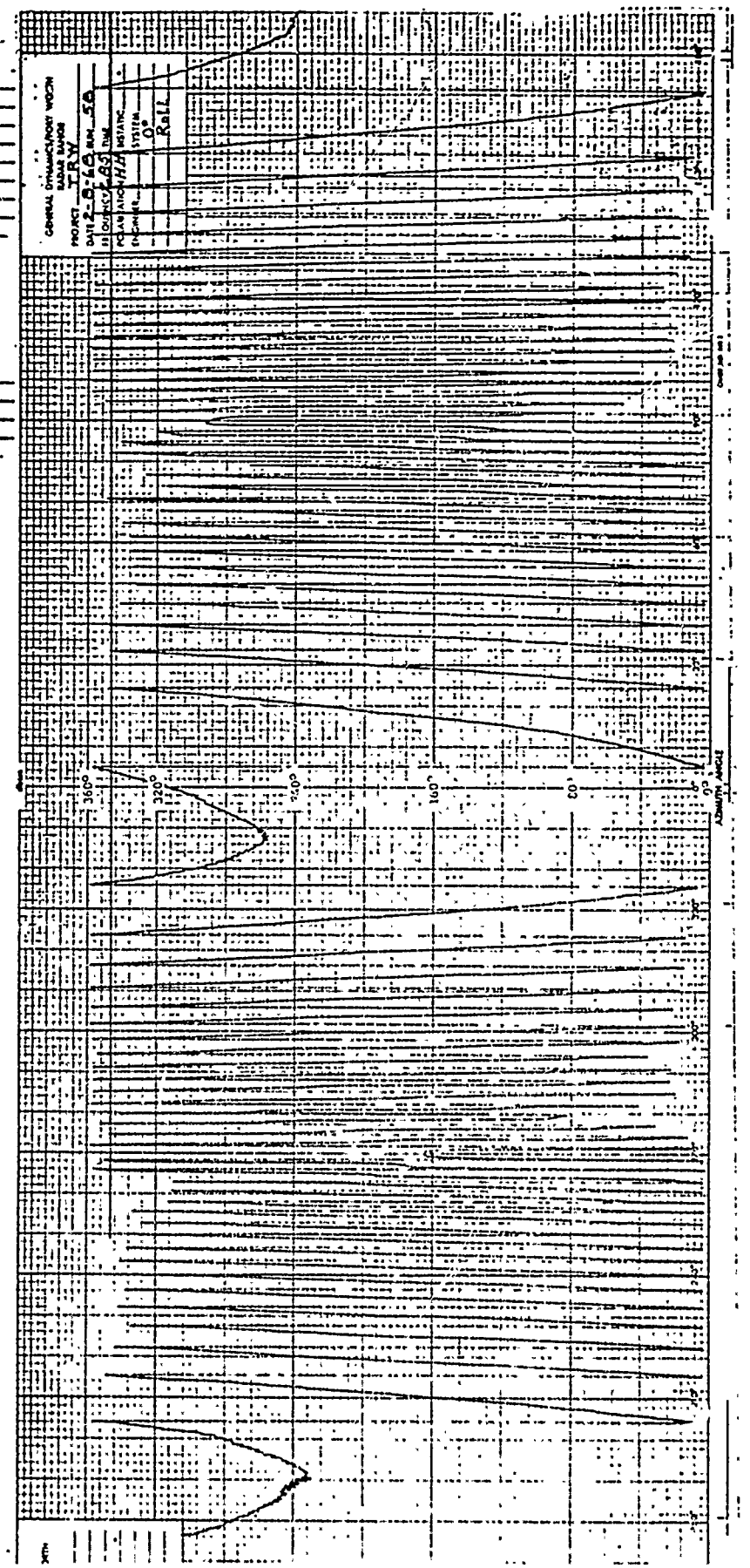

Fig. D-20 VEHICLE 001 PHASE RESPONSE; S-BAND, HH POLARIZATION, 0-DEGREE ROLL

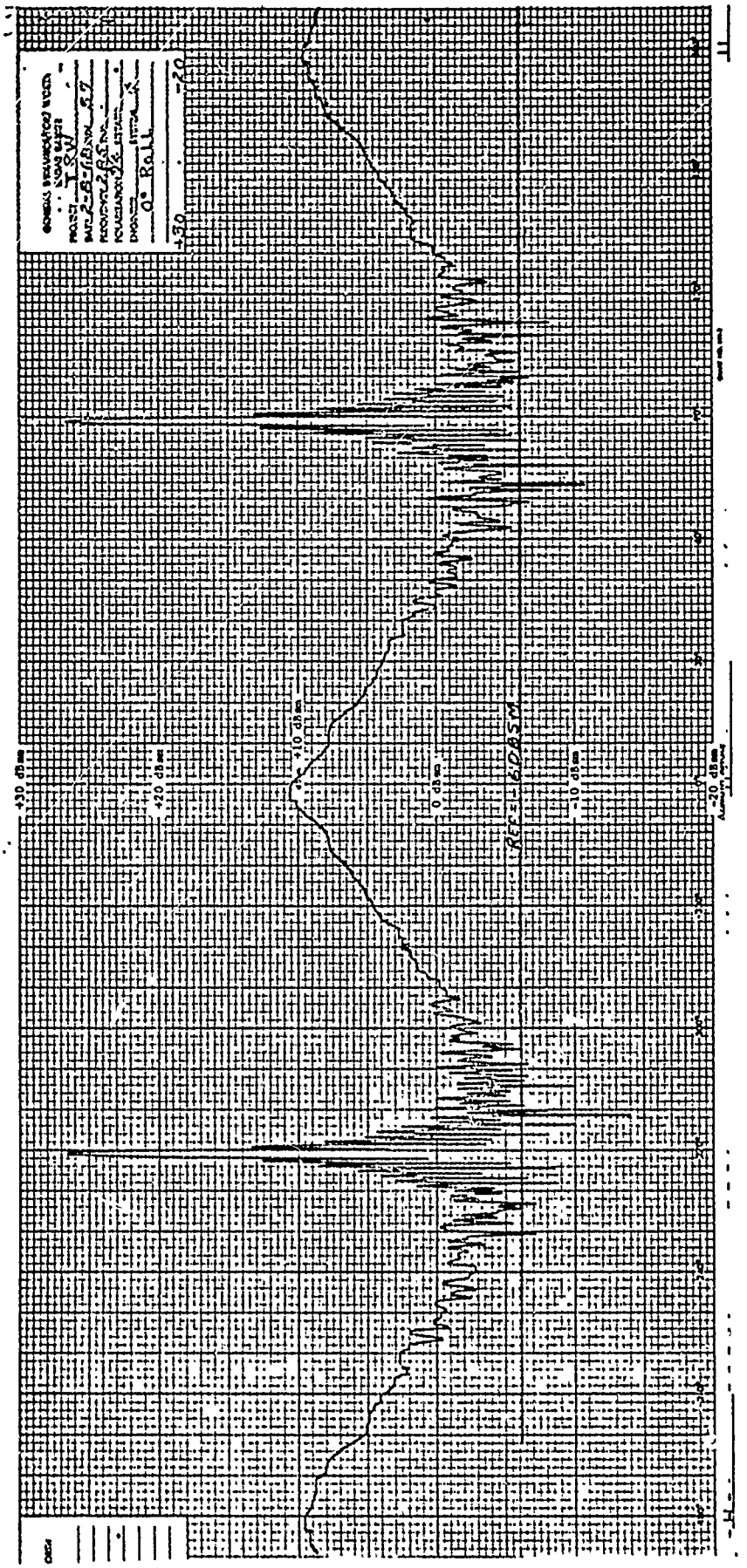

Fig. D-21 VEHICLE 001 AMPLITUDE RESPONSE; S-BAND, $\pi/4$ $\pi/4$ POLARIZATION, 0-DEGREE ROLL

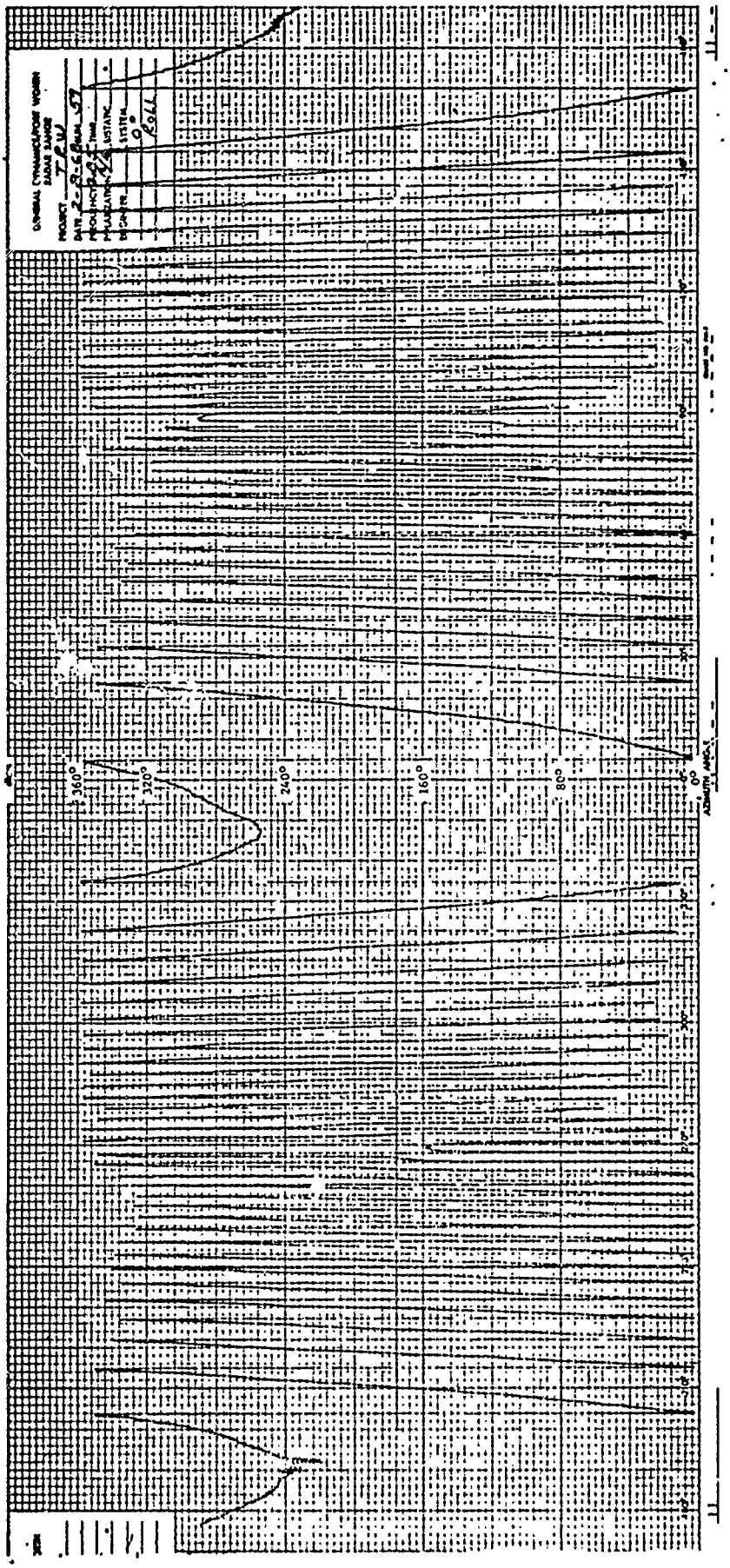

Fig. D-22 VEHICLE 001 PHASE RESPONSE; S-BAND, $\pi/4$ $\pi/4$ POLARIZATION, 0-DEGREE ROLL

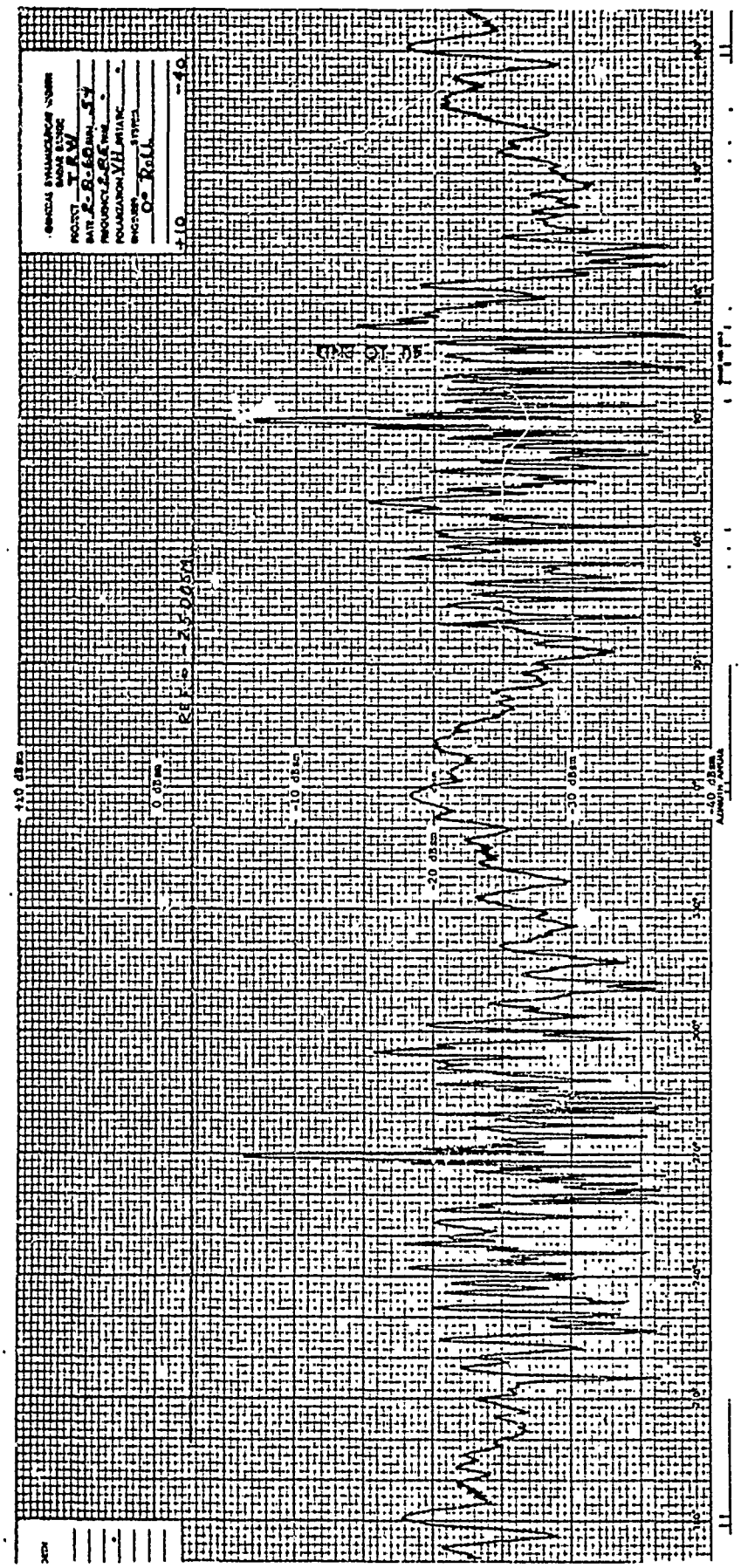

Fig. D-23 VEHICLE 001 AMPLITUDE RESPONSE; S-BAND, VH POLARIZATION, 0-DEGREE ROLL

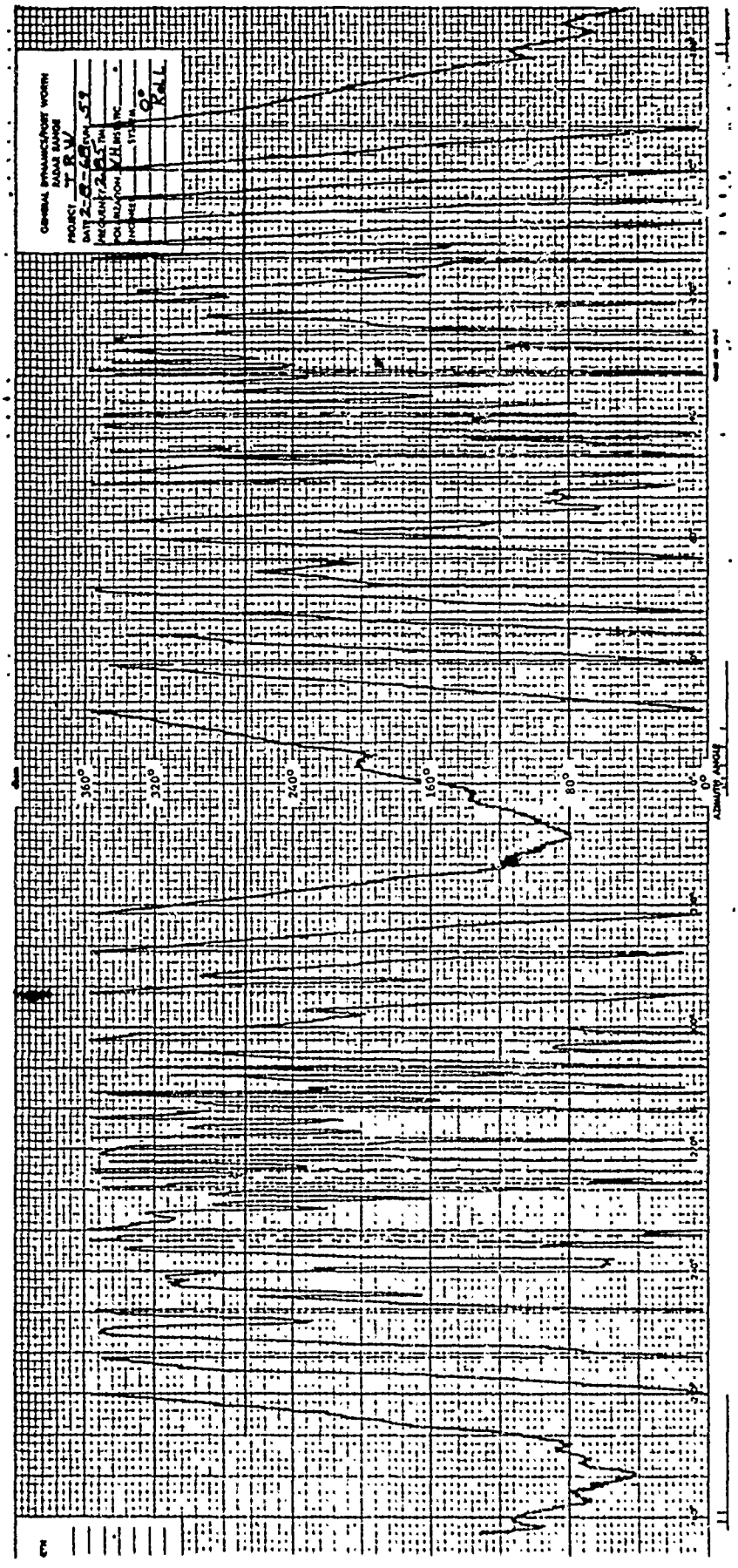

Fig. D-24 VEHICLE 001 PHASE RESPONSE; S-BAND, VH POLARIZATION, 0-DEGREE ROLL

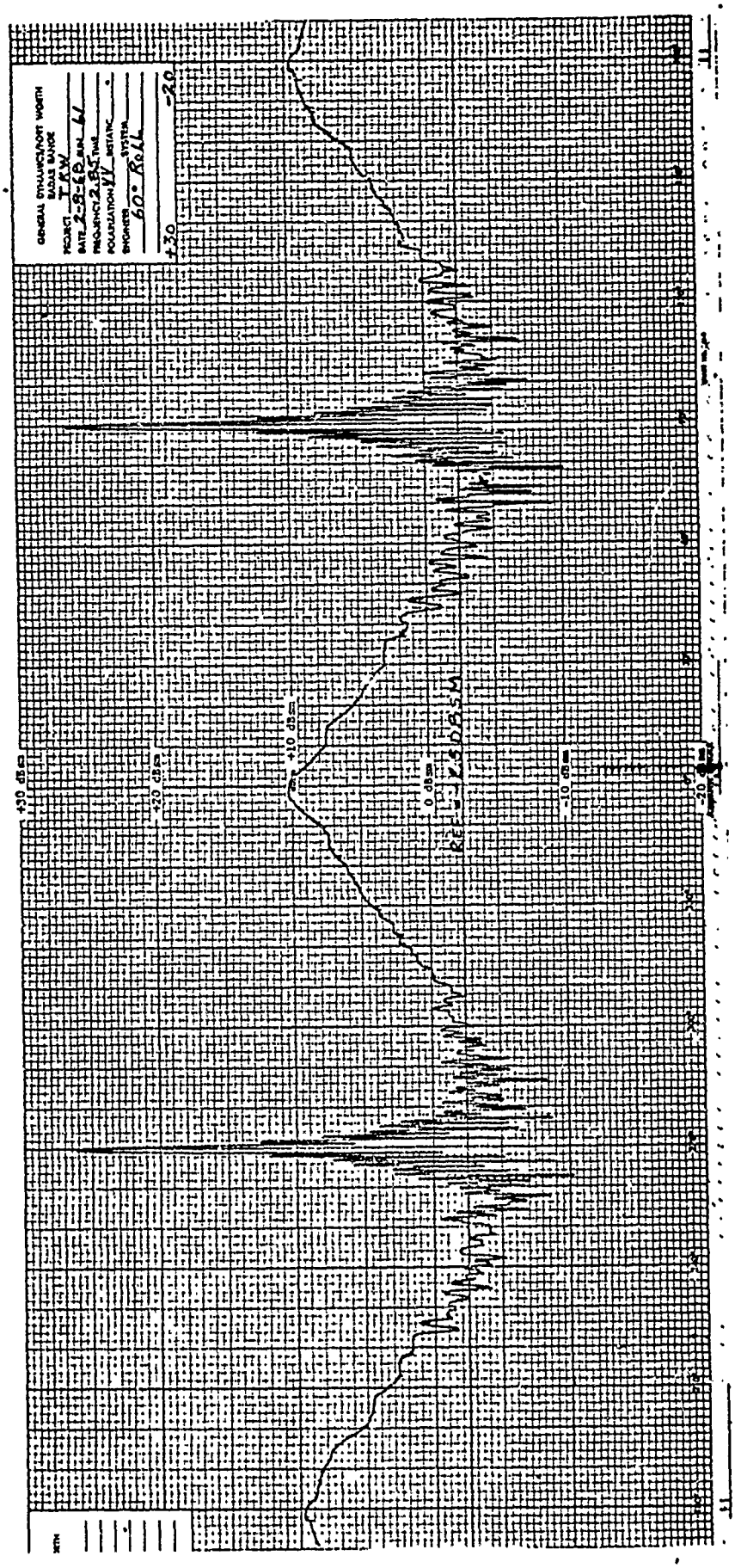

Fig. D-25 VEHICLE 001 AMPLITUDE RESPONSE; S-BAND, VV POLARIZATION, 60-DEGREE ROLL

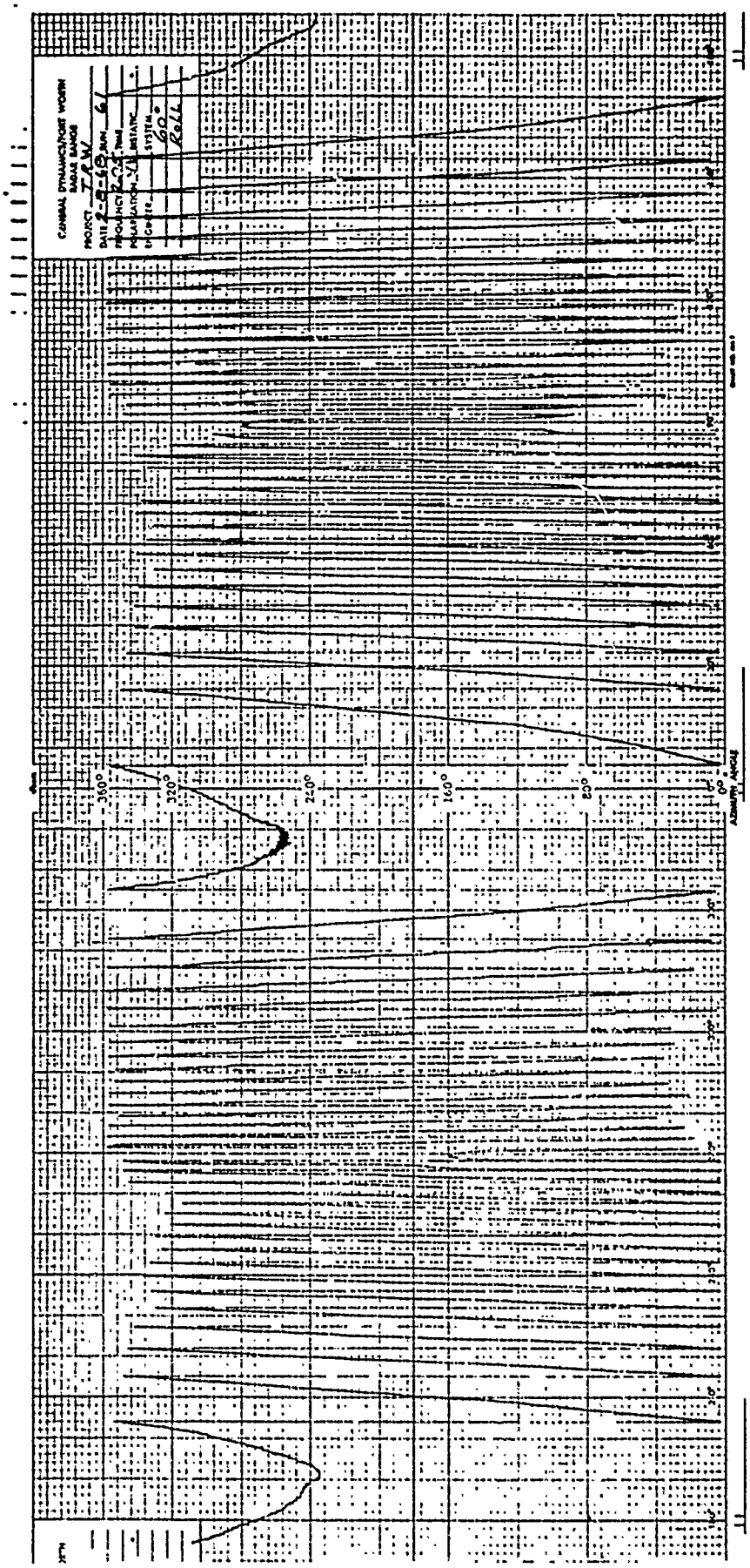

Fig. D-26 VEHICLE 001 PHASE RESPONSE; S-BAND, VV POLARIZATION, 60-DEGREE ROLL

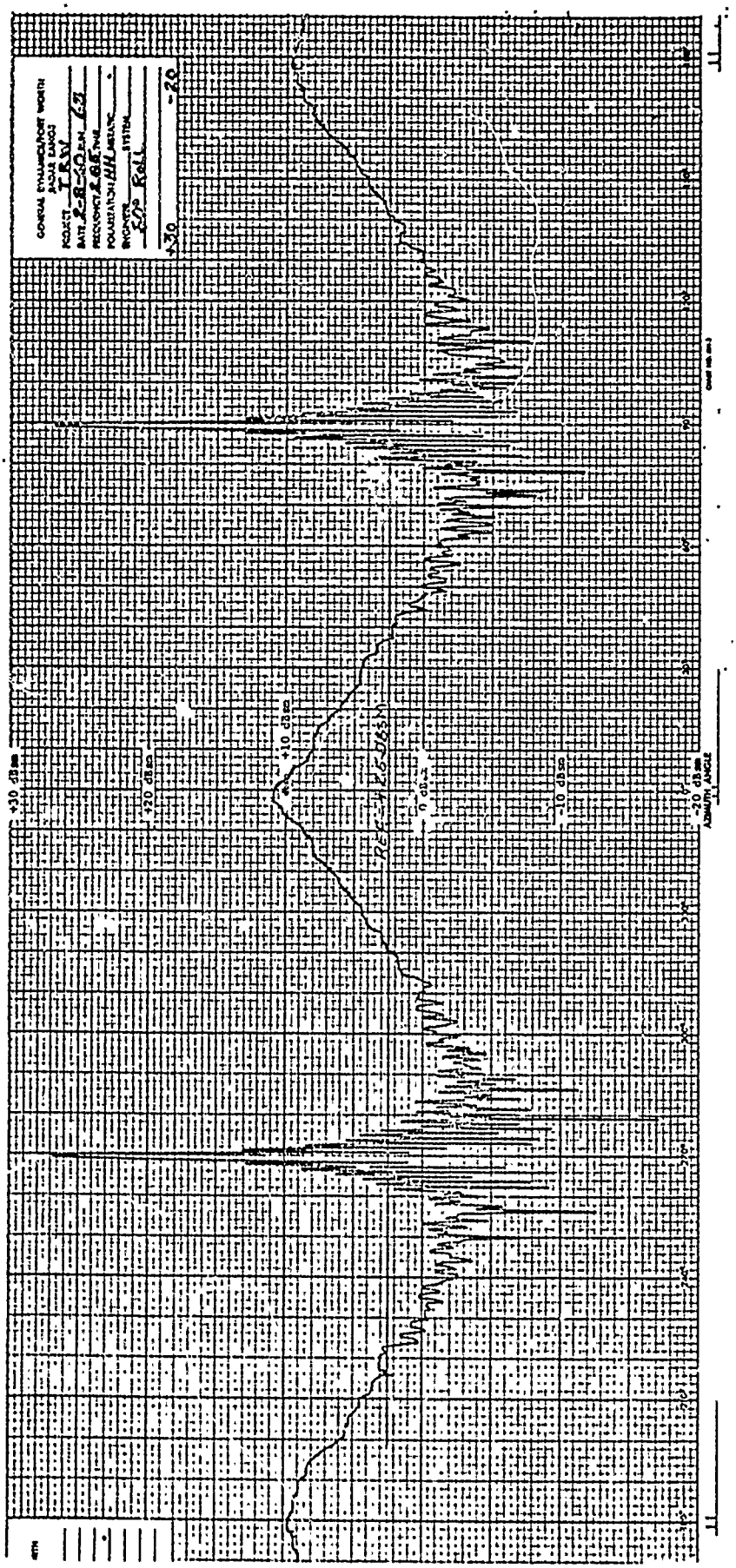

Fig. D-27 VEHICLE 001 AMPLITUDE RESPONSE; S-BAND, HH POLARIZATION, 60-DEGREE ROLL

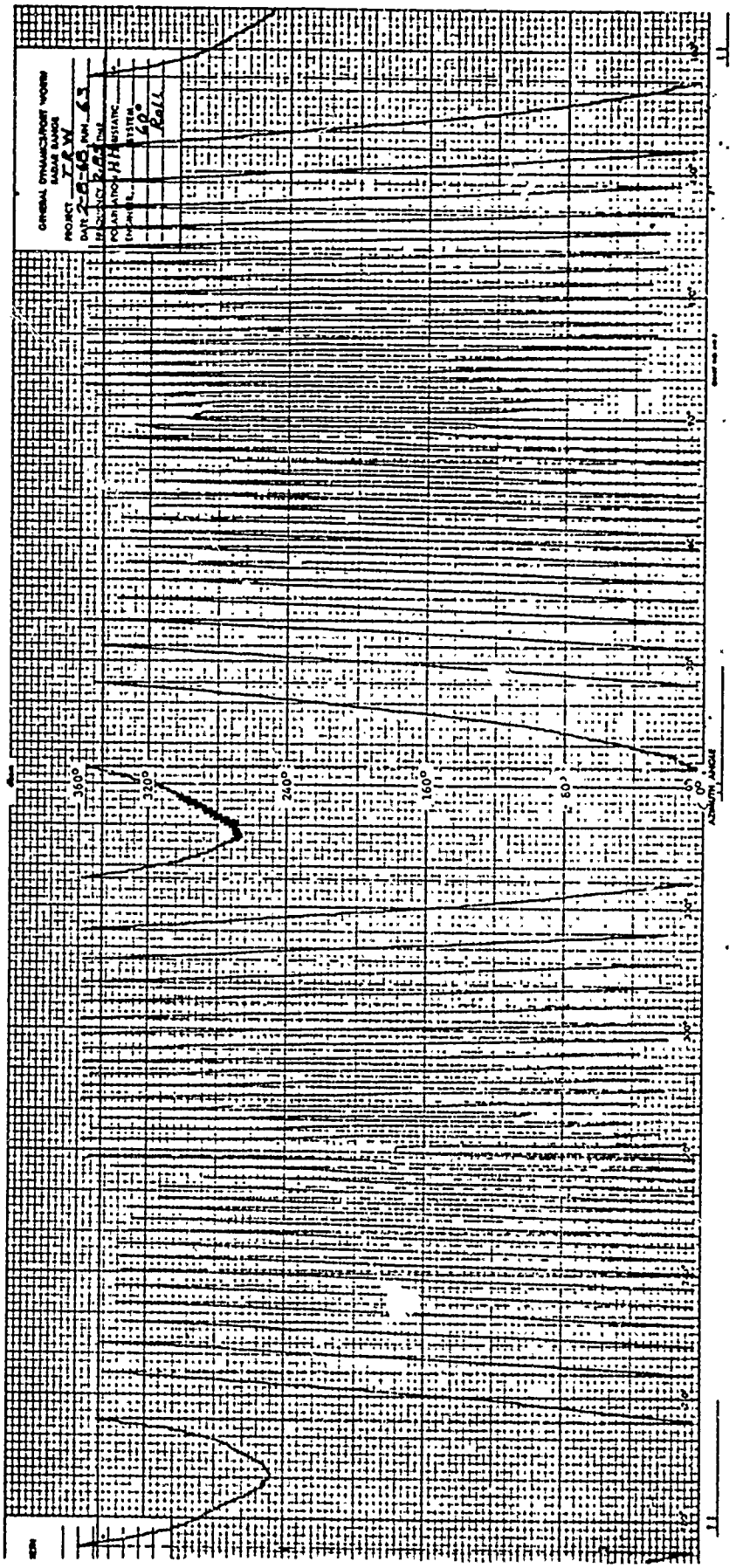

Fig. D-28 VEHICLE 001 PHASE RESPONSE; S-BAND, HH POLARIZATION, 60-DEGREE ROLL

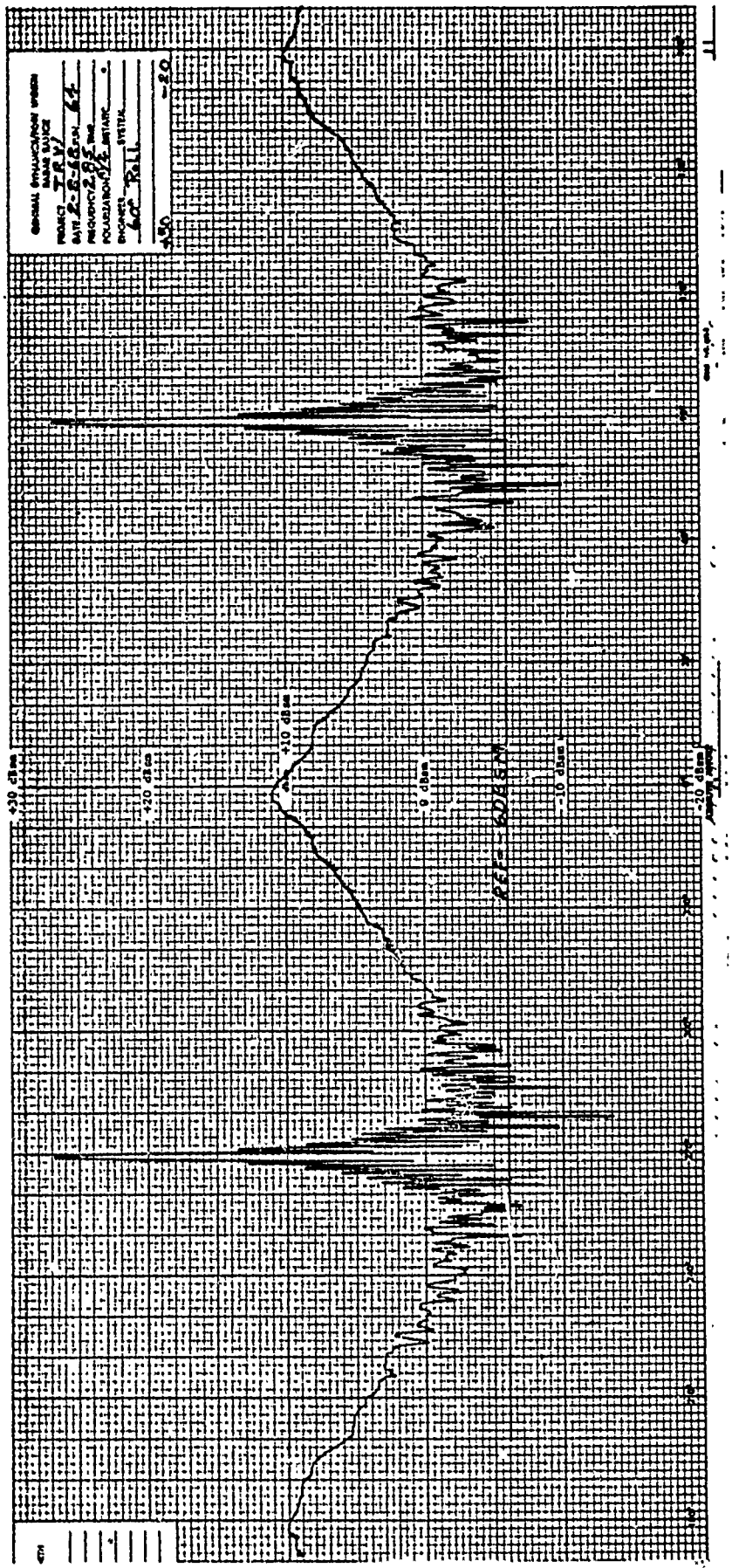

Fig. D-29 VEHICLE 001 AMPLITUDE RESPONSE; S-BAND, $\pi/4$ $\pi/4$ POLARIZATION, 60-DEGREE ROLL

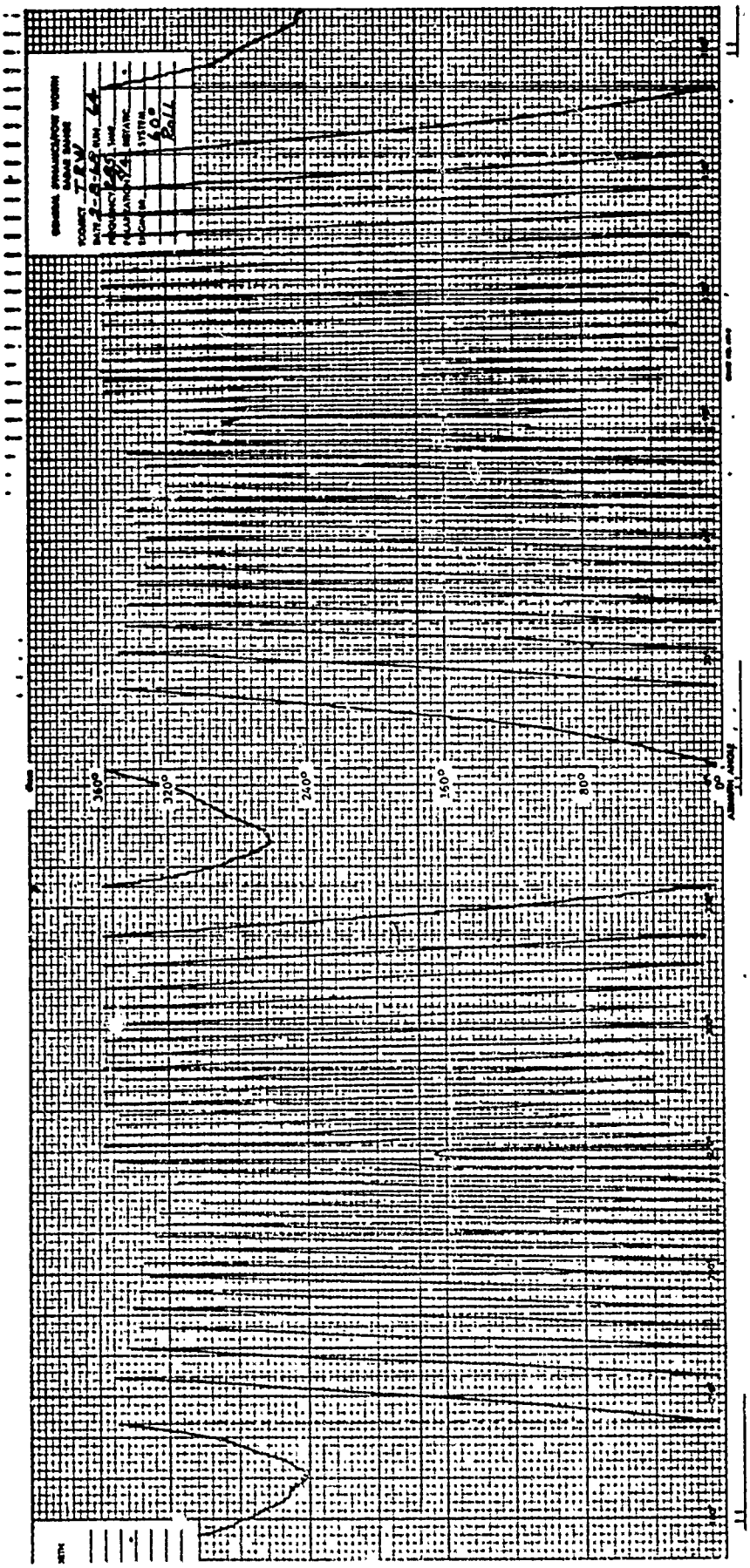

Fig. D-30 VEHICLE 001 PHASE RESPONSE; S-BAND, $\pi/4$ $\pi/4$ POLARIZATION, 60-DEGREE ROLL

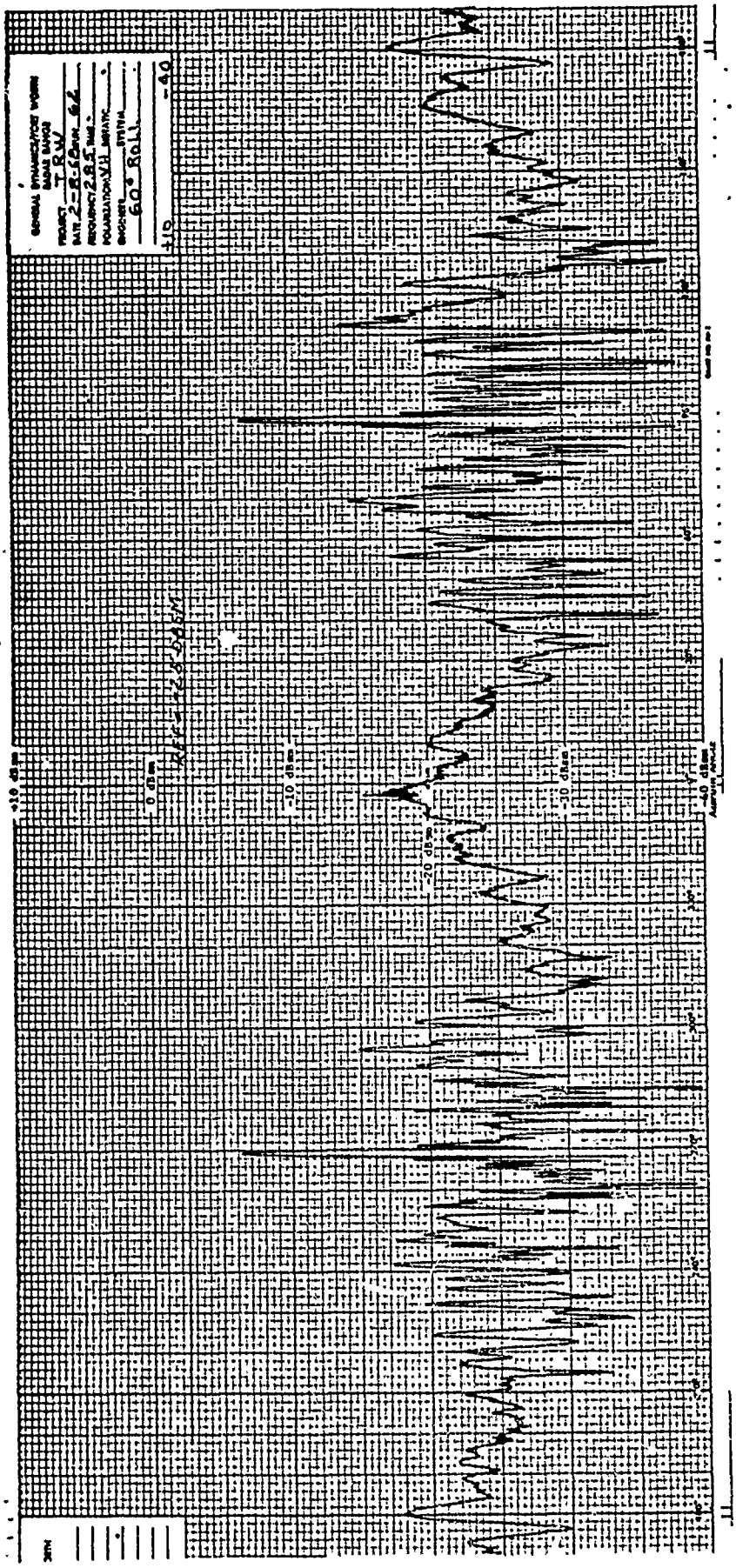

Fig. D-31 VEHICLE 001 AMPLITUDE RESPONSE; S-BAND, VH POLARIZATION, 60-DEGREE ROLL

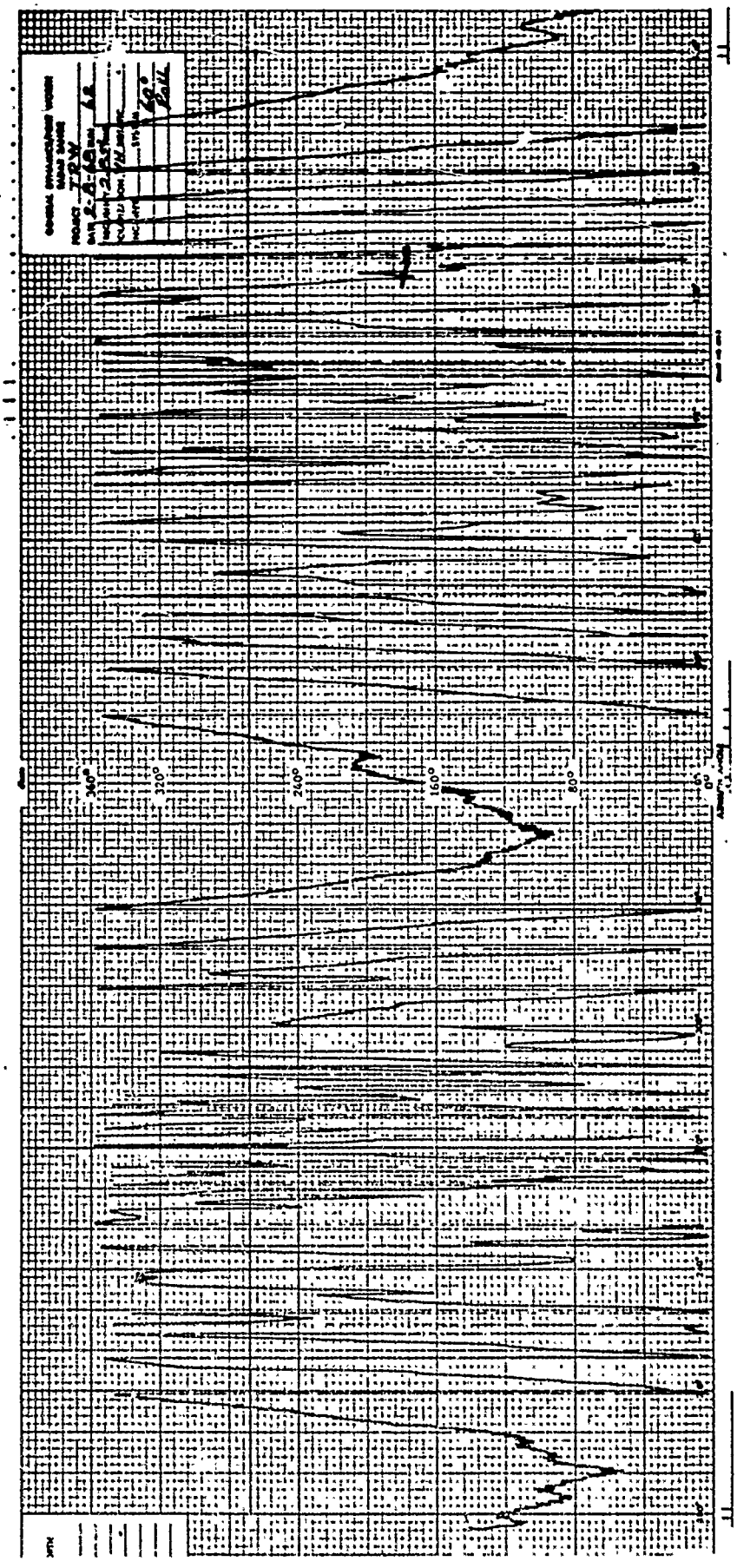

Fig. D-32 VEHICLE 001 PHASE RESPONSE; S-BAND, VH POLARIZATION, 60-DEGREE ROLL

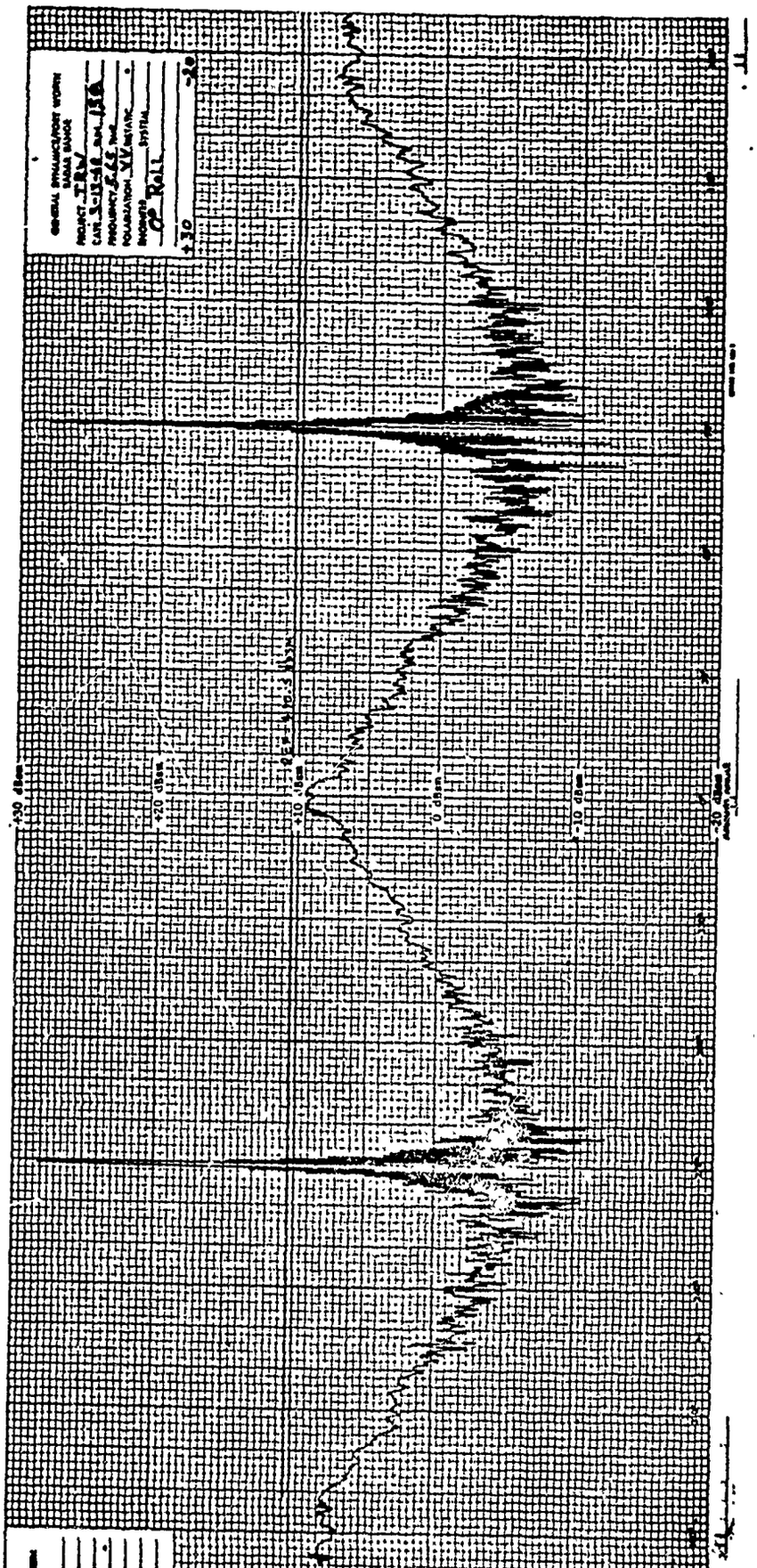

Fig. D-33 VEHICLE 001 AMPLITUDE RESPONSE; C-BAND, VV POLARIZATION, 0-DEGREE ROLL

D-34

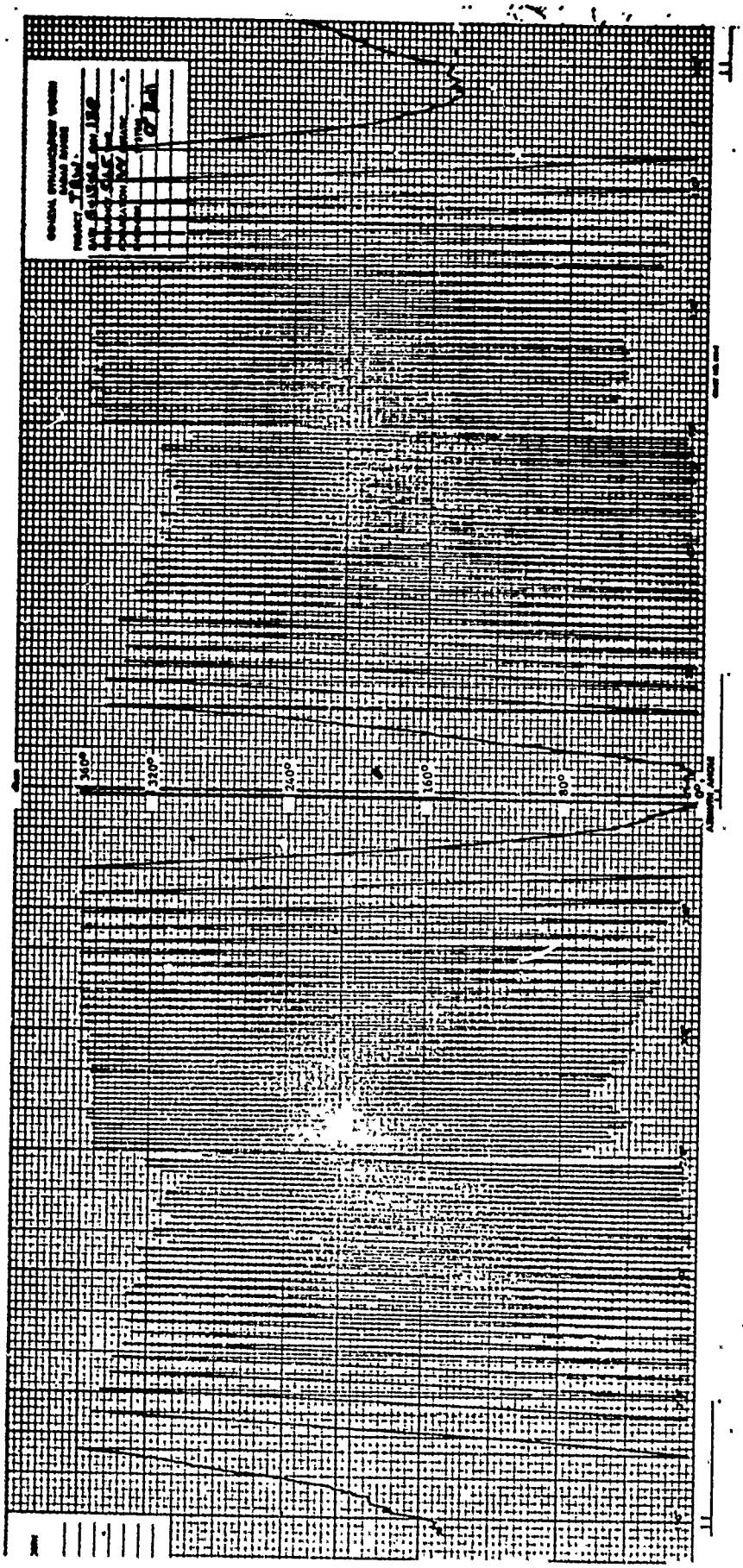

Fig. D-34 VEHICLE 001 PHASE RESPONSE; C-BAND, VV POLARIZATION, 0-DEGREE ROLL

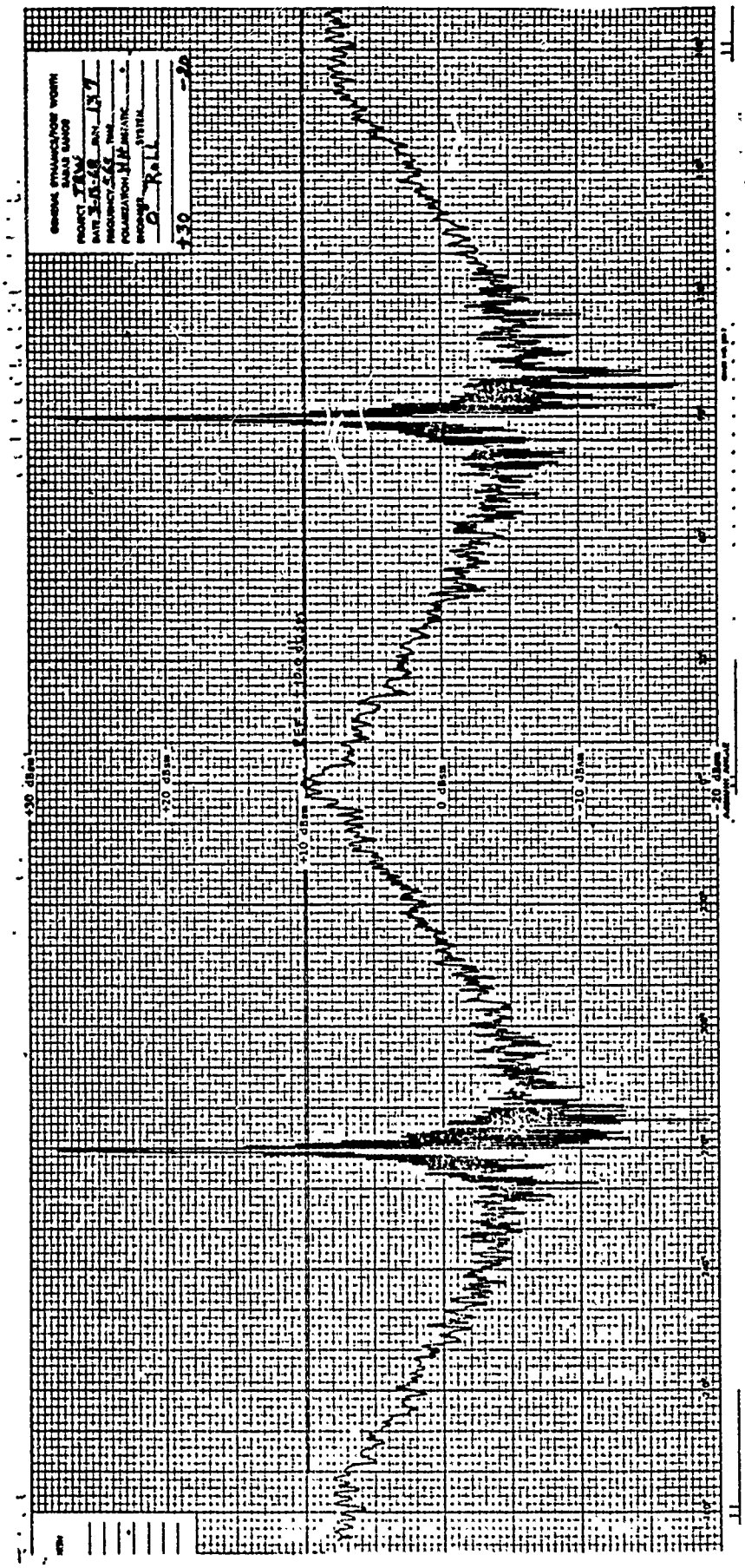

Fig. D-35 VEHICLE 001 AMPLITUDE RESPONSE; C-BAND, HH POLARIZATION, 0-DEGREE ROLL

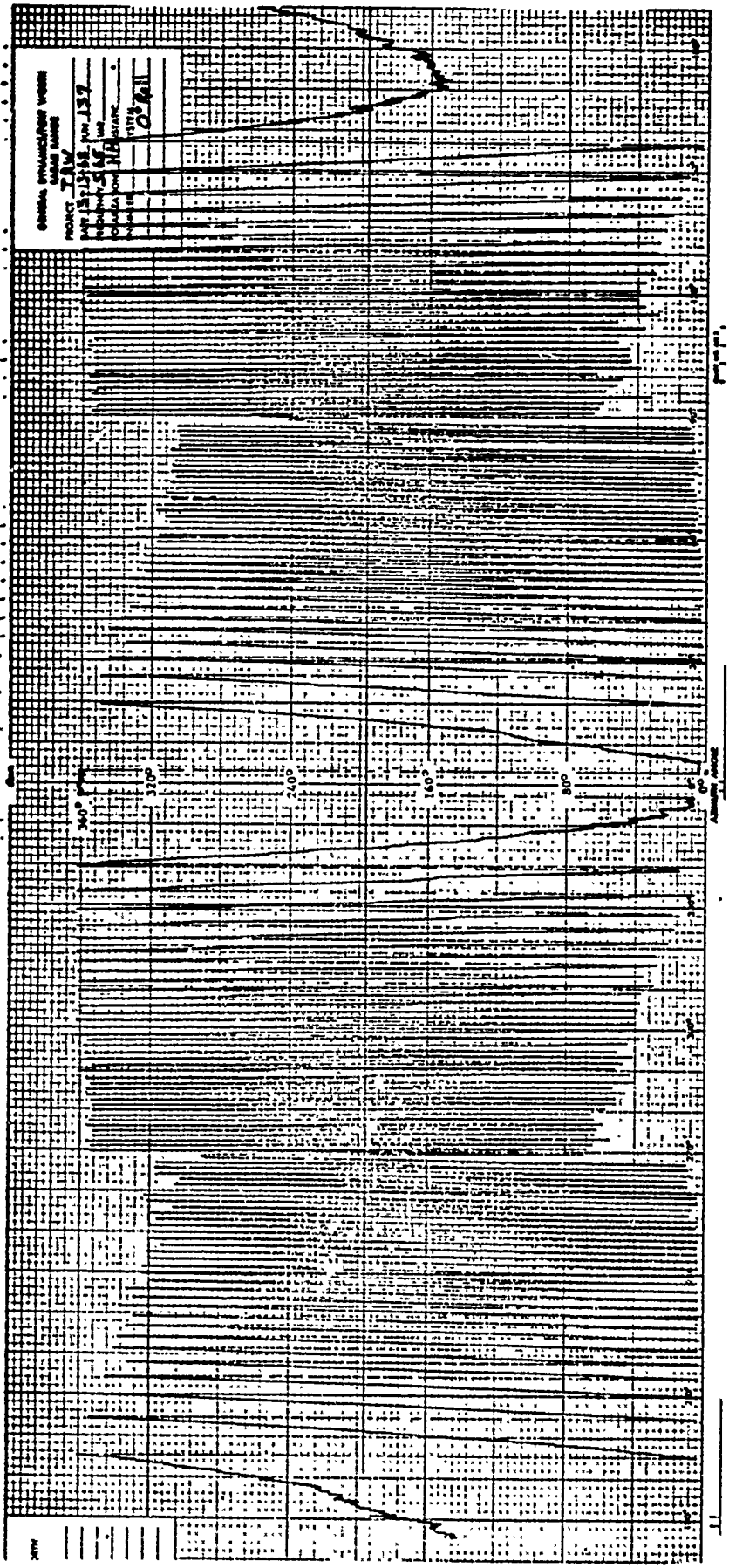

Fig. D-36 VEHICLE 001 PHASE RESPONSE; C-BAND, HH POLARIZATION, 0-DEGREE ROLL

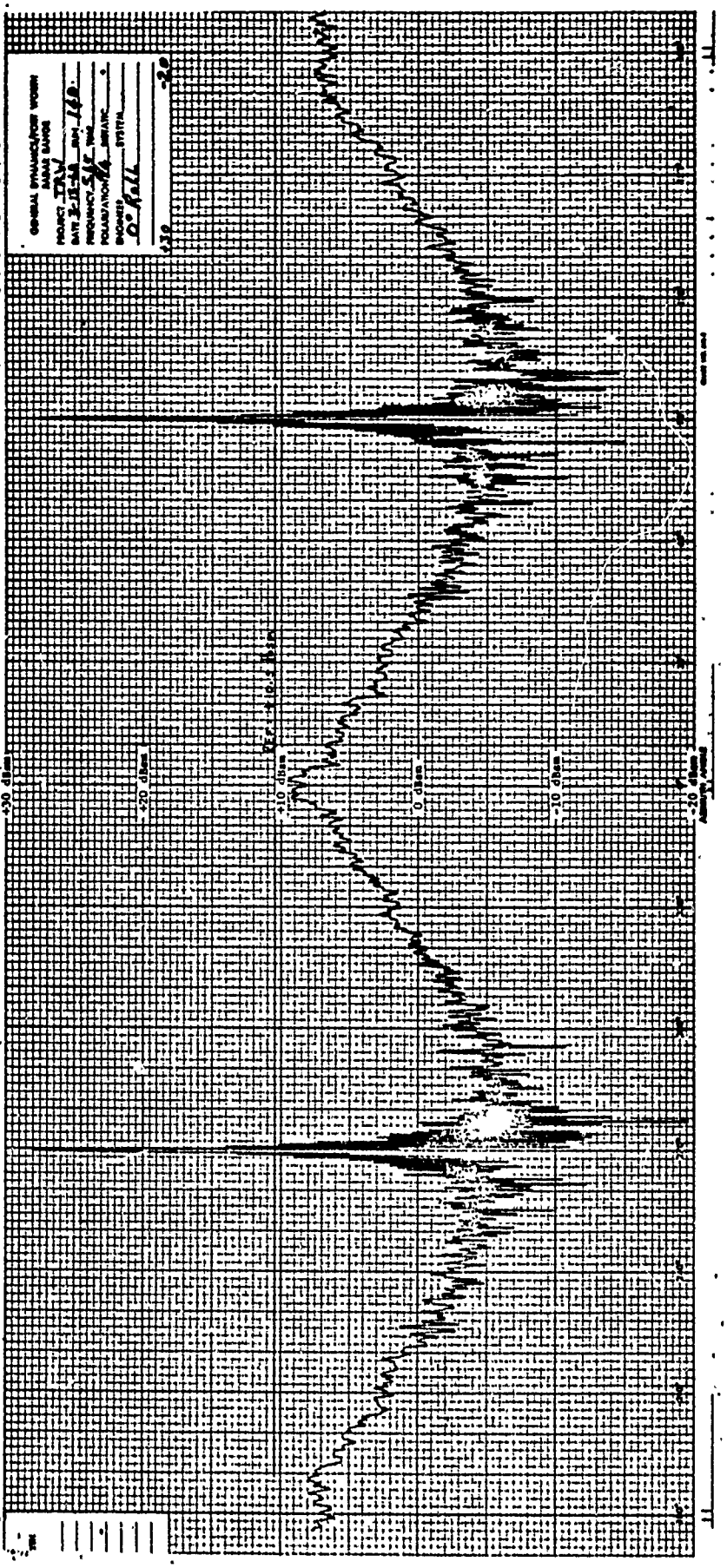

Fig. D-37 VEHICLE 001 AMPLITUDE RESPONSE; C-BAND, $\pi/4$ $\pi/4$ POLARIZATION, 0-DEGREE ROLL

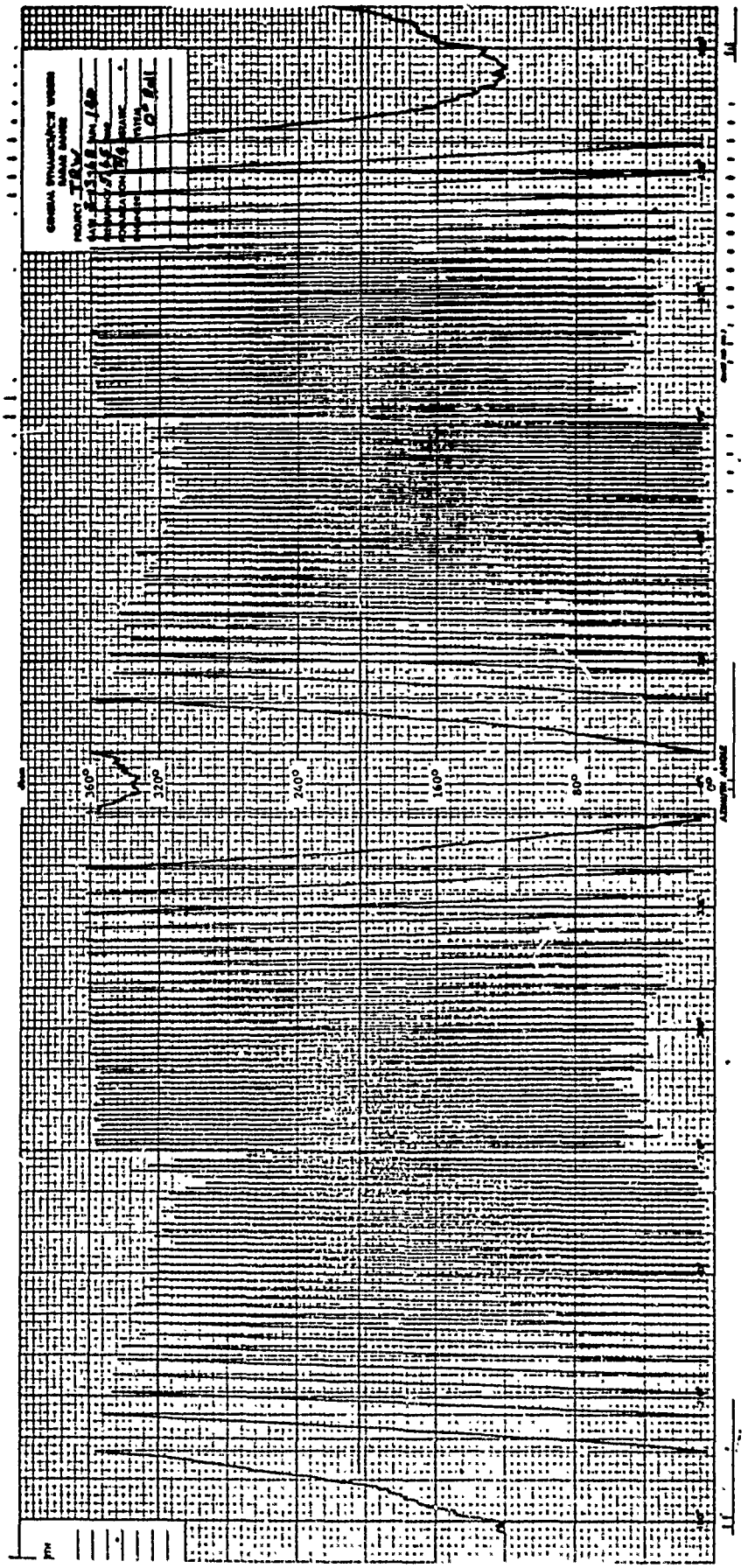

Fig. D-38 VEHICLE 001 PHASE RESPONSE; C-BAND, $\pi/4\pi/4$ POLARIZATION, 0-DEGREE ROLL

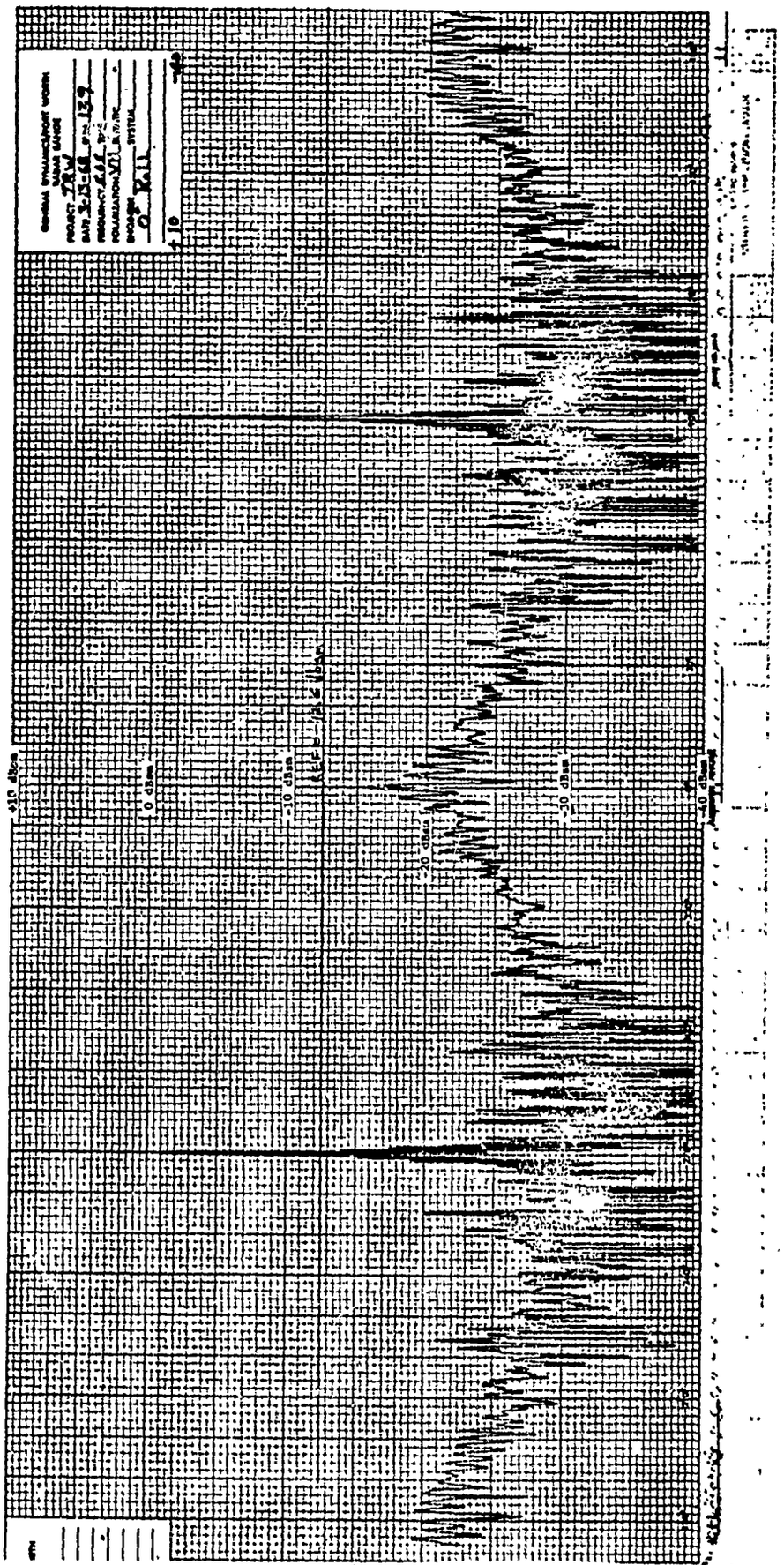

Fig. D-39 VEHICLE 001 AMPLITUDE RESPONSE; C-BAND, VH POLARIZATION, 0-DEGREE ROLL

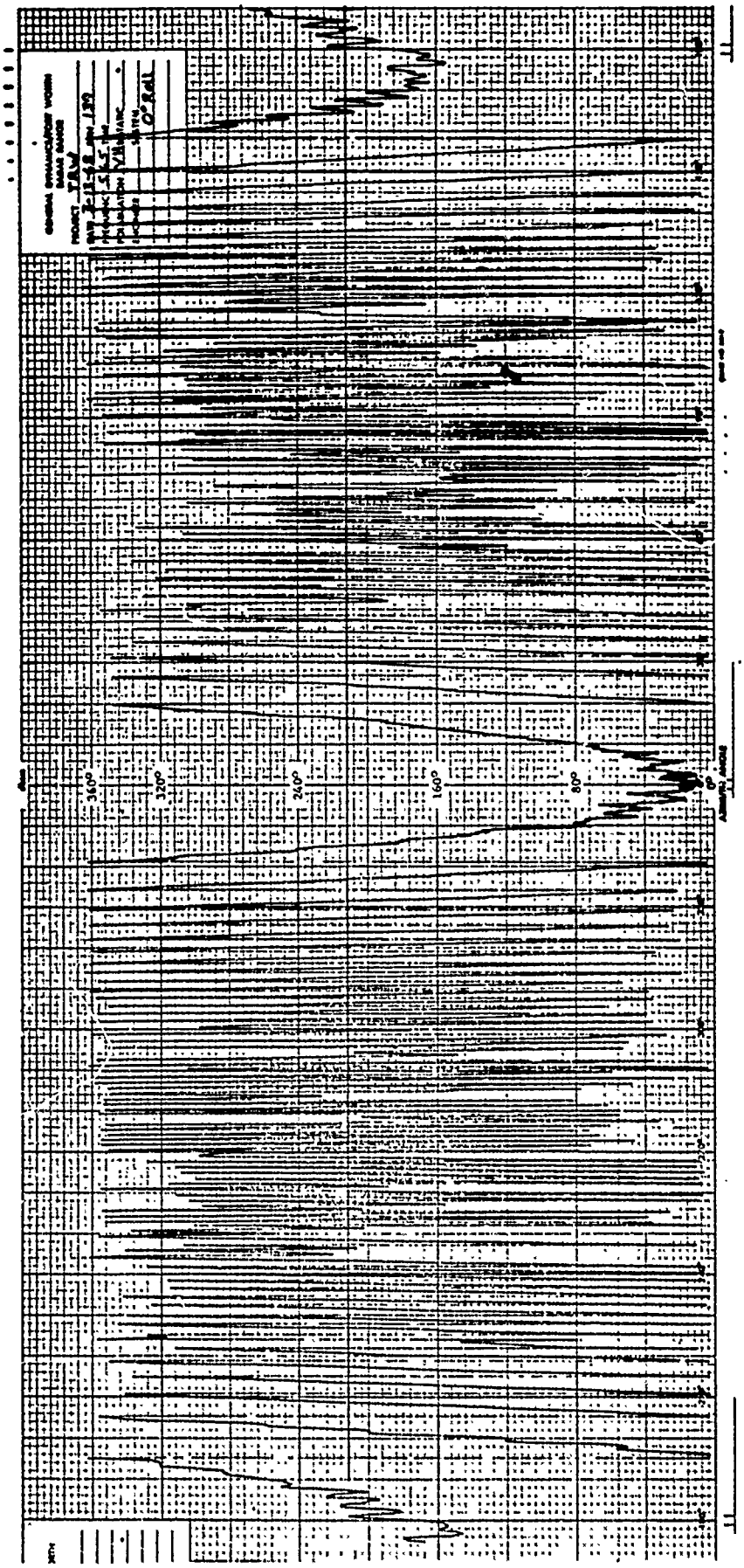

Fig. D-40 VEHICLE 001 PHASE RESPONSE; C-BAND, VH POLARIZATION, 0-DEGREE ROLL

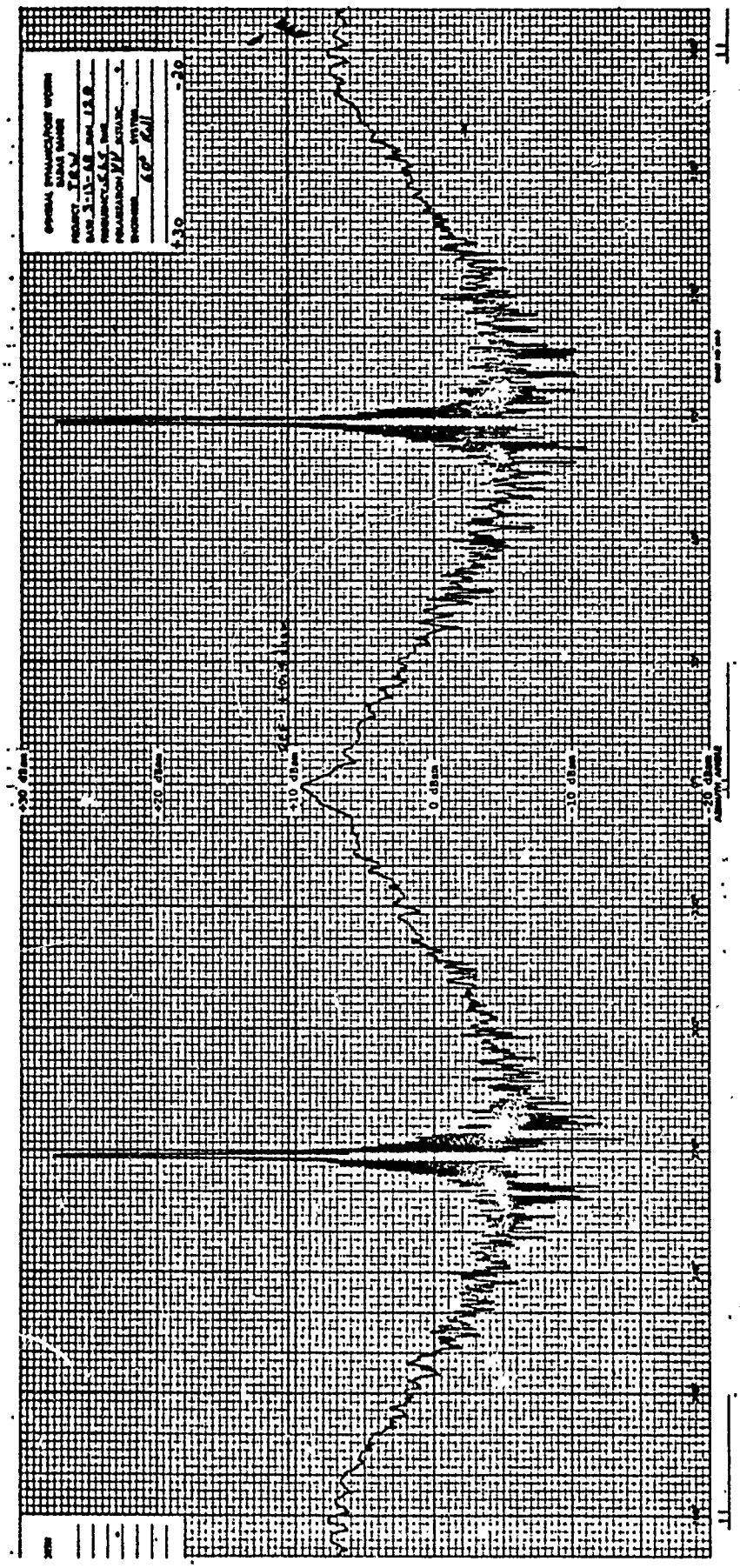

Fig. D-41 VEHICLE 001 AMPLITUDE RESPONSE; C-BAND, VV POLARIZATION, 60-DEGREE ROLL

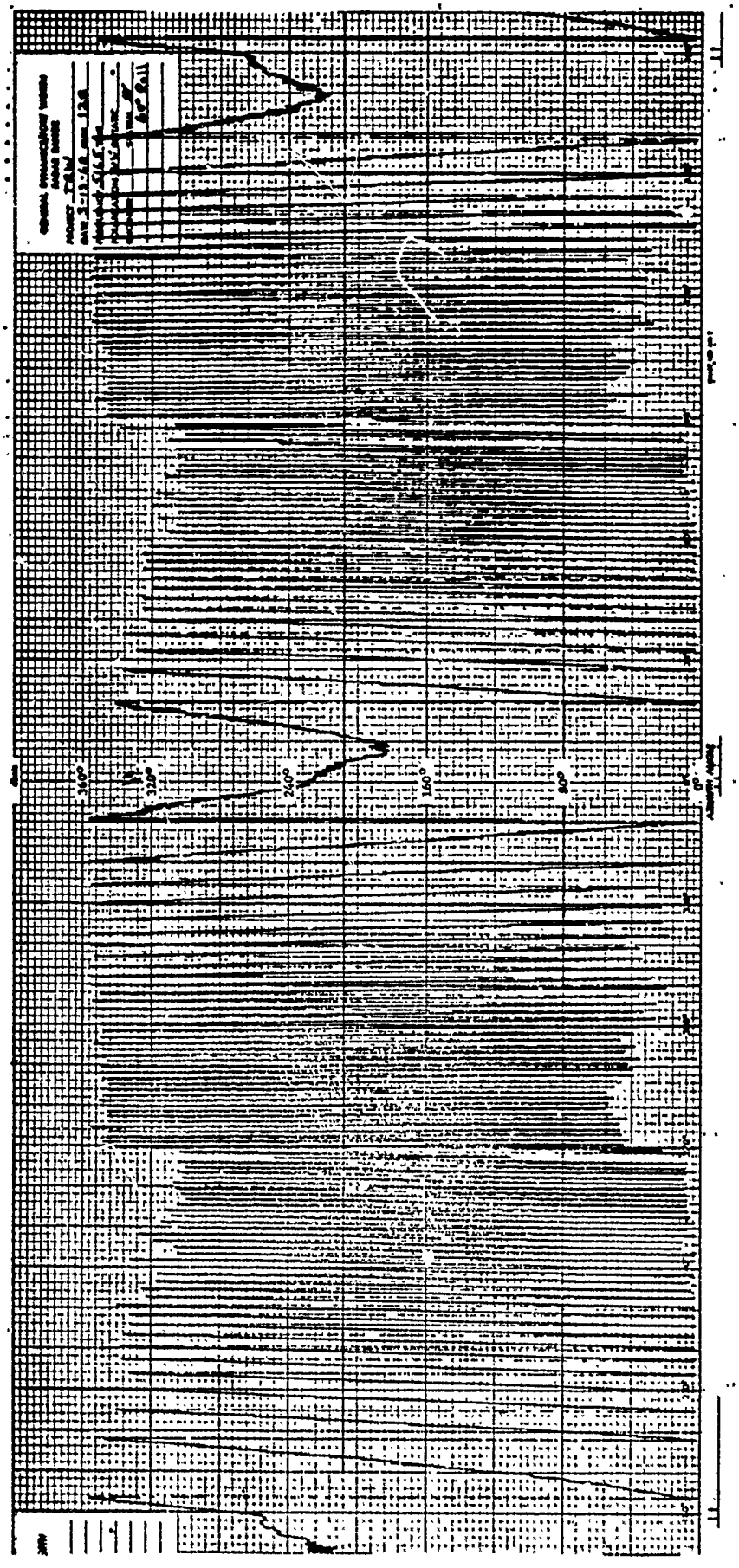

Fig. D-42 VEHICLE 001 PHASE RESPONSE; C-BAND, VV POLARIZATION, 60-DEGREE ROLL

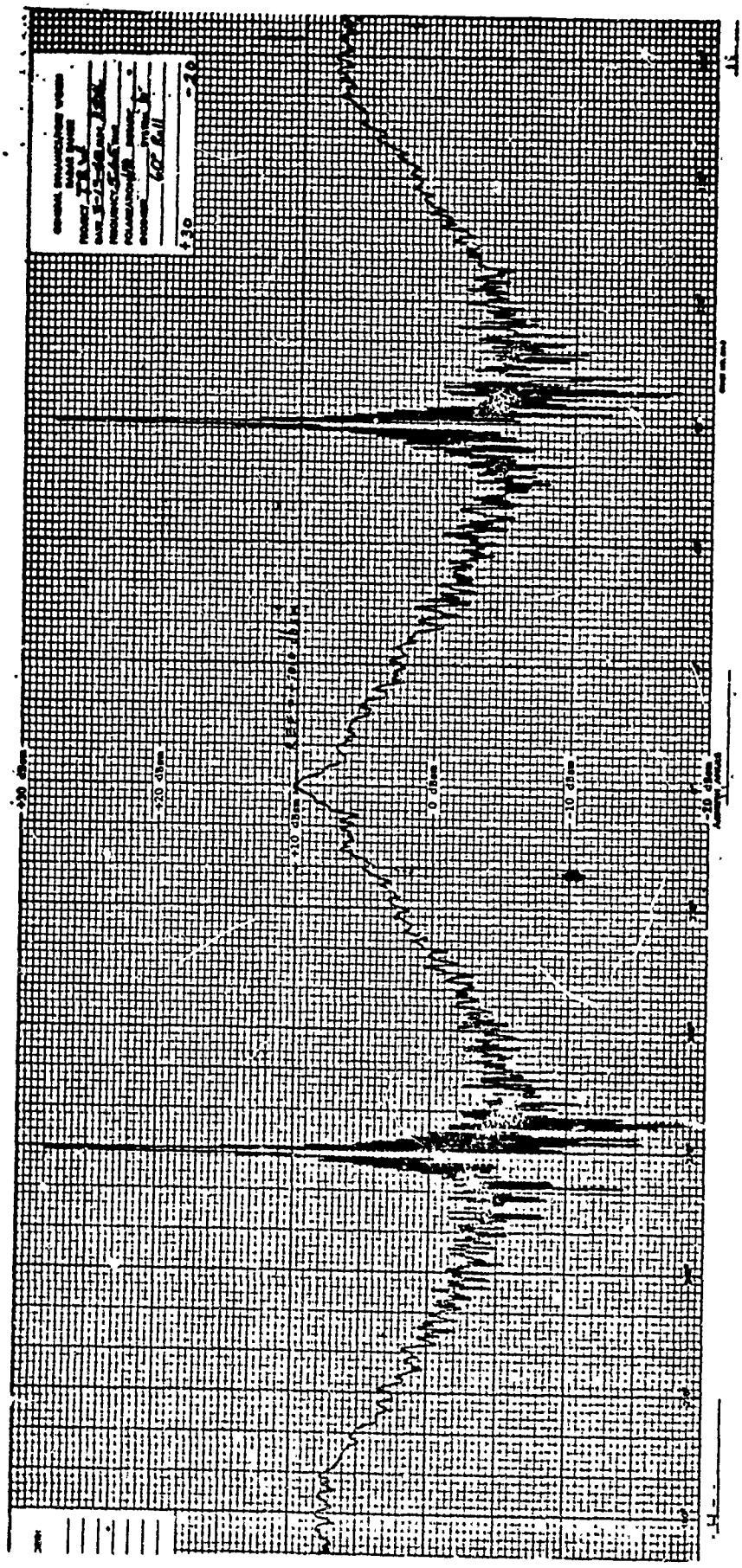

Fig. D-43 VEHICLE 001 AMPLITUDE RESPONSE; C-BAND, HH POLARIZATION, 60-DEGREE ROLL

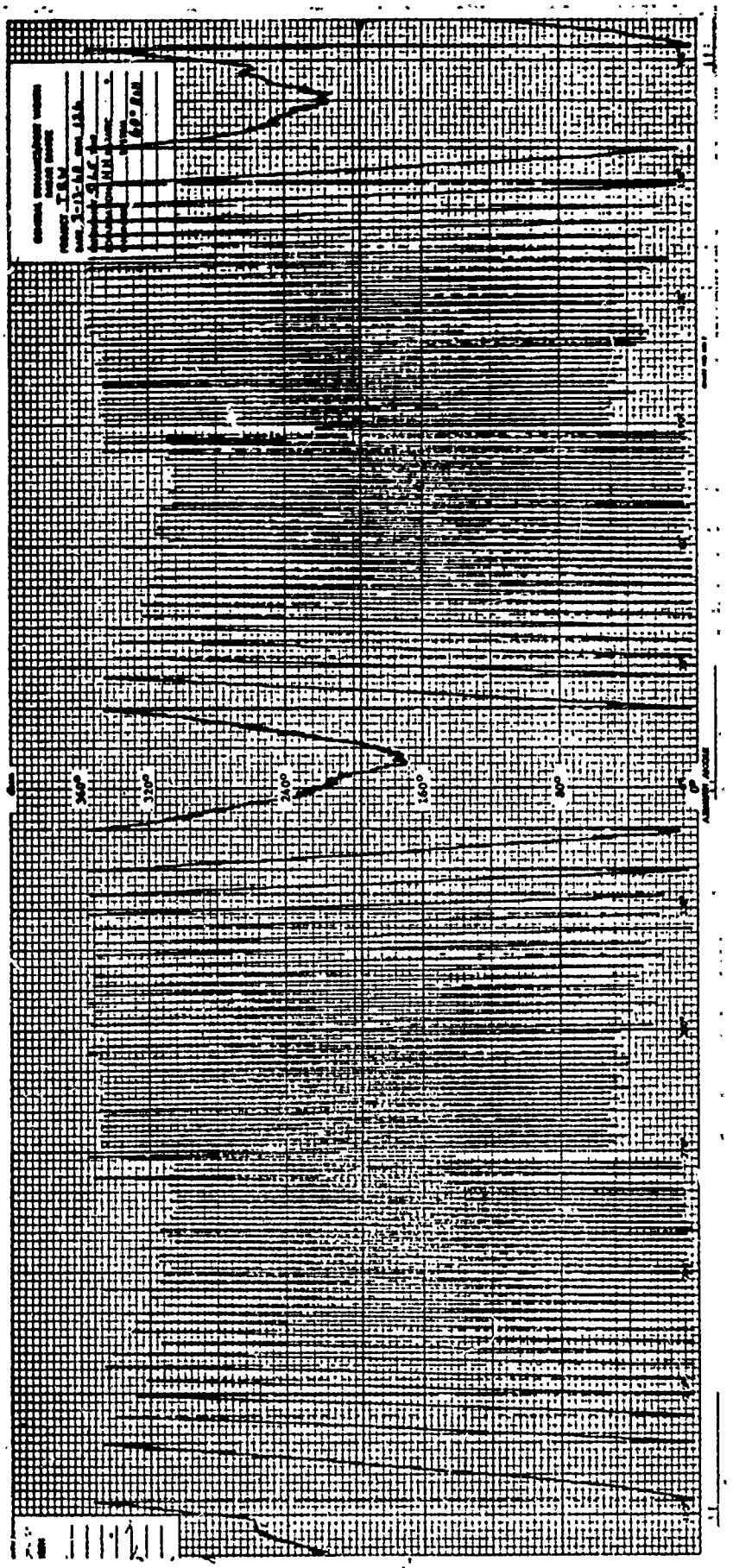

Fig. D-44 VEHICLE 001 PHASE RESPONSE; C-BAND, HH POLARIZATION, 60-DEGREE ROLL

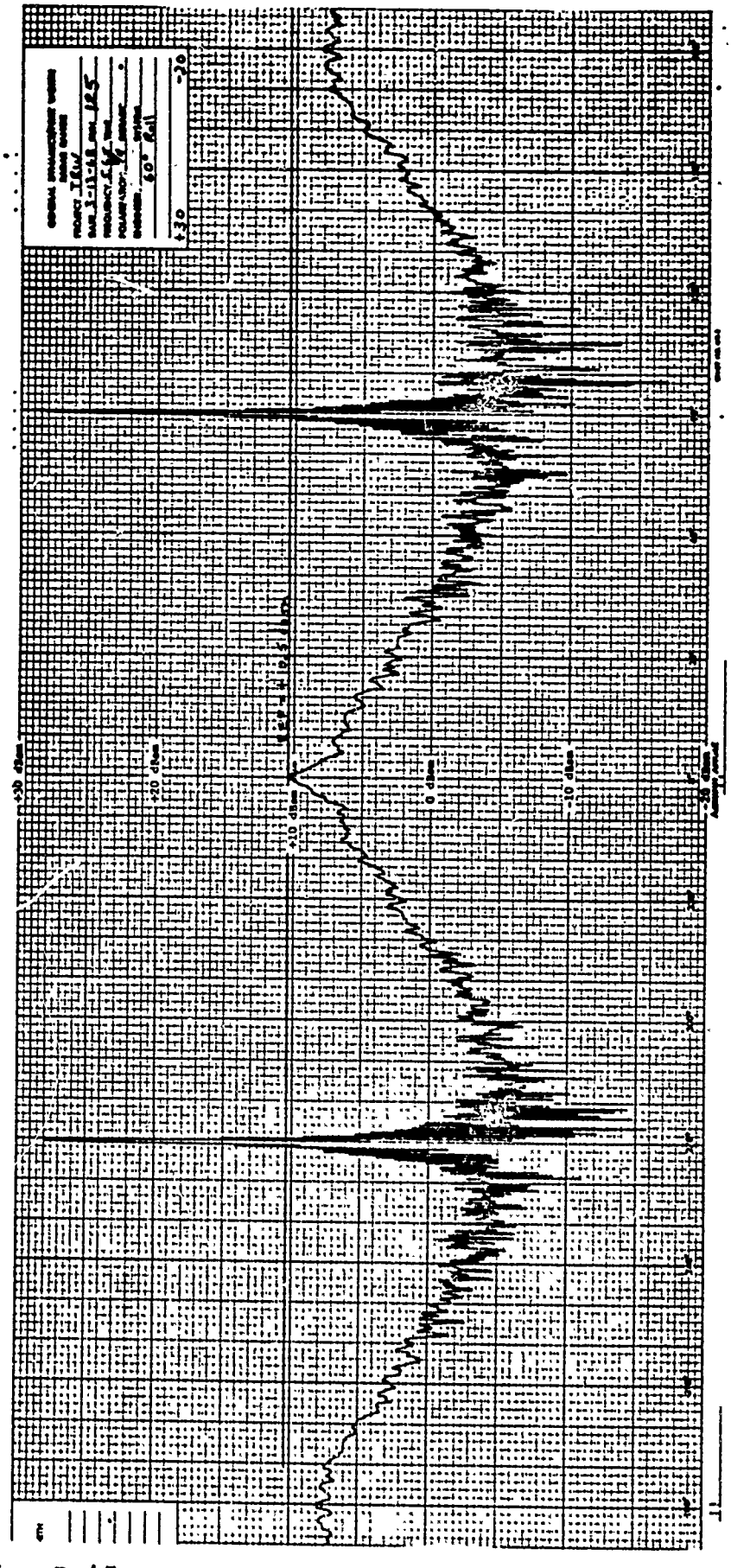

Fig. D-45 VEHICLE 001 AMPLITUDE RESPONSE, C-BAND, $\pi/4$ $\pi/4$ POLARIZATION, 60-DEGREE ROLL

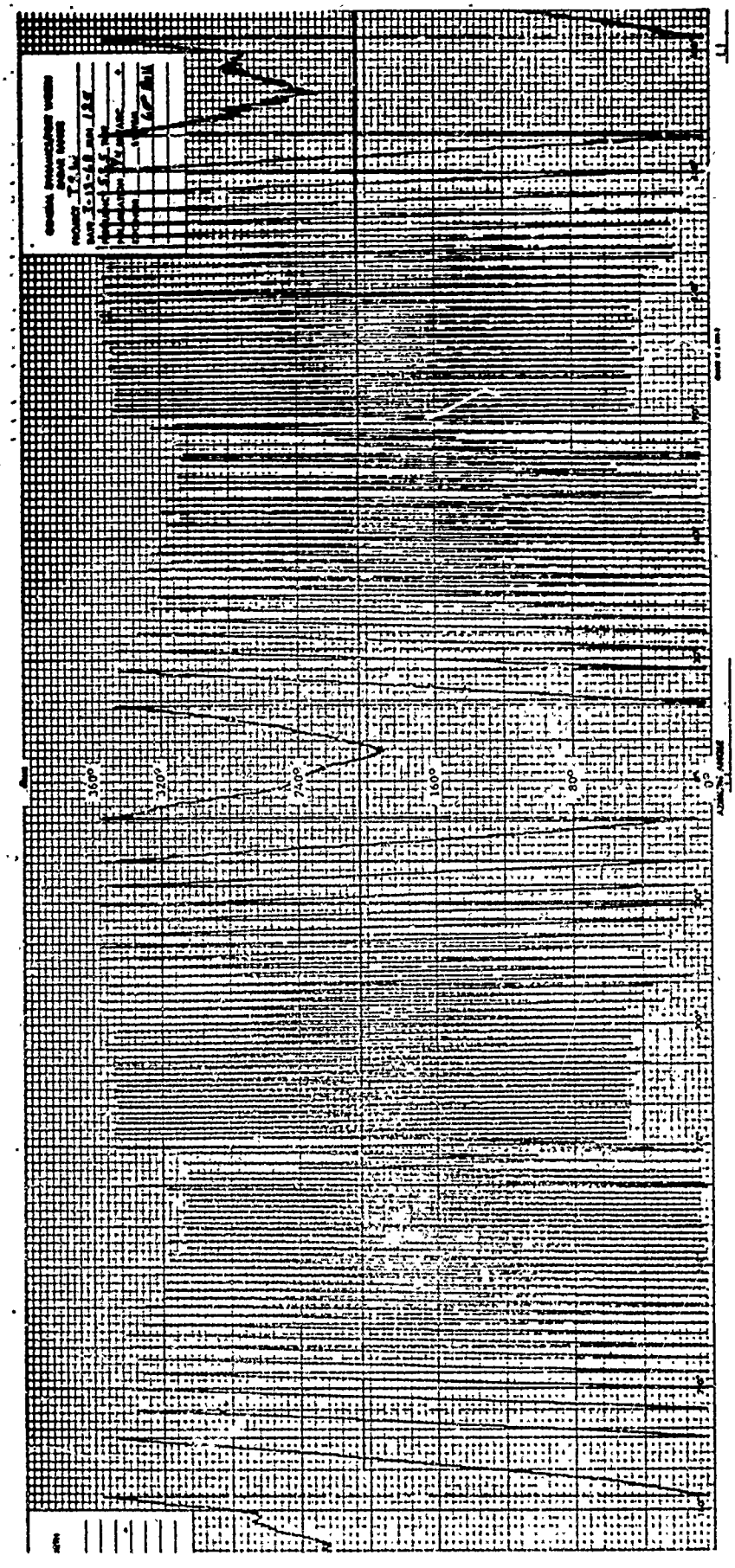

Fig. D-46 VEHICLE 001 PHASE RESPONSE; C-BAND, $\pi/4$ $\pi/4$ POLARIZATION, 60-DEGREE ROLL

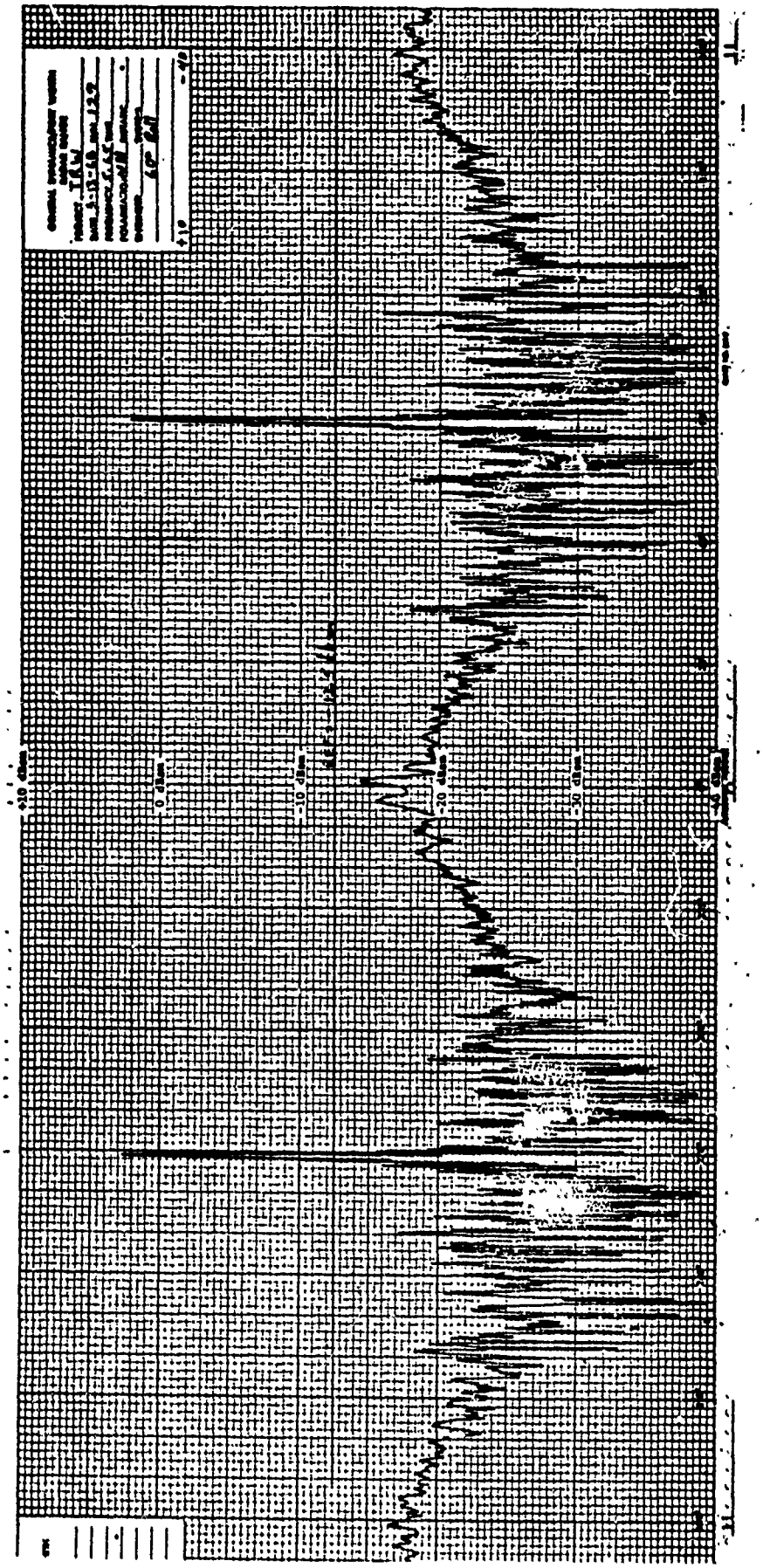

Fig. D-47 VEHICLE 001 AMPLITUDE RESPONSE; C-BAND, VH POLARIZATION, 60-DEGREE ROLL

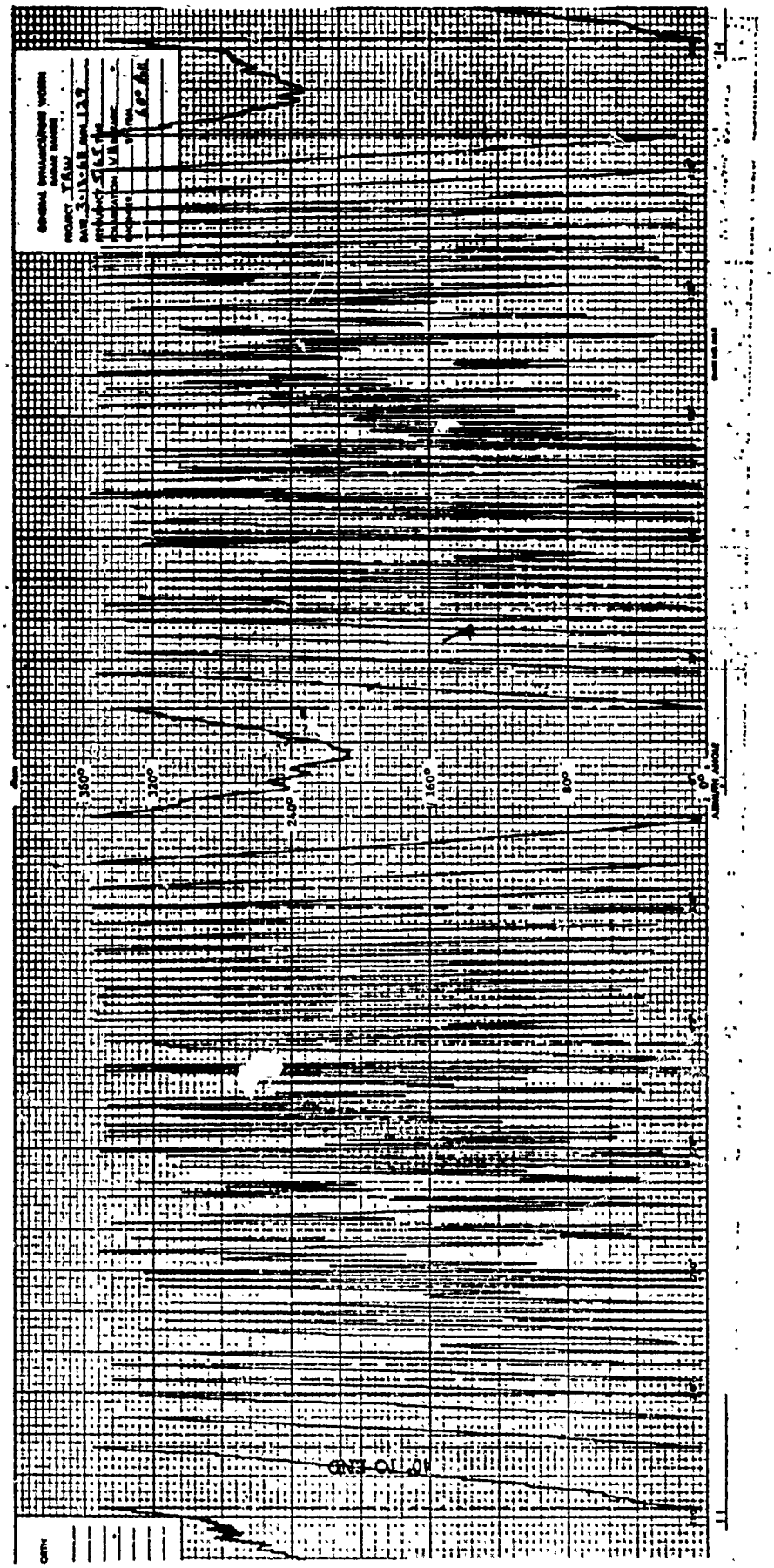

Fig. D-48 VEHICLE 001 PHASE RESPONSE; C-BAND, VH POLARIZATION, 50-DEGREE ROLL

THIS PAGE INTENTIONALLY LEFT BLANK

APPENDIX E

PHYSICAL OPTICS FORMULATION OF RADCAT VEHICLE RESPONSE

The Radar Calibration Target is basically composed of an 8-foot cylinder with 2:1 oblate spheroidal ends; the configuration and dimensions are illustrated in Figure E-1. At the spheroid-cylinder joint ($\rho = a$, $z = \pm \ell/2$), the generator curves are continuous but have discontinuous second derivatives. A plane wave impinging onto the target with an incident angle θ_o with respect to the z-axis and can be expressed, for e^{iwt} harmonic time variation, as

$$\bar{H}^i \begin{pmatrix} V \\ H \end{pmatrix} = \begin{pmatrix} \hat{\theta} \\ \hat{\psi} \end{pmatrix} H_o \, e^{jk_o(z\cos\theta_o + x\sin\theta_o)}$$

Without unnecessary detail, the physical optics integral for the backscattered magnetic field can, in general, be expressed in the following form,

$$\bar{H}^S \begin{pmatrix} V \\ H \end{pmatrix} (\theta_o) = \begin{pmatrix} \hat{\theta} \\ \hat{\phi} \end{pmatrix} K_o \left| \hat{S} \cdot \int_{S_1} \hat{n} \, e^{j2k_o(z\cos\theta_o + x\sin\theta_o)} \, dS \right| \tag{1}$$

where $K_o = jk_o \, H_o \, e^{-jk_oR_o}/2\pi R_o$, η is the unit normal vector at any point on the scatterer's surface, and S_1 denotes the illuminated surface of the scatterer. It can be noted that, in the case of physical optics approximations, the scattered wave is always found to have the same polarization as the

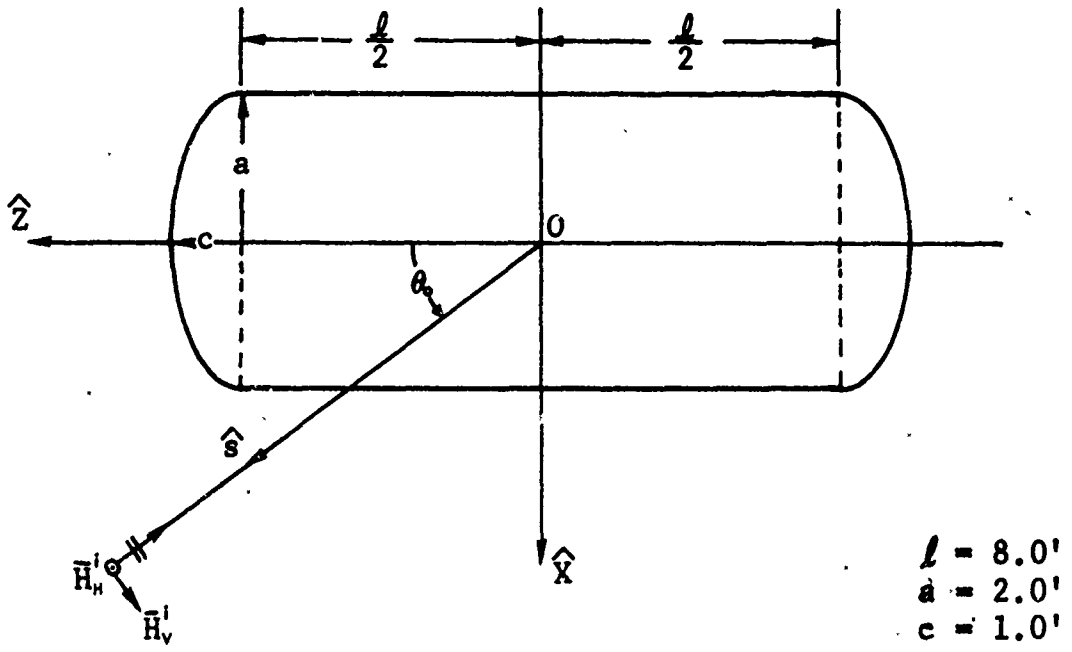

Figure E-1. RADCAT TARGET GEOMETRY

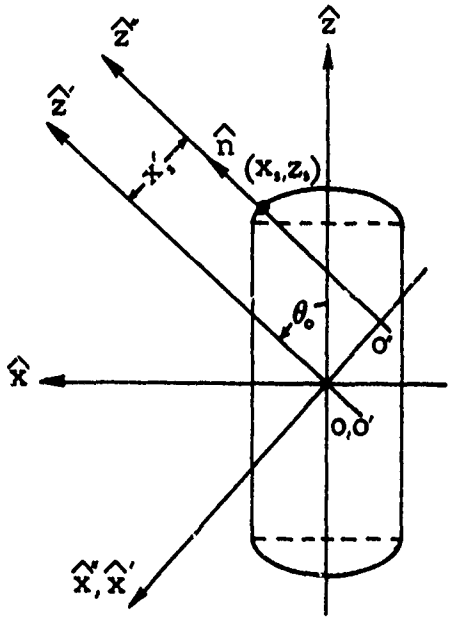

Figure E-2 TRANSFORMATION OF COORDINATES

incident wave. Therefore, $\bar{H}^{S}_{\binom{V}{H}}(\theta_o)$ can be denoted by $H(\theta_o)$.

The illuminated surface on the target can be conveniently divided into the cylindrical and the oblate spheroidal portions; therefore, $H(\theta_o) = H_c(\theta_o) + H_{os}(\theta_o)$. The solution of the cylindrical surface is well known [3] and can be summarized as the following integral,

$$H_c(\theta_o) = K_o(a\sin\theta_o) \int_{-\ell/2}^{\ell/2} \int_{-\pi/2}^{\pi/2} \cos\phi e^{j2k_o(z\cos\theta_o + a\sin\theta_o\cos\phi)} \, d\phi \, dz$$

$$= K_o(a\ell\sin\theta_o) \left\{ \frac{\sin(k_o\ell\cos\theta_o)}{k_o\cos\theta_o} \right\} \int_{-\pi/2}^{\pi/2} e^{j\beta\cos\phi}\cos\phi \, d\phi$$

where $\beta = 2k_o a \sin\theta_o$. Since β is generally large, one can use the method of stationary phase to find the asymptotic solution of the integral. Thus,

$$H_c(\theta_o) = \frac{H_o e^{-jk_o R_o}}{2\sqrt{\pi R_o}} \left(\ell\sqrt{k_o a\sin\theta_o}\right) \left\{ \frac{\sin(k_o\ell\cos\theta_o)}{k_o\ell\cos\theta_o} \right\} e^{j(2k_o a\sin\theta_o + \pi/4)} \tag{2}$$

Similarly, if the physical optics integral is applied to the oblate spheroidal ends, the scattered magnetic field becomes

$$H_{os}(\theta_o) = K_o \int_{S_1} \left\{ \frac{C^2}{a^2}\left(\frac{X}{z \mp \frac{\ell}{2}}\right) \sin\theta_o + \cos\theta_o \right\} e^{j2k_o(x\sin\theta_o + z\cos\theta_o)} \, dx \, dy$$

where $(z \mp \frac{\ell}{2}) = \pm \frac{c}{a}\sqrt{a^2-x^2-y^2}$, and the $\pm$ sign distinguishes each end of the target. However, the solution to this integral is not straightforward primarily due to the difficulty encountered in the determination of the boundary of the illuminated area as a function of aspect angle θ.

For the above reason, an alternative approach is taken for the large, smooth scatterer. In this case the scattering contribution of the oblate spheroid is dominated by that from the specular point. It can be shown that the specular point on an oblate spheroid occurs at the coordinant point (x_s, z_s) where

$$x_s = a^2 \sin\theta_o / \sqrt{a^2\sin^2\theta_o + c^2 \cos^2\theta_o}$$

$$z_s = \pm \frac{\ell}{2} + (c^2 \cos\theta_o / \sqrt{a^2\sin^2\theta_o + c^2 \cos^2\theta_o})$$

The problem can be simplified by transformations of coordinate systems by first rotating the x and z coordinates through an angle θ_o around the y-axis and then translating the new coordinates along the new x-axis an amount x_s' (see Figure E-2) by use of the rotation given by

$$x_s' = x_s\cos\theta_o - z_s\sin\theta_o = \mp \frac{\ell}{2}\sin\theta_o + \frac{(a^2 - c^2)\sin^2\theta_o}{2\sqrt{a^2\sin^2\theta_o + c^2\cos^2\theta_o}}$$

$$z_s' = x_s\sin\theta_o + z_s\cos\theta_o = \pm \frac{\ell}{2}\cos\theta_o + \sqrt{a^2\sin^2\theta_o + c^2\cos^2\theta_o}$$

and with the translation given by

$$x_s'' = 0$$
$$z_s'' = z_s'$$

It is clear that, with the above transformations, the scattered magnetic field reduces to,

$$H_{oc}(\theta_o) = K_o \int_{S_1''} e^{j2k_o z''(x'',y'')} dx'' dy'' \qquad (3)$$

This expression can be recognized as the double integral which can be solved asymptotically for large k_o through use of the method of stationary phase [4]. First, the expression for z"(x",y") is expanded into a Maclaurin series about the specular point, $[0, 0, z_s''(0,0)]$ therefore,

$$z''(x'',y'') = z_s''(0,0) + \left.\frac{\partial z''}{\partial x''}\right|_o x'' + \left.\frac{\partial z''}{\partial y''}\right|_o y'' + \left.\frac{\partial^2 z''}{\partial x''^2}\right|_o \frac{x''^2}{2}$$
$$+ \left.\frac{\partial^2 z''}{\partial x'' \partial y''}\right|_o x''y'' + \left.\frac{\partial^2 z''}{\partial y''^2}\right|_o \frac{y''^2}{2} + \ldots$$

Since the first partial derivatives are zero at the specular point, Equation 3 reduces to

$$H_{os}(\theta_o) = e^{j2k_o z_s''} K_o \int_{S_1''} \exp\left[j2k_o\left(p\frac{x''^2}{2} + q\frac{y''^2}{2} + rx''y'' + \ldots\right)\right] dx'' dy''$$

where p, q, and r are respectively the second partial derivatives at the specular point. By the use of the method of stationary phase, the series can be terminated in the

second derivative, and the limits of integration can be extended to infinity. Thus, the expression can be reduced to

$$H_{os}(\theta_o) = \frac{H_o\, e^{-jk_oR_o}}{2R_o} \left(\frac{1}{\sqrt{|pq - r^2|}}\right) e^{j2k_oz_s''}$$

for a convex surface.

The term under the square root sign has a simple geometrical interpretation. If K is the Gaussian curvature of the surface, then $K = pq - r^2$. Thus,

$$H_{os}(\theta_o) = \frac{H_o\, e^{-jk_oR_o}}{2\sqrt{\pi}\, R_o} \sqrt{\pi R_1R_2}\; e^{j2k_oz_s''}$$

where R_1 and R_2 are the principal radii of curvature of the oblate spheroid, and R_1R_2 can be shown to be

$$a^4c^2/(a^2\sin^2\theta_o + c^2\cos^2\theta_o)^2.$$

Hence,

$$H_{os}(\theta_o) = \frac{H_o\, e^{-jk_oR_o}}{2\sqrt{\pi}\, R_o} \left\{\frac{\sqrt{\pi}\, a^2c}{a^2\sin^2\theta_o + c^2\cos^2\theta_o}\right\} e^{j2k_o \pm\left(\frac{\ell}{2}\cos\theta_o + \sqrt{a^2\sin^2\theta_o + c^2\cos^2\theta_o}\right)} \tag{4}$$

It is interesting to note that this is exactly the geometrical optics solution of the oblate spheroid with the appropriate phase variation for the specular point. Therefore, for a large, smooth scatterer with finite principal radii of curvature the physical optics solution reduces

exactly to the geometrical optics result. It may be mentioned in passing that since this solution is based on physical optics approximation (thus, the VV and HH components are equal), this target will not produce cross-polarized scattered component at any arbitrary orientation to the radar.

THIS PAGE INTENTIONALLY LEFT BLANK

APPENDIX F

1/2-SCALE MODEL MEASUREMENTS

The signatures contained in this appendix correspond to the long-pulse amplitude and phase response of a 1/2-scale perfectly conducting model of the RADCAT Vehicle. Measurements performed at S-band, C-band, and X-band frequencies and transmitter/receiver polarizations of V/V, H/H, $\pi/4/\pi/4$, and V/H are presented herein. These data have been reproduced from an earlier report which documented the scale model measurements program (Reference 2). The addition of 6-dB to the 1/2-scale model response at 2.56 gigahertz corresponds to the full-scale model response at 1.28 gigahertz. Similar scaling of the signatures at 5.7 and 11.3 gigahertz would correspond to the full-scale response at 2.85 and 5.65 gigahertz, respectively. The title block appearing in the upper right-hand corner of each analog trace documents the measurement frequency and polarization.

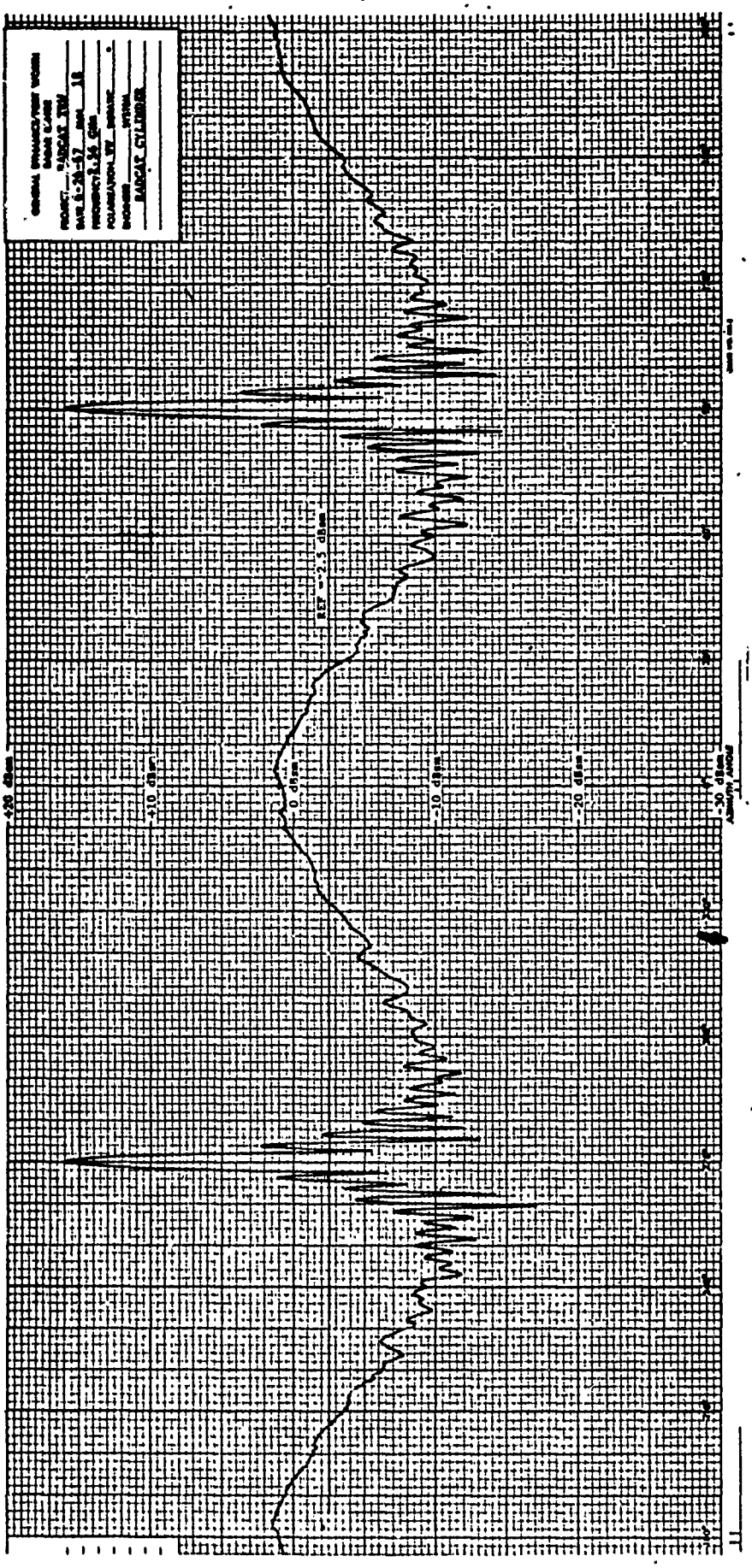

Fig. F-1 HALF-SCALE MODEL AMPLITUDE RESPONSE; S-BAND, VV POLARIZATION

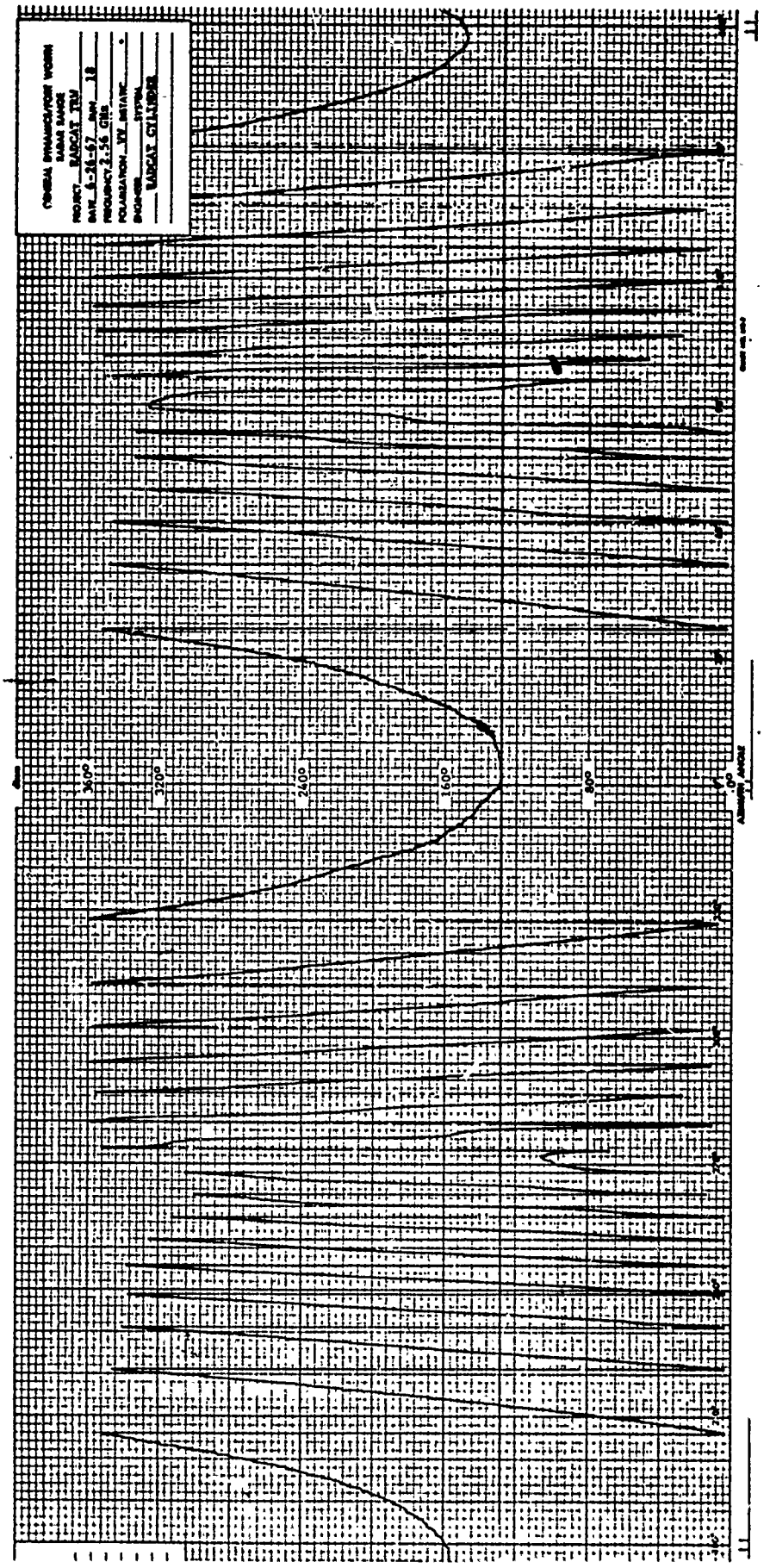

Fig. F-2 HALF-SCALE MODEL PHASE RESPONSE;
S-BAND VV POLARIZATION

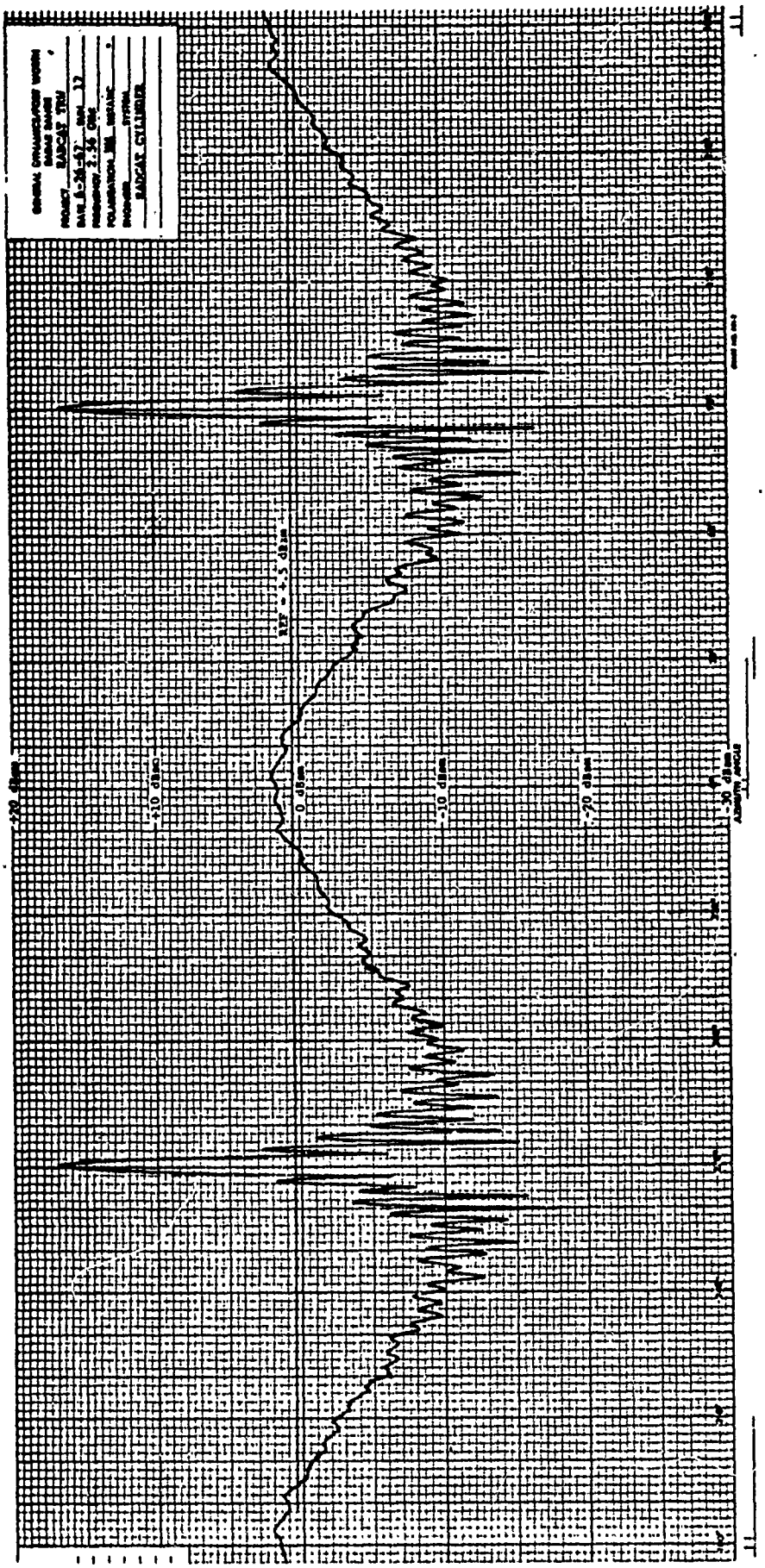

Fig. F-3 HALF-SCALE MODEL AMPLITUDE RESPONSE; S-BAND, HH POLARIZATION

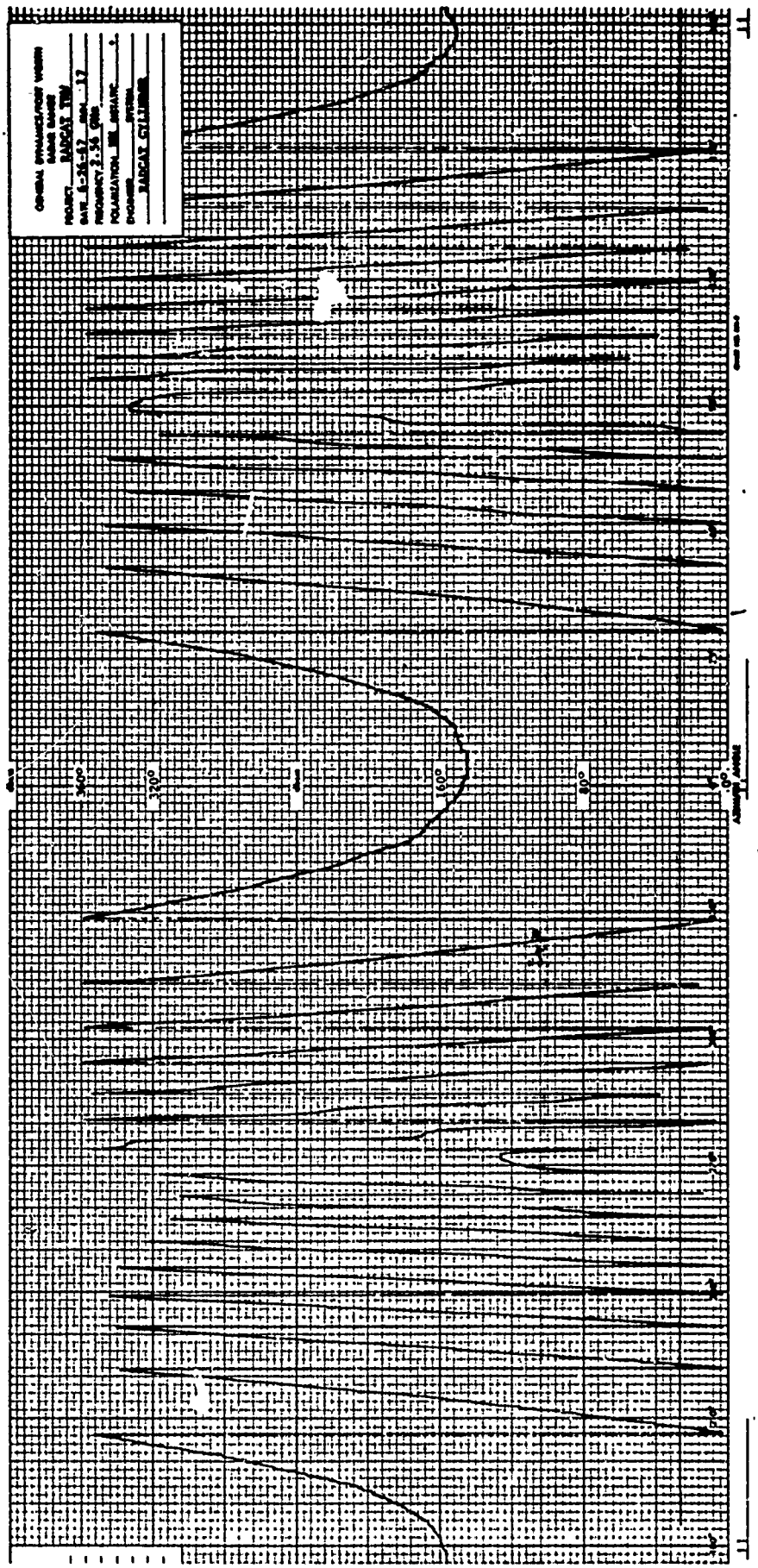

Fig. F-4 HALF-SCALE MODEL PHASE RESPONSE; S-BAND, HH POLARIZATION

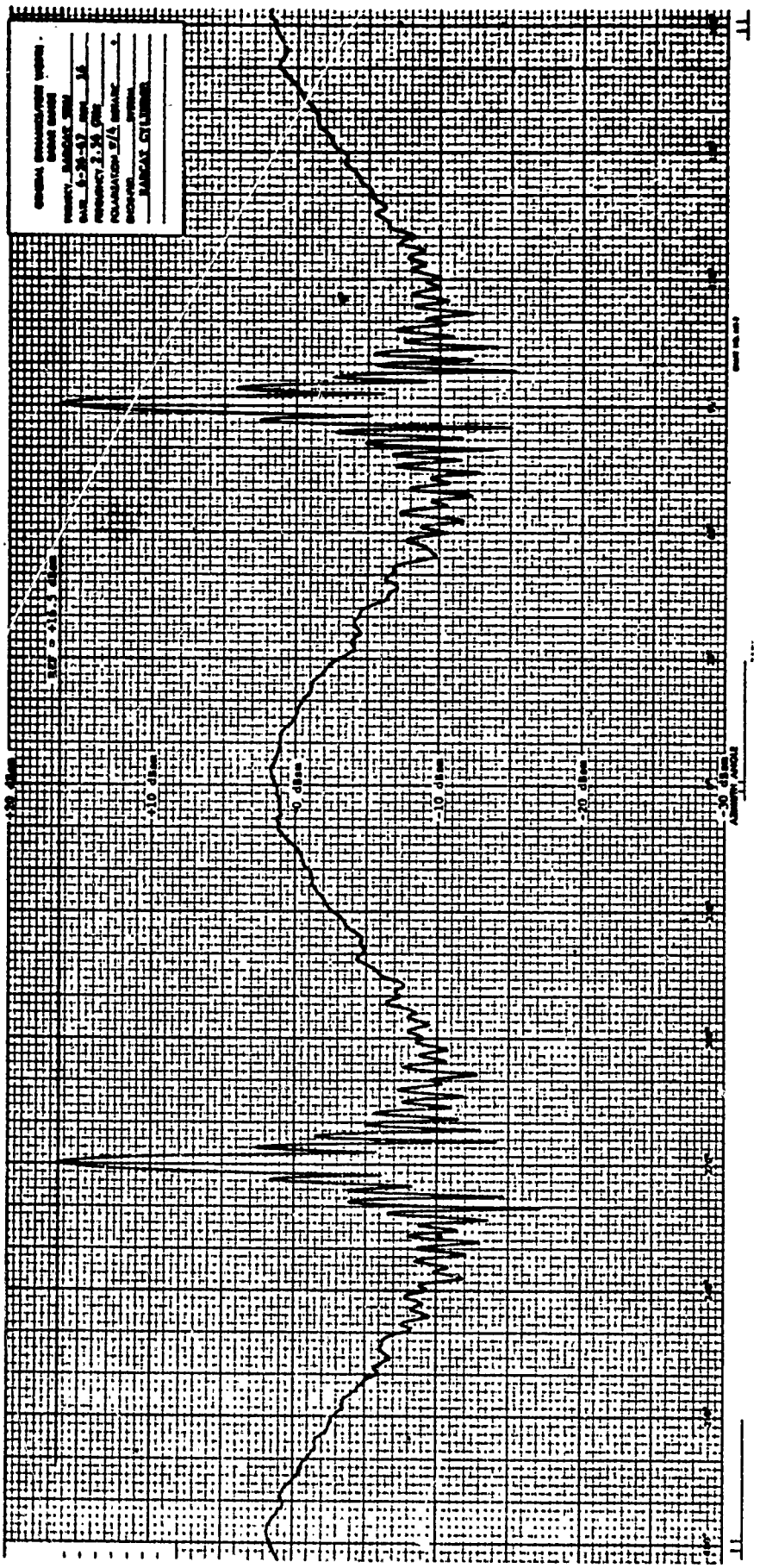

Fig. F-5 HALF-SCALE MODEL AMPLITUDE RESPONSE; S-BAND, $\pi/4$ $\pi/4$ POLARIZATION

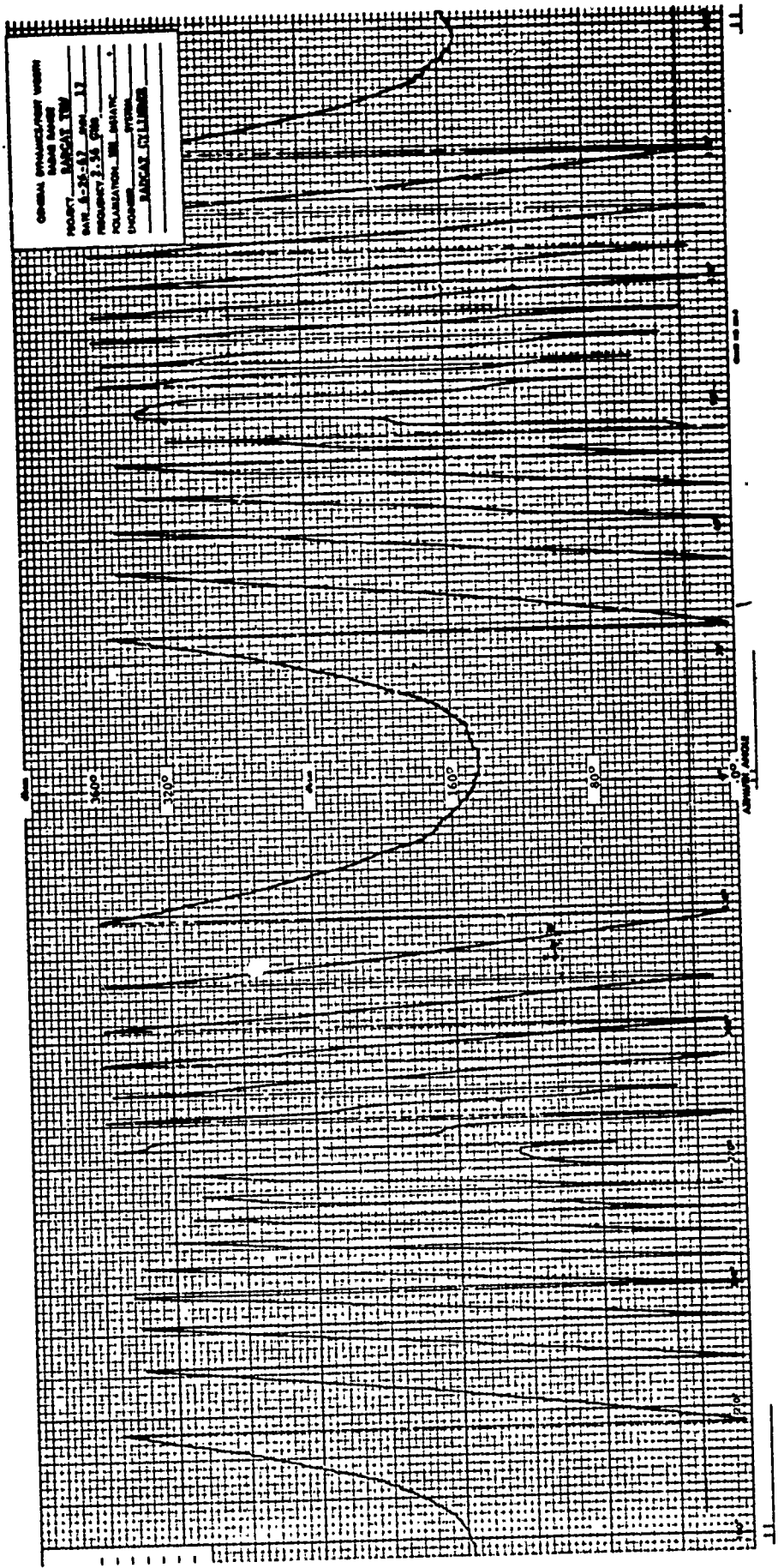

Fig. F-4 HALF-SCALE MODEL PHASE RESPONSE;
S-BAND, HH POLARIZATION

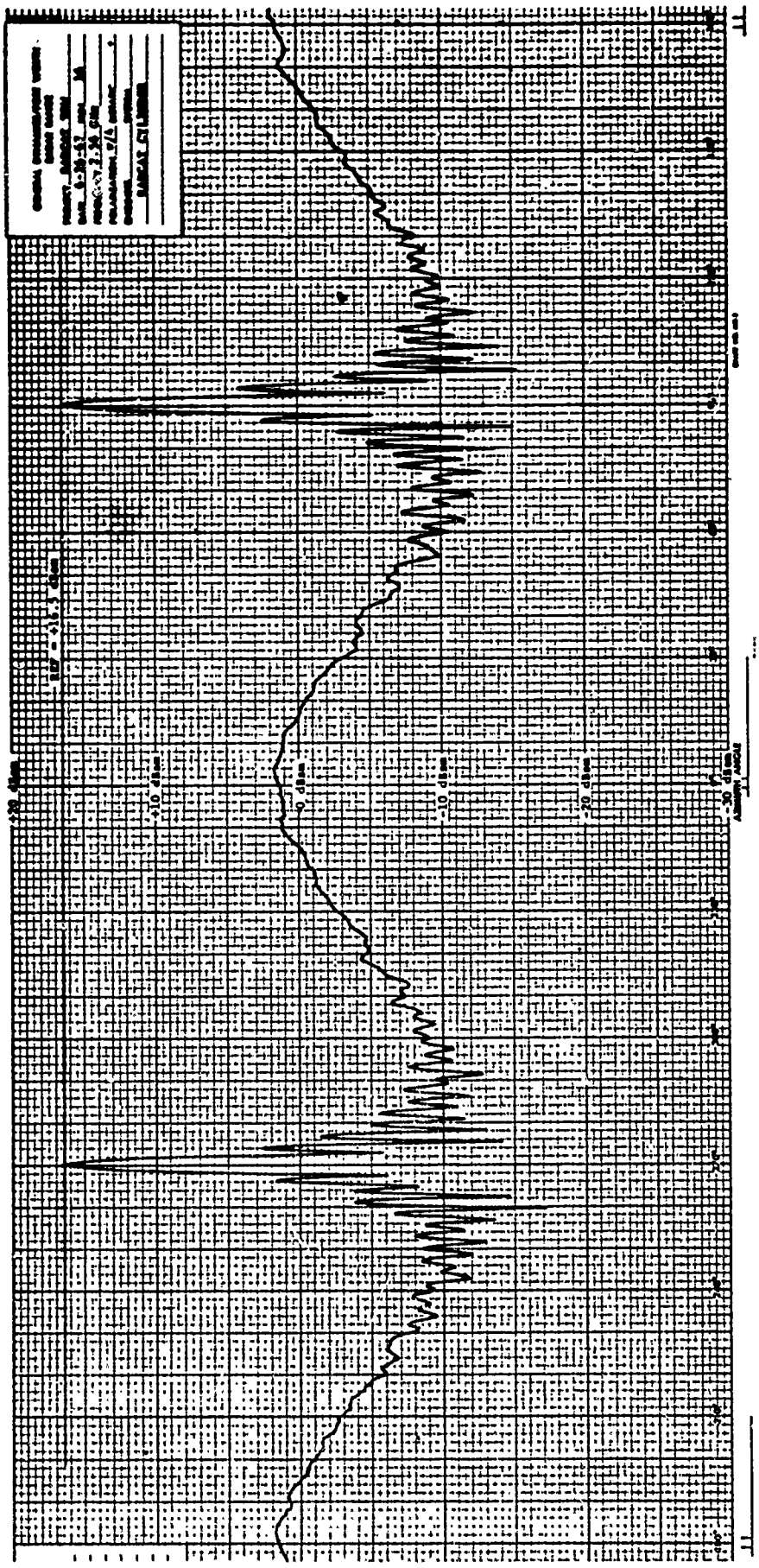

Fig. F-5 HALF-SCALE MODEL AMPLITUDE RESPONSE; S-BAND, $\pi/4$ $\pi/4$ POLARIZATION

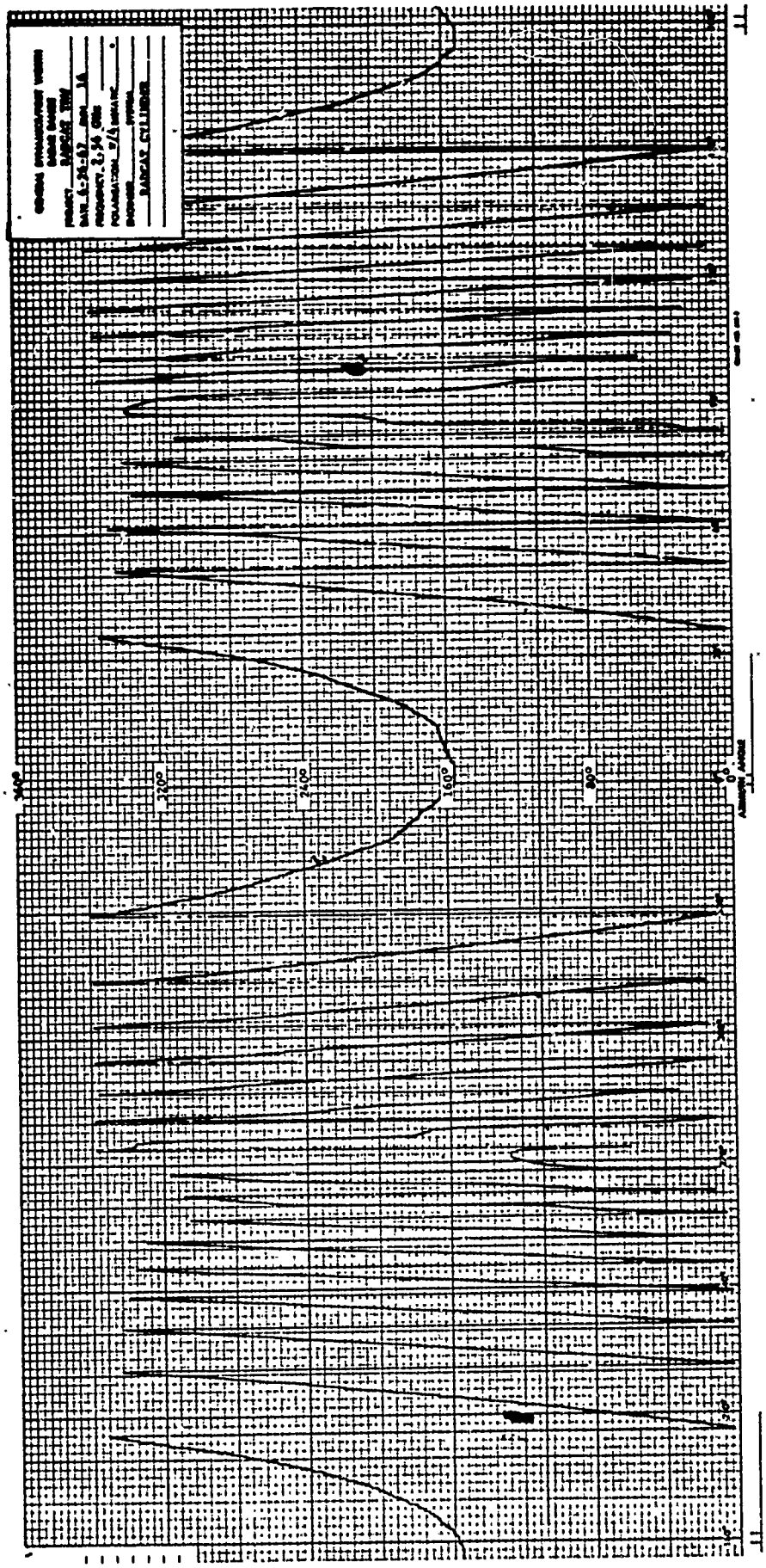

Fig. F-6 HALF-SCALE MODEL PHASE RESPONSE; S-BAND, $\pi/4$ $\pi/4$ POLARIZATION

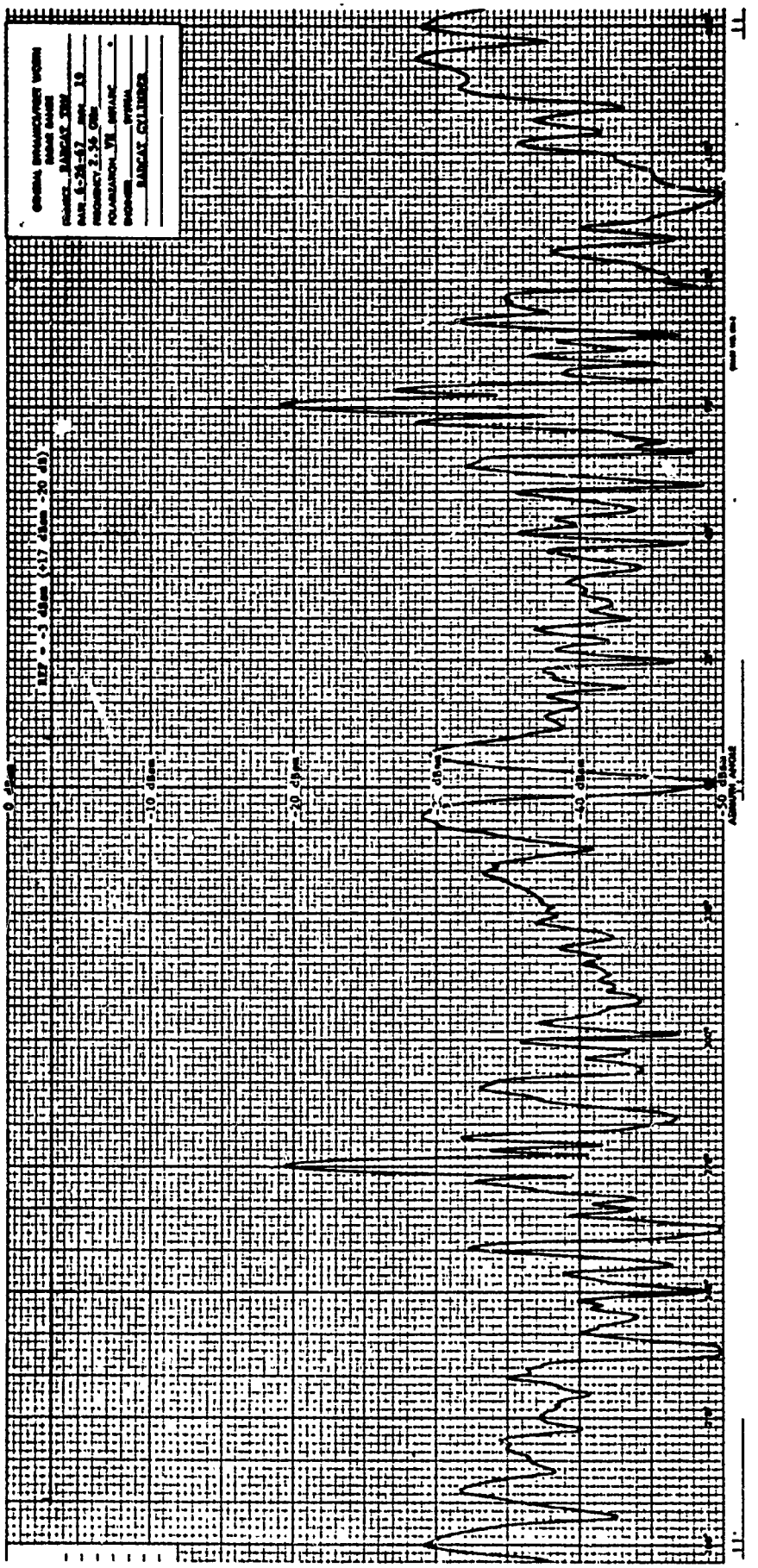

Fig. F-7 HALF-SCALE MODEL AMPLITUDE RESPONSE; S-BAND, VH POLARIZATION

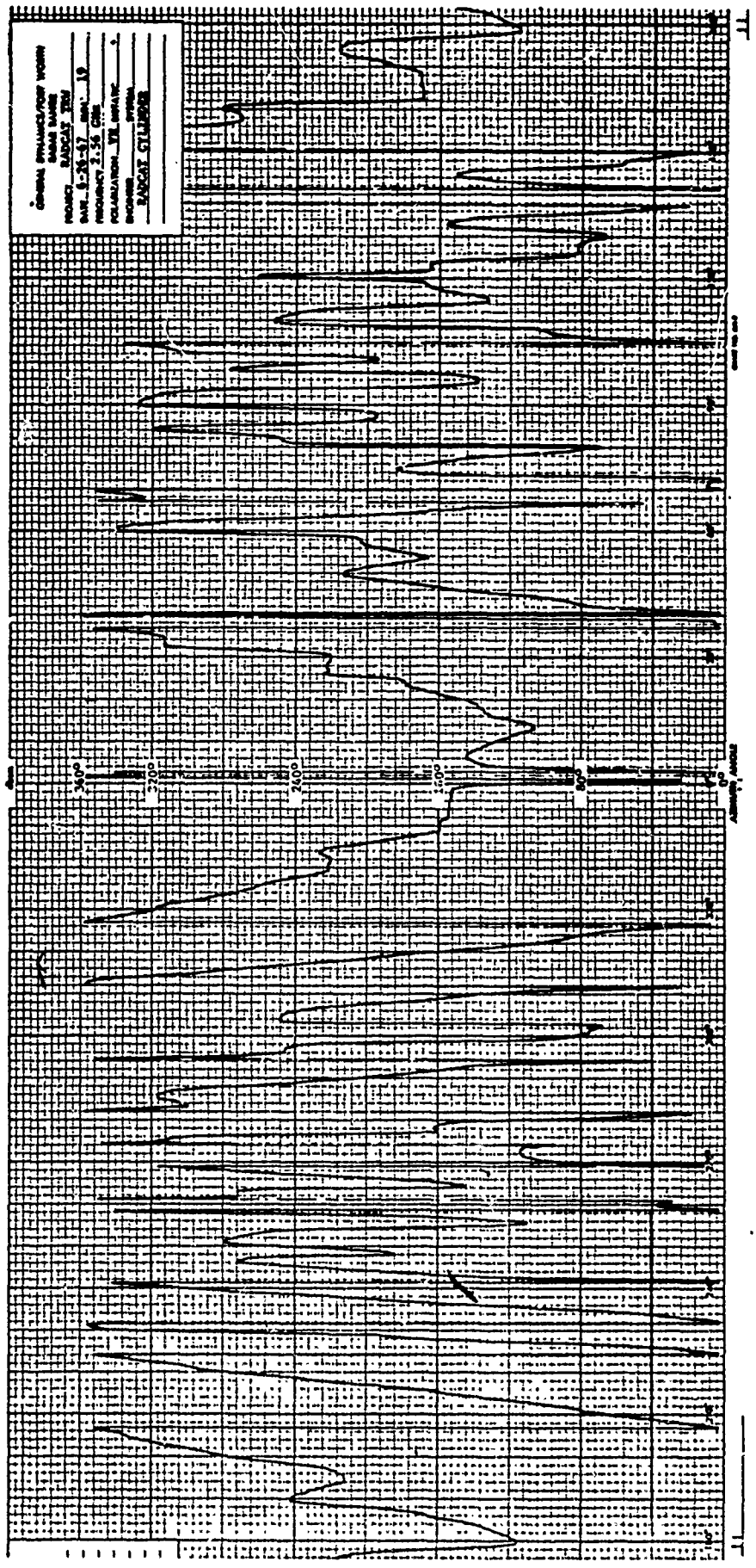

Fig. F-8 HALF-SCALE MODEL PHASE RESPONSE;
S-BAND, VH POLARIZATION

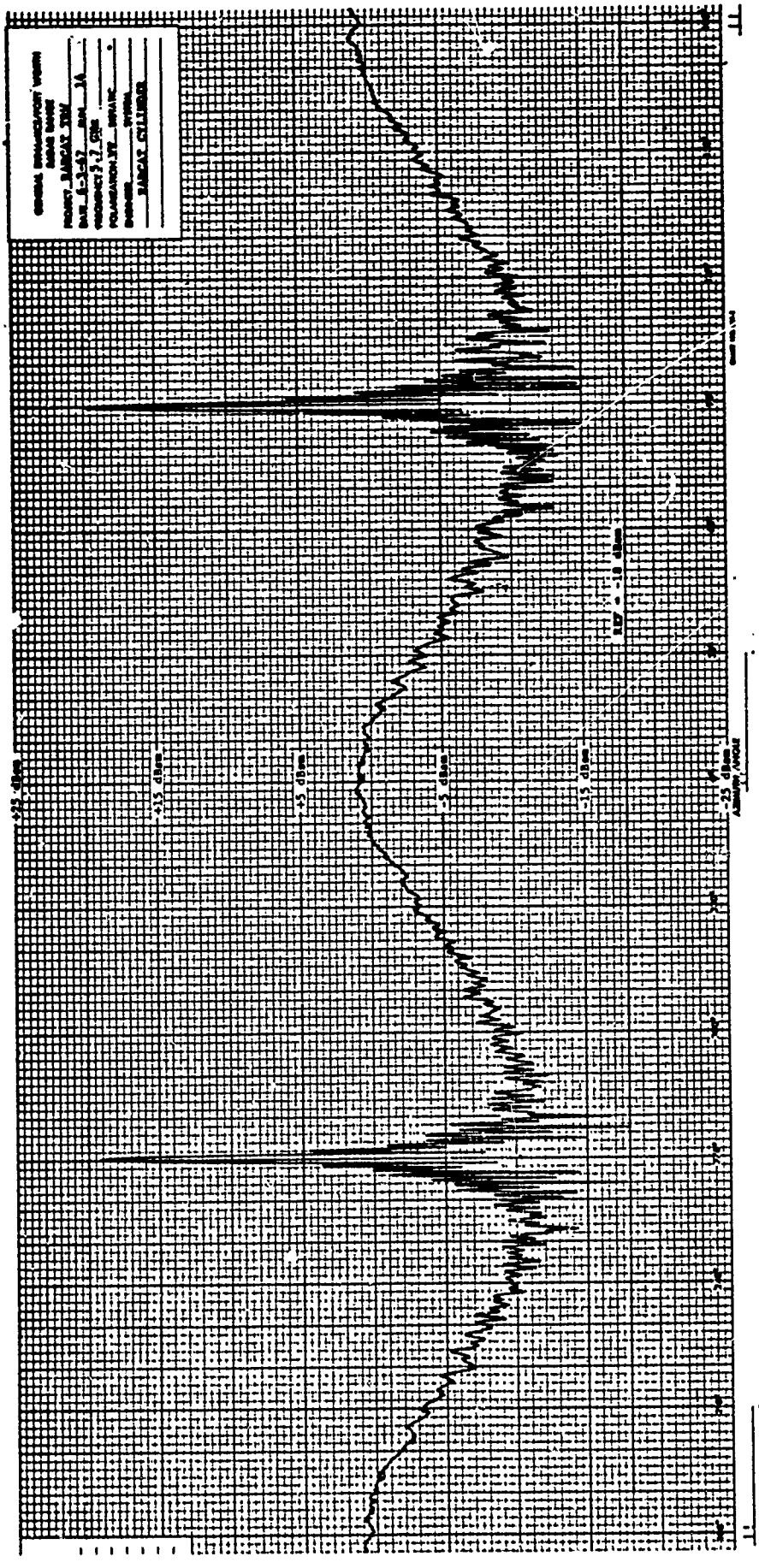

Fig. F-9 HALF-SCALE MODEL AMPLITUDE RESPONSE; C-BAND, VV POLARIZATION

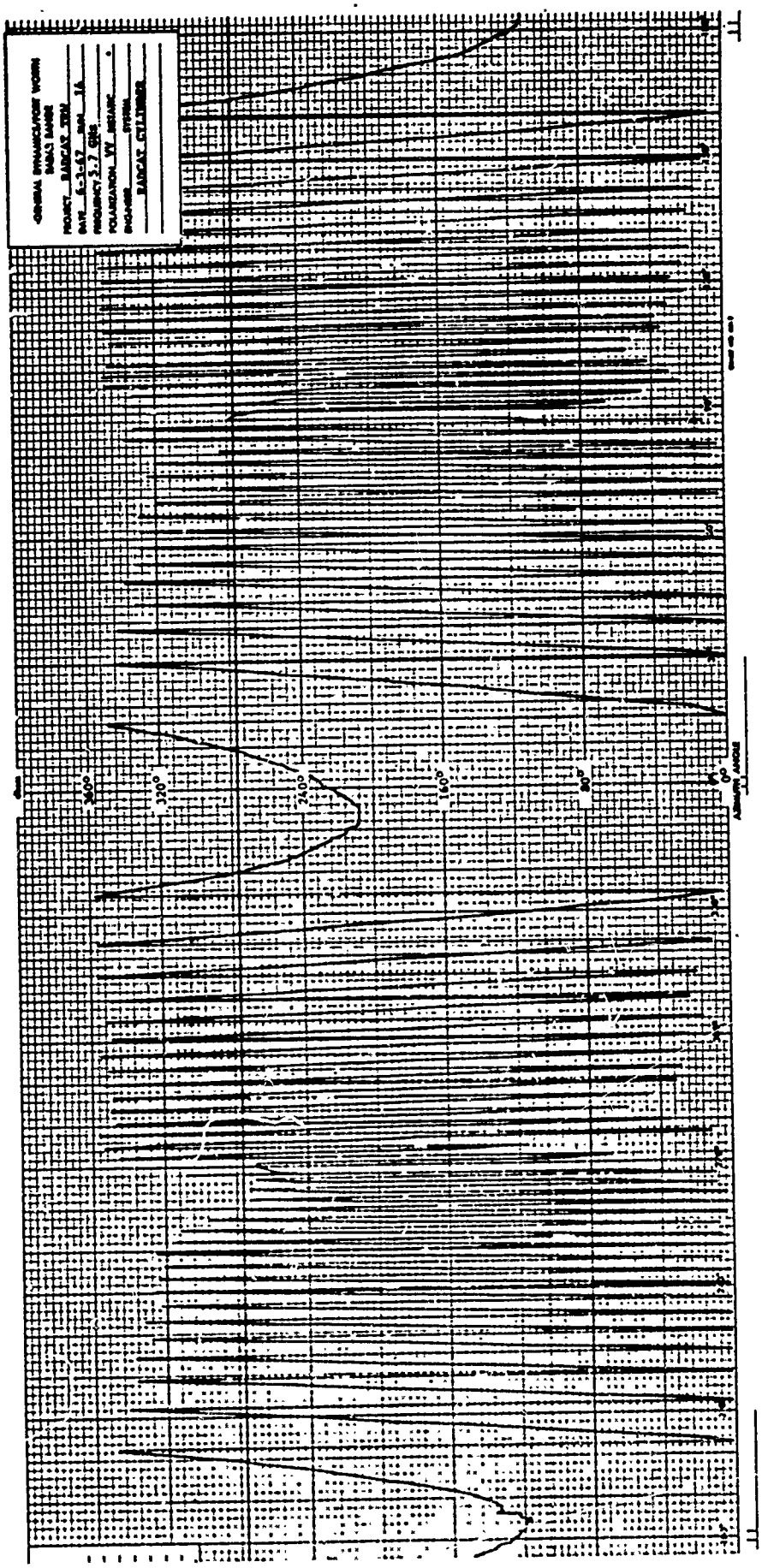

Fig. F-10 HALF-SCALE MODEL PHASE RESPONSE; C-BAND, VV POLARIZATION

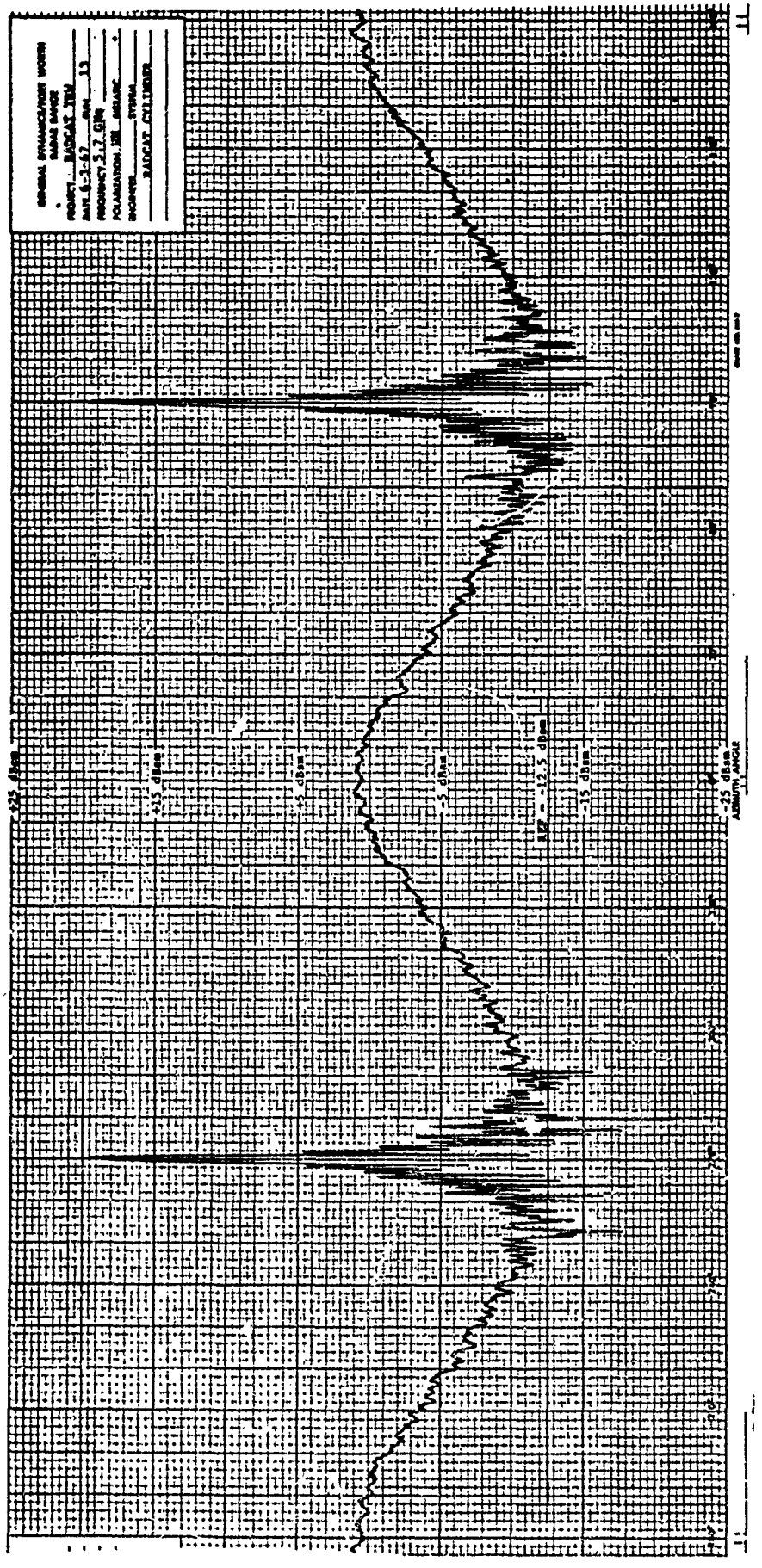

Fig. F-11 HALF-SCALE MODEL AMPLITUDE RESPONSE; C-BAND, HH POLARIZATION

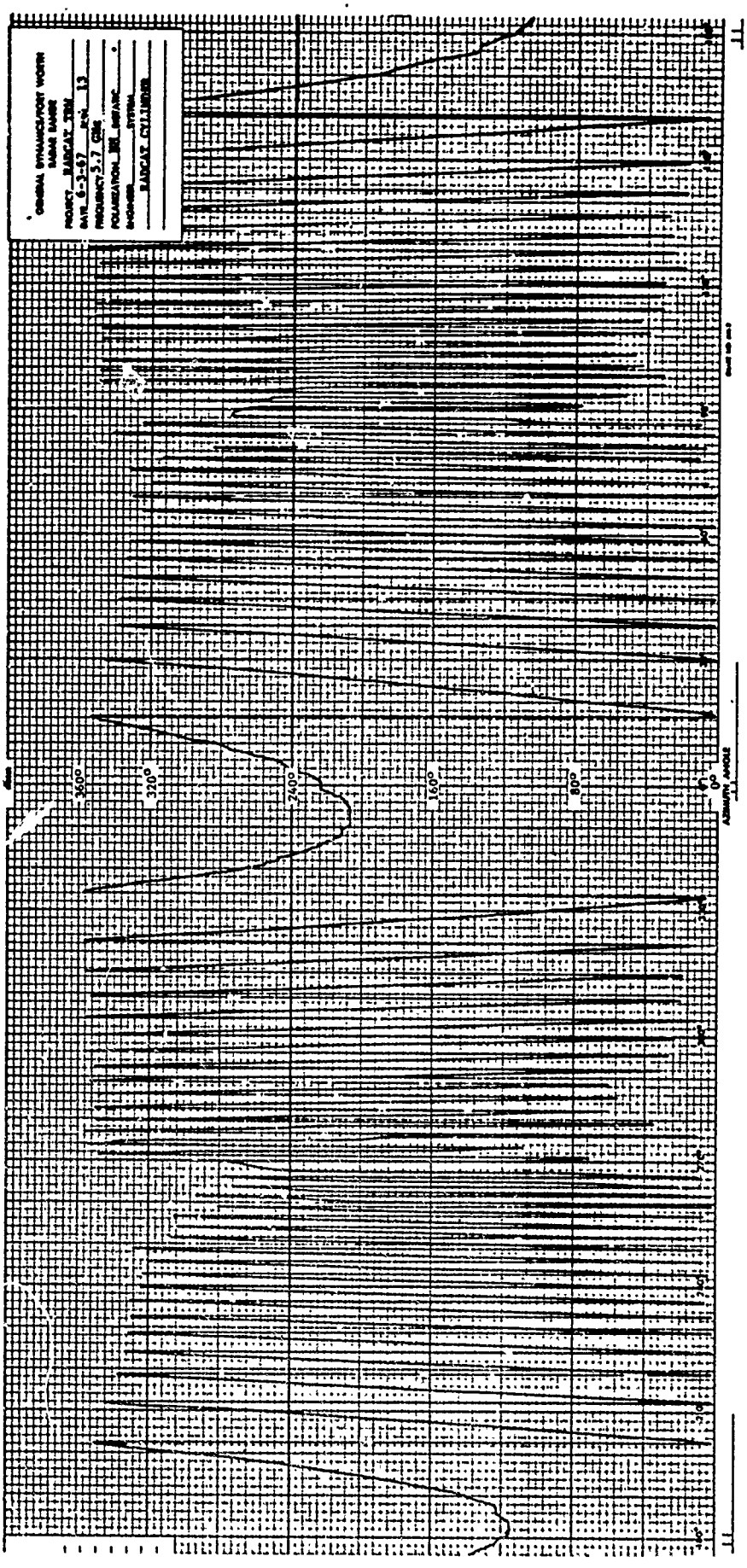

Fig. F-12 HALF-SCALE MODEL PHASE RESPONSE; C-BAND, HH POLARIZATION

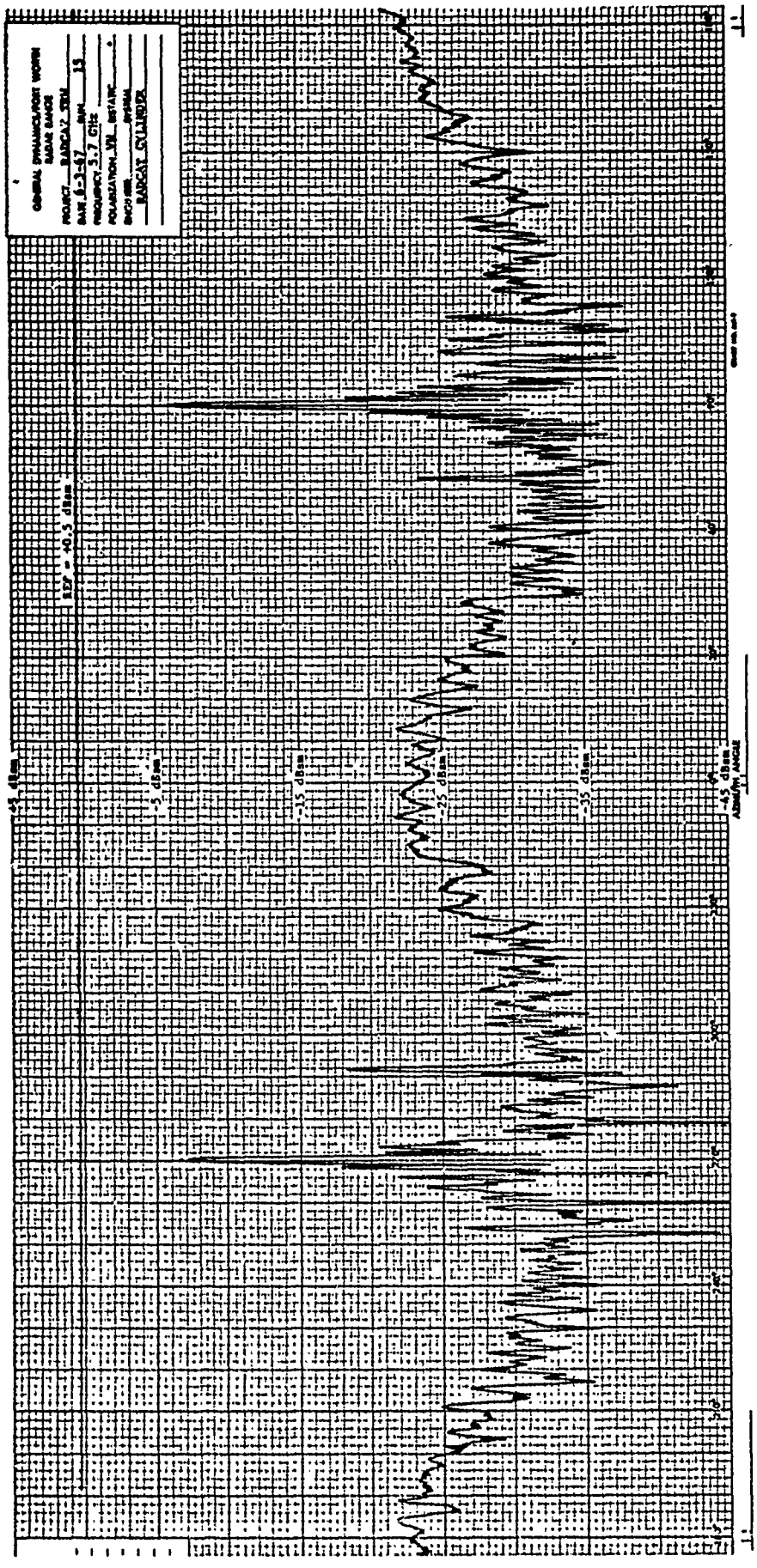

Fig. F-13 HALF-SCALE MODEL AMPLITUDE RESPONSE; C-BAND, VH POLARIZATION

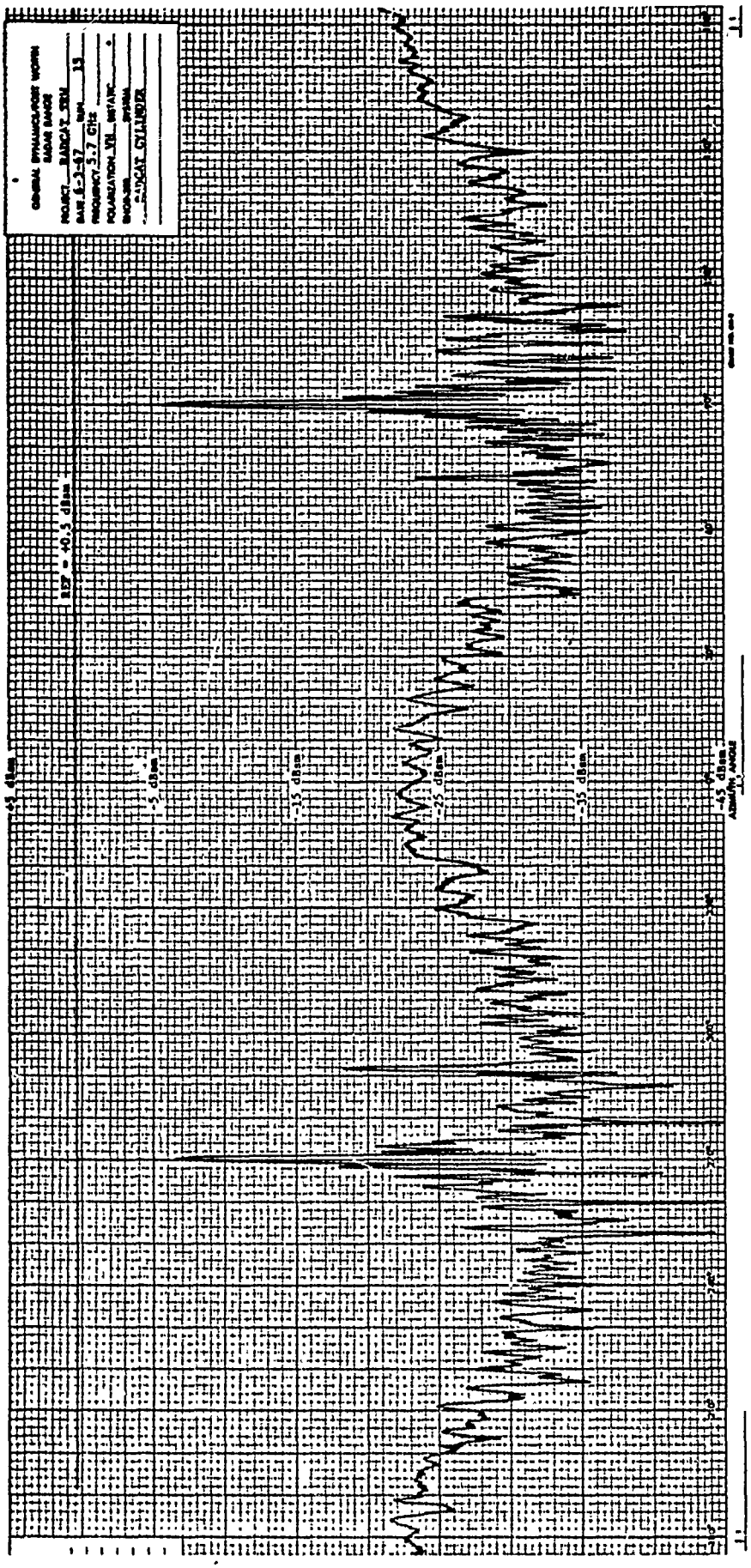

Fig. F-13 HALF-SCALE MODEL AMPLITUDE RESPONSE; C-BAND, VH POLARIZATION

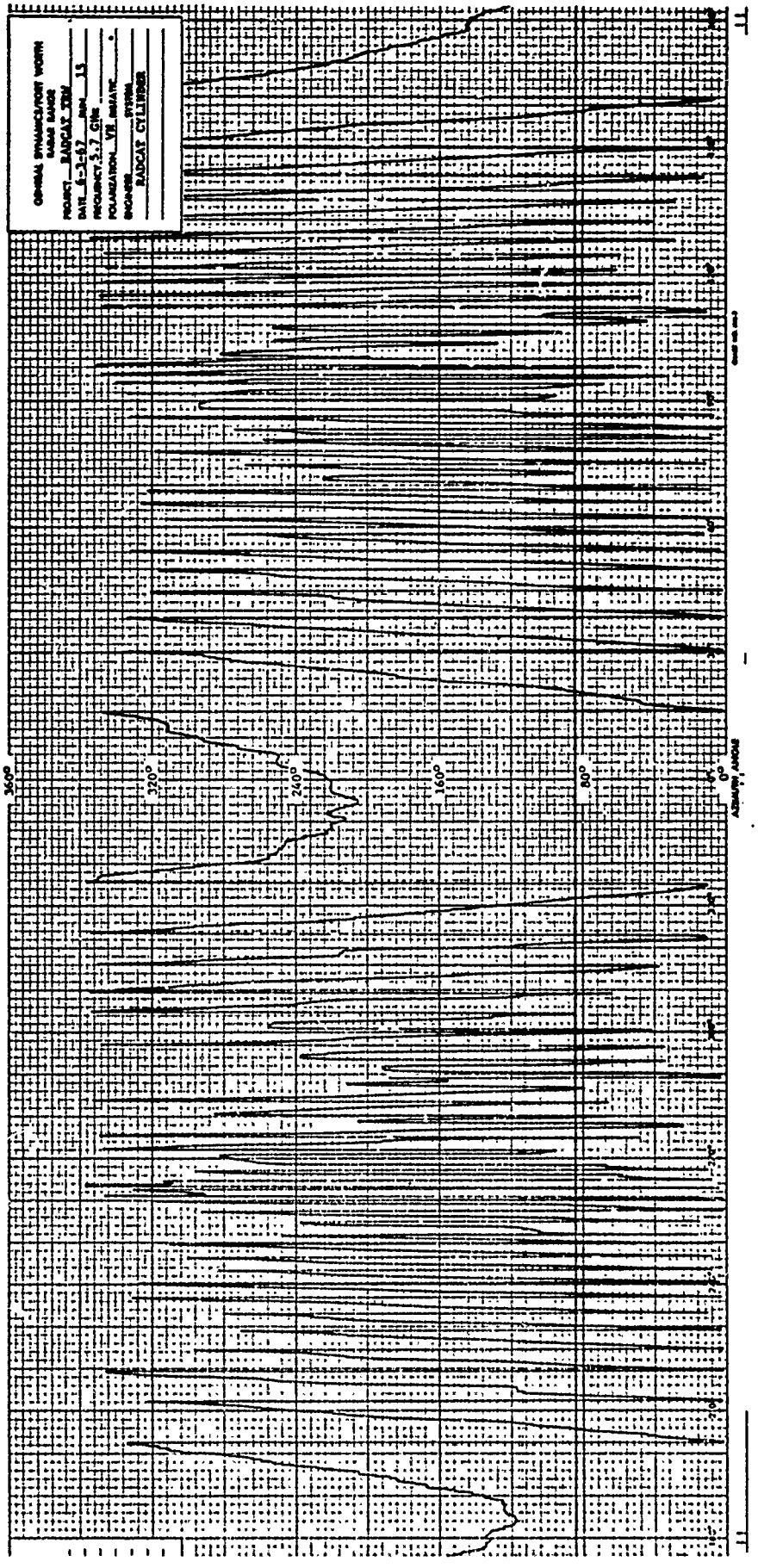

Fig. F-14 HALF-SCALE MODEL PHASE RESPONSE; C-BAND, VH POLARIZATION

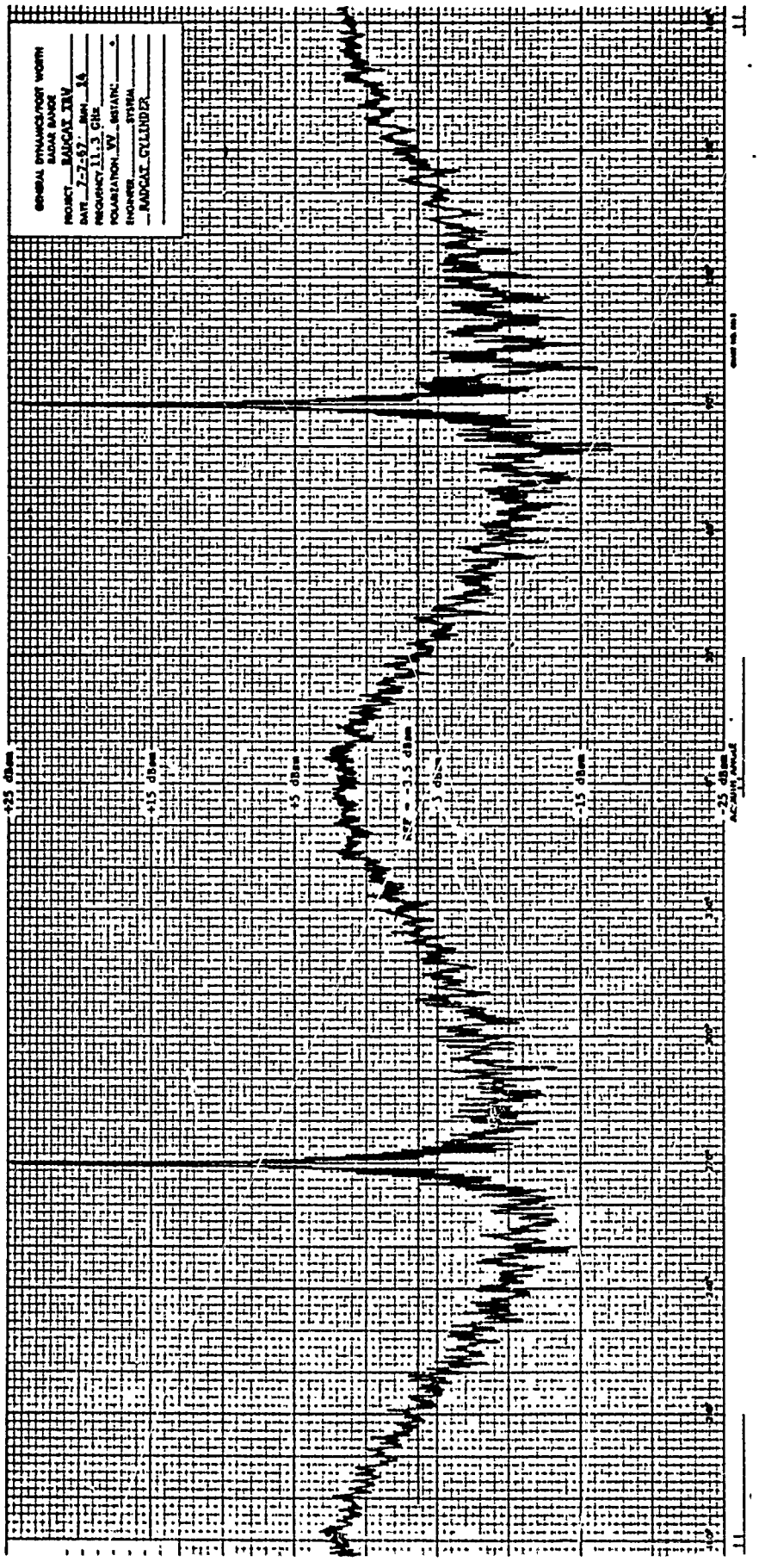

Fig. F-15 HALF-SCALE MODEL AMPLITUDE RESPONSE; X-BAND, VV POLARIZATION

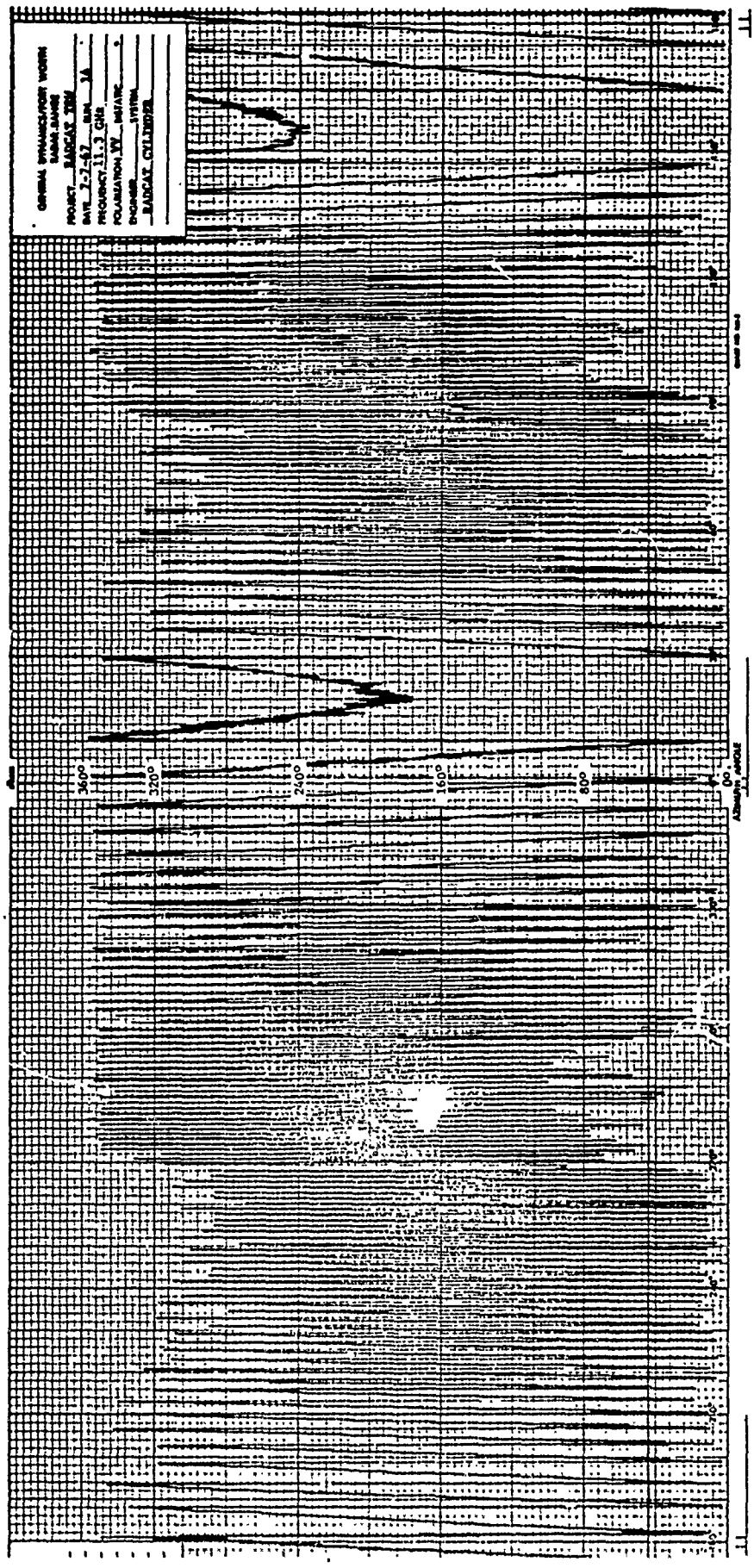

Fig. F-16 HALF-SCALE MODEL PHASE RESPONSE; X-BAND, VV POLARIZATION

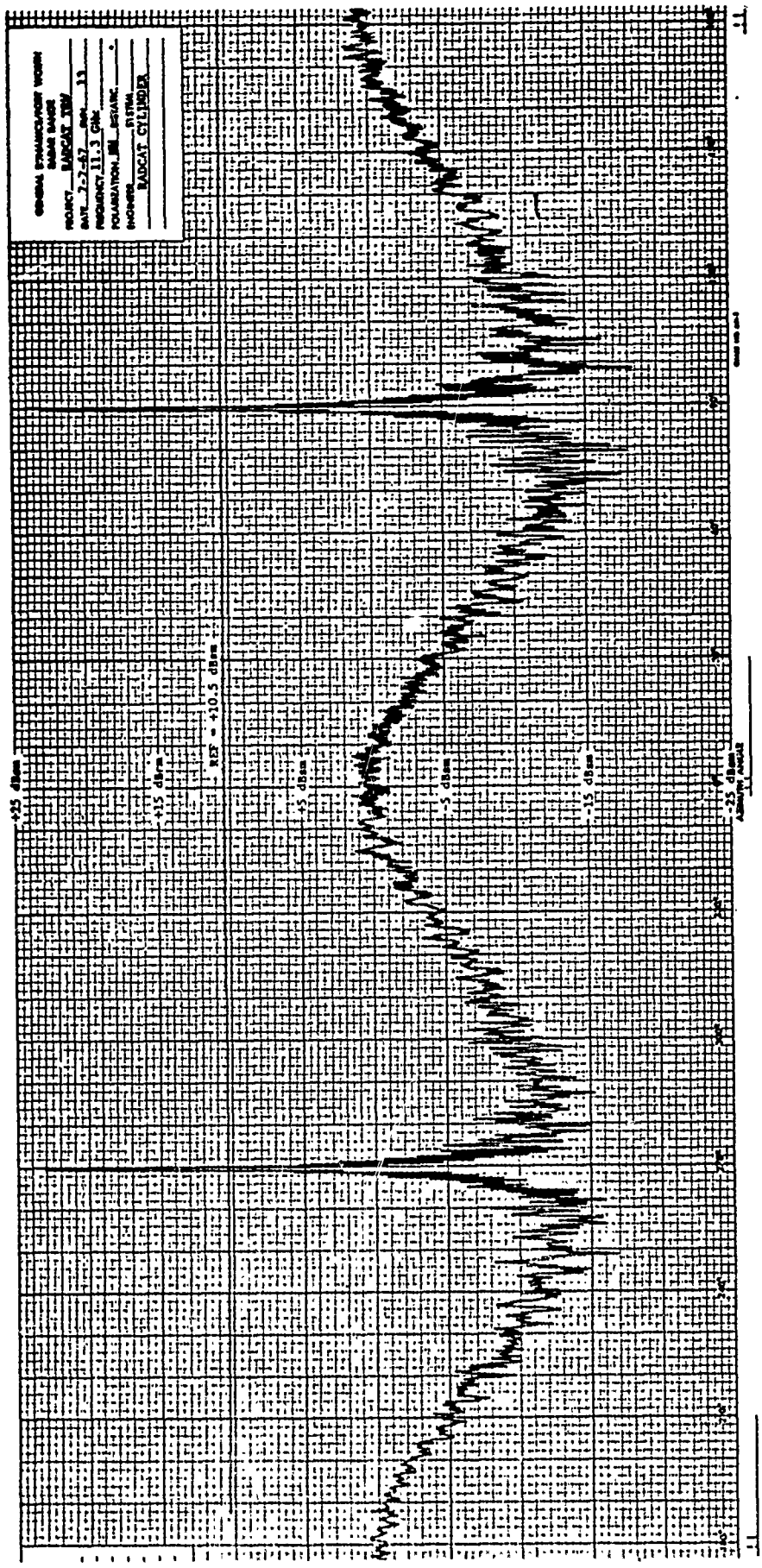

Fig. F-17 HALF-SCALE MODEL AMPLITUDE RESPONSE; X-BAND, HH POLARIZATION

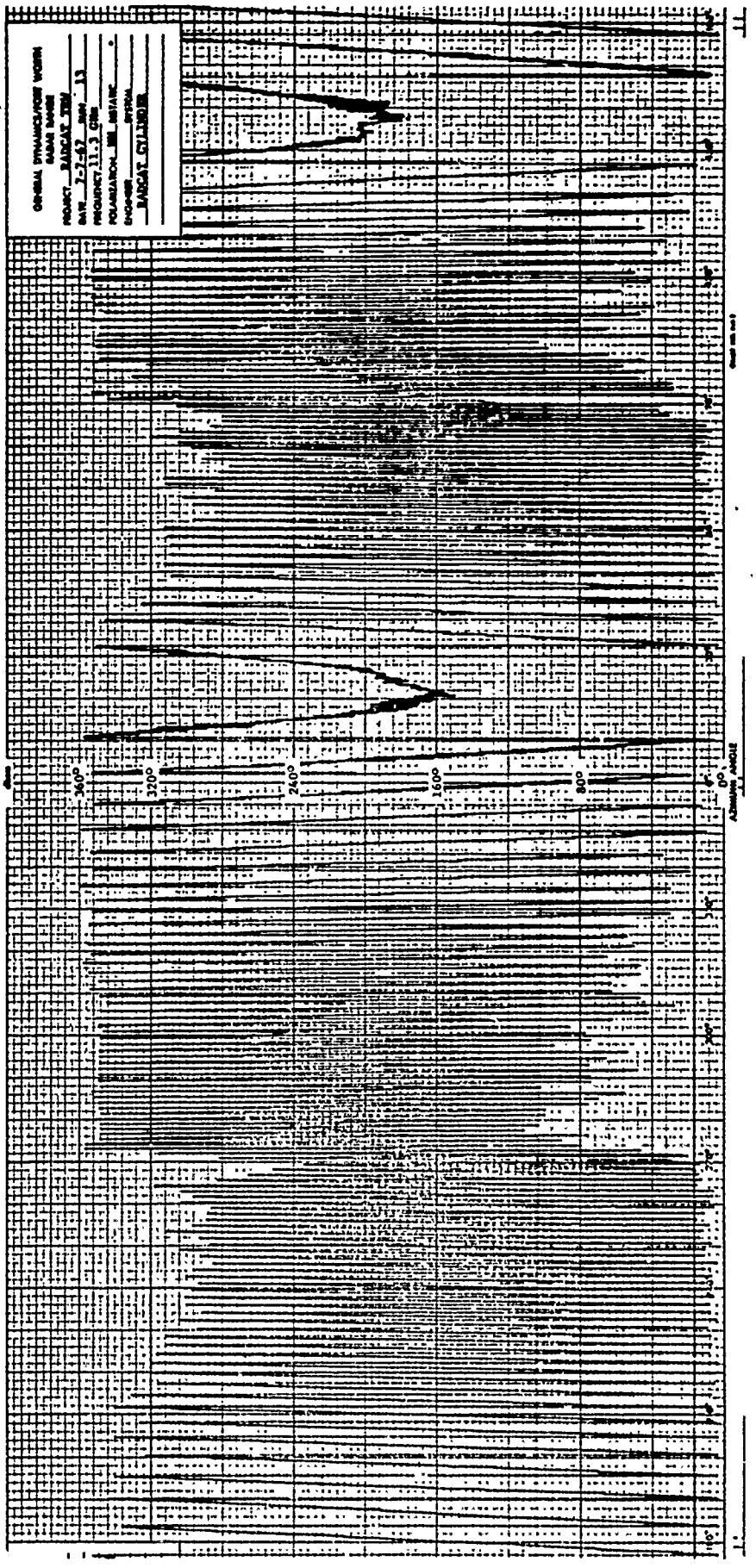

Fig. F-18 HALF-SCALE MODEL PHASE RESPONSE; X-BAND, HH POLARIZATION

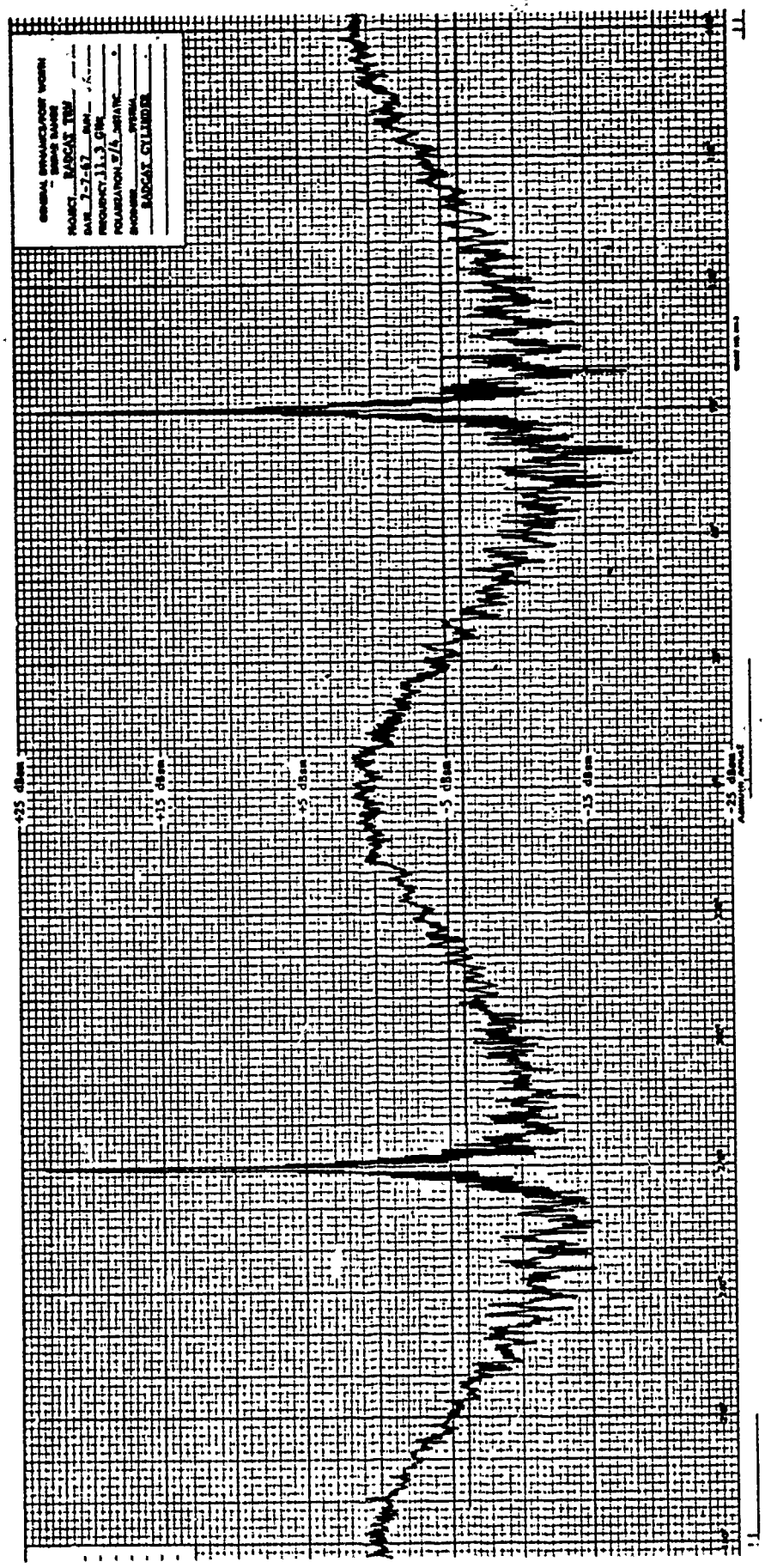

Fig. F-19 HALF-SCALE MODEL AMPLITUDE RESPONSE; X-BAND, $\pi/4$ $\pi/4$ POLARIZATION

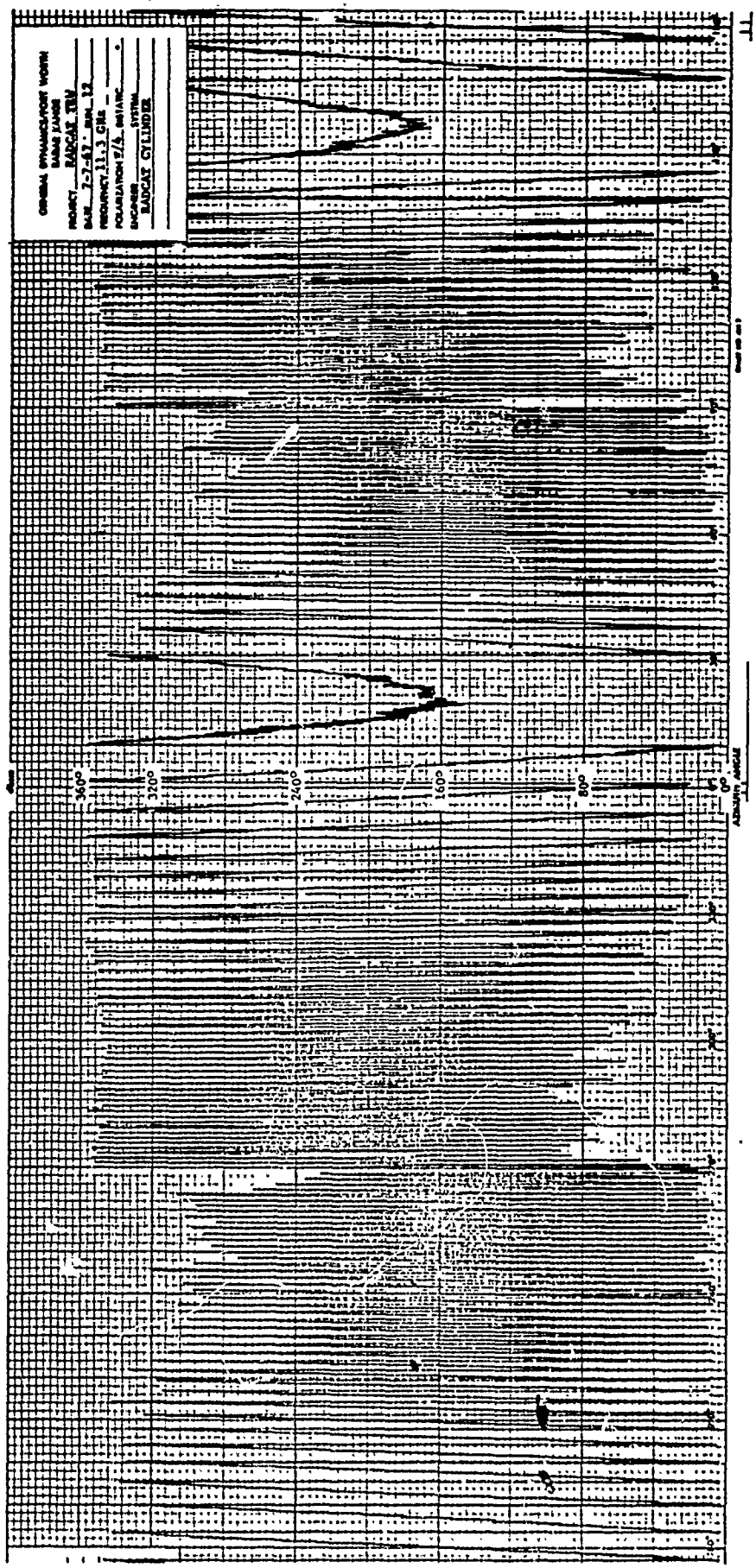

Fig. F-20 HALF-SCALE MODEL PHASE RESPONSE; X-BAND, $\pi/4$ $\pi/4$ POLARIZATION

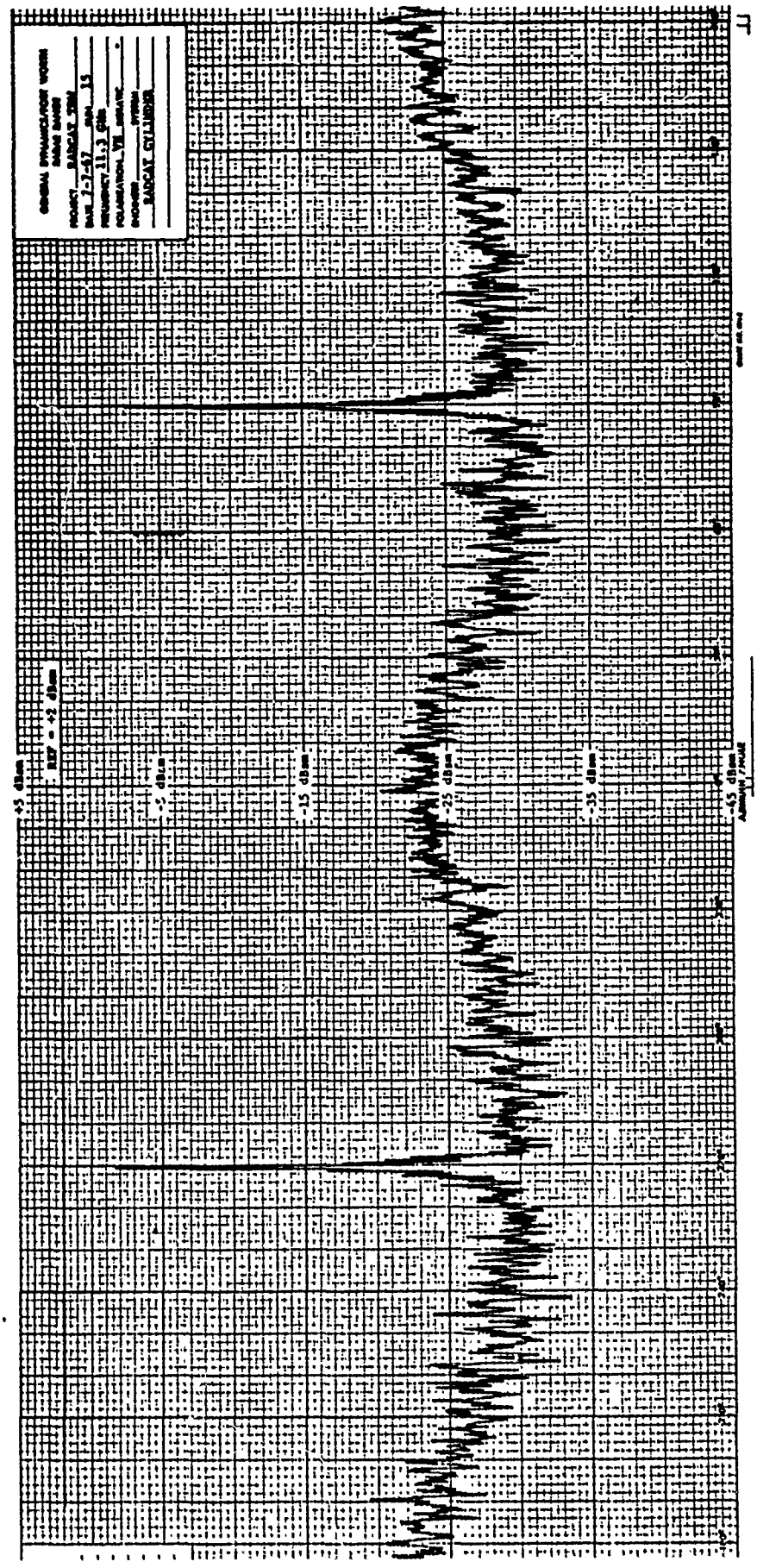

Fig. F-21 HALF-SCALE MODEL AMPLITUDE RESPONSE; X-BAND, VH POLARIZATION

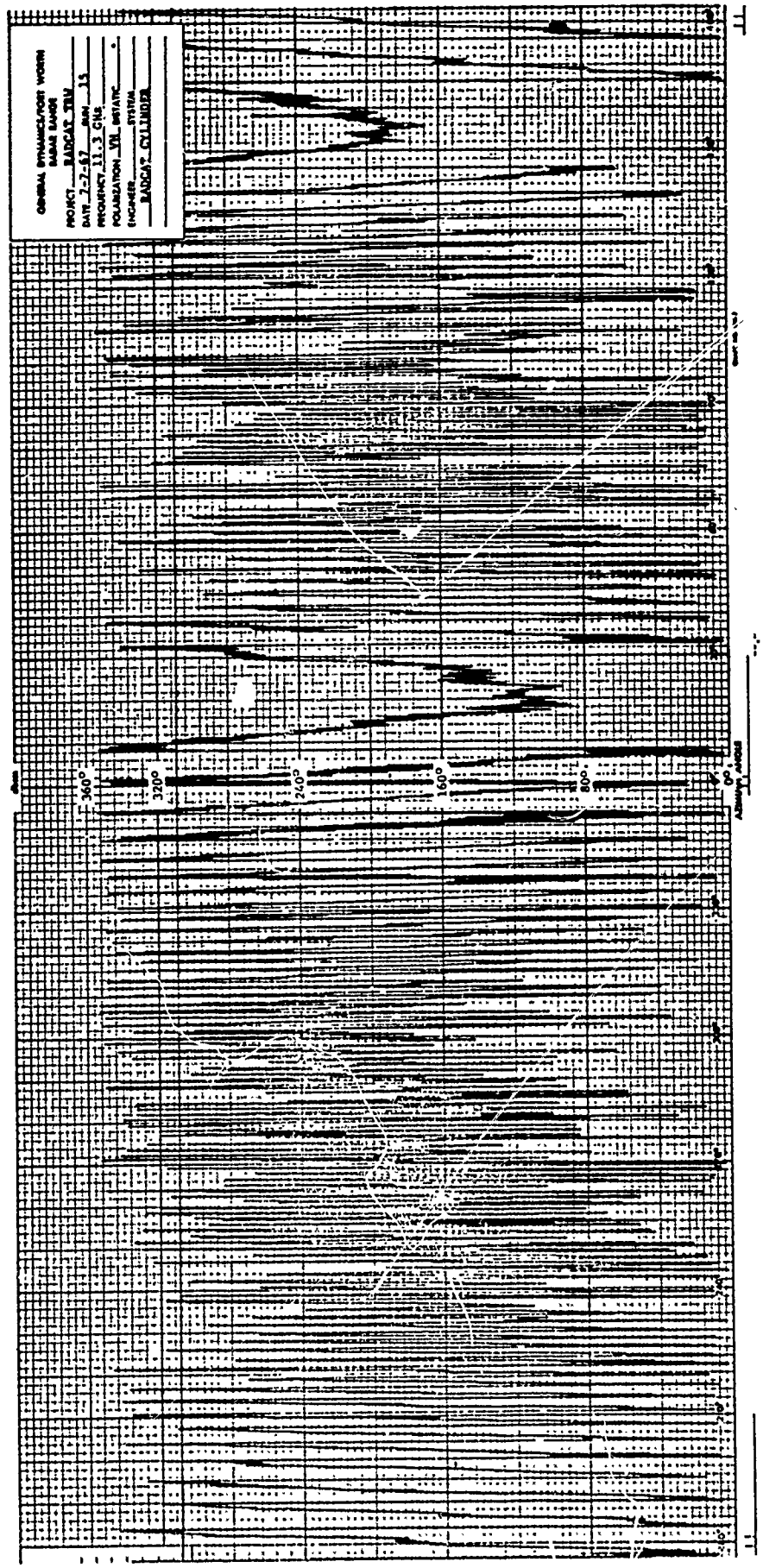

Fig. F-22 HALF-SCALE MODEL PHASE RESPONSE; X-BAND, VH POLARIZATION

THIS PAGE INTENTIONALLY LEFT BLANK

R E F E R E N C E S

1) "RADCAT Cylinder and Luneburg Reflector Scattering Matrix and Short-Pulse Measurements", General Dynamics Report FZE-688, 1 September 1967

2) "RADCAT Target Scattering Matrix", General Dynamics Report FZE778, 15 May 1968

3) Hiatt, R. E. and T. M. Smith (1966), Radar Scattering Investigation, RADC-TF-66-35, (Rome Air Development Center, Rome, N.Y.)

4) Born, M. and E. Wolf (1965), Principles of Optics, (Pergamon Press, Oxford)

UNCLASSIFIED
Security Classification

DOCUMENT CONTROL DATA - R & D

(Security classification of title, body of abstract and indexing annotation must be entered when the overall report is classified)

1. ORIGINATING ACTIVITY *(Corporate author)*
General Dynamics Corporation
Convair Aerospace Div., P.O. Box 748
Fort Worth, Texas 76101

2a. REPORT SECURITY CLASSIFICATION
UNCLASSIFIED

2b. GROUP

3. REPORT TITLE
(U) RADCAT Radar Measurement Program

4. DESCRIPTIVE NOTES *(Type of report and inclusive dates)*
Final Report - 15 Aug 71 to 15 Nov 71

5. AUTHOR(S) *(First name, middle initial, last name)*
Dave O. Cisco

6. REPORT DATE	7a. TOTAL NO. OF PAGES	7b. NO. OF REFS
24 November 1971	270	4

8a. CONTRACT OR GRANT NO.
F30602-72-C-0025

b. PROJECT NO.
Z6590000

c.

d.

9a. ORIGINATOR'S REPORT NUMBER(S)
FZE-1143

9b. OTHER REPORT NO(S) *(Any other numbers that may be assigned this report)*
RADC-TR-72-7

10. DISTRIBUTION STATEMENT
Approved for Public release. Distribution Unlimited.

11. SUPPLEMENTARY NOTES
Daniel L. Tauroney
OCTT
AC315 330-2925

12. SPONSORING MILITARY ACTIVITY
US Army Advanced Ballistic Missile Defense Agency; Commonwealth Buldg. 1320 Wilson Blvd. Arlington VA 22209

13. ABSTRACT

The results of a radar cross section measurement program involving the precision Radar Calibration Target (RADCAT) Vehicle 002 are presented in the Final Report. Coherent long-pulse signatures obtained at measurement frequencies of 1.28, 2.85, and 5.65 gigahertz are presented and discussed in relation to similar data obtained in 1967 on the RADCAT Vehicle 001. Short-pulse measurements, coherent at 5.65 gigahertz and noncoherent at 2.4 gigahertz, were also obtained on RADCAT Vehicle 002 and are presented. Comparisons are made between the long-pulse response of Vehicles 001 and 002, between signatures of Vehicles 001, 002, and those from a half-scale model of the calibration target, and between the long-pulse response of Vehicles 001, 002, and the computed response based on a physical optics formulation.

DD FORM 1473

UNCLASSIFIED

14. KEY WORDS	LINK A		LINK B		LINK C	
	ROLE	WT	ROLE	WT	ROLE	WT
Radar and Radio Target Detection						
Radar Techniques (Detection)						
Scientific Data Analysis						
Scientific Data Reduction						